MECHANISM OF ADAMTS13 REGULATION

EXPLORING THE MECHANISM OF ADAMTS13 REGULATION

BY

HASAM MADARATI, B.Sc., M.Sc.

A Thesis Submitted to the School of Graduate Studies in Partial Fulfillment of the Requirements for the Degree

Doctor of Philosophy

McMaster University

McMaster University DOCTOR OF PHILOSOPHY (2022) Hamilton, Ontario (Health Sciences – Medical Sciences – Blood and Vasculature)

TITLE: Exploring the mechanism of ADAMTS13 regulation

AUTHOR: Hasam Madarati, B.Sc., M.Sc.

SUPERVISOR: Colin A. Kretz, Ph.D.

NUMBER OF PAGES: xiv, 262

ABSTRACT

Studies demonstrated ADAMTS13 possesses unique properties with a mystifying regulatory mechanism. ADAMTS13's role is in its proteolytic function to its VWF. The disparity in the hemostatic balance between ADAMTS13 activity and the distribution of VWF multimers could result in the bleeding disorder Von Willebrand Disease (VWD) or the thrombotic disorder thrombotic thrombocytopenic purpura (TTP). ADAMTS13 is constitutively secreted as an active protease, yet VWF retains its capacity to recruit platelets. This ability makes ADAMTS13 an enigmatic protease with an unknown regulatory mechanism.

Currently, the postulated regulatory mechanism of ADAMTS13 is in its open/closed conformation, yet ADAMTS13 activity is retained in both forms. Literature showed that few proteases are capable of degrading ADAMTS13 *in-vitro*. We hypothesize that the partial degradation of ADAMTS13 regulates its activity, thereby stabilizing VWF and promoting thrombosis.

The goals of this project were to develop and optimize *in-vitro* plasma BioID to identify novel interactions to ADAMTS13, validate novel interactions, identify proteases capable of degrading ADAMTS13 and their proteolytic sites, and develop protease-resistant ADAMTS13 mutants as novel therapeutics to thrombotic disorders.

We optimized the BioID technique to be used *in-vitro* in plasma, to study novel interactions with ADAMTS13. Our results identified novel potential interactions with vitronectin or plasminogen. Validation studies disregarded vitronectin's interaction and

confirmed plasminogen's interaction through the CUB and Kringle domains in a lysine-dependent manner.

Further, the list of proteases capable of degrading ADAMTS13 was expanded to include FXIa and neutrophil-derived proteases including Cathepsin G, elastase, and hPR3. Activated neutrophils played a stronger role than coagulation proteases in degrading ADAMTS13 *in vivo*, while also demonstrating that elastase is a more potent regulator. Proteolytically degraded sites on ADAMTS13 were identified and proteolytic-resistant ADAMTS13 mutants were produced accordingly, which we aim to be utilized as a novel therapeutic to thrombotic disorders.

ACKNOWLEDGMENTS

Special thanks to everyone who has supported me throughout this journey. It is a great privilege and honour to partake in this project, and I am very grateful for the opportunity to complete my Ph.D. in Medical Sciences at McMaster University

With great gratitude, I would like to thank:

Alhamdulilah, all praises to Allah for the strength and His blessing in completing this thesis and for providing me with the following people in my life whom of which have supported me in various ways

My parents, Dr. Mohamad Yahya Madarati and Nawal Fattal, for their unconditional and blessed support, love, and care especially during the COVID-19 hardships

My wife, Sana Birawi for her continuous "hand-in-hand" support, for being my pillar of strength, and for being patient with me on finishing this project

My family, for their patience, unconditional support and care

The Birawi Family for being like a second family to me and for their unconditional support and care

My nephew and nieces, the three cupcakes, for always putting a smile on everyone's face

My supervisor, Dr. Colin Kretz for his guidance and feedback on this project, and mentorship and assistance in writing and editing this thesis

My committee, Dr. Peter Gross and Dr. Jeffrey Weitz for their commitment and evaluation of this work along with their incredible guidance and feedback

My external examiner, Dr. Walter Kahr, for taking the role of an examiner and evaluating this work at such a short notice

My previous mentors, Dr. Yousef Haj-Ahmed, Dr. Bernard Lam, Dr. Candace Panagabko, Dr. Matilda Baptist, Dr. Parthajit Mukherjee, and Dr. Jeffrey Atkinson, for being the initiators of my journey in research and guiding me towards the PhD summit

My lab mate, "Dr." Kanwal Singh for being like a brother to me and for his support on all experimental work and motivation on the completion of this thesis

My lab mate, "Dr." Taylor Sparring for her support on all experimental work

Dr. Tammy Truong and Dr. Shana Aadl Shaya for their support on all experimental work, publication, and guidance

Abdulsalam Birawi and Ahmed Al-Azem for their continuous motivation in completing this thesis and guidance on the pursuit of a career

Sahar Sohrabipour for her assistance and guidance on all neutrophil related projects

Andrew Kwong for his assistance and guidance on all proteomics related studies

Dr. Jim Fredenburgh for his assistance and guidance on the BiaCore SPR related studies

Christine Wu, Papiha Joharapurkar, Veronica DeYoung for their work on the proteolytic degradation of ADAMTS13

All other friends and colleagues, including but not limited to Rawaa Hussain, Neha Sharma, Jaskirat Arora, Cherie Teney, Timothy Wong, Rex Huang, Andrew Chan, and Dr. Ran Ni for all the great memorable moments

McMaster University and CANVector for funding this project

Everyone who has taken the time to read, edit, comment, and listen to my research project

TABLE OF CONTENTS

LIST OF FIGURES

LIST OF TABLES

1. INTRODUCTION

1.1. Hemostasis

1.1.1. Overview of Hemostasis

The cardiovascular system is responsible for delivering oxygen and nutrients throughout the body. Circulating blood delivers the needed supplements to the various organs and cells via the blood vessels, arteries, or veins, which are pumped from the heart towards the organs and back to the heart, all while maintaining homeostasis, a state of internal stability. The cardiovascular system can be disrupted by vascular injury, leading to blood loss. The hemostatic system responds to vascular injury by generating a blood clot at the site of damage to prevent excessive blood loss and maintain the flow of blood to downstream organs and tissues.

Hemostasis is the term used to describe the cessation of bleeding. It is the process of maintaining blood in a fluid state and exists as a balance between coagulation and anticoagulation (1). Disruption of the hemostatic balance can lead to excessive bleeding or thrombosis, a pathological blood clot that can lead to tissue ischemia, a restriction of blood supply to tissues, and cell death (2). The luminal layer of blood vessels is lined with endothelial cells, which maintains the fluidity of blood by expressing and releasing anticoagulant factors. If a blood vessel is damaged, a subendothelium layer consisting of a procoagulant surface is exposed. Through a cascade of events near the procoagulant surface, which involve platelets, coagulation factors, and other proteins, a blood clot is formed to reduce the loss of blood outside the circulatory system (3, 4).

The hemostatic model consists of four major steps (5). Immediately following vascular damage, blood vessels contract to reduce blood flow (vasoconstriction). Next, platelets are recruited and aggregate to form an initial platelet plug (primary hemostasis). The coagulation system is initiated leading to the generation of thrombin, which deposits fibrin to stabilize the platelet plug (secondary hemostasis). Finally, tissue repair is facilitated by the fibrinolytic system, which degrades blood clots (tertiary hemostasis) (6).

During vasoconstriction and at the time when endothelial cells are damaged, the vessel wall halts the expression of anticoagulant mediators, such as thrombomodulin, and will secrete proteins that initiate the formation of blood clots, such as von Willebrand factor (VWF) (5). Following vasoconstriction, are two distinct yet overlapping mechanisms for blood clot formation, the formation of a platelet plug and the formation of a fibrin clot.

1.1.2. Primary Hemostasis: Platelet-Plug Formation

Platelets, VWF, and a disintegrin and metalloprotease with thrombospondin motifs 13 (ADAMTS13) are a few of the key players involved in the formation of the hemostatic plug. In a balanced hemostatic system, 150,000 to 450,000 platelets per microliter circulate in an inactivated and non-adhesive state, with a circular shape and a size of 2-3 µm (7). The role of platelets in hemostasis revolves around their activated state. In response to vascular injury, platelets are activated through various pathways that allow them to undergo a procoagulant conversion. This activation triggers a morphological change, converting platelets from their circular shape to a round shape with finger-like projections (8). The

change in shape includes the exposure of a procoagulant PS surface, whereby the assembly of coagulation factor complexes, the intrinsic- and extrinsic-tenases prothrombinase complex, takes place (9, 10). In addition, the activation of platelets triggers the release of molecules that further promote platelet recruitment and aggregation (8, 11, 12).

The recruitment of platelets to an injured vessel is controlled by Von Willebrand Factor (VWF). VWF is a large multimeric circulating protein that binds to the exposed subendothelial collagen at sites of vessel injury (13). Due to the presence of shear from blood flow, collagen-bound VWF unravels into a long-string structure that binds to the $GP1b_{\alpha}$ receptor on circulating platelets (14, 15). The bound platelets become activated on the collagen surface via the interaction of the GPVI platelet receptor and collagen (13, 16). During the signaling events for the activation of platelets, the cytosolic concentration of Ca^{2+} is increased, which activates the adenosine diphosphate (ADP) signaling pathway (12). ADP, initially released from damaged endothelial cells, acts on platelet's P2Y1 and P2Y12 receptors, causing further platelet activation and further release of ADP (12). Activated platelets release thromboxane A2 (TxA2), which stimulates vasoconstriction, and further amplifies the activation of platelet (6). Activated platelets release their granule contents, including fibrinogen and VWF, which promote further platelet aggregation and the formation of the fibrin clot (16–18). Furthermore, additional agonists such as TF and thrombin are also released which promote clot formation through the secondary hemostasis (10, 19). Platelet aggregation and the formation of a platelet plug continue to grow as additional VWF binds to the immobilized platelet aggregates, capturing additional platelets

to the growing clot (20). The size formation of the platelet plug is controlled by ADAMTS13, which proteolytically degrades unraveled VWF (Figure 1) (20).

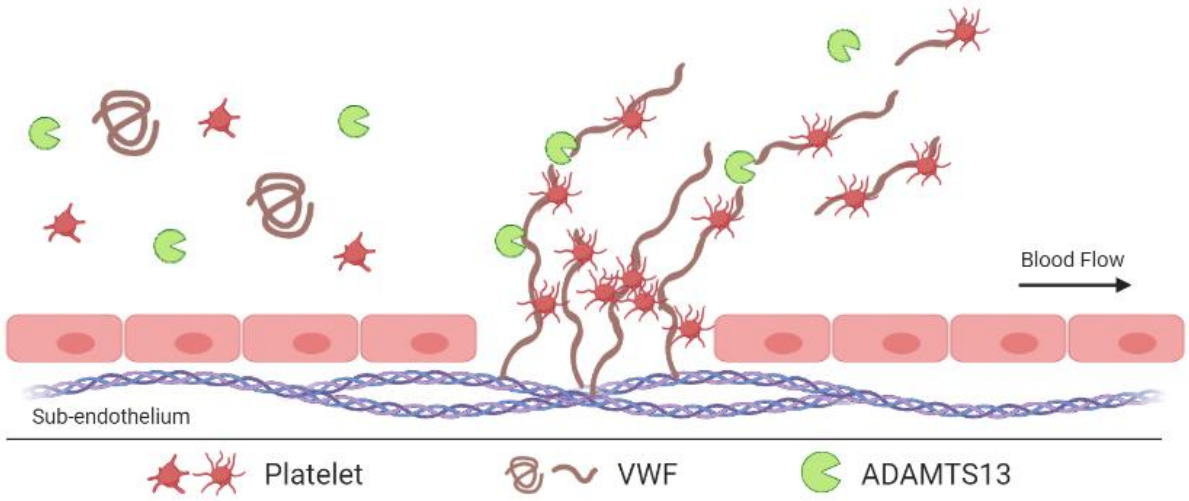

Figure 1 - Platelet Plug Formation – Role of Platelets, VWF, & ADAMTS13.

The globular shape VWF multimer binds to the exposed collagen at the sub-endothelium, unravels from the shear force applied by the flow of blood, and tethers platelets to the site of vascular injury. Platelets then adhere to collagen, which stimulates platelet activation and aggregation. ADAMTS13 regulates VWF's capacity to recruit platelets by regulating the size of the unraveled VWF multimers (21).

1.1.3. Secondary Hemostasis: The Coagulation Cascade

The coagulation system is largely comprised of serine proteases and their cofactors that ultimately regulate the formation of an insoluble fibrin matrix to stabilize the platelet plug (1, 3, 4, 22). Coagulation is initiated through an extrinsic or intrinsic pathway to generate the serine protease thrombin, which activates platelets and converts fibrinogen into fibrin (Figure 2).

The extrinsic pathway begins with a vascular injury and the exposure of extravascular tissue factor (TF) (3). TF is a transmembrane glycoprotein that is expressed by vascular smooth muscle cells, adventitial fibroblasts, pericytes, and circulating monocytes (3, 23, 24). Expression of TF provides a hemostatic barrier by quickly initiating coagulation after injury (23). TF binds circulating FVII, which autoactivates into FVIIa by cleavage of an internal peptide bond at Arg_{152}-Ile_{153} (25). The TF remains bound to FVIIa to form the extrinsic tenase complex (25). This complex, created on a phosphatidylserine (PS) membrane, activates FX into FXa (22).

The intrinsic pathway also referred to as the contact system pathway, begins by activation of FXII through a negatively charged surface, in the presence of Zn^{2+} (4). Physiological activators of FXII include nucleic acids (DNA, RNA), activated platelets, dense granules, polyphosphates, and neutrophil extracellular traps (NETS) (4, 26, 27). FXII activation can be further amplified by the kallikrein system. FXIIa activates FXI into FXIa in the presence of Ca^{2+}, which activates FIX into FIXa (4, 22). FIXa assembles with its

cofactor FVIIIa on negatively charged membrane surfaces to form the intrinsic tenase complex, which rapidly activates FX into FXa (22).

The intrinsic and extrinsic coagulation pathways converge into the common pathway resulting in the formation of the prothrombinase complex (22). FXa binds to FVa in the presence of calcium on PS-containing membrane surfaces to form the prothrombinase complex, which converts prothrombin to thrombin (6).

Thrombin is the final effector of coagulation and converts soluble fibrinogen into insoluble fibrin (28). Fibrin monomers are generated then polymerized upon the release of the fibrinopeptides A & B (FPA & FPB) and through the binding of α chains and γ chains of adjacent fibrin monomers (28). Thrombin also activates FXIII, which crosslinks fibrin chains to yield a more stable fibrin clot (28–30). The fibrin clot is capable of trapping red blood cells and white blood cells, resulting in a complex mesh of insoluble fibrin, aggregated platelets, and other hematopoietic cells (31).

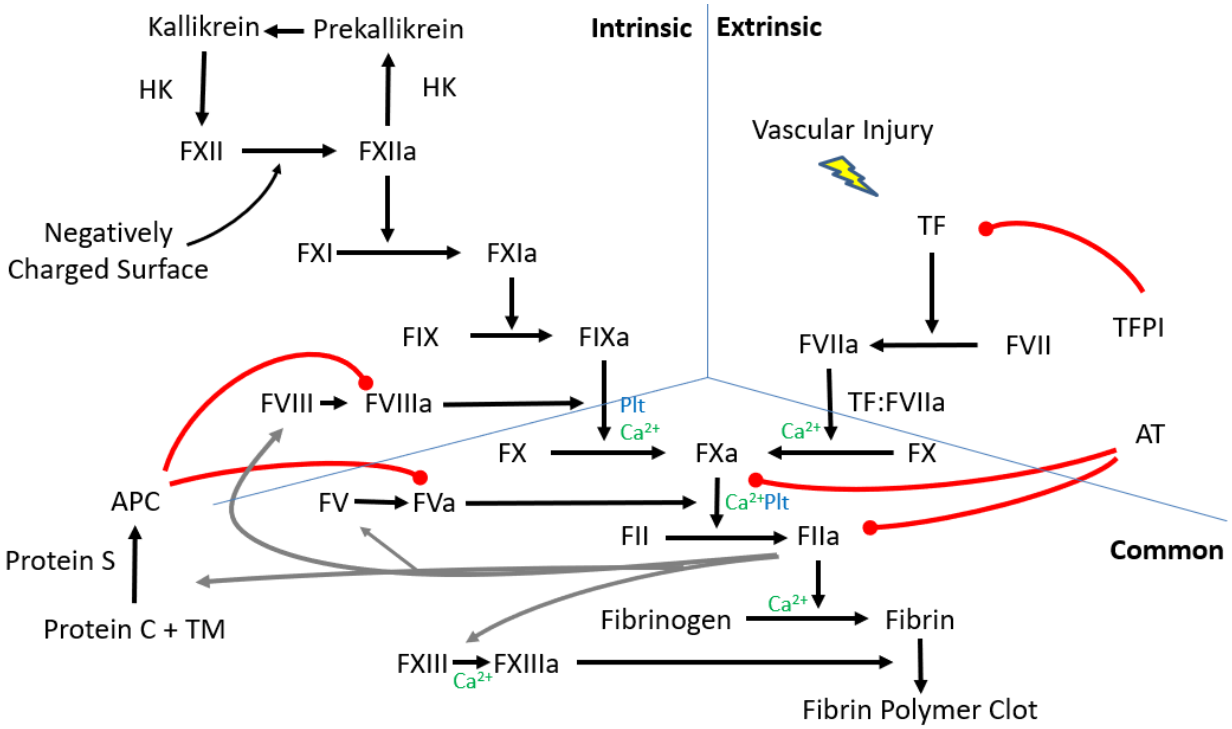

Figure 2 - The Coagulation Cascade.

The coagulation system is divided into the intrinsic, extrinsic, and common pathways. The extrinsic pathway begins with a vascular injury and the activation of FVII by TF (3, 25)*. Intrinsic pathway begins by activation of FXII though negatively charged surfaces, or Kallikrein* (4, 29)*. The two pathways merge at the activation of FX. Cofactors as* Ca^{2+} *and platelet surfaces (Plt). Feedback activations are highlighted in grey for positive feedback loop, or in red for negative feedback loops.*

The initial production of thrombin may not be sufficient to counter the blood loss at the site of vascular damage. Thus, many positive feedback loops take place throughout the coagulation system, which further amplifies the production of thrombin (29, 32). Besides the generation of fibrin, thrombin can activate the endothelium, which provides anionic phospholipid surface, and platelets, which are a major source of FVa activation (29, 32). In terms of the coagulation factors, thrombin is also capable of activating FVIII into FVIIIa, FV into FVa (minor in comparison to the release of FVa by α-granules), FXI into FXIa in the presence of platelets (29, 32). Although thrombin is the major activator of FVIII, FXa can also activate FVIII (29, 32). The positive feedback loops will amplify the system uncontrollably without the presence of regulators such as natural anticoagulants.

The coagulation system has three natural anticoagulants that regulate the system: activated protein C (APC), antithrombin (AT), and tissue factor pathway inhibitor (TFPI) (22). Activated Protein C (APC) is the activated form of the zymogen and vitamin K-dependent anticoagulant Protein C (33). APC, along with protein S, regulates coagulation by cleavage and degradation of FVa and FVIIIa (33). APC is generated on demand in response to thrombin generation, whereby thrombin activates protein C in the presence of thrombomodulin (TM) and endothelial protein C receptor (EPCR) (33). Secondly, antithrombin (AT) is a serine protease inhibitor that inhibits serine proteases such as thrombin (FIIa), FIXa, FXa, FXIa, and FXIIa (34, 35). AT is constantly active and its adhesion to the serine proteases is increased in the presence of the physiological heparan sulfate or by the therapeutic administration of heparins (34, 35). Heparins enhance AT's affinity to thrombin by accelerating the bridging of AT to thrombin (34). Thirdly, Tissue

Factor Pathway Inhibitor (TFPI) is an extrinsic pathway inhibitor that inactivates FVIIa by targeting TF (25). The expression of coagulation factors and natural anticoagulants is also influenced by the hematopoietic cells within the cardiovascular system.

1.1.4. Tertiary Hemostasis: Fibrin Clot Breakdown

The healing process for a blood vessel injury begins at the tertiary hemostasis stage when the fibrinolytic system generates plasmin to break down the fibrin clot (6). Fibrinolysis is dependent on the enzyme tissue plasminogen activator (tPA), which is released by activated endothelial cells following vascular injury and converts plasminogen to its active form, plasmin (36, 37). Plasminogen and tPA bind to fibrin, which serves as a cofactor to accelerate plasminogen activation into plasmin (38). Within the clot, plasmin degrades fibrin releasing fibrin degraded products. Because plasminogen activation by tPA requires fibrin, plasmin generation is restricted to the site of thrombus formation (39). This localization of plasmin is significant since its action is non-specific and will not only degrade fibrin, but also other factors such as FV and FVIII (37). Other plasminogen activators that are not dependent on fibrin include urokinase, FXII, and kallikrein (37). In addition, in the contact portion of the intrinsic pathway, FXII and kallikrein produce bradykinin from high-molecular weight kininogen while bradykinin is the most specific and potent stimulus for tPA release (37). This emphasizes the involvement of the intrinsic pathway's early components (high-molecular weight kininogen, prekallikrein, and FXII) in fibrinolysis and bradykinin generation rather than coagulation (37). The serine protease

inhibitor plasminogen activator inhibitor-1 (PAI-1) regulates fibrinolysis by targeting and inhibiting tPA and urokinase from activating plasminogen (39). Alpha-2 antiplasmin is a serine protease inhibitor that specifically targets plasmin. Increased PAI-1 levels have been associated with an increase in the occurrence of thrombosis in cancer patients (38). Thus, effective activation of plasminogen into plasmin regulates clot clearance.

1.1.5. Role of Hematopoietic Cells in Hemostasis

Hematopoietic cells are derived from stem cells of the bone marrow and are differentiated into mature blood cells such as platelets, erythrocytes, and leukocytes (40). The contribution of platelets to hemostasis is well known and established. Other hematopoietic are increasingly recognized for their role in hemostasis and thrombosis through their expression and secretion of coagulation activators or inhibitors, and/or in providing a negatively charged surface to assemble coagulation factor complexes (10, 19, 41).

1.1.5.1. Role of Red Blood Cells in Hemostasis

Red blood cells (RBC) are primarily responsible for transporting oxygen to body tissue and cells (42). The role of RBCs in hemostasis was investigated during the first clinical observation, in 1910, when anemic patients demonstrated prolonged bleeding time irrespective of their platelet count (43). Originally, it was thought that platelets were

responsible for coagulation and the role of RBCs in hemostasis was not well known. However, investigations have revealed that abnormally high hematocrit levels, such as those with polycythemia vera, are more vulnerable to thrombotic disorders (44). The hemostatic balance can be disrupted by changes in the hematocrit level which is influenced by any of the following underlying effects: an increase in blood viscosity, the formation of RBC aggregates, RBCs binding to the vessel wall, the release of procoagulant microvesicles, the ability of free hemoglobin to suppress free nitric oxide (a platelet inhibitor) during hemolysis, RBCs migration towards the center of blood flow that pushes platelets toward the vessel wall, varying the levels of VWF and FVIII, or the availability of procoagulant phosphatidylserine surface which helps in the assembly of coagulation factor complexes and accelerate clot formation (43–51).

1.1.5.2. Role of White Blood Cells in Hemostasis

White blood cells (WBC), also referred to as leukocytes, are a family of hematopoietic cells that play a role in the body's immune. WBCs may contribute to blood clot formation in several ways including expression of procoagulant mediators such as TF, expression of proteases capable of inactivating natural anticoagulants, or in providing a negatively charged surface for the assembly of coagulation factor complexes (52–54).

Monocytes are the largest type of white blood cells that differentiate into macrophages or dendritic cells. Their main function is to combat infection through phagocytosis, antigen presentation, or cytokine production (55). Unlike other leukocytes,

monocytes exposed to bacterial lipopolysaccharide (LPS) have been shown to express TF both *in-vitro* and *in-vivo* (24, 52, 56). Furthermore, monocytes can release MMP-1 and MMP-9, which cleave and inactivate tissue factor pathway inhibitor (TFPI), which can accelerate clot formation (57). This activity may be accelerated at sites of vessel injury or inflammation because monocytes can be recruited by VWF through the interaction of the monocyte's β2 integrin and an LLG motif in the A2 and D3 domains of VWF (58–60).

Eosinophils are another type of white blood cells and are more involved in an inflammatory response yet can predict the likelihood of a cardiovascular event (54). However, the involvement of eosinophils in hemostasis is not as prevalent as in neutrophils. Similar to neutrophils, activated eosinophils will secrete eosinophil extracellular traps (EETs) that are composed of a mesh-like network of DNA, histones, and granular proteins (61). This mesh-like network can bind and kill bacteria extracellularly (61). Also, EETs primary function is to kill bacteria, yet are also capable of activating platelets and promoting thrombus formation (62). Targeting EETs and preventing their formation was proven to diminish thrombus formation *in-vivo* (62). Furthermore, activating eosinophils, through an agonist such as ADP, provides a negatively charged surface capable of further enhancing thrombin generation and contributing to hemostasis (63).

Another two types of white blood cells are basophils and mast cells (64). In terms of hemostasis, basophil count can be used to predict the likelihood of a cardiovascular event or cardiovascular-related mortality through increased thrombin activity (65). Both basophils and mast cells store histamine and heparin within their secretory granules (41, 66). Once activated, histamine and heparin are secreted into the cardiovascular system to

induce an inflammatory response and trigger coagulation (41, 66). Despite heparin being an anticoagulant that can inactivate thrombin through AT; mast cells-derived heparin has been proven to initiate coagulation by activating FXII through the kallikrein-kinin cascade (67–69).

Neutrophils are the most abundant white blood cell and are the first line of defense in an innate immune response (70, 71). The role of neutrophils in hemostasis is pleiotropic, affecting both procoagulant and anticoagulant pathways (71). Neutrophils possess anticoagulant properties that lead to a faster breakdown of blood clots. For example, neutrophil elastase cleaves native plasminogen (Glu-plasminogen) to yield an angiostatin-like molecule containing plasminogen's K1-3 domains (72–74). Elastase-cleaved plasminogen is a better substrate for the plasminogen activators, u-PA, and t-PA than native plasminogen (72). Thus, neutrophil elastase promotes a faster breakdown of blood clots through the fibrinolytic system. In addition, another neutrophil-secreted enzyme Myeloperoxidase (MPO) produces reactive oxygen species (ROS) (75). These ROS partially inactivate various coagulation factors such as FV, FVIII, and FX (75). The inactivation of coagulation factors slows down the coagulation cascade system, hence providing neutrophils with an anticoagulant role within the hemostatic system.

Neutrophils also possess procoagulant properties that lead to a faster formation of blood clots. Upon activation, neutrophils degranulate and release neutrophil extracellular traps (NETs). NETs are a mesh-like structure composed of DNA, histones, and secreted granular proteins (76). The main function of NETs is to entrap, immobilize and kill pathogens (76). The presence of negatively charged DNA fragments released during the

activation of neutrophils can initiate coagulation through the intrinsic pathway by promoting FXII autoactivation (71, 77). Also, neutrophils contribute to hemostasis via the release of histones H3 and H4 which activate platelets and promote platelet aggregation (57, 71). Like monocytes, neutrophils release proteases that can degrade natural anticoagulants (57, 71). For example, cathepsin G and elastase cleave the natural anticoagulants antithrombin (AT), thrombomodulin (TM), protein C, and TFPI (53, 71, 78, 79). In addition, neutrophils release proteases such as elastase and hPR3 which are capable of degrading both ADAMTS13 and VWF *in vitro* (80, 81). Whether neutrophils have a direct function in disrupting the ADAMTS13/VWF axis is unknown, neutrophils may play a role in regulating ADAMTS13 activity through proteolysis.

1.2. Von Willebrand Factor

VWF, von Willebrand Factor, is a plasma multimeric glycoprotein that tethers platelets to the site of vascular injury and binds to and stabilizes FVIII in circulation (82). Deficiency of VWF results in a bleeding disorder referred to as von Willebrand Disease (VWD).

1.2.1. Discovery of VWF

In the mid-1920s, the scientist Erik von Willebrand first identified an inheritable bleeding disorder that demonstrated prolonged skin bleeding time in a 5-year-old girl (83,

84). The child had a history of significant mucosal bleeding, yet interestingly, had normal clotting time and clot retraction (83, 85). Von Willebrand's analysis revealed that the "new" bleeding disorder was caused by the absence of a plasma factor, which resulted in extended bleeding time without affecting coagulation time or clot retraction (86, 87). In the early 1960s, two *in-vitro* studies identified decreased platelet adhesion as a result of this bleeding order (88, 89). By the late 1960s, the bleeding disorder was pinpointed to a deficiency of FVIII and another plasma factor (84, 90, 91). However, it was not until the 1970s that a breakthrough in the diagnostic and identification of VWD took place thanks to the advancements in molecular techniques. In the early 1970s, ristocetin was identified to induce platelet aggregation, and its use in the quantification of platelet adhesion was the first reliable test in the diagnostic of VWD (92, 93). In addition, with the advancements in immunoassays, Zimmerman identified and termed the multimeric glycoprotein VWF, and by the mid-1980s, the VWF gene was isolated and cloned (94–96).

1.2.2. Expression of VWF

The VWF gene is on chromosome 12, whereby its mRNA encodes for a 2813 amino acid protein (97). VWF contains a 22 amino acid signaling peptide, a 741 amino acid propeptide, and a 2050 amino acid mature protein (98).

During the biosynthesis process of VWF, the translocation of the newly synthesized VWF protein to the endoplasmic reticulum ensues protein folding whereby many of the disulfide bonds are formed including the bond, Cys2771-2773’ and Cys2771’-2773 in the

CK domains of two monomers, which is responsible for the C-terminal dimer formation (99). Upon dimerization, the signaling peptide is removed, and glycosylation ensues as the protein is carried to the Golgi (Figure 3) (100). In the Golgi, pro-VWF dimers multimerize through disulfide bond formation between the D3 domains of two dimers into a "head-to-head" and "tail-to-tail" formation, and the propeptide is then cleaved by furin to produce a mature unit of VWF (101). VWF multimers are then secreted through Weibel Palade bodies from endothelial cells and α-granules from platelets into the bloodstream, which results in ultra-large VWF multimers that require processing into more hemostatically balanced multimer sizes (102, 103).

Human VWF is secreted as a multimeric protein consisting of a variable number of subunits that can reach 40 µm in length, and longer under pathological conditions (103–105). These findings were reiterated in a review by Springer whereby he indicated that as many as 3500 monomers can form VWF tubules with 5 µm in length in Weibel palade bodies (pH 5.4), which extend to ~250 µm in length when released into the blood stream (pH 7.4) (106). As a monomer, VWF is 250 kDa in size, and as a multimer in circulation, VWF varies in size distribution with a molecular weight ranging between 500 kDa and over 10,000 kDa (97). In a balanced system, the average concentration of VWF is about 10 µg/mL in circulation (107).

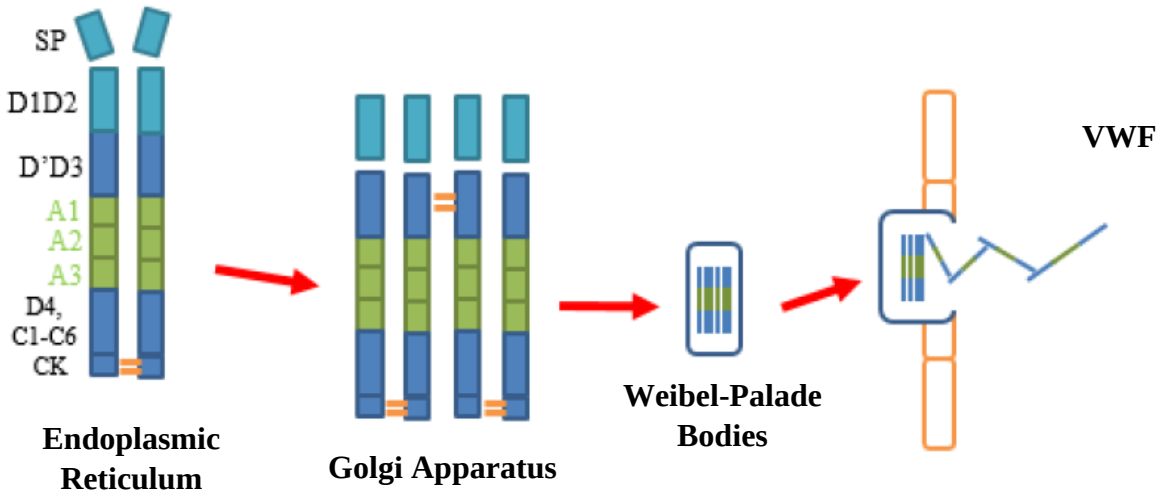

Figure 3 - Multimerization of VWF.

After proteolysis of the signaling peptide, VWF dimerizes via the CK domain at the Endoplasmic Reticulum, then further via the D3 domain at the Golgi (102, 103). *The multimerization process is achieved through a 'head-to-head' and 'tail-to-tail' formation via disulfide bonds at D3 and CK domains.*

1.2.3. VWF Structure

The domain organization of VWF encoded from the VWF gene is as followed: SP (signaling peptide), D1D2 (propeptide), D'D3 (FVIII binding site), A1 (collagen, and platelet receptor $GP1_{b\alpha}$ binding site), A2 (ADAMTS13 proteolytic site), A3 (collagen-binding site), D4, C1-C6, and CK domains (Figure 4) (96, 102, 103). Many of these domains contribute to the role of VWF in hemostasis through functional binding sites or cleavage sites, while others are involved in the biosynthesis process and the multimerization of VWF (108). VWF also contains many cysteines (234 cysteines out of 2813 amino acids), resulting in several disulfide linkages that give VWF its unique structure and functions (109).

The propeptide plays an important role in the multimerization of VWF and the packing of VWF into Weibel-Palade Bodies and α-granules. VWF propeptides from adjacent dimers assemble into a helix bringing dimers into proximity to each other (110). After that, disulfide isomerase activity of the propeptide catalyzes disulfide formation of the adjacent dimers, resulting in multimer formation. The acidic pH of the Golgi maintains the association between the propeptides and the newly multimerized mature protein. The mature multimer radiates outwardly from the helical core of the propeptides, and the compact configuration is maintained as VWF is packaged into Weibel-Palade body storage organelles (110). Furthermore, deletion of the propeptide prevents VWF multimerization

at the D3 domains but has no effect on the dimerization process at the CK domains (111, 112). Furthermore, the pH difference between the endoplasmic reticulum (pH 7.2) and trans-Golgi network (pH 6.2) is needed for the multimerization process to occur (113, 114). The slightly acidic pH in the Golgi, along with the absence of chaperones, creates an unfavorable environment for disulfide bond formation. However, Purvis *et al* demonstrated that VWF can overcome that challenge via the formation of a transient intracellular disulfide bond between the propeptide and VWF D3 domain, similar to the works of a disulfide isomerase (115). Wagner *et al*, along with others, also revealed that the propeptide is required for the successful packing of VWF multimers into Weibel-Palade bodies by demonstrating that the propeptide is needed for the formation of storage granules (116–118).

The D'D3 domains within the mature VWF subunit contain the binding region for FVIII. These set of domains are associated with the stability of FVIII in hemostasis by protecting FVIII from proteolysis and prolonging its half-life (119, 120). Mutations within this region leading to an impaired VWF-FVIII interaction result in rapid clearance of FVIII (121). This effect is observed in VWD type 2N patients displaying hemophilia A-like symptoms. In addition, the inability of furin to cleave VWF propeptide due to mutations in the furin cleavage site prevents FVIII from binding to VWF D'D3 domains, possibly due to steric hindrance (122–124).

The three central 'A' domains on VWF are important to VWF's role in hemostasis. Each VWF A domain consists of a hydrophobic β-sheet core surrounded by amphipathic α-helices (125). This results in a folded, globular conformation that shields the functional

binding sites or cleavage sites of VWF. In its globular state, VWF does not readily interact with its binding partners such as platelets or collagen, and VWF is not readily available for proteolysis by its cleaving enzyme ADAMTS13 (102, 103). In circulation, the presence of shear stress unwinds VWF which facilitates the force-dependent cleavage of VWF multimers by ADAMTS13 (126). Depending on the blood vessel size, the shear rate and rheological stress applied differs. In veins, where the rate and force are the lowest, the mean wall shear rate is 15 – 200 (/s), and force is 0.7 – 9 (Dyn/cm^2) (126). Whereas those numbers increase to 300 – 800 and 450 – 1600 (/s) in rate, and 13.5 – 36 and 20.2 – 72 (Dyn/cm^2) in large arteries and arterioles respectively (126).

The A1 domain, amino acids 1277 – 1453, contains the platelet's binding site, whereby the VWF A1 domain binds to the GP1bα receptor of platelets (102, 103, 127). Mutations in the A1 domain, such as I1309V, are observed in VWD patients type 2B (128). These patients demonstrate a gain-of-function mutation whereby VWF has increased affinity to the platelet receptor GP1bα, resulting in platelet agglutination and a bleeding phenotype (128). In addition to binding to platelets, the VWF A1 domain was found to bind to heparin, sulfatides, and collagen VI (129–132). The heparin-binding domain within the VWF A1 domain demonstrated an additional role of VWF beyond hemostasis and in angiogenesis by binding to growth factors and promoting angiogenesis and tissue regeneration (130). Sulfatides, sulfated glycosphingolipids, were found to bind to the A1 domain of VWF at a site overlapping the GP1bα-binding site and disrupting the binding interaction between VWF and GP1bα (131). Collagen VI, an abundant component of the

fibrillar subendothelium of the arteries, was also found to bind to the A1 domain of VWF emphasizing the role of VWF in hemostasis in arteries (132).

The A2 domain, amino acids 1498 – 1665, contains the proteolytic site for ADAMTS13 (102, 103, 127). When VWF experiences sufficient shear forces of 5000 s^{-1} or higher (133), the A2 domain unfolds and exposes the Tyr^{1605}-Met^{1606} bond to ADAMTS13 for proteolysis (21). Mutations in the A2 domain, such as G1629E, increase the susceptibility of VWF to cleavage by ADAMTS13 (134). This effect results in a decrease in the size distribution of VWF multimers, resulting in reduced VWF-platelet binding capacity and the bleeding phenotype observed in VWD type 2A patients (135). Unlike the other A domains, the A2 domain does not contain the α4-helix, which may play a role in the unfolding and refolding of the A2 domain required for VWF proteolysis by ADAMTS13 (136). In addition, the A2 domain contains a calcium-binding site that is postulated to also play a role in the folding mechanism of the A2 domain. Xu *et al* demonstrated an increase in the refolding rate of the A2 domain in the presence of Ca^{2+}, thus Ca^{2+} stabilizes the refolding of the A2 domain (137). Lastly, due to the nature of the folded state of the A2 domain, studies have utilized several techniques to study the effect of ADAMTS13 on the VWF A2 domain. These techniques include a truncated form of VWF A2 domain, such as VWF73, which avoids the requirement of shear, or a cone-plate viscometer that mimics shear, or denaturants, such as urea, which unfold the A2 domain (21, 126, 138–140).

Evaluating the proteolytic activity of ADAMTS13 becomes a challenge due to the natural folded state of the A2 domain on VWF. VWF A2 domain can be exposed through

shear force or denaturants such as urea, or mutations on VWF (21, 140). Thus, three techniques were developed to study the proteolytic activity of ADAMTS13 on VWF. These include the use of cone-plate viscometer, FRETS-VWF73, and the use of a denaturant reagent such as urea. The cone-plate viscometer is a shearing device made of a rotating cone on top of a stationary plate. The rotating cone applies a varying amplitude of centrifugal force onto VWF, mimicking the rheological effect present in the cardiovascular system and exposing the A2 domain of VWF (126, 138). Another technique to study the activity of ADAMTS13 is the use of a truncated form of VWF, such as VWF73, whereby fluorescence resonance energy transfer technology is incorporated. FRETS-VWF73 is an assay that utilizes the VWF73 peptide along with a fluorophore and a quencher near VWF's proteolytic site (139). The VWF73 peptide is a subsection of the VWF A2 domain which includes VWF's proteolytic site (Y1605-M1606) and excludes the amino acids responsible for the folding of the A2 domain; thus, the proteolytic site is readily available (139). The assay was designed to avoid the requirement of shear FRETS-VWF73 which allows to quantitatively analyze the activity of ADAMTS13 in real-time in a clinical setting (139). Lastly, the use of denaturants such as urea unravels the A2 domain of VWF, whereby ADAMTS13 cleaves VWF before both proteins are completely denatured (21, 140).

The A3 domain, amino acids 1691 – 1871, contains the collagen's binding site, whereby the VWF A3 domain binds to collagen (102, 103, 127). In response to vascular injury, VWF binds to exposed collagen types I and III via its A3 domain (141). The interaction between the negatively charged residues on the A3 domain and the positively charged residues on collagen is what allows the binding to occur (141). Few mutations in

the A3 domain, such as S1731T, have been identified and characterized demonstrating a qualitative defect in the binding of VWF to collagen, yet the multimeric distribution pattern is normal (142). However, other mutations within the A3 domain, such as L1696R, demonstrated a combined qualitative defect in the binding to collagen, and a qualitative defect (143). In addition, similar mutations also observed another qualitative defect whereby VWF's ability to bind to platelets also decreased (143). The administration of purified wild-type VWF was able to correct this defect, yet the binding to collagen remained abnormal (143).

The D4 domain of VWF is involved in the compacting of VWF into Weibel-Palade bodies. D4, along with A2 and A3 domains come together to form a flower bouquet-like structure that assists in the packing of VWF into the Weibel-Palade bodies (144). More specifically, the flower arrangement is known as raceme, whereby the structure arrangement contains three pairs of flower-like globules followed by a stem-like structure (144). Under electron microscopy, the distal domains C1-CK are observed as stem-like structures (144).

With 201 VWC domains found in 70 human proteins, the C domains of VWF (VWC) are prevalent in the motifs of extracellular proteins (145). Typically, VWC domains are small with a size of ~10 kDa and range between 75 to 100 amino acids in length (145). The C1-C6 domains of VWF are involved in the secretion process of VWF. Despite the lack of a resolved crystal structure of the VWF C domains, analysis of a typical C domain structure showed 10 conserved cysteine residues and the formation of 5 disulfide bridges between each pair (146). Shapiro *et al* demonstrated through mutations of these cysteine

residues to alanine, that individual or paired mutations resulted in impaired secretion of VWF and retained VWF in the endoplasmic reticulum (146). In addition, partial or complete deletions of the C domains also resulted in similar retention, suggesting that the C domains are required for normal VWF assembly and secretion (146). Furthermore, the unique C4 domain, unlike other C domains in VWF, contains a platelet-integrin binding domain (145). The structure of the C4 domain is "unusually kinked", whereby the platelet-integrin binding loop is exposed for binding to the platelet GPIIb/IIIa receptor (145, 147). The binding of VWF to this receptor activates platelets and contributes to platelet aggregation at sites of vessel injury (147).

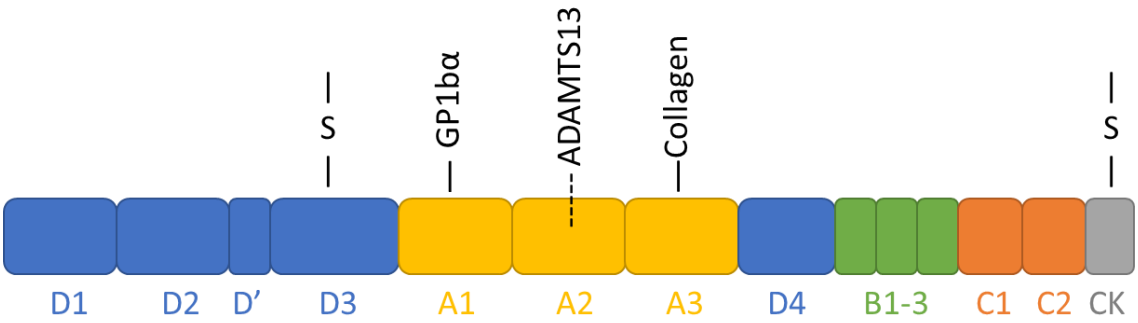

Figure 4 - Classical Domain Organization of VWF.

VWF multimerizes through a "head-to-head" and "tail-to-tail" formation by disulfide bonds at D3 and CK domains (102). *The 3 A domains are: A1 for binding to platelet receptor GP1bα, A2 for proteolysis by ADAMTS13, and A3 for binding to collagen.*

1.2.4. Role of VWF Beyond Hemostasis

As previously discussed, the primary role of VWF in hemostasis is in the tethering of platelets at the site of vascular injury (102). However, further studies have revealed VWF as a multi-functional protein with involvement in other systems such as sepsis, atherosclerosis, and angiogenesis.

Sepsis is a life-threatening illness in response to an extreme infection whereby neutrophils release NETS to trap and handle the bacteria in the circulation system (148). VWF is recruited by bacteria during sepsis by attaching to immobilized VWF on activated endothelial cells in the bloodstream and disrupting VWF's physiological functions such as platelet recruitment and coagulation (149). Studies have demonstrated that NETS have been found to promote thrombosis which is mediated through the binding of DNA and histones to the A1 domain of VWF (150, 151). In addition, during sepsis, VWF levels are increased which contribute to platelet consumption, microvascular thrombosis, and organ damage (150, 151).

Atherosclerosis is a chronic lipoprotein-driven disease whereby there is a build-up of fatty lesions that consist of cholesterol, fat, and inflammatory and thrombotic factors that lead to the formation of an atherosclerotic plaque (152). During atherosclerosis, ultra-large VWF immobilized to endothelial cells recruit and activate platelets which promote vascular inflammation through an increase of inflammatory markers and oxidative stress (153).

Inflammatory markers such as P-selectin and VCAM-1 are leukocyte adhesion mediators which promote leukocyte recruitment onto the endothelial cell surface at the atherosclerotic lesions (154, 155). As the atherosclerotic plaque begins to grow and rupture, thrombosis is induced, and VWF contributes to the growth of the atherosclerotic clot by recruiting additional platelets (153). Furthermore, an *in-vivo* study has pinpointed that endothelial cell-derived VWF, and not platelet-derived VWF, was responsible for promoting atherosclerosis by promoting platelet adhesion and vascular inflammation (156). Deficiency in VWF has been shown to provide a protective effect against atherosclerosis (157). In addition, using ADAMTS13 as a therapeutic agent has been proven to reduce vascular inflammation and plaque formation during early atherosclerosis as demonstrated by Gandhi *et al* during their examination of atherosclerotic plaques in ADAMTS13$^{-/-}$ mice (158).

Angiogenesis is the process whereby new blood vessels are formed from pre-existing ones (159). Dysregulated angiogenesis can be a result of many disorders such as diabetes, cancer, and pathological angiogenesis is referred to as angiodysplasia (160). Angiodysplasia was found to be associated with VWD (161). During an *in-vitro* study on angiogenesis, suppressing the expression of endothelial VWF increased the formation of the capillary tube network (161). Furthermore, the study demonstrated that intracellular VWF inhibits vascular endothelial growth factor receptor 2 (VEGFR-2), a receptor that is responsible for promoting endothelial proliferation, migration, and sprouting in the early stages of angiogenesis (161–163). Also, using an *in-vivo* model, VWF$^{-/-}$ mice were shown to promote angiogenesis (161). Relating this observation to VWD patients, blood

outgrowth endothelial cells (BOECs) isolated from VWD patients demonstrated enhanced angiogenic properties (161). Overall, these data suggest VWF to have a regulatory role in angiogenesis, whereby the lack of VWF promotes the formation of new blood vessels (161).

In relation to ADAMTS13, since ADAMTS13 regulates the size distribution of VWF multimers, and that VWF plays additional roles beyond hemostasis; one can postulate that ADAMTS13 may also have additional roles beyond hemostasis that are indirect and are possibly a result of VWF processing.

1.3. ADAMTS13

ADAMTS13 is a 180 kDa plasma metalloprotease protein that is responsible for the proteolytic degradation of VWF (164, 165). The ADAMTS13 gene has been mapped to chromosome 9q34, whereby its mRNA sequence of 4550 bp after processing encodes for a 1427 amino acid pre-cursor unit of ADAMTS13 (166). The ADAMTS13 gene encodes for a 29 amino acid signaling peptide, 45 amino acid propeptide, and a 1353 amino acid mature protein (164, 166).

ADAMTS13 is predominantly synthesized in the liver by hepatic stellate cells and secreted into circulation as an active enzyme (167). In addition, ADAMTS13 expression was found in kidneys whereby glomerular endothelial cells were found to express and secrete ADAMTS13 as well (168). Furthermore, using real time-PCR, ADAMTS13 was found to express in the spleen, lungs, and the brain as well (167). However, the primary

source of ADAMTS13 is in its expression by the hepatic stellate cells, and further investigating these cells may provide a further understanding in the regulation of ADAMTS13 in TTP (167).

1.3.1. Discovery of ADAMTS13

The history of ADAMTS13 predates its discovery and is centered on the thrombotic disorder TTP. In the mid-1920s, the first case, of what was later classified as TTP, was diagnosed in a 16-year old female patient (169). The patient presented anemia followed by paralysis and a coma (169, 170). Two weeks later, the patient died, and her autopsy revealed occlusive thrombi in the arterioles and capillaries (169). Moschowitz's diagnosis was written as a powerful "poison" with hemolytic and agglutinative properties (169). Later in 1960, Schulman reported a similar diagnosis in an 8-year old patient, who also presented several episodes of anemia and thrombocytopenia (171). However, she responded well to plasma infusion treatments (171). By the late 1970s, Upshaw reported a similar diagnosis in a 29-year old woman; however, her first episode was reported as early as 6 months of age (172). Following these incidents, the examiners postulated that a lack of a plasma protein responsible for platelet agglutination or the survival of RBCs was the cause of this unknown disease (173). In addition, the use of plasma transfusion recovered the levels of such protein; thus, the term Upshaw-Schulman Syndrome was coined for this disease (173). By the early 1980s, Moake *et al* reported the presence of ultra-large VWF (UL-VWF) multimers present in similar patients (174). Moake *et al* also postulated the presence of a

VWF “depolymerase” that is responsible for regulating the size of VWF multimers (174). However, it was not until the late 1990s that VWF “depolymerase” was identified and isolated (175, 176). In 2001, several studies examining the structure of VWF “depolymerase” identified this protein as a novel member of the ADAMTS family, and thus the term ADAMTS13 was coined (177–179).

1.3.2. ADAMTS Family

ADAMTS13 is part of the ADAMTS protease family and a member of the Metzincin protease superfamily (180). The ADAMTS family consists of 19 metalloproteases and 7 ADAMTS-like proteins that lack protease activity and the metalloprotease domain (181, 182). The 19 metalloproteases of the ADAMTS protease family are generally not well characterized but are thought to help shape the extracellular matrix (ECM). For example, ADAMTS2 cleaves procollagen into activated collagen fibrils, which plays a major role in the structure and stability of fibrous tissue (183).

All members of the ADAMTS protease family consist of a signaling peptide, a propeptide, a metalloprotease domain (M), disintegrin-like domain (D), thrombospondin type 1 motif (T), cysteine-rich domain (C), spacer domain (S), and varying other C-terminal domains (181, 182). The additional domains could be additional T repeats, CUB domains (complement C1r/C1s, sea urchin epidermal growth factor, and bone morphogenetic protein), mucin domain, Gon-1 like domain, or a PLAC domain (protease and lucinin) (181, 182).

The most common shared feature within this family of proteases is the metalloprotease domain. This domain contains a highly conserved consensus sequence, HEXXHXXGXXH, whereby the histidines coordinate a zinc atom, and along with glutamic acid residue, carry out the enzyme's catalytic function (181, 182). Following this sequence is a methionine residue, which forms a curve in the structure known as the Met-turn, which provides a binding pocket for the zinc atom and is conserved throughout the Metzincin family of proteins (184, 185).

Another common feature that is shared amongst this family of proteins is the cleavage of the propeptide by a protein, such as furin, that activates the ADAMTS protein for its proteolytic function (186). Generally, the function of the ADAMTS proteins, apart from ADAMTS13, revolves around the extracellular matrix. In addition, the activity of the ADAMTS proteins, apart from ADAMTS13, is regulated by metalloprotease inhibitors such as tissue inhibitors of metalloproteinases (TIMPs) (187).

The ADAMTS proteins are further categorized depending on their function. The class of proteoglycanases, enzymes that are capable of cleaving proteoglycans such as aggrecan, include ADAMTS-1, -4, -5, -8, -9, -15, and -20 (181). Another class of enzyme, procollagen N-peptidase, include ADAMTS-2 which is capable of cleaving collagen types I, II, and III (188). ADAMTS proteins that share a similar homology to ADAMTS-2, such as ADAMTS-3 and ADAMTS-14, are also capable of cleaving collagen *in-vitro* (181). Other members of the ADAMTS family of proteins, apart from ADAMTS13, have not been well characterized.

Despite the sequence similarities and homology that are shared between ADAMTS13 and the ADAMTS family of proteins, ADAMTS13 remains the most unique member of the ADAMTS family because of its unique properties and function.

1.3.3. Structure of ADAMTS13

ADAMTS13 shares the same first part of the protein, pro-MDTCS, as other ADAMTS proteins but differs at the C-terminal (167, 180). Unlike the other ADAMTS proteins, ADAMTS13 possesses seven additional thrombospondin type-1 repeats and two additional CUB domains (Figure 5) (167, 180). The additional domains have been shown to play a role in the conformational activation of ADAMTS13 (189, 190).

The propeptide of ADAMTS13 is different than the propeptide of other ADAMTS proteins and matrix metalloproteases (MMPs). First, the propeptide of ADAMTS13 is shorter, ~41 amino acids, compared to the typical ~200 amino acids in size (164). Second, the propeptide of MMPs may assist in protein folding, or in regulating the catalytic activity of the protease via a cysteine switch whereby a cysteine residue binds to and occludes access to the Zn^{2+} ion in the active site (191, 192). Interestingly, the ADAMTS13 propeptide is unique and does not possess either property (164). While the ADAMTS13 propeptide is cleaved during the expression and secretion of ADAMTS13, its attachment to ADAMTS13 does not hinder the ADAMTS13 activity, and ADAMTS13 is capable of cleaving VWF multimers with and without the propeptide present (164). These data suggest

that the propeptide is a vestigial feature of evolution and has lost its function in ADAMTS13.

The ADAMTS13 metalloprotease domain function is the hydrolysis of the VWF scissile bond (21). The metalloprotease domain of ADAMTS13 shares few similarities with other metalloproteases, such as reprolysin or adamalysin, which include the highly conserved metalloprotease active site motif (HEXXHXXGXXH), and an adjacent Met-turn that provides a Zn^{2+}-binding pocket (21). ADAMTS13's active site's Glu225 residue, 3 His residues (184, 190, 193), and the Zn^{2+}-bound ion coordinate a water molecule that drives hydrolysis of the scissile bond (21). Furthermore, ADAMTS's active site is known to have three Ca^{2+} binding sites, based on the crystal structure (194, 195). First, the amino acid residues Glu83, Asp173, Cys281, and Asp284 coordinate the first Ca^{2+} binding site (194, 196). These residues are conserved throughout the ADAMTS family and appear to facilitate low-affinity Ca^{2+} binding (194, 196). Second, the amino acid residues Glu164, and Asp166 coordinate the second Ca^{2+} binding site along with one or more of the following residues Asn162, Asp165, and/or Asp168 (194, 196). However, amino acid substitutions on any of the amino acids in this site did not affect the calcium-binding ability of ADAMTS13 (194, 196). Third, the amino acid residues Asp187, and Glu212 coordinate the third Ca^{2+} binding site along with Asp182 or Glu184 (194, 196). In addition, amino acid substitutions on the amino acids involved in this site resulted in a drastic decrease of Ca^{2+}-dependent ADAMTS13 activity; thus, postulating this site to be involved in high-affinity Ca^{2+} binding (194, 196). The location of the Ca^{2+} binding sites in a loop near the active site and within

the metalloprotease domain suggests that Ca^{2+} binding offers structural stability, which is required for effective VWF proteolysis (21).

The disintegrin domain shares structural features with the viper venom disintegrin but lacks the canonical cysteine arrangement and therefore does not inhibit platelet aggregation nor bind to other integrins (21, 197). For ADAMTS13, the disintegrin domain shares similarities to the cysteine-rich domain in structure and contains critical exosites involved in binding VWF and positioning the scissile bond for proteolysis by the metalloprotease domain (21). In addition, the disintegrin domain contains a flexible linker that allows the disintegrin domain to be positioned towards one end of the metalloprotease active site (21). Furthermore, several studies have alluded to the importance of the disintegrin domain in the specificity and proteolysis of VWF. de Groot *et al* demonstrated that mutations to the residues Arg349 and Leu350 in the Disintegrin domain decreased the proteolytic activity of ADAMTS13 by 5- to 20- fold when cleaving a truncated VWF A2-domain substrate, VWF115 (193). Moreover, Xiang *et al* demonstrated that mutations to the residues Ala1612 and Asp1614 in the A2 domain of VWF decreased the proteolytic activity of ADAMTS13 by 6.5- fold, when cleaving VWF115 (198). Bringing all this together, these amino acid residues are involved with the positioning of VWF onto ADAMTS13 for cleavage (198).

Thrombospondin type-1 (TSP) repeat motifs are homologous to the thrombospondin type-1 protein that interacts with cell adhesion receptors (21). ADAMTS13 contains 8 TSP repeats, whereby TSP-1 is between the disintegrin domain and the cys-rich domain, and TSP repeats -2 to -8 are between the spacer domain and the

CUB domains (21). Between TSP-4 and TSP-5, and TSP-8 and the CUB domains are two linker regions referred to as T4L, and T8L respectively (21). Four TSP repeats within ADAMTS13 including TSP-2, -5, -6, and -8, contain the region CSVSCG, which is a binding region for the cell surface receptor CD36 (199). ADAMTS13 binds to the cell surface receptor CD36 via TSP-1 repeats, where it is localized to the VWF-platelet complex and optimally positioned to cleave VWF (199). Furthermore, the later TSP repeats, TSP-5 to -8, along with the CUB domains are involved in mediating the binding of ADAMTS13 onto VWF's D4-CK domains (200, 201). Moreover, the earlier TSP repeat, TSP-1, is involved in mediating the exosite binding of ADAMTS13 onto VWF which assists in orienting the scissile bond towards the active site of ADAMTS13 (21, 201). Further explanation of both interactions is discussed in the following section ADAMTS13 conformation.

The ADAMTS13 Cysteine-rich domain is analogous to the other members of the ADAMTS protein family's Cysteine-rich domain by having 10 conserved cysteine residues (21). For ADAMTS13, the functions of the cys-rich and spacer domains were recently shown to interact with a novel exosites binding region within the VWF A2 domain and are therefore involved in the proteolysis of VWF (202).

The spacer domain is one of the most important domains for the function of ADAMTS13. The spacer domain recognizes VWF's A2 domain and initiates the exosite binding interaction between the two proteins (203). In addition, the spacer domain interacts with the CUB domains of ADAMTS13, providing a closed conformation in a scorpion tail-like manner (190, 201, 204). Disruption of this interaction modulates the proteolytic

activity of ADAMTS13 onto VWF (190, 201, 204). Furthermore, the spacer domain was found as a significant target for autoantibodies in acquired TTP patients (205, 206). Studies have demonstrated that mutations within the spacer domain, specifically exosite 3, nearly abolished the binding autoantibodies onto the spacer domain, as well as significantly impaired the proteolytic activity of ADAMTS13 onto VWF multimers (205, 206). For example, the amino acids Arg568, Phe592, Arg660, Tyr661, and Tyr665 in exosite 3 are responsible for this effect, and mutations of these residues are responsible for many of the TTP cases (206).

Figure 5 - Domain Organization of ADAMTS13.

Visual representation of the domain organization of ADAMTS13 (21)*, which consists of metalloprotease (M), disintegrin (D), thrombospondin type-1 (T), cys-rich (C), spacer (S), thrombospondin type-1 repeats (T2-8), and two CUB domains. Within the thrombospondin type-1, repeats are two linker regions, defined as T4L and T8L.*

1.3.4. ADAMTS13 Conformation

Since its discovery, ADAMTS13's active state was explained by its reliance on its proteolytic function on VWF conformation (201). However, recent studies have shown that ADAMTS13 circulates in a closed folded form and its activation is mediated by VWF binding to the D4-CK domain (Figure 6) (189, 190, 201, 204, 207). In a functional study on ADAMTS13, a gain of function mutant (spacer domain substitutions R568K/F592Y/R660K/Y661F/Y66F) demonstrated VWF cleavage activity comparable to that of ADAMTS13 with removed C-terminal domains (T-CUB) (208, 209). By mutating the spacer domain residues responsible for binding to the CUB domains, the mutated residues provide ADAMTS13 with an open conformation that demonstrated similar proteolytic activity to that of the truncated form of ADAMT13 where the T-CUB domains are removed (MDTCS form of ADAMTS13) (208, 209). Similarly, a structural study on ADAMTS13 using electron microscopy and small-angle x-ray scattering profiles of full-length ADAMTS13 and its truncated form MDTCS has shown that ADAMTS13 is in a folded state with the CUB domains folding onto the Spacer domain (189). Thus, a globular structure of ADAMTS13 whereby the CUB domains interact with the spacer domain is being adopted, and the closed/open conformations of ADAMTS13 are the current postulated mechanism of regulation for ADAMTS13 proteolytic activity (189, 190).

The distal TSP-CUB domains, TSP-5-CUB, of ADAMTS13 bind to D4-CK of VWF with a binding affinity of K_d ~80-120 nM (201). ADAMTS13 circulates in the cardiovascular in a closed conformation whereby the CUB domains are bound to the spacer domain of ADAMTS13. Upon interaction with VWF, ADAMTS13's CUB domains bind

onto VWF's domains D4-CK, providing an open conformation for ADAMTS13 and exposing ADAMTS13's spacer domain (190). In addition, the importance of the initial interaction between ADAMTS13 and VWF is further emphasized through the study that demonstrated that the deletion of the ADAMTS13 distal domains, T-CUB domains, has been shown to impair the proteolysis activity of ADAMTS13 (189). As ADAMTS13 binds VWF and adopts an open confirmation, it is relieved from its auto-inhibition and the ADAMTS13 proximal domains, MDTCS, can then bind onto VWF through exosite binding (K_d ~10-20 nM) (210). Starting with the exposed spacer domain, residues Arg568, Arg660, Try661, and Tyr665, or the spacer domain will bind tightly to residues 1659-1668 of the A2 domain of VWF (210). Then, the cys-rich domain along with the disintegrin domain bind onto the VWF's A2 domain and help position the VWF cleavage site into the active site of the metalloprotease domain where the 3 His residues and Zn^{2+} coordinate the binding of Glu225 of ADAMTS13 to the scissile bond of VWF, where VWF is cleaved at Tyr1605-Met1606 (21, 201).

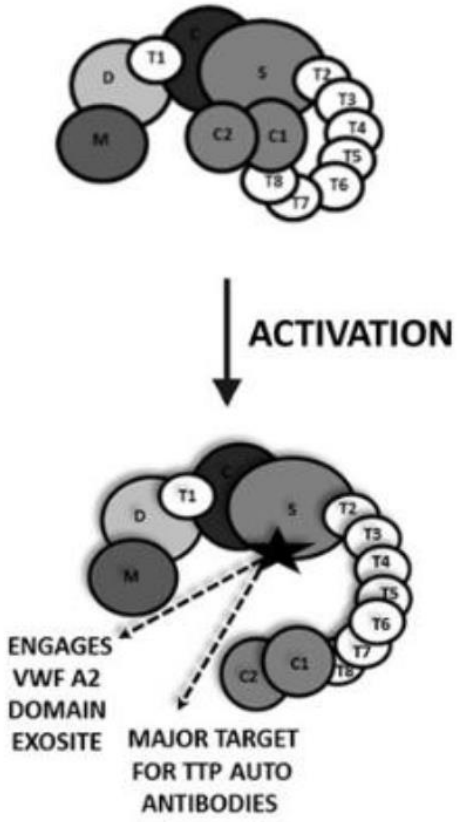

Figure 6 - Conformational Activation of ADAMTS13.

The conformational change model of ADAMTS13 (190). *VWF binding to the TSP-CUB domain releases the CUB domain from the spacer domain, creating an open active conformation of ADAMTS13.*

Despite the fact that the ADAMTS13 open/closed conformation has been proposed as a regulatory mechanism for ADAMTS13, it has been demonstrated that ADAMTS13 is an enzyme that is always active. This is because ADAMTS13 can cleave VWF73 peptide regardless of whether the distal domains, T-CUB domains, are present or not (190). Truncated ADAMTS13, in the form of MDTCS, can cleave VWF73 peptide substrate twice as fast as full-length ADAMTS13 (190). This ability is one of the unique properties of ADAMTS13 that make ADAMTS13 an enigmatic protease to study.

1.3.5. Unique Properties of ADAMTS13

ADAMTS13 has three distinct characteristics that make it an interesting protease to research. First, ADAMTS13 is known to have only one role in biology and that is to cleave its only known substrate, VWF (211). Second, ADAMTS13 is an enzyme that is always active (190). Third, ADAMTS13 has no known natural protease inhibitors making its regulatory mechanism an intriguing subject of research (212).

To date, ADAMTS13's only known biological function is to cleave its only known substrate, VWF. Despite this fact, Kretz *et al* utilized a VWF-phage display to demonstrate that ADAMTS13 is capable of cleaving >1000 unique peptide sequences suggesting that ADAMTS13 does not have exclusive specificity to VWF (213). Having one substrate is unusual since other metalloproteases including ADAMTS proteases have multiple substrates and/or roles (190, 214). For example, ADAMTS5 is a proteoglycanase that is capable of cleaving proteoglycans, such as aggrecan, which is important in the prevention

of progressive diseases of the joints, such as osteoarthritis (181, 215, 216). Through an *in-vivo* study, ADAMTS5, independent of its proteoglycanase activity, demonstrated anti-angiogenic and anti-tumorigenic properties through suppressing B16 melanoma growth in mice (217). In addition, coagulation proteases, such as thrombin, also have multiple substrates. Thrombin is known to cleave fibrinogen into fibrin yet is also capable of cleaving protease-activated receptors and coagulation factors V, VIII, and XIII (30, 218). Hence, ADAMTS13 differs from other proteases in the cardiovascular system in that it has only one role and one substrate in biology.

Second, ADAMTS13 has the unique property of being always active. Unlike other coagulation proteases, ADAMTS13 is synthesized and secreted as an active protease (164). In addition, the deletion of ADAMTS13 distal domains, T-CUB, does not abolish its proteolytic activity towards the VWF73 peptide substrate (190). As a result, ADAMTS13 is a one-of-a-kind protease that is always active and ready to cleave its VWF substrate when it is readily available.

Third, ADAMTS13 has a three-day circulating half-life, emphasizing the resistance of ADAMTS13 to natural inhibitors (212). Other metalloproteases, including other members of the ADAMTS family, are regulated by metalloprotease inhibitors such as TIMPs (187). However, in the case of ADAMTS13, TIMPs demonstrated no inhibitory effect towards ADAMTS13 proteolytic activity (219). This effect was also demonstrated in the case of another natural protease inhibitor α2-macroglobulin (220).

1.3.6. Role of ADAMTS13 Beyond Hemostasis

ADAMTS13's only known function is hemostasis, which it achieves through its proteolytic activity against VWF (21). TTP's biomarker is ADAMTS13, and the primary characterization of TTP is a lack of ADAMTS13 activity (165). Interestingly, ADAMTS13 inactivation does not always cause TTP, but it can play a significant role, as seen in congenital TTP (165, 221). The fact that impaired ADAMTS13 secretion does not always result in TTP suggests that other enzymes, such as elastase from leukocytes, may be involved in controlling VWF multimer levels (222, 223). In this case, other enzymes in biology could take the place of ADAMTS13. However, evolution has selected for ADAMTS13, suggesting it could perform other roles in biology.

Xu *et al* demonstrated that ADAMTS13 controlled key steps in vascular repair and enhanced ischemic neovascularization (224). ADAMTS13$^{-/-}$ mice demonstrated reduced neovascularization through decreased levels of angiopoietin-2 and galectin-3, two proangiogenic proteins involved in vascular maturation and stabilization (224). The role of ADAMTS13 in neovascularization may be indirect and could be a result of VWF processing since VWF was found to be anti-angiogenic through VWF's binding with proangiogenic factor galectin-3 (225, 226).

During a study focused on the development of early atherosclerosis in mice, Gandhi *et al* discovered that ADAMTS13 played a role in reducing excessive vascular inflammation and plaque formation during the early stages of atherosclerosis (158). ADAMTS13$^{-/-}$ ApoE$^{-/-}$ mice demonstrated the increased formation of atherosclerotic

plaque through increased leukocyte adhesion and macrophage recruitment (158). Since elevated VWF levels and reduced ADAMTS13 activity were described in atherosclerosis, and similar conditions, the role of ADAMTS13 on atherosclerosis plaque formation may be indirect and may be a result of VWF processing (158, 227–229).

ADAMTS13 was found to play both roles as proangiogenic and antiangiogenic (230). ADAMTS13 was found to increase cell tube formation, proliferation, and migration; as well as inhibit VEGF-induced angiogenesis (230). The effects of ADAMTS13 were observed via Matrigel tube formation, and cell migration assays through treatment of recombinant ADAMTS13 on human umbilical vein endothelial cells (HUVECs) (230). HUVECs treated with recombinant ADAMTS13 demonstrated increased tube formation and cell migration, establishing ADAMTS13 to be proangiogenic (230). On the other hand, HUVECs treated with recombinant ADAMTS13 and vascular endothelial growth factor (VEGF), a protein that promotes the growth of new blood vessels, had the opposite effect, which demonstrated decreased tube formation and cell formation, prompting ADAMTS13 to be antiangiogenic via the inhibition of VEGF by ADAMTS13 through the interaction of its TSP1 domain (230). Since VWF, as an antiangiogenic factor, is known to inhibit VEGFR2, and low levels of VWF are known to promote angiogenesis; it is likely the angiogenesis effect of ADAMTS13 is dependent on whether ADAMTS13 is acting on VWF or VEGF (161–163, 230). If ADAMTS13 is acting on VWF, which allows VEGF to act on VEGFR2, angiogenesis is promoted; whereby if ADAMTS13 is acting on VEGF, which allows VWF to act on VEGFR2, anti-angiogenesis is promoted.

All these identified roles were associated with the interactions of VWF. Hence, whether these roles are directly dependent on the activity of ADAMTS13 or are a result of the size of VWF multimers distribution or both is unknown. To examine this, one could utilize ADAMTS13$^{-/-}$ and VWF $^{-/-}$ mice and study whether VWF deficiency could correct ADAMTS13 deficiency. The insight from the study would provide a better understanding of ADAMTS13's overall role in biology.

1.3.7. Regulation of ADAMTS13

The mechanism of ADAMTS13 regulation is not well understood. However, its activity must be regulated at sites of vessel injury for VWF to retain its capacity to recruit platelets.

Coagulation proteases are secreted into circulation in the form of a zymogen, whereby coagulation factors remain inactive until a specific bond within the inactive protein is cleaved by an activator (231). For example, the zymogen form of thrombin, referred to as prothrombin, remains inactive until the cleavage of two peptide bonds by the prothrombinase complex (232). This zymogen to protease conversion reaction serves to spatially and temporally regulate thrombin activity to sites of vessel injury. However, unlike coagulation factors, ADAMTS13 is not expressed as a zymogen and is instead secreted as an active enzyme (164). Interestingly, even if the cleavage of the ADAMTS13 propeptide during expression is considered an activator, studies have demonstrated that the presence of the propeptide on the secreted ADAMTS13, i.e. pro-ADAMTS13, does not

affect ADAMTS13's proteolytic activity towards VWF multimers. Thus, pro-ADAMTS13 is not a zymogen of ADAMTS13 (164).

Another form of the regulatory mechanism of ADAMTS13 considered is the use of inhibitors. For example, as thrombin diffuses away from a clot, it is rapidly inhibited by α2-macroglobulin, ATIII, and heparin cofactor II (233). Hence, thrombin's activity is spatially and temporally regulated by the combination of zymogen activation and rapid inhibition. Furthermore, metalloproteases including other members of the ADAMTS family are inhibited by metalloprotease inhibitors, such as TIMPs, or other natural inhibitors, such as α2-macroglobulin. For example, TIMP-3 has been shown to inhibit ADAMTS-2 (234). Another example, α2-macroglobulin has been shown to inhibit ADAMTS-4 and -5 (235). In the case of ADAMTS13, neither TIMPs nor α2-macroglobulin were able to inhibit ADAMTS13 (219, 220). Since ADAMTS13 is a metalloprotease that utilizes divalent ions, such as Zn^{2+} and Ca^{2+} in the proteolysis of VWF, the use of an inhibitor capable of limiting the availability of these ions, such as EDTA is considered (236). EDTA has been shown to abolish the activity of ADAMTS13 by chelating the available cations; however, EDTA is not a natural inhibitor and is not of physiological relevance (237). Thus, the ADAMTS13 regulatory mechanism is not through any known natural protease inhibitors.

The currently accepted ADAMTS13 regulatory mechanism is centered on the substrate level and how ADAMTS13 interacts with VWF (190). When ADAMTS13 recognizes and binds to VWF, it changes its conformation from closed to open. The closed conformation indicates that ADAMTS13 is "inactive", whereas the open conformation

indicates that ADAMTS13 is "active" (190). However, even in a closed conformation, the metalloprotease domain, which contains ADAMTS13's active site, is still accessible for proteolytic activity. ADAMTS13's closed conformation folds the CUB domains onto the spacer domain but does not obstruct the metalloprotease domain (189, 201). As a result, even in a closed conformation, ADAMTS13 is an active enzyme, and thus, the regulatory mechanism of ADAMTS13 is not fully understood.

Another form of regulatory mechanism for ADAMTS13 that has not been deeply explored is the possibility that proteolytic degradation of ADAMTS13 regulates its activity. Thrombin, plasmin, and FXIa are capable of proteolytically degrading ADAMTS13 (238, 239). However, the concentration of the proteases and the reaction time utilized were deemed of non-physiological relevance; thus, this form of regulatory mechanism was not explored further (238, 239). Nonetheless, this type of regulatory mechanism for ADAMTS13 was proposed because local high concentrations of proteases at the site of vascular injury are capable of degrading ADAMTS13 and thus may regulate ADAMTS13 activity via proteolytic degradation. Further research into this type of regulatory mechanism, such as a survey of proteins capable of proteolytically degrading ADAMTS13, may lead to a better understanding of how ADAMTS13 activity is regulated. This type of regulatory mechanism for ADAMTS13 is being investigated further in this project.

1.4. The Hemostatic Balance

1.4.1. ADAMTS13 and VWF Axis

Hemostasis is maintained by balancing the mechanisms that promote blood clotting with those that inhibit the formation of a blood clot. Dysregulation in the coagulation system can lead to either excessive bleeding or thrombosis. Thrombosis is caused by an increase in procoagulant factors and the excessive formation of damaging and potentially lethal blood clots. This can result in stroke, myocardial infarction, pulmonary embolism, or deep vein thrombosis, whereby blood does not properly reach the brain, heart, lungs, arm, or leg respectively (22). Uncontrollable blood clots disrupt the supply of oxygen and nutrients or the clearance of metabolic by-products leading to organ damage. On the other hand, tilting the hemostatic balance towards bleeding due to a decrease in coagulation factors or an increase in anticoagulants results in excessive bleeding that could potentially be uncontrollable or fatal (22). The cause of hemostasis imbalance could be acquired or inherited. Acquired imbalance could be a result of a pathogen, physical damage, or a trigger from another disease or condition such as smoking, pregnancy, cancer, obesity, etc. (240). Inherited imbalance is a result of a genetic defect (240). The extent of imbalance varies and is based on the impact the affected factor(s) have on the coagulation system.

In terms of platelet-plug formation, hemostasis is regulated by the balance between the activities of ADAMTS13 and VWF. The activity level of ADAMTS13 regulates the size of VWF multimers, which dictates VWF's platelet recruitment capacity (Figure 7). Mutations in VWF that sensitize VWF to cleavage by ADAMTS13 cause a loss of high

molecular weight multimers, which result in insufficient platelet-binding activity, as seen in the bleeding disorder Von Willebrand Disease (VWD) (211). On the other hand, decreased ADAMTS13 activity, due to the presence of autoantibodies or mutations that impair secretion of ADAMTS13, causes an accumulation of ultra-large VWF multimers, which results in spontaneous binding of multimers to platelets, as seen in the thrombotic disorder thrombotic thrombocytopenic purpura (TTP) (211).

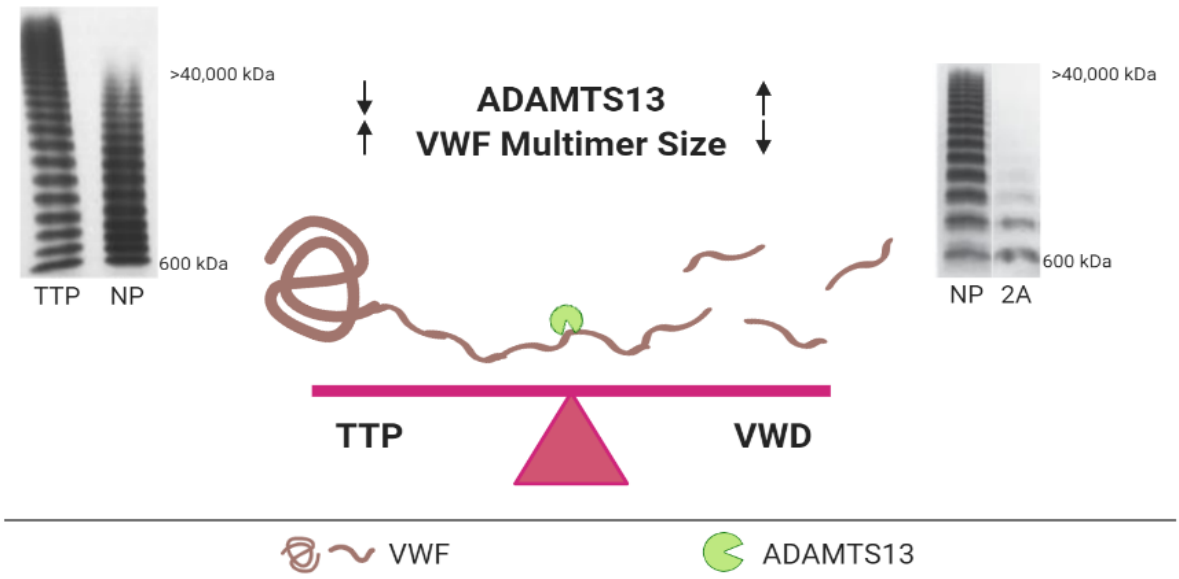

Figure 7 - Hemostatic Balance via ADAMTS13 & VWF.

Hemostatic balance as determined by the activity level of ADAMTS13, which dictates the size of VWF multimers and its capacity to recruit platelets (211). *Mutations in VWF that sensitize VWF to cleavage by ADAMTS13 result in a loss of high molecular weight multimers, and bleeding, as seen in type 2A VWD. Decreased ADAMTS13 activity, due to the presence of autoantibodies or mutations that impair secretion of ADAMTS13, result in an accumulation of high molecular weight multimers, and thrombosis, as seen in TTP.*

1.4.2. Bleeding Disorders (VWD)

Von Willebrand Disease (VWD) is an inherited bleeding disorder characterized by defective platelet adhesion and aggregation that is caused by defects in VWF (103). VWD affects up to 1% of the population and is classified into three types, whereby types 1 and 3 are quantitative defects, and type 2 is a qualitative defect of VWF (102, 241).

The diagnosis of VWD can be challenging because few symptoms, such as bruising or nose-bleeds, can occur frequently in healthy individuals. Also, diagnosing VWD solely on the levels of VWF could be misleading because VWF levels vary widely between individuals based on ethnicity, ABO blood group, and age (147). For example, the mean VWF antigen level of a type O individual is 0.75 U/mL, compared to 1.0 U/mL for the average population (242). However, in combination with low VWF levels, the diagnosis of VWD becomes easier when family history is considered, or the severity of bleeding symptoms has increased (147).

Type 1 VWD accounts for 80% of VWD cases and is classified as a partial quantitative deficiency of VWF (243). Studies have shown this type to be a result of missense mutations in the VWF gene that decrease the amount of VWF that is released into circulation (244–246). In most cases, administering the drug desmopressin stimulates the release of VWF and FVIII and reduces bleeding symptoms (247).

Type 3 VWD accounts for <5% of cases and is associated with a complete, or near-complete, deficiency of VWF in circulation (243). Patients with type 3 VWD exhibit the most severe bleeding phenotype of any VWD subtypes due to lack of VWF and low levels

of FVIII (243). This type of VWD is a result of defects in the VWF gene, including nonsense mutations (248). Thus, unlike other subtypes, type 3 VWD cannot be treated by desmopressin, and is treated using recombinant VWF protein infusions (247).

Type 2 VWD accounts for about 20% of cases and is characterized by a qualitative or functional defect in VWF (243). Type 2 is subcategorized into 2A, 2B, 2M, and 2N depending on the affected function of VWF. Type 2 A is a result of missense mutations in the VWF gene that impair dimerization of VWF assembly, as well as enhance susceptibility to proteolysis by ADAMTS13 (102, 249). Type 2B is a result of missense mutations in the VWF gene that enhance the ability of VWF to bind to platelet GP1bα without the requirement for VWF to bind to collagen first (250). The result is the spontaneous formation of platelet-VWF aggregates that consume the largest high-molecular-weight multimers. Type 2M is a result of missense mutations in the VWF gene, often in the A1 domain, which alters protein conformation and diminishes or decreases the ability of VWF to bind to platelet GP1bα (248). Type 2N is a result of missense mutations in the VWF gene, in the key amino acids of the FVIII binding site within the D' and D3 domains, which alter protein conformation and diminish or decrease the ability of VWF to bind to FVIII (102). Often, individuals with type 2N VWD have a normal VWF multimer distribution pattern (251).

Type 2A VWD is of particular interest due to VWF's increased susceptibility to proteolysis by ADAMTS13. Mutations in the VWF A2 domain provide an open structure whereby the A2 domain is unfolded which allows ADAMTS13 to have easier access to its proteolytic site (249). The mutation R1597W is the most commonly identified mutation in

VWD-2A patients, whereby the stability of calcium within the binding loop is diminished, as well as the folding of the A2 domain, was affected (252). Together, the result of both mechanisms is a decrease in VWF high-molecular-weight multimers, resulting in fewer GP1bα binding sites and less effective formation of platelet-VWF aggregates. Interestingly, the increase in the rate of ADAMTS13 activity is due to the increase in the availability of the substrate, i.e. free proteolytic sites within VWF, and not a direct enhancement of ADAMTS13 activity.

1.4.3. Thrombotic Disorders (TTP)

Decreased ADAMTS13 activity, as a result of impaired secretion or the presence of autoantibodies, will result in increased levels of ultra-large VWF multimers and increased formation of platelet-VWF thrombi, resulting in the thrombotic disorder known as thrombotic thrombocytopenic purpura (TTP) (253). The acronym TTP was derived from the clinical features observed in TTP patients; whereby, thrombotic refers to the formation of blood clots, thrombocytopenia refers to lower than normal platelet levels, and in this case, platelets are depleted in the formation of the blood clots, and purpura refers to the purple bruises caused by bleeding under the skin (165). TTP is a rare and potentially fatal blood disorder that causes the formation of platelet-rich thrombi in the microvasculature (165, 254). If left untreated, TTP is fatal in over 90% of the cases (255, 256). TTP is treated by plasma exchanges which removes pathogenic antibodies and replenishes ADAMTS13 levels and was shown to improve the survival rate of TTP patients to 60-90% (255, 256).

One of the clinical features of TTP is hemolytic anemia, which is characterized by the presence of blood in urine and is due to the tearing of RBCs by the platelet-rich thrombi and the presence of schistocytes, a fragmented part of a RBC (257). Furthermore, many clinical manifestations present in TTP are shared with other forms of thrombotic microangiopathy (TMA). TMA is characterized by microangiopathic hemolytic anemia (MAHA), severe consumption of platelets (thrombocytopenia), and possible organ damage due to the formation of platelet-rich thrombi in the microvasculature (254). However, unlike other forms of TMA, TTP is characterized by the low or absent activity of ADAMTS13, whereby ADAMTS13 activity level of 10% or less, as determined by the clinical assay FRETS-VWF73 (165).

Acquired TTP is an autoimmune disorder characterized by auto-antibodies directed towards ADAMTS13 (258). These antibodies target and inhibit the activity of ADAMTS13 toward VWF, or target ADAMTS13 for removal from circulation resulting in low circulating ADAMTS13 levels (258). Pereira *et al* demonstrated that the majority of antibodies targeting ADAMTS13 observed in acquired TTP target the spacer domain, resulting in an open conformation ADAMTS13 (259).

Interestingly, TTP is an episodic disorder (165). In congenital TTP, also referred to as Upshaw-Schulman syndrome (USS), mutations within the ADAMTS13 gene result in low or no circulating ADAMTS13 (260). These mutations can be either missense mutations that result in an amino acid change that impairs secretion of ADAMTS13 or nonsense/frameshift mutations that result in a premature stop codon and a truncated non-functional protein (260). The treatment for acute episodes of TTP is to replenish

ADAMTS13 levels through therapeutic plasma exchange (261). However, once a patient is treated for an acute episode of TTP, their symptoms subside despite their ADAMTS13 levels remaining low (165). Some patients with congenital TTP may not experience their first episode of TTP until later in life, despite having little to no ADAMTS13 activity (221, 262).

Fujimura *et al* studied 43 congenital TTP patients and examined their first TTP episode (221). Fujimura *et al* demonstrated that only 25 of 43 experienced their first TTP symptoms in childhood before the age of 15 and the remaining patients did not display their first symptom until adolescence or well into adulthood (221). Interestingly, all the individuals that displayed late symptoms of TTP were female, suggesting a potential link to pregnancy or other hormonal changes (221).

Consistent with the heterogeneity of the disease in humans, ADAMTS13 knockout mice exhibited no spontaneous thrombosis or TTP-like phenotype (263). Interestingly, ADAMTS13$^{-/-}$ mice on a mixed-strain C57BL/6J and 129X1/SvJ genetic background exhibited loss of ADAMTS13 activity yet the distribution of VWF multimers was unchanged (263). When the mixed strain was backcrossed into the CASA/Rk genetic background, there was an increase in plasma VWF levels, a decrease in platelet count, and a higher susceptibility of developing spontaneous TTP symptoms (263). In addition, TTP-like symptoms were only induced in the ADAMTS13$^{-/-}$ mice following injection of the bacterial Shiga toxin, which stimulates endothelial cells to release VWF stored in Weibel-Palade bodies (263). While the mouse phenotype from these experiments was similar to that of TTP, the presence of a Shiga toxin due to an infection is associated with hemolytic

uremic syndrome (HUS), and not TTP (86). These experiments demonstrated that increased VWF levels in combination with reduced ADAMTS13 can trigger TTP.

This observation has resulted in the proposal of a 2-hit model hypothesis for TTP. The first hit is ADAMTS13 deficiency, and the second hit is a triggering event such as bacterial infection or major hormonal shifts such as during puberty, pregnancy, or menopause (260, 263, 264). Whether the triggering events are associated with the absence of ADAMTS13 is currently unknown. Overall, this observation points to the lack of knowledge on the pathogenesis of TTP and whether ADAMTS13 has additional roles outside of VWF processing that may contribute to TTP or other cardiovascular disorders.

Beyond TTP, abnormal formation of platelet-VWF thrombi can result in various thrombotic disorders such as myocardial infarction (MI), stroke, venous thromboembolism (VTE), thrombotic thrombocytopenic purpura (TTP), and can even play a role in sepsis (87, 253, 265–267). In all cases, studies have demonstrated that decreased ADAMTS13 levels can increase the risk of cardiovascular diseases (87, 253, 265–267). For MI, decreased levels of ADAMTS13 (levels between 3% - 85%) resulted in patients having a 1.5x higher chance of experiencing MI (87). As for stroke, patients within the lowest quartile (<70% ADAMTS13 activity) had an 11% chance of developing stroke (265). In terms of VTE, patients suffering chronic thromboembolic pulmonary hypertension displayed decreased levels of ADAMTS13 by 23% compared to healthy controls (266). Similarly, and in terms of sepsis, septic patients displayed ~50% lower ADAMTS13 activity compared to healthy controls (267).

Thus, the use of recombinant ADAMTS13 is emerging as a therapeutic treatment option to combat various cardiovascular diseases (268). However, in the case of MI, administering recombinant ADAMTS13 did not prove to decrease the size of MI in a porcine model, but did decrease the size of MI in ADAMTS13$^{-/-}$ mice (269, 270). Thus, the role of ADAMTS13 and its direct effect on various cardiovascular diseases is not fully understood; but may be related to VWF. Further understanding the direct role of ADAMTS13 may lead to novel therapeutics for the beforementioned cardiovascular diseases.

1.5. Proximity-Dependent Biotinylation (BioID)

1.5.1. Concept of BioID

Mapping protein-protein interactions is key to understanding ADAMTS13 and its role in the cardiovascular system. Traditional methods used to identify novel protein interactions include co-immunoprecipitation or column chromatography coupled with gel electrophoresis or crosslinking reagents. However, these approaches rely on the high binding affinity of proteins and may be limited in their capacity to identify proteins that are not soluble in free solution, such as transmembrane proteins. Furthermore, these approaches are a challenge to study proteases because proteases do not form a stable complex with their substrates. Also, these approaches can result in non-specific protein aggregates that are difficult to interpret (271). To overcome these barriers, proximity-dependent biotin identification (BioID) was developed.

BioID is a method for discovering novel protein-protein interactions that uses a promiscuous biotin ligase, BirA*, attached to the protein of interest (272). BioID provides an advantage through the identification of transient/weak interactions because proteins that contact the target are covalently tagged with biotin (273).

Biotin, also known as vitamin H, is a water-soluble vitamin that is part of the vitamin B family and is involved as a cofactor for enzymes in carboxylation reactions (274, 275). Biotin's biological function is dependent on whether it is covalently attached to a carboxylase (276). Within the human body, five biotin-dependent carboxylases maintain metabolic homeostasis through crucial reactions in gluconeogenesis, lipogenesis, and amino acid metabolism (276, 277). Biotinylation is a post-translational modification whereby biotin is covalently attached to a recipient molecule, such as protein (277).

1.5.2. Development of BioID

The process of biotinylation has long been used in the search for novel protein-protein interactions (278). Chemical reagents were developed to artificially biotinylate proteins (278). Together, with the high affinity of biotin to streptavidin, novel protein or ligand interactions could be isolated through streptavidin co-IP and then identified using mass spectrometry analysis (279). Proteins can be biotinylated either chemically or enzymatically, whereby the enzymes responsible for biotinylation are referred to as, BirA* (280).

BirA* is a 35-kDa biotin ligase enzyme derived from *E. coli*, which catalyzes the biotinylation of acetyl-CoA carboxylase and acts as a transcriptional repressor for the biotin biosynthetic operon (280). Biotinylation works in two steps. In the first step, the biotin ligase consumes biotin and adenosine triphosphate (ATP) to generate a highly reactive biotinoyl-5'-adenosine monophosphate (bio-AMP) intermediate (280, 281). In the second step, the biotin ligase docks with a specific peptide sequence on the target protein, allowing the bio-AMP intermediate to react with a specific lysine residue. This reaction results in an amide bond between biotin and the lysine side chain resulting in the release of AMP (280, 281). Wild-type biotin ligase targets a specific subunit of acetyl-CoA-carboxylase, thus the biotinoyl intermediate remains intact in the active site until the specific target is recognized (273). This reaction has been used in molecular biology to biotinylate recombinant proteins using the AviTag (GLNDIFEAQKIEWHE) (282).

A mutagenesis study revealed that the R118G mutated biotin ligase, hereafter referred to as BirA*, became a promiscuous enzyme, with a much lower affinity to the bio-AMP intermediate than the wild-type (280, 283). This mutation caused the premature release of bio-AMP, allowing the "activated" biotin to diffuse away and covalently bind to the first lysine residue with which it interacts, thus covalently marking accessible lysine residues in the vicinity with BirA* (273, 283).

Proximity-dependent biotinylation takes advantage of the capacity of the BirA* to biotinylate proteins within its vicinity without the need for the AviTag sequence. The technique, referred to as BioID, is based on making a fusion protein using the protein of interest with BirA* (272). BirA* activates biotin that covalently attaches to proteins that

interact with the protein of interest within a radius of 10 nm (Figure 8) (280, 284). The biotinylated proteins are then subjected to purification and identification using streptavidin pulldown and mass spectrometry (273).

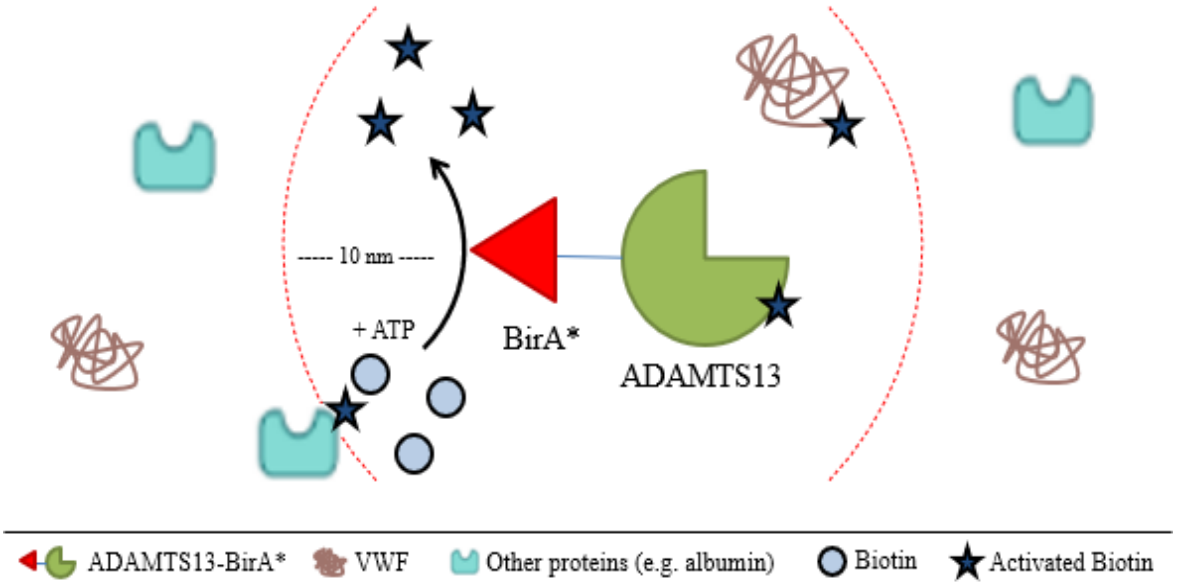

Figure 8 - The Concept of the BioID Technique.

The addition of biotin and ATP to the fusion protein (ADAMTS13-BirA) releases the biotinoyl-5'AMP that biotinylates neighboring proteins within its 10 nm labeling radius* (272). *This result includes the self-labeling of the fusion protein (auto-biotinylation), the labeling of substrates and interacting proteins such as VWF, and the labeling of prominent proteins in the environment such BSA.*

1.5.3. Validation of BioID

The first application of BioID was to map the nuclear lamina's filament protein, lamin A (LaA) (272). Later, the concept of BioID was used in other applications such as in the oncogenic transcription factor, Ewing's sarcoma Ets transcription factor (EWS-Fli-1), in the viral infection HIV-1 focusing on the Gag precursor polyprotein, and much more (273, 285–287).

1.5.4. Advantages of BioID

Discovering novel protein-protein interactions may help provide a better understanding of complex biological systems, like hemostasis. Novel protein-protein interactions are commonly discovered through the utilization of high binding affinity interactions for isolation, and comparison to various libraries for identification. BioID was developed to overcome a few of the challenges faced in the discovery of novel protein-protein interactions by other techniques, such as yeast 2 hybridization, co-immunoprecipitation, and engineered ascorbate peroxidase proximity-labeling.

Yeast 2 hybridization (Y2H) was developed in 1989 and utilizes the yeast *S. cerevisiae*`s transcription factor, GAL4 (288). GAL4 is a transcriptional activator for the expression of galactose-induced genes and consists of two domains, the DNA-binding domain (DBD), and the activator domain (AD) (288). The Y2H system was designed to separate both domains by utilizing a fusion protein system in which the bait protein is attached to the DBD, and the prey protein is attached to the AD. The Y2H system is based

on the cDNA libraries that are expressed recombinantly in the yeast cells. If the bait binds to a protein expressed in the library, the yeast will grow. Therefore, candidate interactions are identified by picking colonies on a plate and sequencing the cDNA (289). However, the interactions are artificial since the interactions take place in the yeast cell and not in their native biological context. Furthermore, proteins that exist in their non-native environment are more susceptible to misfolding (272, 290). Also, the Y2H system often results in a high number of false-positive or false-negative interactions (291). In comparison to BioID, the BioID system allows the identification of weak and/or transient protein-protein interactions, such as the identification of enzymes and their substrates or cofactors (272, 292, 293). In addition, the BioID system allows the preservation of physiologically relevant conditions (272).

Another form of discovery of novel protein-protein interactions is co-immunoprecipitation (co-IP). The principle of co-IP is in the use of a specific antibody against the bait protein, the protein of interest (294, 295). The antibody is designed to be conjugated to beads that are utilized in the isolation process (295). The protein of interest is placed in its natural environment, followed by the addition of the antibody (294). Through a pulldown method, the beads will help isolate the bait protein along with any prey proteins that have a high affinity to the bait protein (295). Subsequently, the isolated proteins are then analyzed using gel electrophoresis, western blots, and then identified using mass spectrometry (294, 295). The advantage of this method over the Y2H is the ability to use the bait protein in its native environment (294). Also, co-IP could be used to identify multi-component complexes (294). However, the limitation of this method is the

high-affinity interaction that is required for the novel protein-protein interactions to be identified after the isolation process (294, 295). Thus, unlike BioID, the co-IP method cannot detect weak or transient interactions.

Another form of discovery of novel protein-protein interactions that is similar to BioID is the engineered ascorbate peroxidase (APEX). The APEX method utilizes a modified ascorbate peroxidase fused to the protein of interest and a hydrogen peroxide-biotin substrate to identify interacting proteins and substrates (296). APEX makes use of an activated phenol-biotin radical intermediate produced by engineered ascorbate peroxidase, which has a half-life of less than 1 ms (296–299). In addition, APEX labeling specificity is to exposed tyrosine residues (300). In comparison to BioID, BirA* labeling specificity is to exposed lysine residues. This may be advantageous to BioID because protein evolution has chosen to have a higher estimated amount of lysine residues present in nature, potentially limiting the number of available identified proteins (301, 302). In addition, the half-life of bio-AMP intermediate produced by BirA* is in minutes compared to the half-life of APEX intermediate which is <1 ms (296–299). The longer half-life results in a larger labeling radius, which may be advantageous depending on the labeling target (300). Furthermore, the use of hydrogen peroxide is toxic to the cellular environment, which limits its use and decreases the labeling sensitivity of the APEX system; unlike biotin and ATP, which are not toxic and provide the BioID system with higher labeling sensitivity (300). Lastly, while the APEX system was evolved to establish higher sensitivity, through APEX2, the BioID system was also evolved, into BioID2 and other forms, to overcome its limitations and challenges (303, 304).

In summary, the BioID system was developed to have higher sensitivity, improved spatial resolution, non-toxic substrate, the ability to label under physiologically relevant conditions, and detection of weak or transient interactions.

1.5.5. Evolution of BioID

BioID was developed to overcome challenges and barriers imposed by conventional protein-protein interactions discovery methods. However, the BioID method does have its limitations with the size of BirA*, and its long labeling time of 15-24 hrs (300).

BioID utilizes the promiscuous biotin enzyme, R118G mutant BirA*, isolated from *E. coli* (272, 280). Through a database search, another BirA*, isolated from *A. aeolicus* was identified (304). Through modifications of this BirA*, including an R40G mutation, another promiscuous BirA* was established and termed BioID2 (304). The BioID2 system was evaluated for comparison to the BioID system in the lamin A network by the same founding group and displayed the following advantages (304). The BioID2 system utilizes a smaller, 27 kDa, BirA* that was able to improve localization of the fusion protein intracellularly (304). Furthermore, the BioID2 required less biotin, 3.2 µM of biotin, compared to the original method which required 50 µM of biotin, for the same amount of labeling (304). In a similar observation, the minimal amount of biotin required for the label was 0.01 µM BioID2 and 0.1 µM for BioID (304). Furthermore, the BioID2 system was optimal at higher temperatures, 50°C, in comparison to 37°C for the BioID system (304). Thus, BioID2 provided advantages over the founding BioID system.

Recently, new advances have been made on BioID and BioID2 in an effort to reduce the labeling time. Using a yeast display-based direct evolution, two more advanced BirA*, TurboID, and miniTurbo, were identified (305). These variants were selected using a mutagenesis library of BirA* displayed on the surface of yeast and the cells that expressed the most active variant of BirA* were selected. The stringency of the selection was increased following each round of selection to identify an optimized BirA* variant with the fastest labeling time, and highest labeling activity. As a result, TurboID and miniTurbo were established. TurboID is a 35 kDa protein with 15 mutations, and miniTurbo is 28 kDa with 13 mutations relative to the original BirA* (305). Through comparison via the labeling of the cytosolic proteins in a HEK293 cell system, both enzymes displayed higher labeling efficiency of ~3-6 fold higher at an early time point of 10 min, and ~15-23 fold higher at a later time point of 18 hrs, in comparison to the wild type BirA* (305). Furthermore, the number of labeled proteins by TurboID in 10 minutes was the same as the amount labeled by the original BirA* in 18 hrs (305). In comparison, miniTurbo displayed ~1.5-2 fold less labeling than TurboID, but displayed less labeling in the absence of exogenous biotin, suggesting miniTurbo to be more specific (305). Comparing the quantification of the labeled proteins, both TurboID and miniTurbo demonstrated similar enrichment patterns in a 10-minute reaction time, compared to a labeling reaction of 18 hrs for the original BirA* (305). At lower temperatures, 30°C, labeling via TurboID and miniTurbo was detected, unlike in the use of BirA* which was undetectable (305). Overall, TurboID and miniTurbo overcame BioID's greatest challenge of long labeling reaction times, which expands the potential applications of BioID. The evolved properties of BirA* are compared in Table 1.

TurboID and miniTurbo were discovered after this project was initiated, and thus, the BioID2 system was utilized.

Table 1 - Comparison of the Various BirA* Enzymes.

	BioID1	BioID2	Turbo-ID	Mini-Turbo
Host	*E. coli*	*A. aeolicus*	*E. coli*	*E. coli*
Mutation	R118G	R40G	15 mutations from BioID	Δ of N-terminal domain and 13 mutations from BioID
Discovery	Roux - 2013	Kim - 2016	Branon - 2018	Branon - 2018
Reference	(272)	(304)	(305)	(305)
Size (kDa)	35.4	27	35	28
Labelling Radius (nm)	~10	~10-15	~35	
Optimal Temperature (℃)	37℃	50℃	30℃	30℃
Advantages		Size, higher temperatures, less biotin required (10x less than BioID)	Labeling period (10-minutes compared to 18 h in BioID), labeling in the absence of exogenous biotin, lower temperatures	Size, similar advantages to TurboID (but not as fast)
Limitations	Size		Labeling accuracy	

1.5.6. Other Forms of BioID

Initially, BioID was developed to identify proteins in eukaryotic cells. Since then, BioID was implemented in other mammalian cells, unicellular organisms, and host-pathogen systems (273). Other forms of BioID were further established into other environments and adapted into other forms of technique, such as *in planta*, *in-vivo* (i-), *in-vitro* (iv-), two-component- (2C-), and Split-, BioID (306–310).

In planta, BioID adapts the BioID technique in a whole plant system (306). The plant system faces unique and different challenges compared to a eukaryotic cell system, whereby the plant system has low cytoplasmic volume relative to cell wall mass, high levels of unique enzymes such as proteases, phosphatases, and rubisco, all of which may interfere with the labeling protein reactions (306). Transgenic plants expressed BirA* as unconjugated or fused with protein of interest, HopF2 (306). In planta BioID was validated through the positive control of previously known interaction, Hopf2-RIN4 as demonstrated in the leaf tissues of *A. thaliana* plant by Khan *et al* (306).

IBioID, also referred to as *in-vivo* BioID, adapted the BioID technique in an *in-vivo* murine model, as demonstrated in mapping the synaptic complex in the brain network of a mouse by Uezu *et al* (307). The group utilized adeno-associated viral constructs for the expression of the inhibitory or excitatory postsynaptic proteins fused with BirA*, unconjugated BirA* (307). The identification of labeled proteins validated this technique through the finding of over 100 previously known interactions along with 27 foreign

proteins (307). However, further studies were needed to validate the discovery of the novel interactions.

IvBioID, also referred to as *in-vitro* BioID, also adapted the BioID technique in an *in-vitro* model, as demonstrated in mapping the kinetochore components during mitosis by Remnant *et al* (308). Stable Hela cell lines were generated for the expression of CENP-A-BirA* and unconjugated BirA*, and biotin was provided exogenously (308). In a cell pellet form, the cells took up the exogenous biotin, and the BirA* labeled the proximal proteins *in-vitro* (308). This technique was validated through the identification of previously known interactions (308).

2C-BioID, also referred to as 2-component BioID, is an evolved form of the BioID technique in a eukaryotic cell model, as demonstrated in mapping the lamin A network by Chojnowski *et al* (309). The group utilized the FKBP:FRB oligomerization system to establish a more specific BioID assay (309). This method was validated in mapping the network of lamin A-associated polypeptide 2β (LAP2β) (309).

Split-BioID was developed by Schopp *et al* and validated via the application of the method to the miRNA-mediated silencing pathway, GIGYF2 protein was uncovered as a novel regulator (310). The design of split-BioID is similar to 2C-BioID in the sense of a two-component system; however, split-BioID utilizes the reattachment of the BirA* subdomains instead (310). As the BirA* is reattached, its activity is restored and the proteins within proximity are labeled (310). The advantage of this method is the ability to focus on mapping multi-protein complexes (310).

Despite the various advancements in the BioID technique, none have utilized the concept in a plasma system.

1.5.7. *In-Vitro* BioID in Plasma

In less than a decade, the BioID technique has developed into different forms, and been utilized in various biological samples. However, BioID has not yet been applied to plasma or other acellular environments. The use of BioID in a plasma system provides unique challenges and overcoming these will provide great advancement in the field of protein-protein network research and cardiovascular research.

Blood plasma is a yellow liquid that serves as the base of whole blood (311). Plasma is separated from whole blood via centrifugation, whereby the majority of hematopoietic cells are removed (311). Plasma contains numerous enzymes and ions that are activated during the blood collection process if an anticoagulant, such as citrate, was not used (312). The use of an anticoagulant to prevent the natural process of blood clotting makes studying coagulation factors in a physiologically relevant environment more difficult (313). For example, using sodium citrate in the blood collection process prevents coagulation factor activation by chelating free ions such as Ca^{2+}, rendering the coagulation factors as inactive proteins (314). This result provides a limitation in the study of ADAMTS13 as the activity of ADAMTS13 is also dependent on Ca^{2+} which may be chelated and unavailable in the presence of sodium citrate (236). In addition, the use of sodium citrate may attenuate BirA*'s labeling efficiency because BirA* hydrolyzes ATP in the form of MgATP, which

requires Mg^{2+} (315). Also, plasma is known to be rich in ATPases and phosphatases, which challenge the availability of ATP and limit its half-life in circulation (316). Unlike a cell-based BioID system, ATP is provided by the cell system itself, and biotin is added exogenously. However, the availability of ATP and biotin in plasma is a challenge that must be addressed through exogenous administration of both substrates, which will require optimization. Nonetheless, overcoming these obstacles will provide a novel discovery tool in further understanding and advancing the discovery of the hemostatic system network, potentially leading to a better understanding of various hemostatic disorders and potential novel therapeutics. Here, we develop the BioID technique to an *in-vitro* model to study the hemostatic protein, ADAMTS13, in plasma (Figure 9).

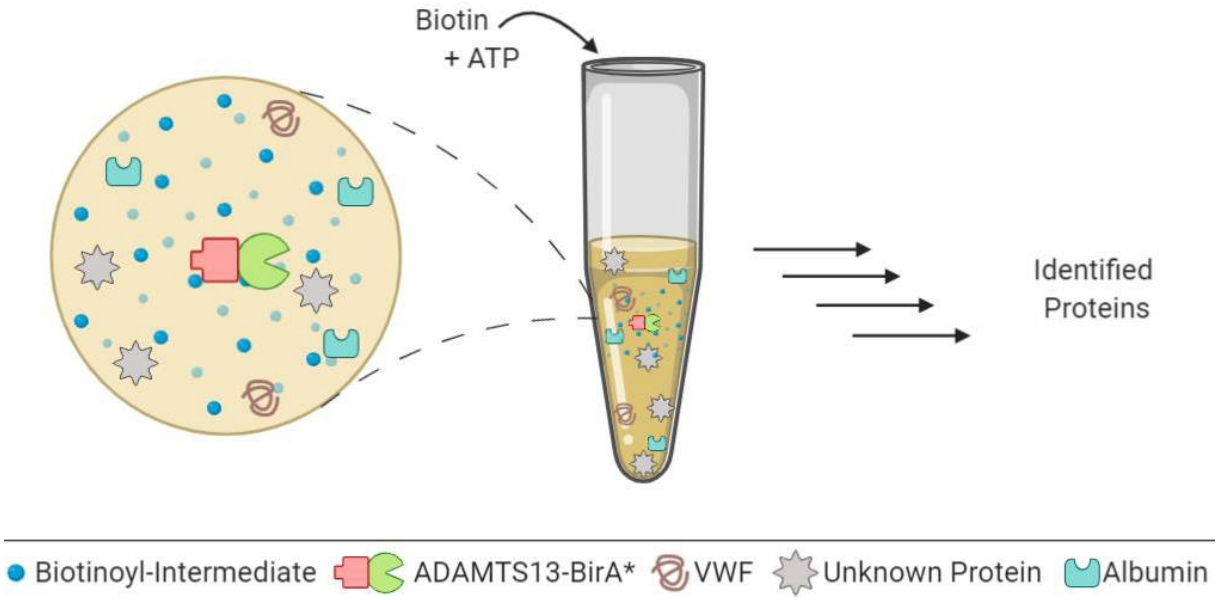

Figure 9 - *In-Vitro* Plasma BioID.

Fusion protein (ADAMTS-BirA), or unconjugated BirA*, is added to the citrated plasma along with ATP and biotin. BirA* activates the biotinoyl-intermediate that biotinylates neighboring proteins within its 10 nm labeling radius. The labeled biotinylated proteins are isolated and purified using streptavidin immunoprecipitation, washed, digested, then identified through LC/MS/MS analysis.*

1.6. Objective

The objective of this research project is to: a) develop and utilize the BioID technique in plasma in search of novel ligands to ADAMTS13, b) to utilize our new findings in the interactome of ADAMTS13 and develop a better understanding of its regulation, and c) to leverage this knowledge to design variants of ADAMTS13 that may serve as effective antithrombotic therapies.

2. MATERIALS and METHODS

2.1. Cloning of ADAMTS13 and BirA* Genes

2.1.1. Polymerase Chain Reaction

The cloning design strategy was developed using SeqBuilder 14 (DNASTAR Lasergene) and the OligoAnalyzer tool (IDT – Integrated DNA Technologies). Primers were designed to avoid possible hairpin structures and dimerization. Each junction primer set was designed with an overlap region of 15-25 bases to facilitate the Gibson Assembly reaction. The melting temperatures, hairpins, and dimers were calculated using Integrated DNA Technologies online (IDT OligoAnalyzer 3.1). Table 2 describes the primer design and the conditions of the PCR reactions for the extracted fragments.

PCR reactions were assembled using primers for each fragment, according to Table 2, and according to the high-fidelity polymerase mastermix protocol (N.E.B.: M0530S). Each reaction took place in a PCR thermocycler (T100 Thermal Cycler, Bio-Rad) and conditions were optimized to the melting temperatures for each primer pair (Table 2). Generally, the cycles consisted of: 1) 95°C, 2 min; 2) 95°C, 30 sec; 3) 60°C, 30 sec; 4) 70°C, 30 sec/kb; 5) 70°C, 10 min; repeating steps 2-4 for a total of 30 cycles. Negative control reactions, in which the DNA template was absent, were performed in parallel. Additional sequences of interest were (Kozak, Cox2 signaling sequence, 6x His-tag, FLAG-tag, TEV protease site, and a GS or AP linker between ADAMTS13 and BirA*) added alongside the ADAMTS13 and BirA* genes of interest.

Table 2 - PCR Conditions in the Extraction of DNA Fragments of Interest

The following is a list of all the primers used in the PCR extraction of the genes of interest and their sequences (5' to 3'):

Bold – primer, non-bolded – overhang, *italicized* – overlap

Primer1	**Primer2**	**Gene**	**Tm (°C)**		**PCR (°C)**
			P1	P2	Extension Time (min:sec)
Vector 1 – ADAMTS13-GS-BirA*					
V1P1S (***AAACCCGCTGATCAGCCTCGA)***	V1P1AS (*GCACGAGCCAGCATGGTGGC***TTAAA CGCTAGCCAGCTTGG)**	pcDNA (~5kbps)	68	62.8	2:30
V1P2S (GCTCGGATCT*GCCACC**ATGCT GGCTCGTGC***ACTG**)**	V1P2AS (*CACAGCGGCCCACACCCA***GGCCTGC CGTGGCTTA)**	Cox + MDTCS (~2kbps)	65.1	64.4	1:00
V1P3S (*TGGGTGTGG**GCCGCTGTG***CGT GGG**)**	V1P3AS (*CCGCTGCCTCCCCCT*GAGCCACCAC C**GGTTCCTTCCTTTCCCTTCCA)**	TSP+ CUB (~2.25kbps)	66	64	1:00
Vector 2 – BirA*-FLAG					
V2P1S (***AAACCCGCTGATCAGCCTCGA)***	V2P1AS (*GCACGAGCCAGCATGGTGGC***TTAAA CGCTAGCCAGCTTGG)**	pcDNA (~5kbps)	68	62.8	2:30
V2P2S (GCTCGGATCT*GCCACC**ATGCTG GCTCGTGC***ACTG**)**	V2P2AS (*GTTCTTGAA**GGCATTGG***ATTGGAAG TACAG**)**	Cox (~0.15kbps)	65.1	64	0:30
V2P3S (*CCAATGCC**TTCAAGAAC***CTGAT CTGGCTGAA**)**	V2P3AS (*ATCGTCTTTGTAGTC*GGAACCACC**GC TTCTTCTCAGGCTGAACTC)**	BioID2 (~0.75kbps)	64.2	62.6	0:30

2.1.2. Agarose Gel Electrophoresis

The PCR reactions were assessed on 1% agarose gel (1 g/ 100 mL TAE (40 mM Tris, 20 mM acetic acid, 1 mM EDTA, pH 8.0) buffer, ethidium bromide (0.2-0.5 μg/mL)). The PCR reactions were mixed with 6x loading dye (Thermo Scientific: R0611) and loaded onto the agarose gel alongside 100 bp or 1 kb bp marker ladders (Thermo Scientific: SM024, SM1331). The gel ran at 80V for ~1hr and was then imaged under UV light (BioRad: ChemiDoc XRS+, QuantityOne Software).

If multiple bands were present, the band of interest was cut out and purified according to the QIAquick Gel Extraction Kit (QIAGEN: 28706). In the presence of only one band with the correct size, the PCR reaction was purified using QIAquick PCR Purification Kit (QIAGEN: 28106). The eluted DNA fragments were collected into ddH_2O and quantified using absorbance at 260 nm on the NanoDrop.

2.1.3. Gibson Assembly

Purified DNA fragments were assembled into the final construct using Gibson Assembly. The Gibson reaction method is based on a mixture of enzymes (5’ exonuclease, DNA polymerase, and DNA ligase) that stitch together DNA fragments with overlapping double-stranded sequences under isothermal conditions (50°C) (317). The Gibson assembly reaction was performed in accordance with the kit provided by New England Biolabs (N.E.B.: E5510S). This mixture consisted of 10 μL of 2x master mix and 0.1 pmols of each DNA fragment to a total reaction volume of 20 μL using ddH_2O. The reaction was

placed on a thermocycler (T100 Thermal Cycler, BioRad) at 50°C for 1 hour, then 1.0 µL of the Gibson assemblies were transformed into 50 µL chemically competent TOP-10 and XL-GOLD$_{10}$ *E. coli* cells.

2.1.4. Chemical Transformation

Gibson assemblies were transformed into chemically competent TOP-10 and XL-GOLD10 *E. coli*. Each tube of 50 µL chemically competent cells was thawed on ice for 20 minutes before adding 1.0 µL of the Gibson assembly reaction (~10 ng of DNA) was added. The cells and DNA mixture were incubated on ice for 30 minutes, then heat shocked at 42°C for 45 seconds. After that, the cells were placed on ice for 2 minutes, before 200 µL of SOC broth (N.E.B.: B9020S) was added. The cells mixture was placed in an incubator shaker to grow at 37°C for 1 hour at 200 rpm. Using sterile techniques, 50-100 µL of the transformed competent cells were plated on LB agar plates containing ampicillin at 100 µg/mL and grown overnight at 37°C.

To identify the correct assembly of constructs, individual colonies were picked and placed in a culture tube containing 5 mL of LB media with 100 µg/mL of ampicillin to grow overnight in a shaking incubator at 37°C and 200 rpm. From the grown culture, a frozen stock was made, or the plasmid DNA was extracted.

2.1.5. *E. coli* Freeze Stocks

An *E. coli* freeze stock was prepared by pelleting 1 mL of the grown culture at 16000 xg for 5 minutes then resuspending the pellet in 1 mL of LB media containing 25% glycerol and stored at -80°C in a cryovial. Plasmid DNA was extracted using the QIAprep Spin Miniprep kit (QIAGEN: 27106) and 4 mL of the grown *E. coli* culture.

2.1.6. Diagnostic PCR Reactions

Diagnostic PCR reactions were performed to validate the Gibson Assembly. Primers were designed as previously described in section 2.1.1. Table 3 describes the primer design and the conditions of the PCR reactions for the sequencing primers, primers set ~200 bases away from each junction. PCR reactions using the Gibson assembly reactions and sequencing primers (Table 3) were run (refer to section 2.1.1) with the exception in the use of a standard fidelity polymerase (GoTaq Green Mastermix, Promega: M712B).

PCR reactions were assessed by agarose gel (refer to section 2.1.2) Product size of ~360-400 bp indicated correct assembly. Plasmid DNA templates from correct samples were sent out to Mobix Lab (McMaster University, Hamilton, ON) for sequencing using the sequencing primers used in the PCR reactions (Table 3). The resulting sequences were of ~600-800 bp sequenced in the direction of each sequencing primers. The sequencing results were analyzed using SeqMan Pro 14 and compared to the published ADAMTS13

and BirA* sequences (NCBI: AAL11095.1 and Addgene: 36047). A detailed vector map was then constructed using SeqBuilder 14.

Table 3 - PCR Conditions in the Sequencing of the Assembled Junctions

The following is a list of all the primers used in the PCR extraction of the genes of interest and their sequences (5' to 3'):
Bold – primer, non-bolded – overhang, *italicized* – overlap

Junction (length – bp)	**Primer 1**		**Primer 2**		**Tm (°C)**		**PCR (°C)**
	Name	Sequenced Region	Name	Sequenced Region	P1	P2	Extension (min:sec)
Vector 1 and 4 – ADAMTS13-GS/GSA-BirA*							
pcDNA/CoxM (~400)	V1S1F (TAATACGACTCACTATAGGGAGAC)	Vector-Cox-M	V1S1R (AGGTTGGCTGTGATATTTGGA)	M-Cox-Vector	60.5	62.1	0:30
S/TSP (~420)	V1S2F (CCTGGAGGAGATCCGCATCT)	S-TSP	V1S2R (CAATGTCTTCAGGAGGCTGCC)	TSP-SC	65.1	65.1	0:30
CUB/BirA* (~390)	V1S3F (CAGGTGCTCTACTGGGAGTCA)	CUB-GS/GSA-BirA*-FLAG-Vector	V1S3R (TTCTCGAACTCCTTGGGGTTC)	BirA*-GS/GSA-CUB	64.9	63.8	0:30
BirA*/pcDNA (~360)	V1S4F (CCTGAAGAAGTTCAAGGAGAA)	BirA*-FLAG-Vector	V1S4R (AGGAAAGGACAGTGGGAGTGG)	Vector-FLAG-BirA*-GS/GSA-CUB	59.8	65.6	0:30
Vector 8 – BirA*-FLAG							
pcDNA/BirA* (~370)	V1S1F (TAATACGACTCACTATAGGGAGAC)	Vector-Cox-BirA*-FLAG-Vector	V1S3R (TTCTCGAACTCCTTGGGGTTC)	BirA*-Cox-Vector	60.5	63.8	0:30
BirA*/pcDNA (~360)	V1S4F (CCTGAAGAAGTTCAAGGAGAA)	BirA*-FLAG-Vector	V1S4R (AGGAAAGGACAGTGGGAGTGG)	Vector-FLAG-BirA*-Cox-Vector	59.8	65.6	0:30

2.2. Protein Expression

2.2.1. HEK 293 Cells

Frozen 1 mL stocks of HEK 293TRex, obtained from Dr. Ginsburg's lab (University of Michigan, MI), were thawed and resuspended in 9 mL Dulbecco's Phosphate-Buffered Saline buffer (DPBS: 2.7 mM KCl, 1.47 mM KH_2PO_4, 136.9 nM NaCl, 8.10 mM Na_2HPO_4), pelleted at 500 xg for 5 minutes, then resuspended and plated in 10 mL of pre-warmed to 37°C complete media (DMEM (Dulbecco's Modified Eagle's Medium, Sigma: D6046), 10% FBS (Fetal Bovine Serum, Wisent: 098450) and penicillin-streptomycin (Wisent: 450-201-EL)) onto a 10-cm dish in an incubator set to 37°C and 5.0 CO_2.

At ~70% confluency, cells were passaged in a 1:5 split ratio. Media was aspirated and the cells were washed with 10 mL DPBS. The DPBS was aspirated and 1 mL of 0.25% trypsin-EDTA (GIBCO: 25200-056) was added. After 5 minutes, the cells were collected using 9 mL of DPBS, pelleted as described above, plated in a 1:5 split ratio, and grown (refer to section 2.2.1).

2.2.2. HEK 293 Freeze Stocks

Frozen stocks of HEK 293TRex cells were made at the early generations of growth (N = 2-4). Cells at ~70% confluency were trypsinized, washed, pelleted (refer to section 2.2.1), and resuspended in freeze stock media (DMEM + 20% FBS + 10% DMSO). Stocks

of 1 mL aliquots were made in cryovials and stored at -20°C overnight. The frozen cells were placed in a closed Styrofoam box and placed at -80°C for 16-24 hours, for a gradual decrease in temperature, then in liquid nitrogen (-120°C) for long-term storage.

2.2.3. Stable Expression System (Flp-In TRex)

ADAMTS13-BirA* fusions, BirA*, and a negative (dH2O) control were transfected using Lipofectamine 3000 into HEK 293TRex cells. HEK 293FlpIn/TRex cells are engineered cells designed for the creation of stable cell lines using the Flp-In TRex system (ThermoFisher Scientific: K650001). This system utilizes an FRT (Flip-Recombinase integration site) site to integrate the gene of interest into the cells' genome when co-transfected with pOG44, a vector for Flip-Recombinase expression. Cells at 80% confluency were transfected using 20 µg of DNA (1:4, pcDNA 5 FRT:pOG44), 30 µL Lipofectamine 3000, and 40 µL P3000 reagent. The reagents were mixed according to the manufacturer's protocol in 0.5 mL of Opti-MEM (Gibco Life Technologies: 31985-070) media at room temperature for 5 minutes. The two tubes were mixed and incubated for 10 minutes. The media on top of the cells was aspirated, and the lipid-DNA mixture was added. The cells were placed in the incubator, set to 37°C and 5.0 CO_2, for 4 hours. 9 mL of complete media was added, and the cells were grown overnight in the incubator. ~48 hours after transfection, the media on the cells was replaced with 10 mL of fresh pre-warmed complete media. The cells were then incubated for additional 2 days before their media was refreshed again.

Upon successful transfection, as indicated by a large number of healthy cells 5 days post-transfection, Hygromycin B was added as a selection. Initial attempts at selection utilized 200-1000 μg/mL. However, the cells did not look healthy and did not survive. Subsequent attempts utilized lower concentrations of Hygromycin B (25-200 μg/mL) whereby a few cells survived. Healthy cells were transferred to 6-well plates for an easier clustered growth, then back to 10 cm dishes. Media of survived healthy cells were collected and analyzed for protein expression through SDS-PAGE, western blot, and ELISA (specific for ADAMTS13). After confirmation of protein expression, the cells were made into frozen stocks or up-scaled to T-175 cm^2 flask and roller bottles for large-scale protein expression.

2.2.4. Protein Expression

Expression of protein was constitutive, and healthy cells were propagated in complete media containing 200 μg/mL of Hygromycin B in a 10-cm dish for 3 generations, then T175 flasks for 2 generations, then roller bottle. Cells grew in the roller bottle for ~3 days before the complete media containing 200 μg/mL of Hygromycin B, was washed, and aspirated by 50 mL of dPBS twice. FreeStyle media containing AEBSF (0.050 g/L) was used for cell expression. The media was collected every 2-3 days, for 3-6 collections before disposing of the roller bottle.

Conditioned media containing expressed proteins (ADAMTS13-BirA*, BirA* or ADAMTS13) was centrifuged at 4000 x g for 5 minutes then filtered through a 0.45 μm filter. The collected filtered media was frozen at -80°C for storage.

2.3. Protein Purification

The collected filtered media was purified using Q Sepharose (Cytiva: 17051001) and HisPur Ni-NTA Resin (Thermo Scientific: 88221) in accordance with the manufacturer's protocol.

2.3.1. Ion Exchange Chromatography (Q-Sepharose)

The collected filtered media (1-2 L) was thawed overnight at 4°C, then diluted to a 2:1 volume ratio of Tris buffer (25 mM Tris, pH 8.0) to media. For example, 1L of media was added to 2L Tris buffer. The Q Sepharose column was set up with ~10 mL resin bed volume and recharged using 2x bed volume of 0.1 M NaOH followed by 2x bed volume of 0.1 M HCl. The column was then washed using 5x bed volume of Tris buffer.

The diluted media was loaded onto the column overnight at 4°C, and the flowthrough was collected. The column was then washed using 10x bed volume of Tris buffer, and the protein was eluted in ~1-2 mL fractions using 3x bed volume of Tris buffer containing 1 M NaCl (pH 8.0). The eluted fractions were quantified using absorbance at 280 nm on the NanoDrop. Fractions containing high concentrations of proteins were pooled together.

2.3.2. Metal Affinity Chromatography (Ni-NTA)

Pooled Q Sepharose purified fractions were made to conditions like that of the wash buffer (25 mM Tris, 0.5 M NaCl, 10 mM imidazole, pH 8.0) of the NiNTA purification. The pooled fractions were diluted in Tris buffer to a NaCl concentration of 0.5 M; and imidazole, to a concentration of 10 mM, was added and the pH was adjusted to 8.0 accordingly. The column was set up with ~4 mL resin bed volume (Ni-NTA resin, Thermo Scientific: 88221) and 20 mL of the wash buffer was passed.

The media was then passed through the column followed by a wash step using ~40 mL of the wash buffer. The proteins were then eluted in ~1 mL fraction using 12 mL of elution buffer (25 mM Tris-HCl, 0.5 M NaCl, 250 mM imidazole, pH 8.0). The eluted fractions were quantified using absorbance at 280 nm on the NanoDrop. Fractions containing high concentrations of proteins were pooled together and concentrated using a centrifugal concentrator at 4400 xg for 0.5 – 1 hour (MWCO of 10 kDa and 30 kDa for BirA* and ADAMTS13-BirA*/ADAMTS13 respectively). Concentrated samples were buffer exchanged, as described by the manufacturer, using the PD-10 desalting columns (GE Healthcare: 17-0851-01) into PBS buffer (10 mM Na_2HPO_4, 1.8 mM KH_2PO_4, 137 mM NaCl, 2.7 mM KCl, pH 7.4).

2.4. Protein Validation

2.4.1. Polyacrylamide Gel Electrophoresis (SDS-PAGE)

Polyacrylamide gel electrophoresis, SDS-PAGE, was used to separate proteins in the samples from the purification process. Up to 15 µL (~2-5 µg), of protein sample, was mixed with 4x SDS-PAGE loading buffer (BioRad: 161-0747) containing beta-mercaptoethanol and were incubated on a heating block at 95°C for 5 minutes. The samples, alongside 8 µL of a protein marker (BioRad: 1610374), were loaded on a 4-20% SDS-PAGE gel (BioRad: 456-8086). The gel ran, in SDS-PAGE running buffer (25 mM Tris, 192 mM glycine, 0.1% SDS), at 60 V for 12 minutes then 160 V for 40 minutes. The gel was then set up for either a total protein stain or a western blot for detection of total or specific proteins.

2.4.2. Total Protein Stain (SYPRO-RUBY)

Total protein stain was performed using SYPRO-RUBY (BioRad: 170-3125) in accordance with the manufacturer's protocol. The gel was washed 2x with 15 mL Fixative buffer (40% methanol, 10% acetic acid) for 15 minutes each on a table-top shaker, then stained overnight using 15 mL of SYPRO-RUBY reagent covered from light. Then the stained gel was washed 2x with 15 mL of wash buffer (10% methanol, 7% acetic acid) for 15 minutes each, followed by a quick 2-minute wash using $_{dd}H_2O$ before being imaged using ChemiDoc Imager System (Bio-Rad) and analyzed using the Image Lab Software (Bio-Rad, version 5.2.1).

2.4.3. Western Blot

Western blot was used to detect expressed proteins according to their respective tags. The western blot was set up, as directed by BioRad, in the transfer buffer, and the transfer was performed overnight at 30 V at 4°C. After completion, the nitrocellulose membrane (or PVDF membrane pre-soaked in methanol for 30 seconds) was removed into a clean tray and blocked in 10 mL of block buffer (5% non-fat dry milk, TBS (20 mM Tris, 150 mM NaCl) with 0.005% Tween20) for a minimum of 2 hours. The block buffer was refreshed and the antibody anti-FLAG-HRP (Sigma: SLBP6948V) or anti-ADAMTS13 (Abcam: ab28274) was added at a dilution factor of 1/10000 or 1/1000 respectively. The membrane was incubated with the primary antibody on a shaker for 2 hours or overnight at 4°C. The block buffer mixture was removed, and the membrane was washed 6 times with 10 mL of TBST wash buffer (TBS, 0.05% Tween20) for 5 minutes each, on a shaker, and discarding the wash buffer after each time.

If the primary antibody was not HRP conjugated, such as in the case of the anti-ADAMTS13 antibody, a secondary antibody was required. In this case, the membrane was washed 3 times instead of 6, then a secondary antibody, rabbit anti-mouse HRP-conjugated antibody, was added at a dilution factor of 1/10000 and incubated on a shaker for 1 hour. The block buffer mixture containing the secondary antibody was removed and the membrane was washed 6 times with 10 mL of TBST wash buffer (TBS, 0.05% Tween20) for 5 minutes each, on a shaker, and discarding the wash buffer after each time.

The membrane was transferred to a clear plastic wrap and the HRP substrate solution (400 µL of Clarity peroxide solution (Bio-Rad: 102030832) mixed with 400 µL with Clarity luminol (Bio-Rad: 102030830)) was added. Imaging was performed on the ChemiDoc Imager System (Bio-Rad) using the MultiChannel option and the Image Lab Software (Bio-Rad, version 5.2.1).

2.4.4. ADAMTS13 Activity (FRETS-VWF73)

FRETS-VWF73 (AnaSpec: AS-63728-01) is a fluorescence-quenching substrate used to measure the VWF-proteolysis activity by ADAMTS13. The 100 µL reaction took place in a Corning black dark bottom non-treated 96-well plate (Fisher Scientific: 07-200-590) with the final concentrations being 2 nM ADAMTS13 and 1 µM FRETS-VWF73 prepared and diluted in FRETS buffer (20 mM Tris-HCl, 25 mM $CaCl_2$, 0.005% Tween-20, pH 7.4). The activity was measured using SpectraMax M3 (Molecular Devices) fluorescence mode at λ_{ex} = 340 nm and λ_{em} = 450 nm. The fluorescence was measured every thirty seconds for at least 4 hours and the rate of proteolysis was determined by linear regression of the initial slope of the change in RFU vs time using SoftMax Pro (version 5.4). The activity of ADAMTS13 is determined by monitoring the change in fluorescence intensity over time. The values calculated were based on the initial slope of the increasing fluorescence, defined as R^2 value 0.9 and above. By varying the concentration of the ADAMTS13 used in the assay, the specific rate of proteolysis could be evaluated. The specific proteolytic activity of ADAMTS13 was determined by varying the concentration

range of ADAMTS13 between 0.5 and 10 nM, then calculated using the rate of proteolysis divided by the concentration utilized.

2.5. BioID ADAMTS13

2.5.1. *In-Vitro* BioID in Plasma

To note, although the literature has proven the use of this technique for intracellular labeling to be effective, none have used this technique for an *in-vitro* type assay in plasma. We challenge this concept by supplying our own ATP and are optimizing the conditions that will allow us to look for interacting proteins to ADAMTS13 in plasma.

Total reaction volumes of 100 µL containing ADAMTS13-BirA* or BirA* (100 nM) or no protein (PBS), 90 µL citrated pooled normal plasma (PNP), ATP (1 mM), and biotin (50 µM), were made and incubated for 4 hours on a top-over-bottom rotator at 37°C. 10-20 µL of Streptavidin-agarose bed volume (Thermo Scientific: 20349) per reaction was washed 3x in 10x bed volume BioID wash buffer (TBS + NaCl: 20 mM Tris, 450 mM NaCl, pH to 7.6) while pelleted at 500 xg for 3 minutes, and was added to the plasma mixture along with BioID wash buffer up to 1 mL.

The immunoprecipitation (IP) was performed on a top-over-bottom rotator at room temperature for 3 hours. The IP was then washed 5x in 1 mL BioID wash buffer while incubating each wash for 5 minutes in a top-over bottom rotator at room temperature and pelleting the resin at 500 xg for 3 minutes. 25 µL of SDS-PAGE loading dye (β-mercaptoethanol included) was added to the beads and the mixture was heated at 95°C for

5 minutes. The samples were then loaded onto a polyacrylamide gel and were separated using SDS-PAGE followed by analysis through total protein stain and/or western blot (refer to sections 2.4.2. and 2.4.3. respectively).

2.5.2. Optimization of BioID in Plasma

Prior to the use of the developed protocol, various protein (ADAMTS13-BirA* / BirA*) concentrations (25-100 nM), varying the time length of the reaction (4 hours to overnight), and adding additional ATP (+1 mM every hour for 4 hours), were also tested. In the ATPase inhibitors experiments, the BioID reactions were performed (refer to section 2.5.1), except for three inhibitors (2 mM $NaVO_4$ (pH 10), 1 µM IBMX, 5 nM NBTI), or 3 mM EDTA, or TBS (no inhibitor), that were added during the labeling reaction.

2.5.3. LC/MS/MS Sample Preparation

For mass spectrometry analysis (liquid chromatography-tandem MS (LC/MS/MS)), 1 mL of plasma was used, and the plasma mixture was mixed up to 2 mL with BioID wash buffer. In addition, streptavidin agarose beads (Thermo Scientific: 20357) were used instead, and the samples were washed with 2 mL of BioID wash buffer for 1 min, for 5 times; followed by 3 washes using 50 mM ammonium bicarbonate (pH 8.0). The samples were sent to SPARC-BioCentre (Sick Kids Hospital, Toronto) for urea/DTT treatment, alkylated using iodoacetamide, trypsin digested, separated, and analyzed using liquid chromatography-tandem MS (LC/MS/MS).

2.5.4. LC/MS/MS Data Analysis

Results from LC/MS/MS analysis of the BioID ADAMTS13 experiments were quantitatively analyzed using Scaffold 4 (Proteome Software). The quantitative values of spectral counts of the identified proteins were selected under the parameters of 95% threshold for protein, and 95% threshold for peptides. Identified peptides were searched in a Human Proteome database, along with the sequence of the streptavidin synthetic construct and the BirA* BioID2 R40G sequence, for the identification of the corresponding proteins. Quantitative spectral counts were extracted from the Scaffold 4 software and inputted into RStudio for significant analysis. Significance was calculated using a one-way ANOVA with a posthoc Tukey HSD test through RStudio.

2.5.5. Measuring ATP Concentration (Luciferase)

The consumption/stability of ATP in plasma was measured using the CellTiter-Glo 2.0 Assay (Promega: G9241), in accordance with the manufacturer's protocol, along with using the luminescence reading (500 ms) from FlexStation 3 (Molecular Devices) and the results were analyzed using SoftMax Pro (v. 5.4) and GraphPad Prism 6.

Total reaction volumes of 100 µL containing ADAMTS13-BirA* or BirA* (100 nM) or no protein, 90 µL citrated pooled normal plasma (PNP), ATP (1 mM), biotin (50 µM), various ATPase inhibitors (3 mM EDTA, 2 mM $NaVO_4$ (pH 10), 1 µM IBMX, 5 nM NBTI, or TBS (no inhibitor)) were made. Everything except the ATP was added to pre-warmed plasma at 37°C and was incubated for 15 minutes. The timed reaction began with

the addition of ATP (1 mM). At each time point, 5 µL of the reaction was diluted in 370 µL (1:75 dilution) of TBS buffer and placed in liquid nitrogen for a quick freeze. The reaction was stopped at 4 hours or as designated. Frozen aliquots were thawed on a bench top and mixed at a 1:1 ratio of sample to Luciferase (40 µL Cell Titre Glo2 reagent, 3 mM $MgCl_2$). The measurement was read in a 96-well opaque plate (refer to section 2.5.5) alongside a standard curve of ATP (0.1 µM – 100 µM) prepared in TBS.

2.5.6. Different Anticoagulants

Plasma with a different anti-coagulant was also tested during the optimization of the *in-vitro* BioID in plasma technique. Citrated pooled normal plasma was recalcified to a final concentration of 20 mM $CaCl_2$. Hirudin, to a final concentration of 50 µg/mL (32.8 µM), was immediately added to the recalcified plasma. The BioID assay using the hirudin-based plasma was performed as described in section 2.5.1.

2.6. Validation of Novel Interactions

2.6.1. ELISA Plate Binding Assay

Total reaction volumes of 100 µL containing 5 µg/mL vitronectin or 5 µg/mL bovine serum albumin (BSA) in PBS were added to wells of a clear 96-well microtiter plate for 2 hours. Samples were discarded and the wells were blocked with 200 µL TBST + 5% BSA for 2 hours. The block was discarded, and the wells were washed 3 times in 200 µL TBST each time. Next, increasing concentrations of FLAG-tagged ADAMTS13-BirA* or

BirA* (0 – 400 nM) in 100 µL of ADAMTS13 kinetic buffer (20 mM Tris-HCl, 150 mM NaCl, 10 mM $CaCl_2$, 10 µM $ZnCl_2$, 0.005% Tween-20, pH 7.4) was added to wells coated with vitronectin or BSA, and incubated for 2 hours at room temperature. The plates were washed 3 times with TBST. HRP-conjugated anti-FLAG antibody (Sigma: A8592) was then added at a volume of 100 µL and a dilution factor of 1:20000, for 1 hour. The plates were washed 3 times with TBST. The tetramethylbenzidine (TMB) substrate (Sigma: T0440) was then added at a volume of 100 µL for each well and allowed to react for 5 – 15 minutes. The reaction was stopped using 50 µL of 2.5 M H_2SO_4. Binding was detected by reading the absorbance values at 450 nm using SpectraMax M3 (Molecular Devices) and analyzed using SoftMax Pro (v. 5.4) and GraphPad Prism 6.

2.6.2. BioLayer Interferometry

The following experiment uses ForteBio's biolayer interferometry instrument the Blitz to determine the binding affinity of various substrates/proteins to a protein that is amine-coupled to a biosensor in a static condition.

Reagents were prepared according to the AR2G kit (ForteBio: 18-5095) and AR2G biosensor (ForteBio: 18-5092) instructions. Briefly, the biosensor was re-hydrated in 200 µL of water. The biosensor was then installed onto the Blitz, equilibrated with 4 µL water on a drop holder for 60 seconds. The surface was activated using 200 µL of EDC/NHS mixture for 300 seconds, before incubating with 200 µL of 37.5 nM ADAMTS13 or BSA in 10 mM acetate buffer at pH 5 for 300 seconds. The incubation with protein was repeated

for an additional 300 s. The biosensor was quenched using 200 µL 1 M ethanolamine, pH 8.5 for 300 seconds. Each biosensor was prepared fresh for each experiment.

After preparation, the biosensor was equilibrated in 200 µL of the ADAMTS13 kinetic buffer for 60 seconds. The biosensor was then incubated with 375 nM of analyte (such as VWF, anti-FLAG antibody, vitronectin, actin, or BSA) in 200 µL in ADAMTS13 kinetic buffer for 600 seconds. The association was monitored by inserting the biosensor into the ADAMTS13 kinetic buffer solution containing one of the substrates used, such as VWF, anti-FLAG antibody, vitronectin, actin, or BSA, at 375 nM and 200 µL in volume, for 600 seconds. The biosensor was then incubated with 200 µL of ADAMTS13 kinetic buffer for 600 seconds to monitor dissociation. The biosensor was then exposed to 200 µL of 10 mM glycine buffer, pH 2.5, to regenerate the surface before the experiment was stopped. Analysis was performed using the Blitz Software.

2.6.3. Surface Plasmon Resonance

The following experiment uses GE HealthCare's surface plasmon resonance (SPR) instrument the Biacore T200 to determine the binding affinity of various substrates/proteins to a protein that is amine-coupled to a biosensor in a flow condition.

The binding affinities between soluble full-length recombinant ADAMTS13 or truncated ADAMTS13 (MDTCS) (R&D Systems: 6156-AD-020 and 4245-AD-020 respectively), and various purified proteins including plasminogen (Pg: Glu-, Lys-, Mini-, µ-), inactivated plasmin (VFK-Plasmin), vitronectin (Vn), VWF, FXII, prothrombin,

bovine serum albumin (BSA), Apo(a) and its derivatives were determined by surface plasmon resonance (SPR) on a Biacore T200 (GE Healthcare). Biacore sensor chips (CM5), an amine coupling kit, and acetate buffer (pH 5.0) were supplied from GE Healthcare.

Commercially supplied proteins VWF (Haematologic Technologies: HCVWF-0190), vitronectin (Molecular Innovations: HVN-U), and BSA (BioShop: alb007.500) were utilized. Purified Apo(a) and its derivatives were generously donated by Dr. Michael Boffa's lab (Department of Biochemistry, The University of Western Ontario). All other analytes were generously donated by the labs of Dr. Jeff Weitz and Dr. Paul Kim (TaARI, McMaster University).

Biacore sensor chip (CM5) was rehydrated in HEPES-buffered saline (HBS: 20 mM HEPES, 150 mM NaCl) containing 0.01% Tween-20, 10 mM $CaCl_2$, and 10 μM $ZnCl_2$ at a flow rate of 10 μL/min at 25°C for 60 seconds. The chip surface was activated using EDC/NHS mixture for 300 seconds at a flow rate of 10 μL/min. After that, the activated chip was incubated with HEPES-buffered saline buffer for 60 seconds at a flow rate of 10 μL/min. After that, the chip was incubated with 20 μg/mL ADAMTS13 or MDTCS in 10 mM acetate buffer at pH 4 at a flow rate of 20 μL/min for 30 seconds. The incubation with ADAMTS13 or MDTCS was repeated until response units (RU) started to plateau or reach values greater than 2000 RUs. After that, the chip was incubated with 1 M ethanolamine, pH 8.5 at a flow rate of 20 μL/min for 300 seconds. In the case of a blank control, the protein incubation step was skipped, and the chip was quenched via the ethanolamine promptly. After preparation of the Biacore sensor chip (CM5), full-length ADAMTS13 or MDTCS or a blank (no protein) were immobilized using amine-coupling to 500-1000 RUs.

Binding experiments were performed in HEPES-buffered saline (HBS: 20 mM HEPES, 150 mM NaCl) containing 0.01% Tween-20, 10 mM $CaCl_2$, and 10 μM $ZnCl_2$ at a flow rate of 20 μL/min at 25°C. Increasing concentrations of analyte, 0-7 μM (unless otherwise specified) of the before mentioned protein analytes, containing 5 mM AEBSF (Sigma-Aldrich: 30827-99-7) and 10 μM VFKck, were injected into the designated flow cells for 60 sec (association), followed by running buffer alone for 300 sec (dissociation). Flow cells were regenerated with 0.5 M NaCl for 60 sec. Sensorgrams were analyzed with Biacore T200 evaluation software (v 1.0) and data were transferred to GraphPad Prism (v 9), whereby dissociation constants were determined from the non-linear regression fit of a one-site binding model. This model uses the equation:

$$y=Bmax*XKD+X+NS*X, \quad \text{(equation 1)}$$

where y is the total binding, x is the concentration of ligand, Bmax is the maximum specific binding, KD is the equilibrium dissociation constant which is the concentration of ligand at half-maximum binding at equilibrium, and NS is the slope of nonspecific binding.

Competition experiments were performed utilizing the same buffer conditions and the same setup as the binding experiments. 2 μM Lys-Pg or Glu-Pg were prepared with 5 mM AEBSF, 10 μM VFKck, and increasing concentrations of EACA (Sigma-Aldrich: 60-32-2) or TXA (Sigma-Aldrich: 1197-18-8). Sensorgrams were analyzed with Biacore T200 evaluation software (v 1.0), and data were transferred to GraphPad Prism (v 9), whereby IC50 (concentration of inhibitor that gives 50% binding of the analyte) constants were

determined from non-linear regression fit of a "[inhibitor] vs response – variable slope" model. This model uses the equation:

$$y=Bottom+(Top-Bottom)/(1+(IC50X)HillSlope), \qquad \text{(equation 2)}$$

where y is the total binding, x is the concentration of inhibitor, IC50 is the concentration of inhibitor at the half binding of analyte at half-maximum binding at equilibrium, HillSlope is the steepness of the curve (-1 is standard), and Top and Bottom are plateaus in the units of Y axis, where Bottom is forced to a value of 0.

2.7. Proteolytic Degradation of ADAMTS13

2.7.1 *In-Silico* Analysis of Protease Sensitive Sites in ADAMTS13

Our *in-silico* approach for the identification of proteases capable of proteolytically degrading ADAMTS13 consisted of a search in literature for experimental or computational evidence (81, 238, 239, 318, 319). Online tools capable of predicting cleavage sites proteolytically degraded by specific proteases in a specified peptide sequence, such as PROSPER (Protease specificity prediction server – Monash University), ExPASy Peptide Cutter (SIB Swiss Institute of Bioinformatics), and NEBcutter (v2.0, New England Biolabs) were also utilized (320–322). The search was focused on proteases secreted into the circulatory system.

2.7.2. ADAMTS13 Cleavage Assay

In-vitro proteolysis of ADAMTS13 reactions were made to a volume of 50 µL containing 100 nM rhADAMTS13 (R&D Systems: 6156-AD-020) or purified full length-ADAMTS13 and 50 nM various recombinant protease. ADAMTS13 was incubated for varying time points (0 – 3 h) with various recombinant proteases, at 37°C. Reactions were either analyzed for ADAMTS13 activity using FRETS-VWF73 assay (refer to section 2.4.4) or were stopped using SDS-loading dye and separated via SDS-PAGE under reducing conditions (refer to section 2.4.1). SDS-PAGE gels were either stained using SYPRO-RUBY for total protein analysis or by western blot using polyclonal anti-ADAMTS13 antibody (Abcam: ab28274) and goat anti-rabbit HRP-conjugated antibody (Bir-Rad: 1706515) (refer to sections 2.4.2. and 2.4.3).

2.7.3. Isolation of Neutrophils

10 mL of blood was collected in a 20 mL syringe containing 2.5 mL citrate at room temperature. Then, 2.5 mL of dextran (6% dextran in saline) was drawn up by BD Vacutainer into the citrated blood and mixed slowly 4 times in a figure 8 movement. The leukocyte-rich plasma layer was left to separate through a waiting period of 45 minutes to 1 hour. Histopaque 1077 (Sigma: 10771), at room temperate, and at an equal volume to that of separated leukocyte-rich plasma layer (~6 – 8 mL), was added to a 50 mL tube. The separated leukocyte-rich plasma layer was added slowly to a new 50 mL tube. Using a serological pipette, the plasma layer was transferred and added onto the superficial layer of the Histopaque solution at the slowest rate possible. The plasma-Histopaque mixture was

centrifuged at 1200 rpm, for 20 minutes with an acceleration of 7 and deceleration of 0. The supernatant was aspirated, and 2.5 mL of ACK lysis buffer was added onto the pellet. The pellet was slowly resuspended and incubated in the buffer for 4 minutes. Hank's Balanced Salt Solution (HBSS, GIBCO: 14065-056) was added to 50 mL then centrifuged at 1200 rpm, for 5 minutes, at 4 degrees, with an acceleration and deceleration of 9. After that, the supernatant was discarded and if the pellet was red, the ACK lysis buffer step was repeated. The white pellet, i.e. the neutrophils, was resuspended slowly in 10 mL of RPMI (GIBCO: 11835-030). The cells were counted using trypan blue-PBS solution (GIBCO: 15250-061) and a hemocytometer. The volume corresponding to the number of cells needed in the corresponding experiment was transferred into a new 2- or 15-mL tube, centrifuged at 1200 rpm for 5 minutes, the supernatant was discarded, and the pelleted cells were resuspended in RPMI to the volume required to the corresponding experiment.

Neutrophil-containing reactions were set up in 40 µL volume containing a varying number of neutrophils, $0 – 500 \times 10^3$ cells diluted in RPMI, and 100 nM PMA for activation for 4 hours at 37°C. Neutrophils were activated in the presence or absence of 20 µg/mL DNase 1. After that, 100 nM of recombinant or purified ADAMTS13 in ADAMTS13 kinetic buffer was added to the activated neutrophils, to a total volume of 50 µL. The mixture was incubated for 1 hour at 37°C, then analyzed as described in the proteolysis assay of the ADAMTS13 section 2.7.2. In experiments where the number of neutrophils was constant, 50,000 neutrophils were utilized, and the experiments were run as described in section 2.7.2. In the proteolysis experiments whereby specific inhibitors were utilized,

Sivelstat (elastase inhibitor, Tocris: 3535) and Cathepsin G Inhibitor I (Millipore Sigma: 219372) were utilized and the experiments were run as described in section 2.7.2.

2.7.4. Protease-Resistant ADAMTS13 Mutants

ADAMTS13 mutants were designed using SeqBuilder 14, whereby the T4L, or T8L, or both, regions of ADAMTS13 were mutated to a variable length of GGGS repeats. The T4L mutant represents the mutation GGS$[GGGS]_6$ at W868-A894, the T8L mutant represents the mutation $[GGGS]_{14}$GS at G1134-A1191, and the T4L/T8L mutant represents both mutations. These constructs were termed T4L, T8L, or T4L/T8L mutants according to their mutated regions. The T4L, T8L, and T4L/T8L mutants were genetically synthesized into pcDNA 3.1(+) from Bio Basic Inc. (Markham, ON, Canada). DNA vectors corresponding to each vector, along with wt-ADAMTS13 in pcDNA 3.1(+), were transfected and expressed into HEK 293T cells (refer to section 2.2.3). Expressed proteins, in FreeStyle media, were concentrated using centrifugal filters (Satorius Vivaspin 6 – 30,000 MWCO – VS0622) and quantified using the ELISA kit (R&D Systems: DADT130). Proteolytic degradation assay of ADAMTS13 mutants utilized either 100 nM plasmin, or 50,000 activated neutrophils, and was performed as described in section 2.7.2.

3. RESULTS

3.1. Cloning of ADAMTS13 and BirA* Genes

ADAMTS13-BirA*, with a GS linker $[GGS]_3$ and BirA* were cloned into pcDNA5/FRT using polymerase chain reaction (PCR) and Gibson assembly (Figure 10). Other linkers were considered (including GSA - $[GSA]_2$AGSGEF, AP – $[AP]_7$, and EAAK – A$[EAAK]_2$A spacers) but were abandoned because of difficulty in cloning. The linker peptide sequence between ADAMTS13 and BirA* in each expression construct was varied to identify the ideal sequence that promotes independent folding as well as secretion from the cell. Each expression construct includes: a Kozak sequence for optimal protein translation, Cox2 signaling sequence (replacing ADAMTS13 signaling sequence) to accelerate protein movement through the secretory pathway, a 6x His tag and a FLAG tag for protein purification and detection, and TEV protease site for removal of promoter sequence if necessary (Figure 10).

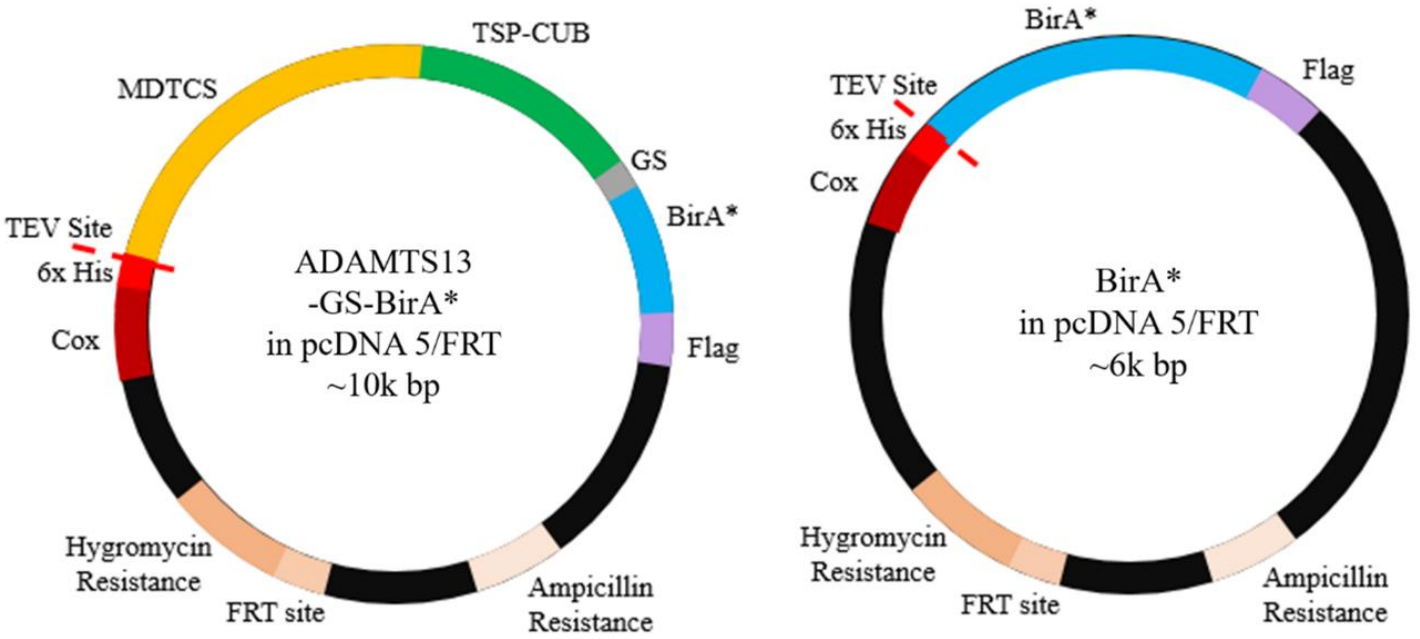

Figure 10 - Vector Maps of ADAMTS13-BirA* and BirA*.

ADAMTS13-BirA and BirA* were assembled into pcDNA 5/FRT vector. Along with that, additional genes of interest were inserted such as: Cox signaling sequence, 6x His-tag, TEV protease site, and FLAG-tag.*

ADAMTS13-BirA* was assembled via extraction of 4 fragments using PCR from the vectors MDTCS-pcDNA 3.1, ADAMTS13-pcDNA3.1, MCS-BioID2-HA, and hFXII-pcDNA 5/FRT (Figure 11), whereas the unconjugated BirA* was assembled via extraction of 3 fragments from the vectors MDTCS-pcDNA 3.1, MCS-BioID2-HA, and hFXII-pcDNA 5/FRT (Figure 11). Multiple troubleshooting factors (additional DNA template, use of DMSO, different primer sets, removal of overhangs, and an annealing temperature gradient) were utilized during the optimization of the PCR reactions.

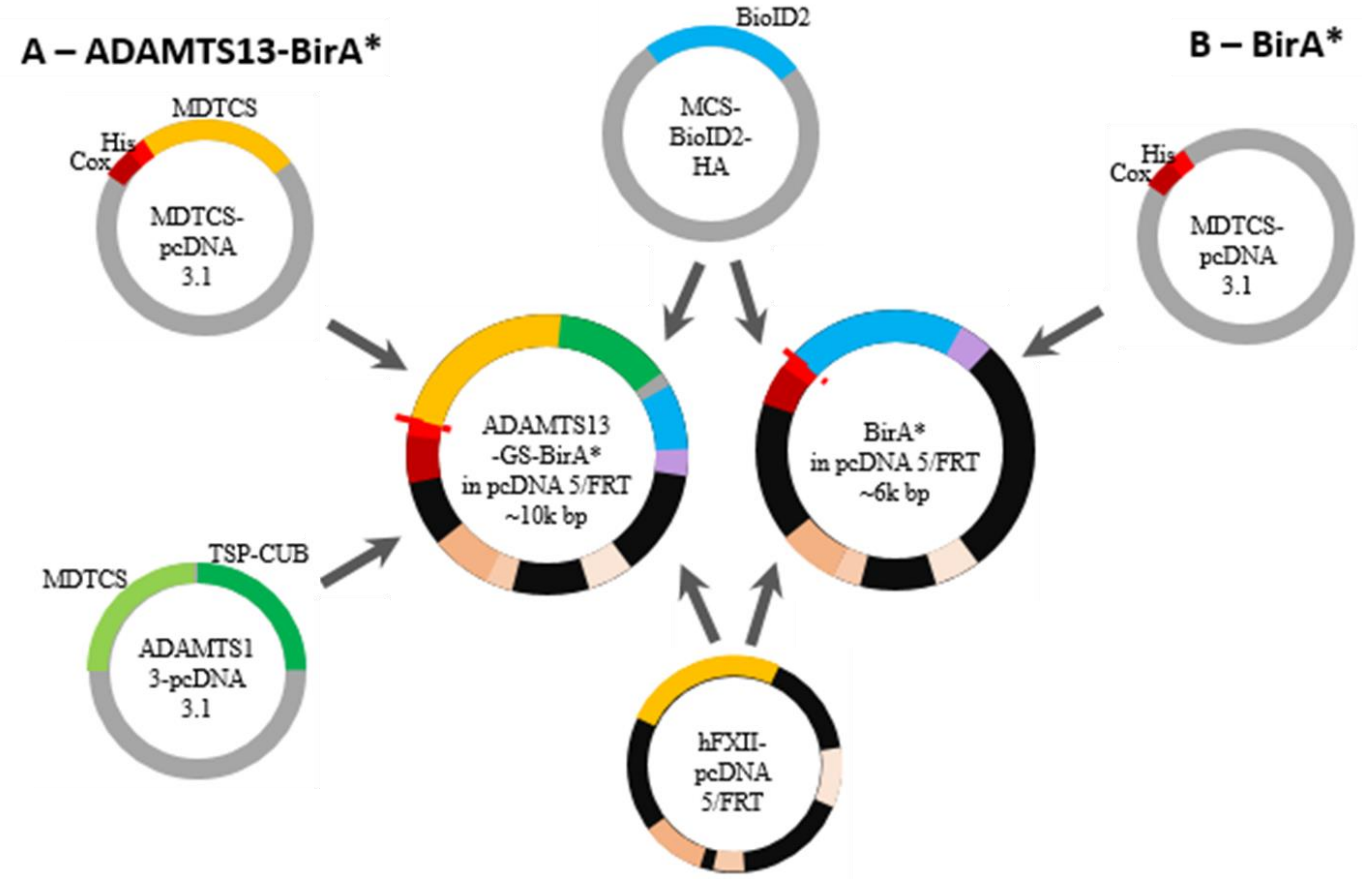

Figure 11 - Assembly Maps of ADAMTS13 and BirA*.

ADAMTS13-BirA (A) and BirA* (B) were assembled from several fragments of interest. The fragments were extracted using PCR under the conditions described in Table 2 and assembled using Gibson assembly.*

After successful extraction of the genes of interest, ADAMTS13-BirA* and BirA* were assembled as described in section 2.1.3. Transforming *E. coli* competent cells yielded a few colonies (1-7 colonies per plate), indicating potential proper assembly of the designed vector. To confirm proper assembly, DNA vectors were isolated from each colony as described in section 2.1.5. and underwent diagnostic PCR tests to verify the cloning procedure (Figures 12-13). In a few cases, the prominent band was double in size than the band of interest, likely a result of PCR laddering, such as BirA*/pcDNA (Figure 12). Furthermore, in the case that a band was missing, the colony was disregarded from future tests. Negative controls whereby non-existing junctions, such as MDTCS/TSPCUB, CUB/BirA* or pcDNA/CoxMDTCS and pcDNA/CoxBirA* were tested in BirA* and ADAMTS13-BirA* respectively (Figure 13). Isolated DNA vectors that have shown the correct assembly of junctions using the diagnostic PCR were further confirmed through sequencing at the MobixLab (McMaster University, Hamilton, ON). Comparing sequencing results to literature, the cloning procedure was determined to be successful as the assemblies were correct and no mutations were identified.

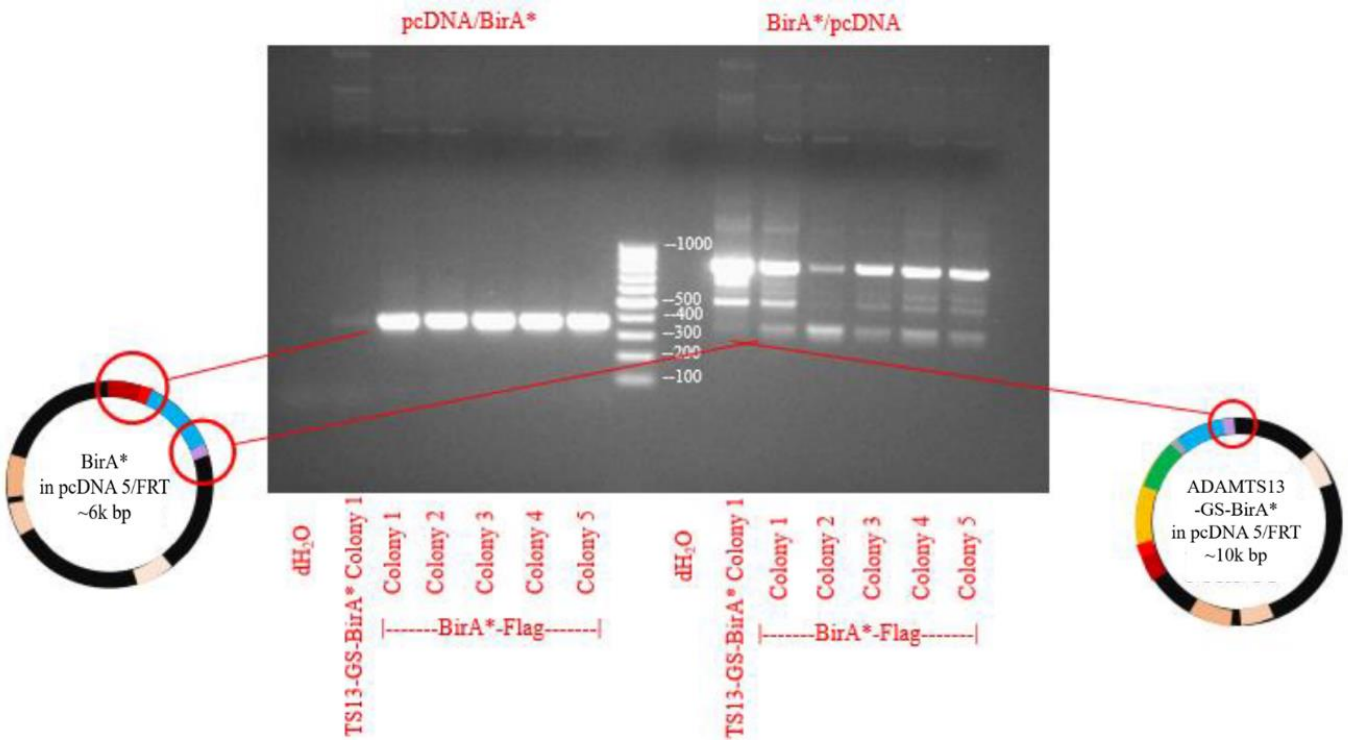

Figure 12 - Confirmation of Assembly - ADAMTS13-BirA* and BirA*.

The correct assembly of the vectors BirA in pcDNA 5/FRT, and ADAMTS13-BirA* in pcDNA 5/FRT was confirmed through PCR at each junction of assembly. Several colonies of BirA* were screened and found to be positive for the N-terminal assembly of the gene, and multiple bands were observed for the C-terminal assembly. Similarly, ADAMTS13-BirA* observed multiple bands for the C-terminal assembly as well.*

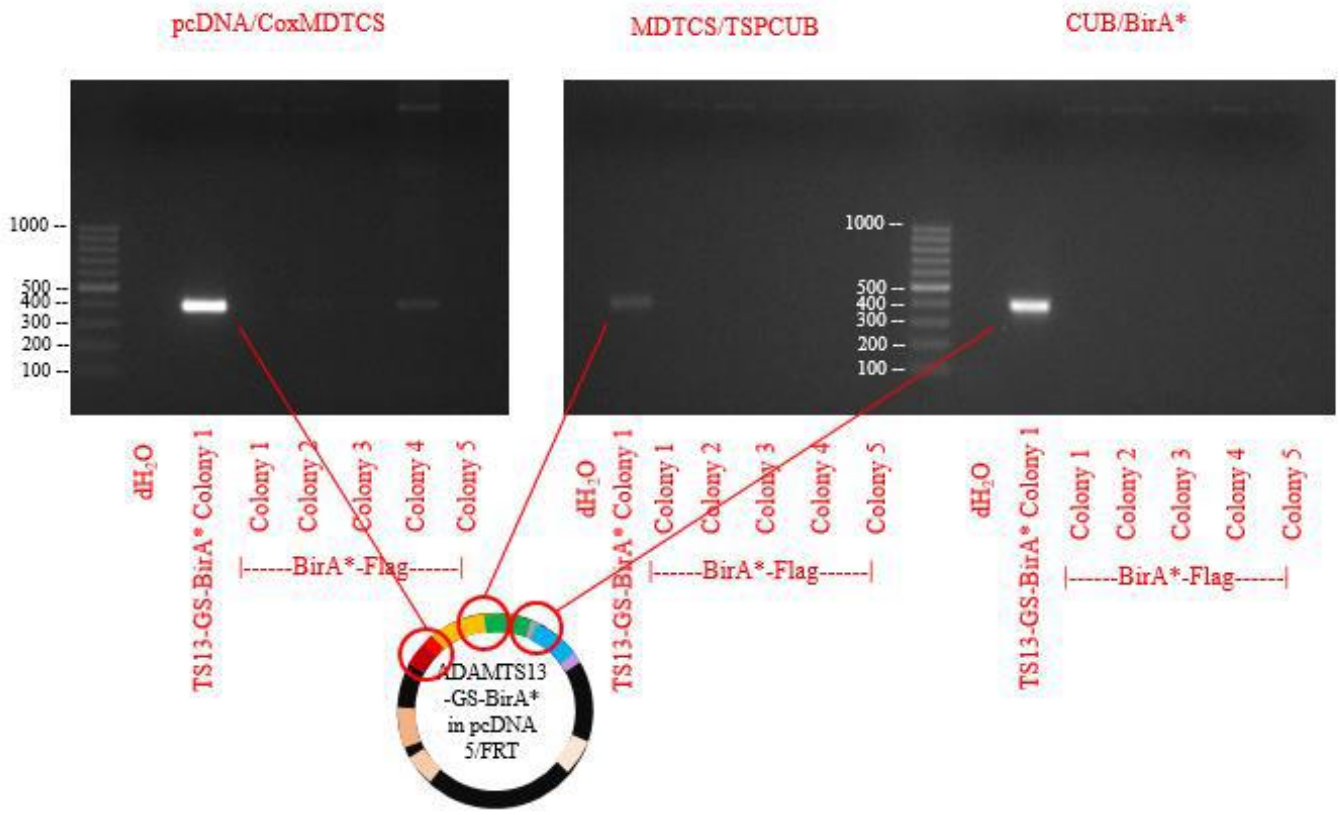

Figure 13 - Confirmation of Assembly - ADAMTS13-BirA*.

The correct assembly of the vector and ADAMTS13-BirA in pcDNA 5/FRT was confirmed through PCR at each junction of assembly. One band was observed at every evaluated junction of the assembled ADAMTS13-BirA*. No bands were observed in the negative control of the BirA* colonies.*

3.2. Protein Expression

3.2.1. Visual Analysis

Successfully transfected HEK 293TRex cells, capable of expressing ADAMTS13-BirA* or BirA*, were propagated until their transfer into roller bottles (refer to section 2.2.4). Expressed proteins were collected, isolated, and analyzed (refer to sections 2.3 and 2.4).

The total protein stain, SYPRO-RUBY, of the purification process of ADAMTS13-BirA* demonstrated a low purity elution fraction (Figure 14A). In addition, the western blot for anti-FLAG protein confirmed the presence of the ADAMTS13-BirA* (~207 kDa) in the eluted fraction (Figure 14B). However, two additional very faint bands were also identified in the western blot, one of which was believed to be a degraded version of the protein, possibly near the CUB domains. Through visual observation, the degraded bands were estimated to make up less than 10% of the total purified ADAMTS13-BirA* protein. Initial attempts to purify the ADAMTS13-BirA* resulted in poor purity and evidence of degradation. Despite several attempts at the optimization of purification protocol, ADAMTS13-BirA* purity was limited to no more than 10% pure (Figure 14).

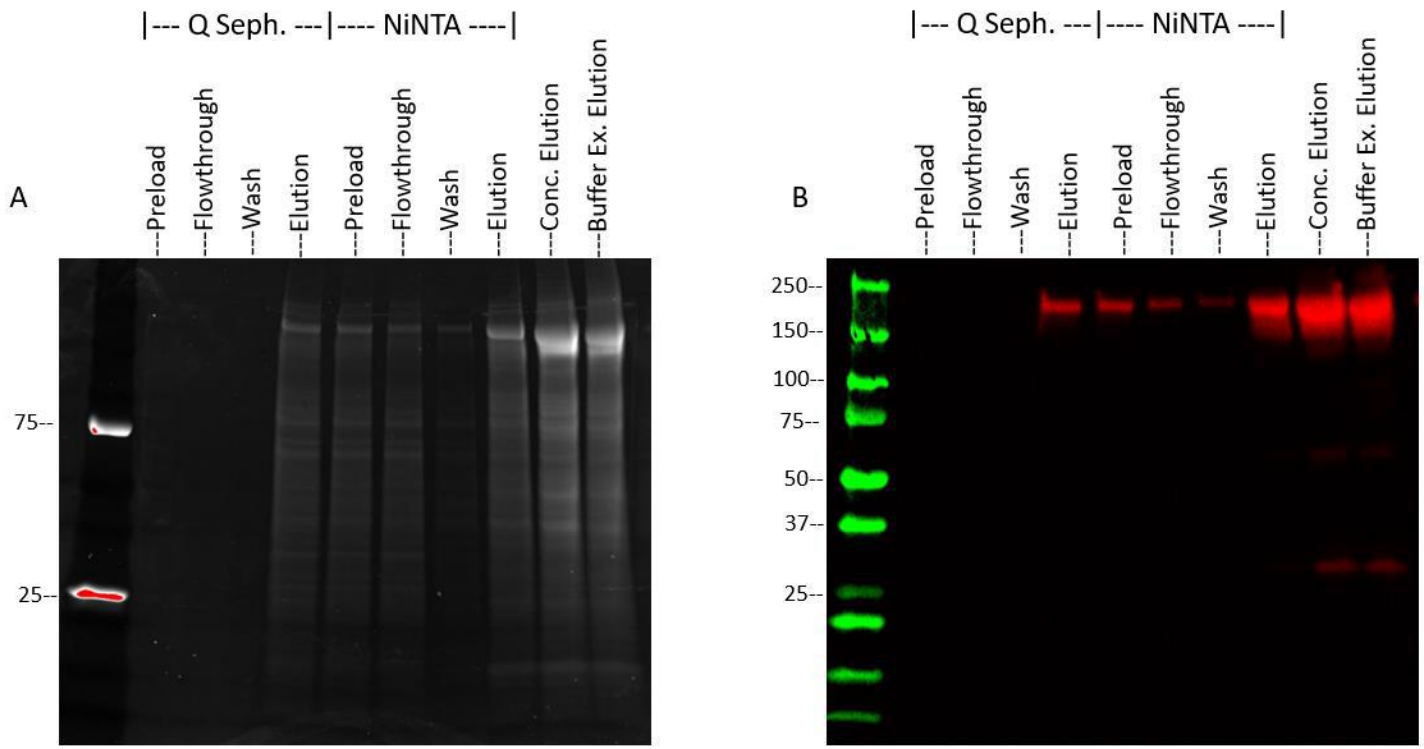

Figure 14 - Purification of ADAMTS13-BirA*.

Purification of ADAMTS13-BirA via anion exchange chromatography (Q Sepharose) followed by immobilized metal affinity chromatography (NiNTA), then separated using SDS-PAGE under reducing conditions and analyzed through a total protein stain (SYPRO-RUBY, A) and a western blot using the anti-FLAG antibody (B).*

Similarly, the total protein stain, SYPRO-RUBY, of the purification process of BirA* demonstrated a low purity elution fraction (Figure 15A). In addition, the western blot for anti-FLAG protein confirmed the correct size of BirA* (~27 kDa) in the eluted fraction (Figure 15B). However, two additional bands, one slightly higher and one slightly lower than the correct sized band, were also observed.

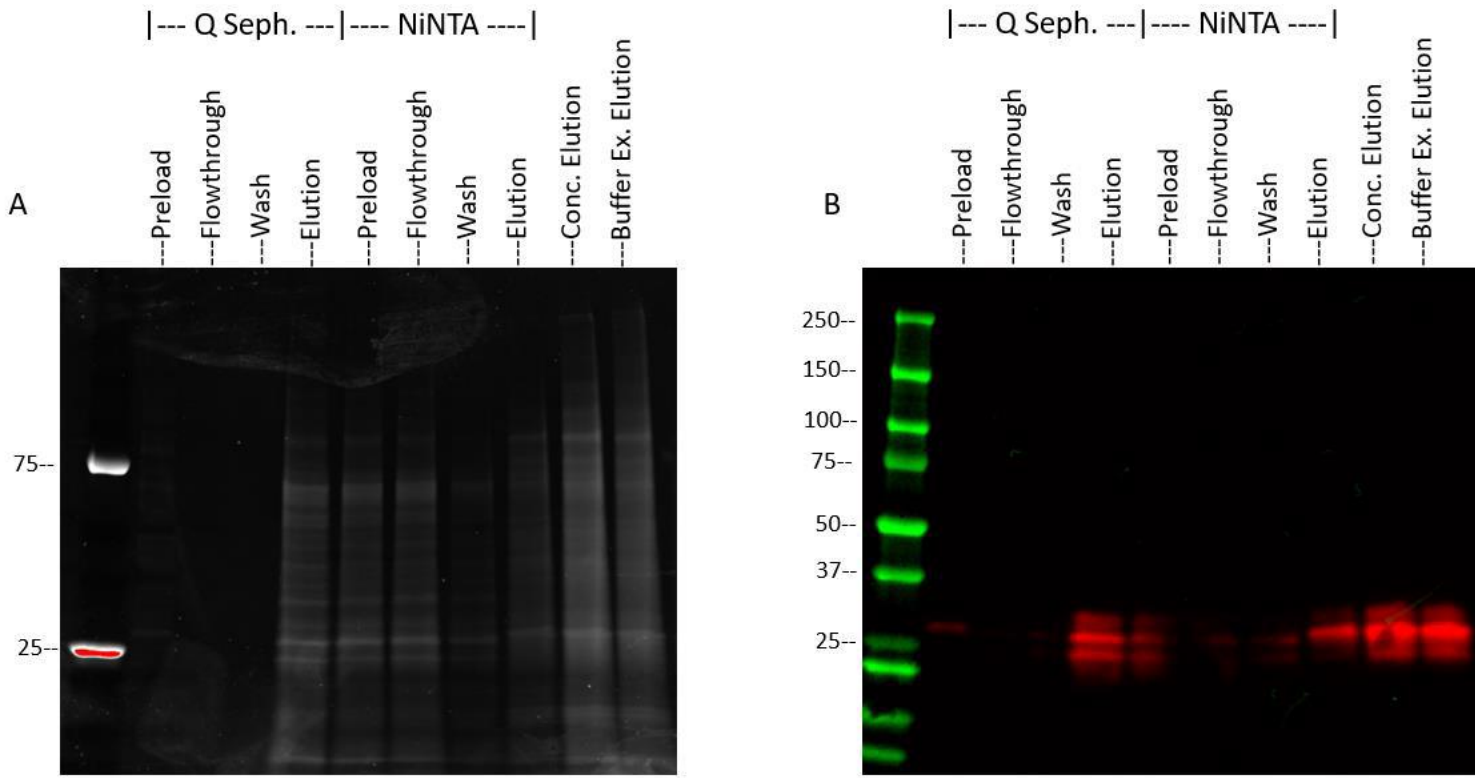

Figure 15 - Purification of BirA*.

Purification of BirA via anion exchange chromatography (Q Sepharose) followed by immobilized metal affinity chromatography (NiNTA), then separated using SDS-PAGE under reducing conditions and analyzed through a total protein stain (SYPRO-RUBY, A) and a western blot using the anti-FLAG antibody (B).*

3.2.2. ADAMTS13 Activity

The proteolysis activity of ADAMTS13 was tested, as fusion and non-fusion protein (refer to section 2.4.4). ADAMTS13-BirA* displayed similar proteolysis rate to that of wt-ADAMTS13, $4.7 \times 10^{-3} \pm 2.3 \times 10^{-4}$ ΔRFU/s/nM and $4.4 \times 10^{-3} \pm 5.0 \times 10^{-6}$ ΔRFU/s/nM respectively (Figure 16). This result indicated that the addition of the BirA* did not affect the proteolytic activity of ADAMTS13 to the VWF substrate VWF73.

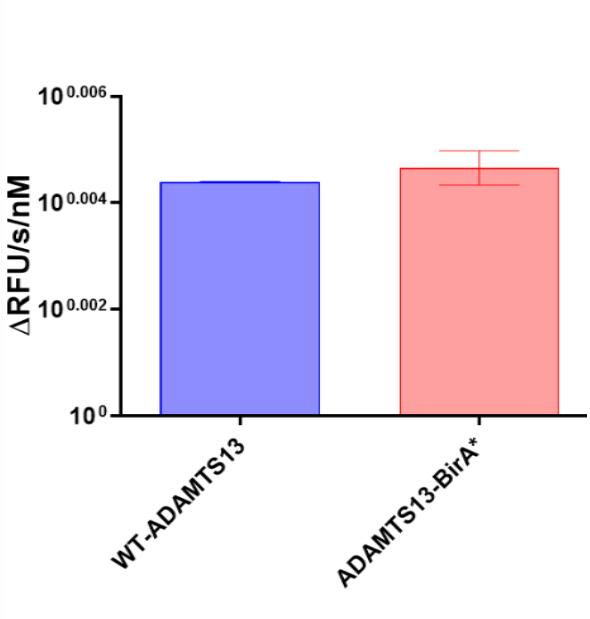

Figure 16 - Enzymatic Activity of ADAMTS13-BirA* (FRETS-VWF73).

The specific activity rate of wt-ADAMTS13 ($4.7 \times 10^{-3} \pm 2.3 \times 10^{-4}$ ΔRFU/s/nM) and ADAMTS13-BirA ($4.4 \times 10^{-3} \pm 5.0 \times 10^{-6}$ ΔRFU/s/nM) to the VWF73 peptide using FRETS-VWF73 assay and varying concentrations of ADAMTS13 (0.5 – 10 nM).*

3.3. BioID ADAMTS13

3.3.1. *In-Vitro* BioID in Plasma

The biotinylation activity of BirA* was tested as a fusion and non-fusion protein. The BioID assay was performed (refer to section 2.5.1) using 250 and 500 nM of BirA* or ADAMTS13-BirA* in citrated plasma. Biotinylated proteins were enriched by streptavidin pulldown and detected using SDS-PAGE and total protein stain (Figure 17). Protein bands of varying molecular weights were observed in samples containing BirA*, whereas no protein bands were observed in the absence of the BirA*. Protein bands with sizes of ~27 kDa and ~207 kDa were observed and resembled the auto-biotinylation of the BirA* and ADAMTS13-BirA* respectively (red arrows, Figure 17). Other bands observed were not identified but are likely non-specific targets given the high concentrations of enzyme used in this assay. These results confirm the biotinylation activity of BirA* in a citrated plasma system, and that the addition of ADAMTS13 does not hinder BirA*'s biotinylation activity.

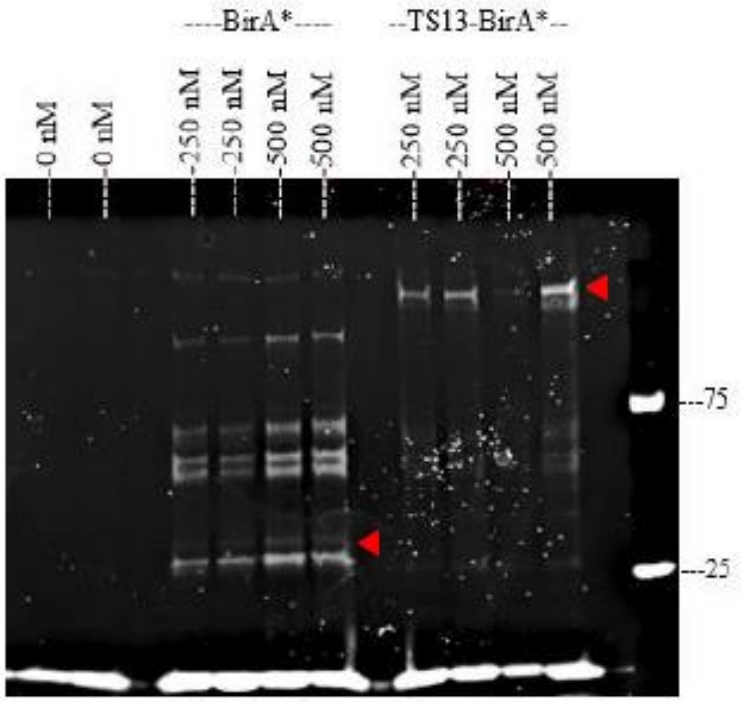

Figure 17 - Confirmation of BirA* Activity.

Labeling of plasma proteins via in-vitro BioID, overnight at 37°C, using increasing concentrations (0 – 500 nM) of the biotin ligase as unconjugated (BirA) or fusion protein (ADAMTS13-BirA*), then isolated using streptavidin-IP and separated using SDS-PAGE under reducing conditions before visual analysis through a total protein stain using SYPRO-RUBY. The red arrows represent the auto-biotinylation of biotin ligases.*

3.3.2. Proof of Concept

The *in-vitro* BioID in plasma technique was validated via identification of the enriched peptides through LC/MS/MS. The BioID assay was performed (refer to section 2.5.1). Results from the mass spectrometry analysis revealed several peptides and proteins, however many were found as a single count and were discarded from the analysis. The total number of proteins found across all samples was 66 proteins, 14 of which were unique to ADAMTS13-BirA* (Table 4 & Figure 18). As expected, the autobiotinylation of ADAMTS13 was identified as the highest number of hits within the sample group, but in only one of the ADAMTS13-BirA* samples (Table 4). The other sample had no protein hits, indicating an unsuccessful biotinylation assay. VWF, the only known substrate for ADAMTS13 and the presumed positive control for this test, was not detected (Table 4) (323). Other proteins that may be of interest going forward and had the highest number of hits within the sample group are actin, tubulin, and vitronectin. However, another attempt at mass spectrometry analysis was needed before further validating the hits. Prior to that, a closer examination of the variables in the BioID assay, such as the concentration of ATP or its stability, to increase the number of hits was conducted.

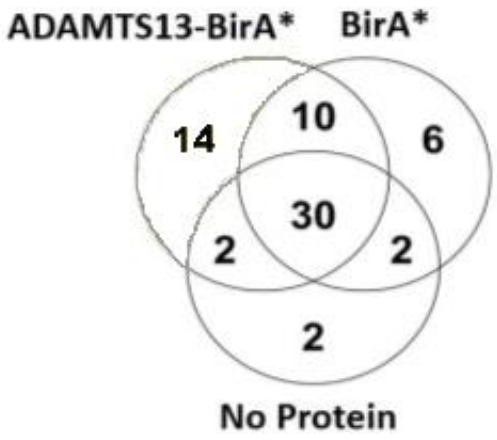

Figure 18 - Mass Spectrometry Results of Initial *In-Vitro* BioID Assay.

Total number of labeled proteins identified from using LC/MS/MS analysis on in-vitro BioID assay of either 25 nM ADAMTS13-BirA, BirA* or no protein, labeled overnight in citrated plasma. The total number of labeled proteins was 66, 14 of which were unique to ADAMTS13.*

Table 4 - Mass Spectrometry Results of *In-Vitro* BioID in Varying Anti-Coagulants

Identified Proteins	**Alternate ID**	**Molecular Weight (kDa)**	**ADAMTS13-BirA***	
			Sample 1	Sample 2
A disintegrin and metalloproteinase with thrombospondin motifs 13	ADAMTS13	154	151	0
Actin, cytoplasmic 1	ACTB	42	13	0
Creatine kinase B-type	CKB	43	2	0
Elongation factor 1-alpha 1	EEF1A1	50	3	0
Heat shock protein HSP 90-beta	HSP90AB1	83	2	0
Immunoglobulin kappa variable 2D-30	IGKV2D-30	13	5	0
Polyubiquitin-B	UBB	26	0	3
Protein RJ1	RJ1	16	3	0
Pyruvate kinase PKM	PKM	58	6	0
Serum paraoxonase/arylesterase 1	PON1	40	5	0
Tubulin alpha-1B chain	TUBA1B	50	15	0
Tubulin beta-4B chain	TUBB4B	50	14	0
UHRF1-binding protein 1-like	UHRF1BP1L	164	0	2
Vitronectin	VTN	54	13	0

3.3.3. Measuring ATP Concentration

The biotinylation activity of BirA* is dependent on ATP and improving the stability of ATP in plasma may yield more reproducible and robust labeling in plasma. According to the literature, the half-life of ATP in plasma is up to 5 minutes (324). The stability of ATP was measured (refer to section 2.5.5), in citrated plasma and in TBS buffer, in the presence or absence of BirA* (Figure 19). Change in ATP concentration was measured using a luciferase assay. ATP concentration was rapidly reduced in citrated plasma with a half-life of minutes, whereas ATP concentration was stable over several hours in TBS buffer. These data suggest that plasma contains proteins, such as ATPase, that is consuming ATP faster than its chemical instability in buffer (322).

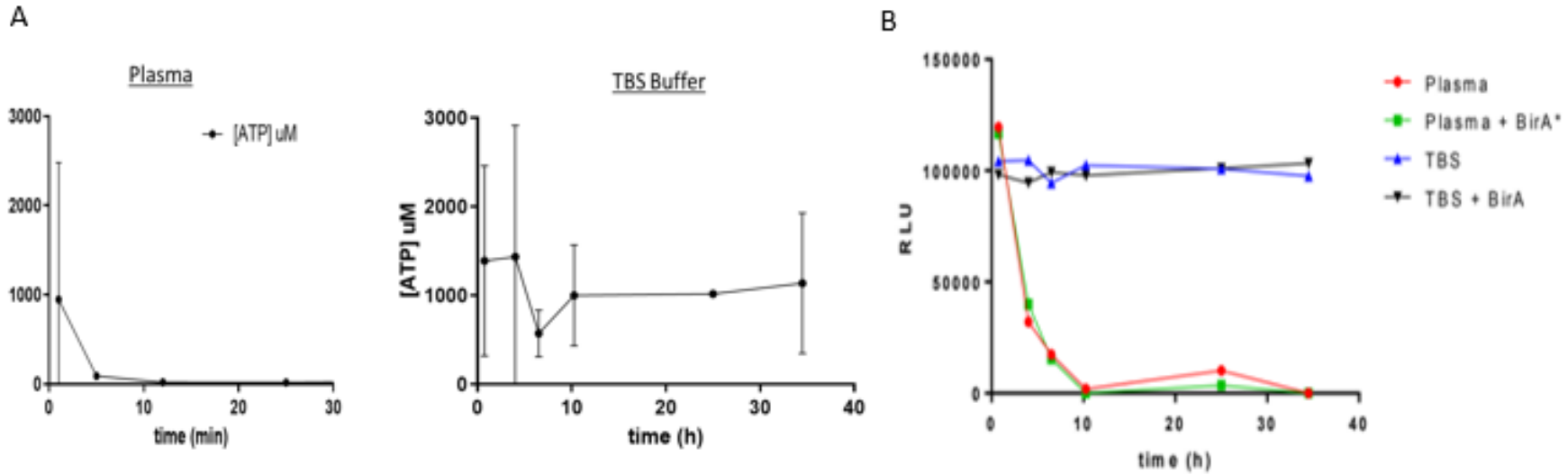

Figure 19 - ATP Stability in Plasma vs Buffer.

A) Measurement of ATP concentration in citrated plasma or TBS buffer. B) Measurement of ATP concentration in citrated plasma or TBS buffer in the presence or absence of BirA, and described as relative luminescence units (RLU), over the course of 36 hours.*

3.3.4. The Use of ATPase Inhibitors

The rapid consumption of ATP in citrated plasma was hypothesized to be caused by ATPase and phosphatase activity. Therefore, ATPase inhibitors were tested for their capacity to stabilize ATP in plasma. Plasma samples were incubated with various inhibitors (3 mM EDTA, 2 mM $NaVO_4$ (pH 10), 1 μM IBMX, 5 nM NBTI, or TBS (no inhibitor)) and the concentration of ATP was measured at different time intervals (Figure 20). EDTA demonstrated the highest preservation of ATP concentration over time. The cocktail of inhibitors ($NaVO_4$, IBMX, and NBTI) and $NaVO_4$ preserved ~40% of the starting ATP concentration at 4 hours, compared to 20% ATP for the no inhibitor condition.

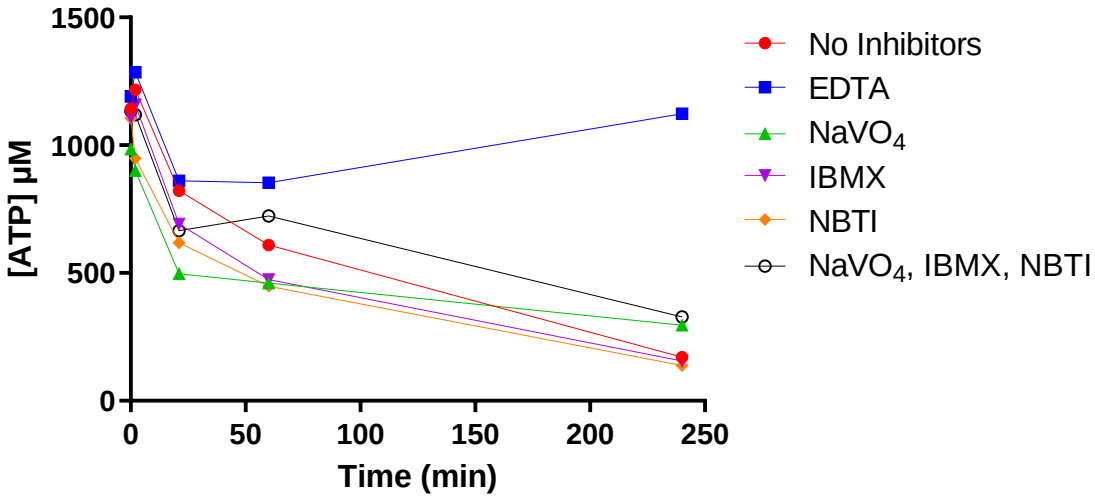

Figure 20 - Effect of Various Inhibitors on ATP Stability.

Measurement of the ATP concentration in citrated plasma in the presence or absence of various inhibitors (3 mM EDTA, 2 mM $NaVO_4$ (pH 10), 1 µM IBMX, 5 nM NBTI, or TBS (no inhibitor)) over the course of 4 hours.

Next, the impact of ATPase inhibitors on BioID labelling efficiency was tested (Figure 21). The presence of the inhibitor cocktail ($NaVO_4$, IBMX, and NBTI) decreased the biotinylation labeling of the plasma proteins, as indicated by the SYPRO-RUBY stain. This result was further confirmed by western blot, as indicated by the bands corresponding to the auto-labeling of BirA* (Figure 21). EDTA, which was the most effective at prolonging ATP concentration in citrated plasma, also inhibited all biotinylation activity in plasma. These data suggest that the presence of the ATPase inhibitors prevented BirA* from consuming ATP; and thus, our aim of further increasing ATP stability through the use of ATPase inhibitors in plasma was abolished.

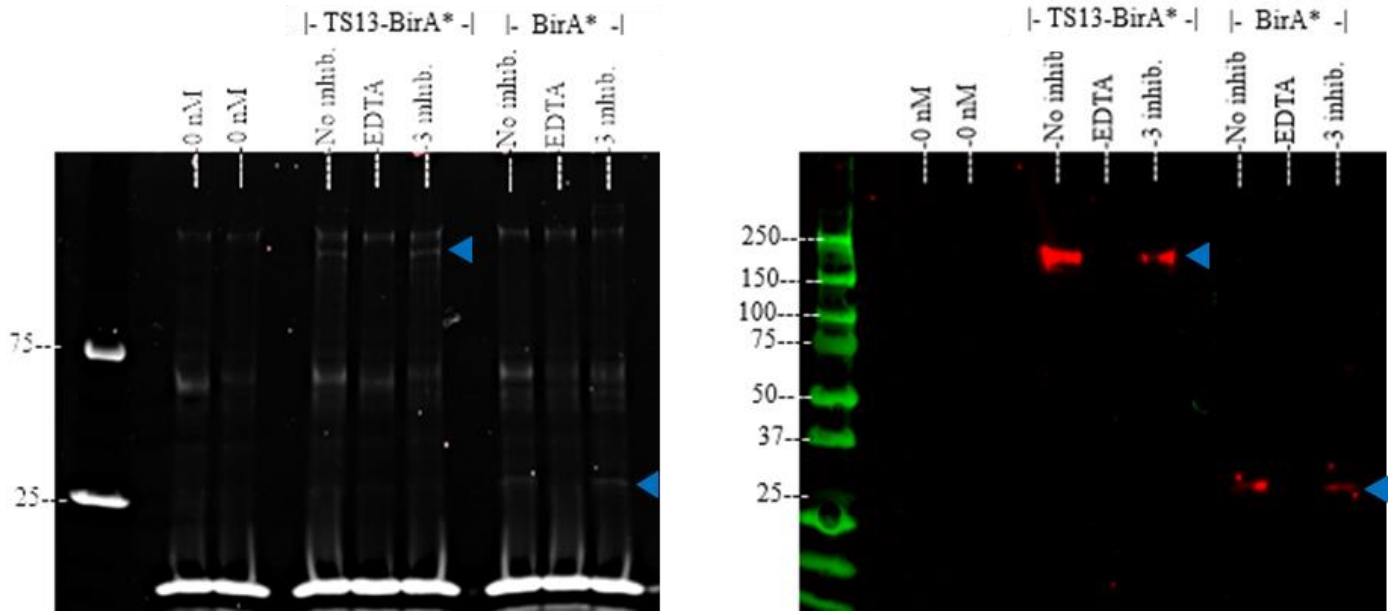

Figure 21 - Effect of Various Inhibitors on BirA* Activity.

Labeling of the plasma proteins via in-vitro BioID using 100 nM ADAMTS13-BirA or BirA*, in the presence or absence of various inhibitors (TBS (no inhibitor), 3 mM EDTA, or 3 inhibitors (2 mM $NaVO_4$ (pH 10), 1 µM IBMX, 5 nM NBTI)), over the course of a 4-hour reaction at 37°C. Labeled proteins were isolated using streptavidin-IP and separated using SDS-PAGE under reducing conditions, before visual analysis through a total protein stain (SYPRO-RUBY, left) and a western blot using the anti-FLAG antibody (right). The blue arrows represent the auto-biotinylation of biotin ligases.*

3.3.5. ATP Supplementation

We next examined whether repeated supplementation of ATP into the BioID assay can yield a greater number of labelled proteins. Therefore, ATP was supplemented at every hour for 4 hours over the course of a BioID assay (Figure 22). The gel analysis of this BioID assay revealed that supplementing ATP increased the labeling of the proteins, as indicated by the intensity of the bands, in the BirA* samples (Figure 22). The addition of ATP to plasma resulted in a dose-dependent increase in plasma protein labeling based on the increase in the intensity of the labeled bands. These data suggest that maintaining high ATP concentrations throughout the labeling experiment may yield more reproducible and robust BioID data in citrated plasma.

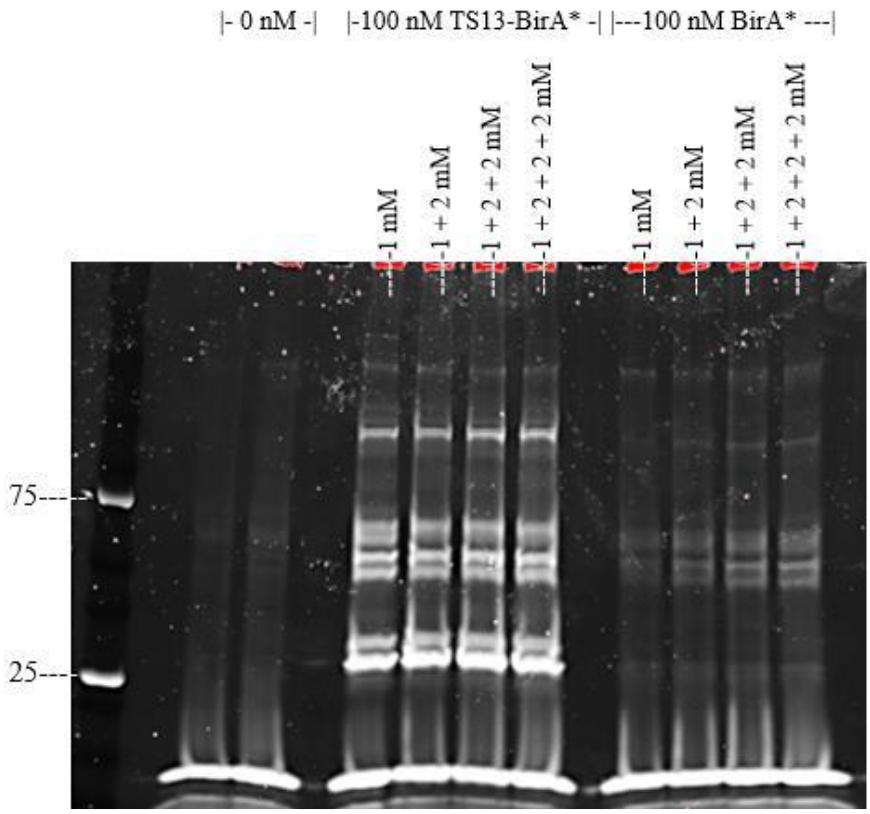

Figure 22 - Effect of ATP Supplementation on BirA* Activity

Labeling of plasma proteins via 100 nM biotin ligase as unconjugated (BirA) or fusion protein (TS13-BirA*), and increasing supplementations of ATP at every hour, for a 4-hour reaction, and visualized as a total protein stain using SYPRO-RUBY.*

3.3.6. Different Anticoagulants

Citrate acts as a calcium chelator to prevent plasma from clotting (312, 313). However, it also chelates other divalent cations like Mg^{2+}, which are important for the phosphatase activity of the BirA enzyme (315). Therefore, we next tested whether collecting plasma in a different anti-coagulant could improve the yields of our BioID assay. Collected citrated pooled normal plasma was recalcified to 20 mM $CaCl_2$ while adding 50 µg/mL of Hirudin, a potent thrombin inhibitor (32.8 µM). The BioID assay was performed (refer to section 2.5.1) with the exception in the use of a larger volume (1 mL). Despite the ATP concentration may be limiting the number of hits, the concentration of ATP remained the same as the previous mass spectrometry run, and additional ATP was not supplemented to maintain a fair comparison of the two anticoagulants.

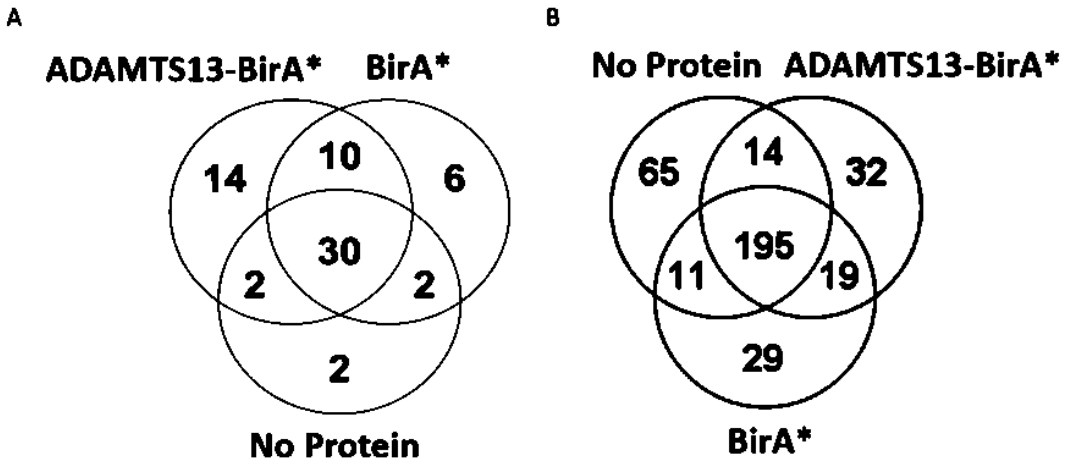

Figure 23 - Mass Spectrometry Results of *In-Vitro* BioID in Varying Anti-Coagulants.

Total number of labeled proteins identified from using LC/MS/MS analysis on in-vitro BioID assay of either 25 nM (A) or 50 nM (B) ADAMTS13-BirA, BirA* or no protein, labeled overnight in citrated plasma (A) or calcified and hirudin-treated plasma (B). In the citrated plasma assay (A), the total number of labeled proteins was 66, 14 of which were unique to ADAMTS13. In calcified and hirudin-treated plasma (B), the total number of labeled proteins was 365, 32 of which were unique to ADAMTS13.*

Results from mass spectrometry analysis found the total number of proteins labelled across all samples were 365 proteins, 32 of which were unique to ADAMTS13-BirA* (Figure 23 B). Whereas, after recalcifying the citrated plasma, the total number of proteins labelled across all samples decreased to 66, 14 of which were unique to ADAMTS13-BirA* (Figure 23 A). Although the number of proteins that were unique to ADAMTS13-BirA* increased compared to the previous run, a closer examination of the mass spectrometry results showed this result was likely due to increased nonspecific labeling and was likely due to insufficient washing of the streptavidin-coated beads following pull-down. Furthermore, through the analysis of one-way ANOVA between each category, and a significance of $p < 0.05$, only 4 proteins were identified for ADAMTS13-BirA* (Table 5). As expected, the autobiotinylation of ADAMTS13 was identified as the highest number of hits within the sample group (Table 5). Comparing these results to the previous attempt (Tables 5-6), only tubulin β-chain (TUBB) was identified in both attempts.

This series of optimization experiments indicate that rapid ATP consumption is the most limiting factor in plasma BioID assays. The optimal plasma BioID protocol, therefore, requires regular supplementation of ATP throughout the labelling period. Additionally, special care was taken during the wash steps following streptavidin IP to change the tubes regularly to reduce the contamination of unlabelled proteins in the mass spectrometry datasets.

Table 5 - Mass Spectrometry Results of *In-Vitro* BioID in Varying Anti-Coagulants.

Labelled Proteins	**Molecular Weight**	**ADAMTS13-BirA*[1]**	
		Citrate	**Hirudin**
A disintegrin and metalloproteinase with thrombospondin motifs 13	154 kDa	151	33
Actin, cytoplasmic 1	42 kDa	13	0
Creatine kinase B-type	43 kDa	2	0
Elongation factor 1-alpha 1	50 kDa	3	0
Heat shock protein HSP 90-beta	83 kDa	2	0
Immunoglobulin kappa variable 2D-30	13 kDa	5	0
Polyubiquitin-B	26 kDa	3	0
Protein RJ1	16 kDa	3	0
Pyruvate kinase PKM	58 kDa	6	0
Serum paraoxonase/arylesterase 1	40 kDa	5	0
Tubulin alpha-1B chain	50 kDa	15	2
Tubulin beta-4B chain	50 kDa	14	2
UHRF1-binding protein 1-like	164 kDa	2	0
Histone, H2B type 1-K	14 kDa	0	3

[1]*Total number of significant peptides identified from using LC/MS/MS analysis on in-vitro BioID assay labeled overnight in citrated plasma or calcified and hirudin-treated plasma.*

3.3.7. Mass Spectrometry – Optimized Conditions

In-vitro plasma BioID was further optimized after the examination of many different variables that played a role in the success of the assay. Such variables include: concentration of BirA*, volume of plasma, type of streptavidin beads (agarose versus magnetic), concentration of biotin, number of washes, and length of incubation periods for labeling, immunoprecipitation, and washes. Previous experiments evaluated the impact of these variables on BioID labeling efficiency using SDS-PAGE and total protein stain (SYPRO-RUBY). These conditions were also evaluated using western blots targeting VWF, BirA*, anti-ADAMTS13, and/or streptavidin.

After many iterations, the optimal plasma BioID assay was performed in replicates of 5. This assay consisted of 100 µM ADAMTS13-BirA* or 100 µM BirA* or no protein (PBS buffer), along with 50 µM biotin and supplementation of 1 mM ATP every hour for 4 hours, added to 1 mL of citrated plasma. Biotinylated proteins were isolated using streptavidin agarose beads. Results from the mass spectrometry data analysis identified an average of 225 proteins in the negative control (no BirA*), 235 proteins with unconjugated BirA*, and 466 proteins with ADAMTS13-BirA* (Figure 24A). Among these, 199 proteins were uniquely present in ADAMTS13-BirA* samples, and 50 proteins that were absent from the negative control samples (no BirA*) but present in both BirA* and ADAMTS13-BirA* indicating some direct interaction with the biotin ligase or non-specific protein labeling (Figure 24A). Proteomics data were further analyzed for significance to ADAMTS13-BirA* ($p<0.05$) using one-way ANOVA, whereby 108 proteins were identified to have significant interaction with ADAMTS13-BirA* (Figure 24B). This

analysis removed proteins with extremely low counts and allowed the analysis of proteins identified in more than one condition to be compared for a significant difference in one condition over the others.

Of the 108 proteins significantly labeled by ADAMTS13-BirA*, 95 are known to be intracellular, 8 are transmembrane proteins, and 5 are extracellular proteins (Table 6). ADAMTS13 was the most abundant protein identified in the ADAMTS13-BirA* BioID reaction, with an average peptide count of 478, and was not identified in the unconjugated BirA* reaction or negative control samples, providing evidence of auto-biotinylation of the fusion protein.

VWF was identified in the ADAMTS13-BirA* reactions with an average peptide count of 1.8. By comparison, VWF had an average peptide count of 0.2 and 0.4 in the BirA* and negative control, respectively. The weak labeling of VWF by ADAMTS13-BirA* may be a result of the reaction being conducted in the absence of flow conditions, and sufficient fluid shear stress is required to optimize their interaction (see discussion) (126, 323). ADAMTS13-BirA* samples were enriched for cell-associated proteins like actin and tubulin, which may reflect the labeling of receptors on the surface of plasma microparticles such as CD36, which is known to bind to proteins containing type 1 thrombospondin domains, including ADAMTS13 (see discussion) (199). The plasma proteins vitronectin and plasminogen were enriched in all samples yet were significantly enriched in the ADAMTS13-BirA* condition and were subsequently tested in validation studies as novel ligands to ADAMTS13.

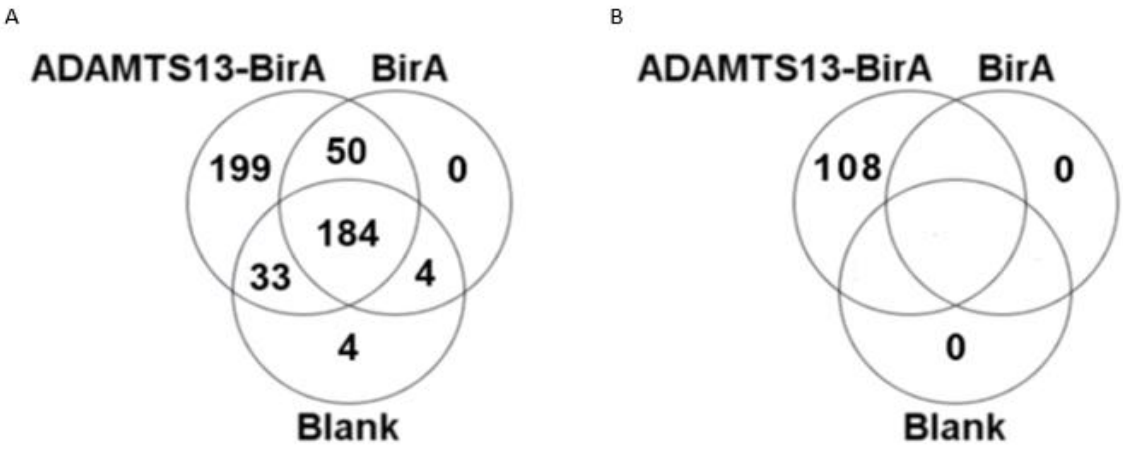

Figure 24 - Mass Spectrometry Results Using Optimized Conditions.

Venn diagram of proteins labeled from BioID assay of 100 nM ADAMTS13-BirA, BirA* or PBS buffer (no protein) in citrated plasma, with 1 mM ATP added every hour, and 50 µM biotin, at 37°C for 4 hours. Labeled proteins were isolated using agarose streptavidin beads, digested with trypsin, analyzed, and identified using LC-MS/MS. A) The numbers represent the number of unique labeled proteins present in each condition. B) The numbers represent the number of unique labeled proteins significant to ADAMTS13-BirA* ($p<0.05$).*

Table 6 - Spectral Counts of Extracellular Proteins Identified Significant to ADAMTS13.

		ADAMTS13 (A)							BirA (B)								No Protein (N)							
		Peptide Count[1]							Peptide Count[1]							A_B pValue[2]	Peptide Count[1]							A_N pValue[2]
Protein	**MW (kDa)**	A1	A2	A3	A4	A5	Avg	S.Dev	B1	B2	B3	B4	B5	Avg	S.Dev		N1	N2	N3	N4	N5	Avg	S.Dev	
A disintegrin and metalloproteinase with thrombospondin motifs 13	154	422	426	351	1021	170	478	286.9	0	0	0	0	0	0	0.0	0.004	0	0	0	0	0	0	0.0	0.004
Vitronectin	54	109	86	68	102	29	78.8	28.6	30	24	29	34	39	31.2	5.0	0.003	24	24	23	33	31	27	4.1	0.005
Plasminogen	91	36	27	10	68	7	29.6	22.0	3	3	6	0	1	2.6	2.1	0.022	2	4	1	0	0	1.4	1.5	0.028
von Willebrand factor	309	2	2	3	2	0	1.8	1.0	0	1	0	0	0	0.2	0.4	0.031	1	1	0	0	0	0.4	0.5	0.015
Stanniocalcin-2	33	2	2	2	1	0	1.4	0.8	0	0	0	0	0	0	0.0	0.003	0	0	0	0	0	0	0.0	0.003

[1]Total number of peptides identified from using LC/MS/MS analysis on in-vitro BioID assay under optimized condition.

[2]Significant analysis for each protein identified between the peptide count in each condition calculated using one-way ANOVA with a posthoc Tukey HSD test through RStudio whereby $p<0.05$ is significant.

3.4. Validation of Novel Interactions

3.4.1. ELISA Plate Binding Assay

The interaction between ADAMTS13 and vitronectin was first tested using an ELISA-plate binding assay. ADAMTS13-BirA* or BirA* were added to a 96-well coated with either vitronectin or BSA (refer to 2.6.1). Increasing concentrations of ADAMTS13-BirA* and BirA* resulted in higher absorbance values, indicating greater binding to the coated proteins (Figure 25). In addition, the binding of ADAMTS13-BirA* and BirA* to vitronectin was higher than to BSA. Although this assay confirmed that ADAMTS13-BirA* can bind to vitronectin, the unconjugated BirA* also bound to vitronectin. Thus, the interaction of vitronectin to ADAMTS13-BirA* may be to that of BirA* and not specific to ADAMTS13. This was subsequently confirmed using SPR, in which wild-type ADAMTS13 did not bind to vitronectin.

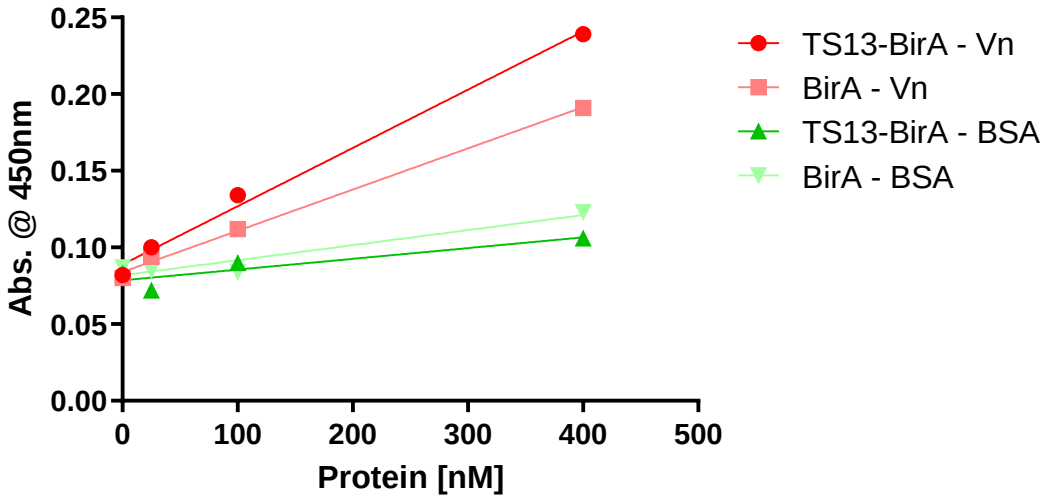

Figure 25 - ELISA Plate Binding Assay.

ELISA plate of ADAMTS13-BirA or BirA* binding to wells coated with 5 µg/mL vitronectin (Vn) or bovine serum albumin (BSA). The wells were blocked with 5% for 2 hours, then increasing concentrations of the FLAG-tagged biotin proteins were incubated with the wells covered with Vn or BSA. Binding was detected with an HRP-conjugated anti-FLAG antibody.*

3.4.2. BioLayer Interferometry

The interaction between potential novel ligands and ADAMTS13 was also examined using ForteBio's BLI instrument, the Blitz. The binding affinity was examined for a change in signal, represented by the binding length (nm), which is read and analyzed by the Blitz software. The binding affinity (K_d) was calculated by the software as determined by a non-linear regression fit curve.

After immobilizing wt-ADAMTS13 onto the biosensor, all tested ligands (VWF, vitronectin, BSA, streptavidin, actin, and anti-FLAG IgG) showed an increase in the signal of the binding signal (Figure 26). The highest value increase was in the presence of anti-FLAG antibody, with a K_d value of 4×10^{-8} M and an R^2 value of 0.95 (Figure 26, Table 7). VWF, the only known substrate for ADAMTS13's, had a K_d value $<1 \times 10^{-12}$ M (Figure 26, Table 7). While it was expected for VWF to have a high affinity, the K_d value observed was outside of the measurable parameters. In addition, performing the assay in the absence of shear makes this K_d value an unreliable affinity estimate. The negative controls, streptavidin, and BSA did display an increase in binding signal, the amplitude of the signal was lower than that of anti-FLAG and VWF's signals (Figure 26, Table 7). In addition, the R^2 value of streptavidin and BSA were <0.9, thus, suggesting that streptavidin and BSA did not bind to wt-ADAMTS13. Vitronectin gave the third-highest amplitude increase in binding signal, with K_d values of 7.2×10^{-8} M and 1.1×10^{-7} M, with an R^2 value of 0.93 and 0.97 respectively (Figure 26, Table 7); suggesting that ADAMTS13 may interact with vitronectin. However, vitronectin also bound to immobilized BSA, suggesting that vitronectin's interactions may be non-specific. Interestingly, actin showed a very low

increase (<0.1 nm) increase in binding signal but displayed a K_d value of 4.2 x 10^{-7} M and an R^2 value of 0.93 (Figure 26, Table 7); suggesting that further tests between ADAMTS13 and actin are recommended.

To further validate the binding affinities between the various analytes and the immobilized ADAMTS13, parallel binding experiments were conducted with BSA-coupled biosensors. After immobilizing BSA onto the biosensors, all tested ligands (vitronectin, ADAMTS13) showed an increase in the signal of the binding signal (Figure 27). Both vitronectin and ADAMTS13 showed an increase in the amplitude of the binding signal and provided K_d values of 4.7 x 10^{-6} M and 4.8 x 10^{-7} M with R^2 values of 0.92 and 0.96 respectively (Figure 27, Table 7). These values were similar in the values of the binding affinities between vitronectin or actin and ADAMTS13, suggesting that the binding interaction between ADAMTS13 and these substrates may be non-specific.

A

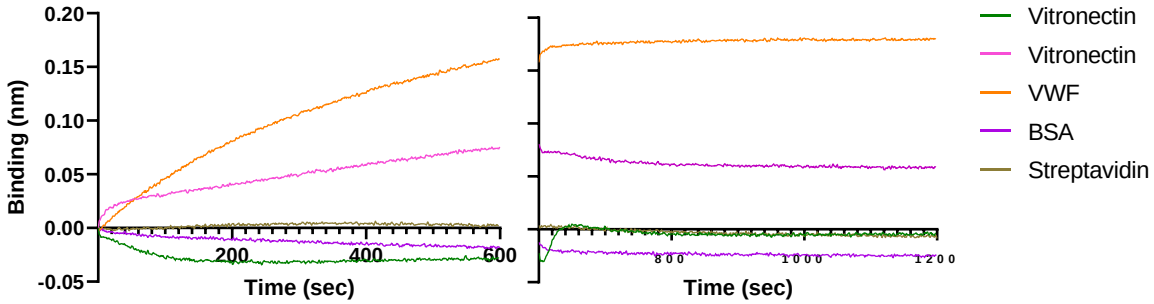
Binding (nm)
0.20
0.15
0.10
0.05
0.00
-0.05
200
400
600
800
1000
1200
Time (sec)
Time (sec)
Vitronectin
Vitronectin
VWF
BSA
Streptavidin

B

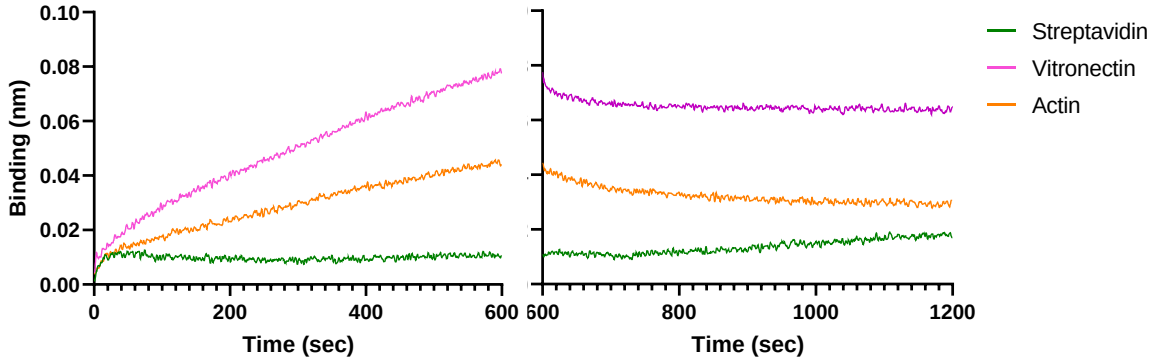
Binding (nm)
0.10
0.08
0.06
0.04
0.02
0.00
0
200
400
600
800
1000
1200
Time (sec)
Time (sec)
Streptavidin
Vitronectin
Actin

C

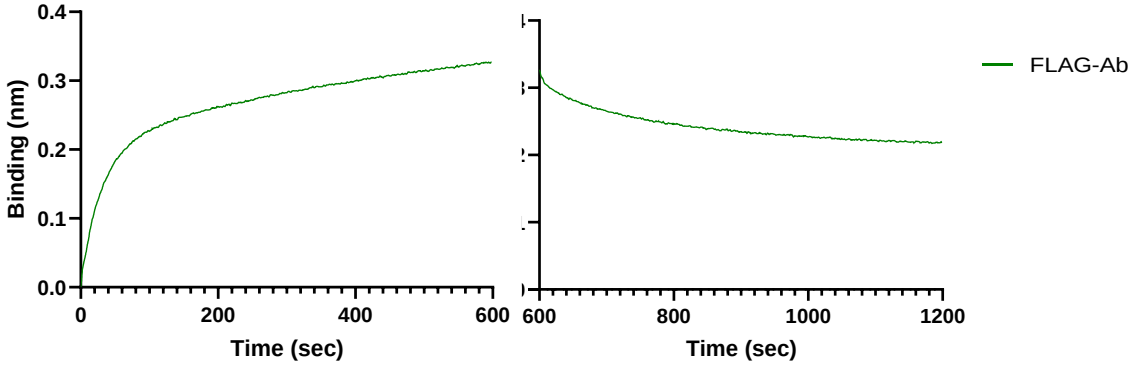
Binding (nm)
0.4
0.3
0.2
0.1
0.0
0
200
400
600
800
1000
1200
Time (sec)
Time (sec)
FLAG-Ab

Figure 26 - Binding Curves of Various Analytes onto Immobilized ADAMTS13 using BLI.

Binding curves (association – left, dissociation – right; trial 1 – A, trial 2 – B, trial 3 – C) of 375 nM of various proteins (vitronectin, VWF, BSA, streptavidin, actin, or FLAG-AB) to immobilized wt-ADAMTS13. The data, as real-time binding curve (colored) were generated through ForteBio's the Blitz software. K_d *values, calculated by the software, are reported in Table 7.*

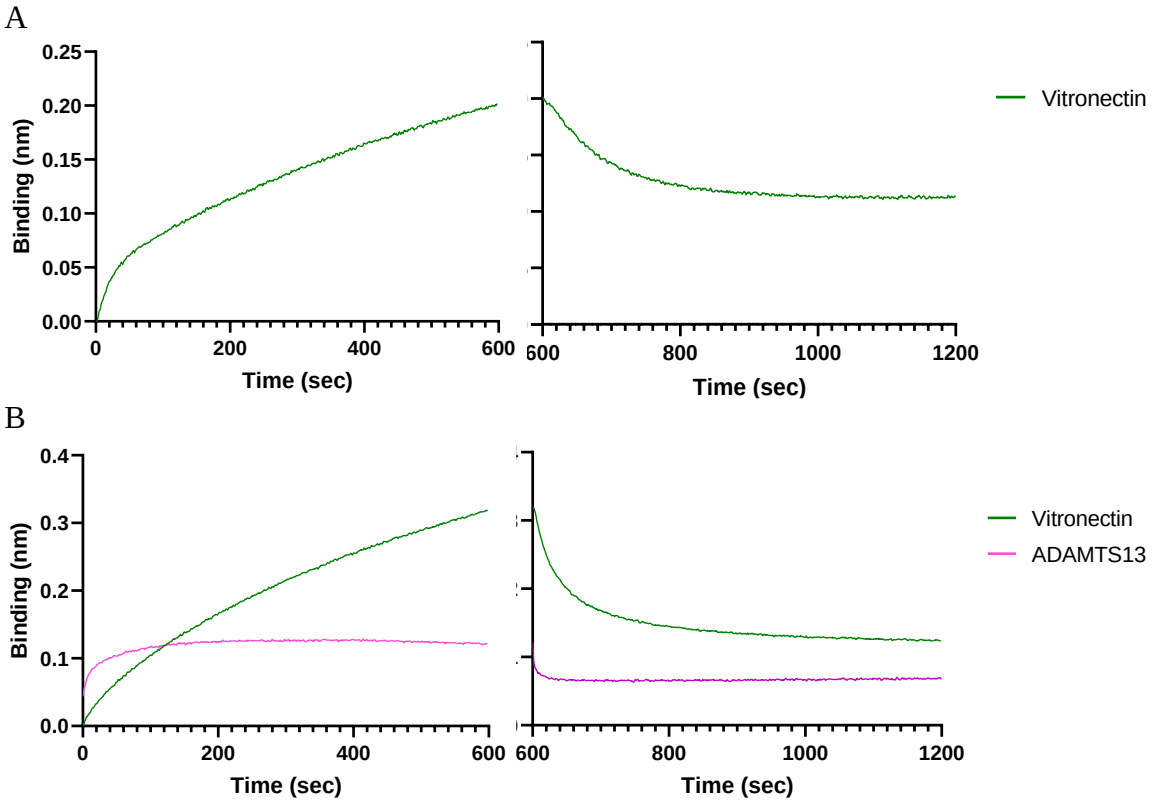

Figure 27 - Binding Curves of Various Analytes onto Immobilized BSA using BLI.

Binding curves (association – left, dissociation – right; trial 1 – A, trial 2 – B) of 375 nM vitronectin or ADAMTS13 to 37.5 nM BSA that was immobilized to a biosensor using amine-coupling. The data was plotted as raw data (colored) and line of best fit (black), and both were generated through ForteBio's the Blitz software. K_d values, calculated by the software, are reported in Table 7.

Table 7 - Binding Affinities of Various Analytes onto Immobilized ADAMTS13 or BSA.

	ADAMTS13		**BSA**	
Analyte	**K_d (µM)**	**R^2**	**K_d (µM)**	**R^2**
Vitronectin	0.1	0	1.2	0.9482
	7.2	0.9284	4.7	0.9231
	0.1	0.9653	N.D.	N.D.
VWF	$<1 \times 10^{-6}$	0.9830	N.D.	N.D.
Streptavidin	2077	0.2835	N.D.	N.D.
	$<1 \times 10^{-6}$	0.0584	N.D.	N.D.
Actin	0.4	0.9274	N.D.	N.D.
FLAG-Ab	4×10^{-2}	0.9541	N.D.	N.D.
BSA	0.1	0	N.D.	N.D.
ADAMTS13	N.D.	N.D.	0.5	0.9632

N.D. – Not Determined

3.4.3. Surface Plasmon Resonance

The binding affinities of vitronectin and plasminogen (Glu-Pg) to immobilized ADAMTS13, were examined using SPR (refer to 2.6.3). Glu-Pg showed a saturable binding profile with increasing concentrations (Figure 28). The K_d of Glu-Pg was calculated to 2.8 ± 0.3 µM. Interestingly, vitronectin also showed an increase in amplitude RUs as the concentration of vitronectin increased. However, a K_d value could not be calculated because the profiles did not saturate at physiologically relevant concentrations. BSA was utilized as a negative control and did not bind to immobilized ADAMTS13.

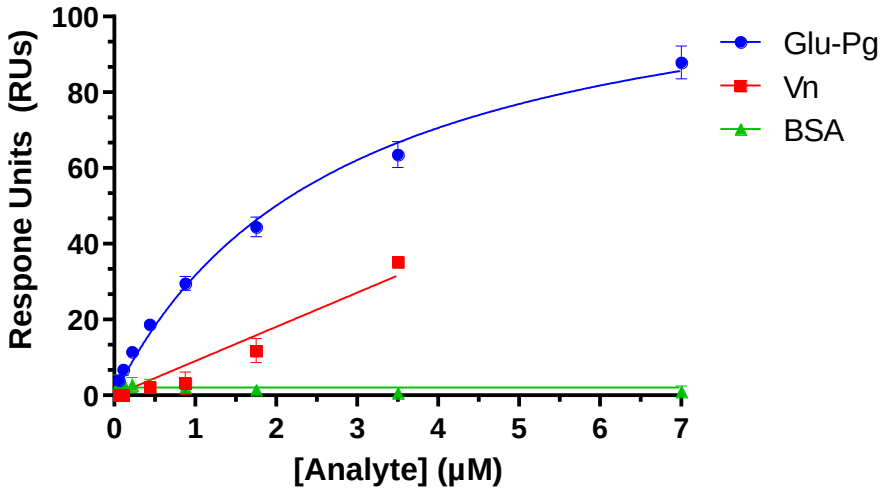

Figure 28 - Binding Curves of Pg, Vn, or BSA onto immobilized ADAMTS13 using SPR.

Glu-Pg, Vn, and BSA at varying concentrations 0-7 µM in HEPES-saline buffer at a flow rate of 20 µL/min were injected onto immobilized ADAMTS13 for 60 seconds and the binding profiles were visualized by Biacore T200 evaluation software.

We next performed binding experiments with vitronectin (Vn), VWF, and a control (BSA) to examine the binding interactions between these analytes and ADAMTS13 or MDTCS.

The binding profile of Vn demonstrated a slight increase in amplitude RUs as the concentration of the interacting Vn increased (Figures 29-31). With 3.5 µM of the analyte, Vn increased to about 20 RUs onto ADAMTS13 and 15 RUs onto MDTCS (Figures 29-31). In comparison to Glu-Pg which saturated at 80 RUs at 3.5 µM (Figure 32), Vn displayed poor binding to ADAMTS13. In addition, with a poor binding profile and a lack of saturation point, the binding affinity of Vn onto ADAMTS13 and MDTCS could not be determined.

Interestingly, VWF multimers, which are reported to have a K_d value of 70-90 nM to ADAMTS13 (200), did not show any binding interaction with ADAMTS13 and MDTCS using SPR and a K_d value could not be calculated (Figures 29-31). This result was likely due to the nature of the Biacore system and the absence of high shear stress that is required. Similarly, BSA, which served as our negative control, also did not display any binding interaction with ADAMTS13 nor MDTCS and a K_d was not determined (Figures 29-31).

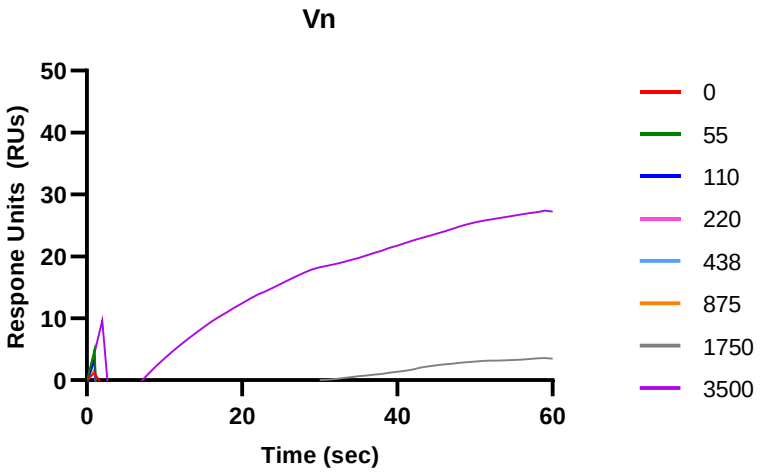
Vn
Respone Units (RUs)
50
40
30
20
10
0
0
20
40
60
Time (sec)
0
55
110
220
438
875
1750
3500

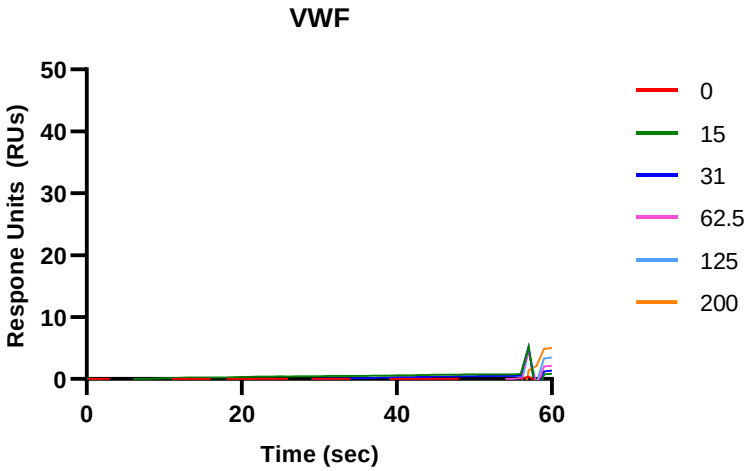
VWF
Respone Units (RUs)
50
40
30
20
10
0
0
20
40
60
Time (sec)
0
15
31
62.5
125
200

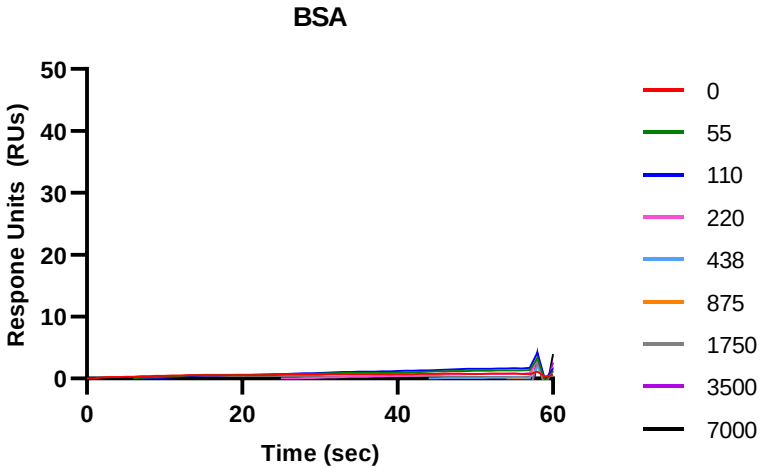
BSA
Respone Units (RUs)
50
40
30
20
10
0
0
20
40
60
Time (sec)
0
55
110
220
438
875
1750
3500
7000

Figure 29 - Binding Curves of Vn, VWF and BSA onto Immobilized ADAMTS13 using SPR.

Vn, VWF, and BSA at varying concentrations 0-7 μM in HEPES-saline buffer at a flow rate of 20 μL/min were injected onto immobilized ADAMTS13 for 60 seconds and the binding profiles were visualized by Biacore T200 evaluation software.

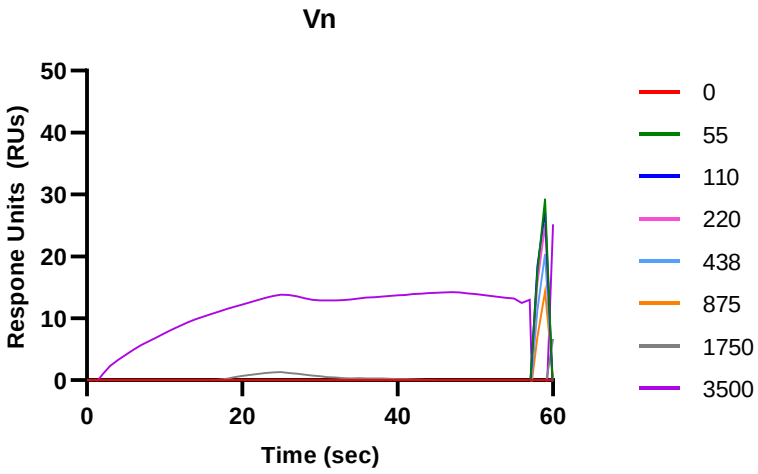
Vn
Respone Units (RUs)
50
40
30
20
10
0
0
20
40
60
Time (sec)
0
55
110
220
438
875
1750
3500

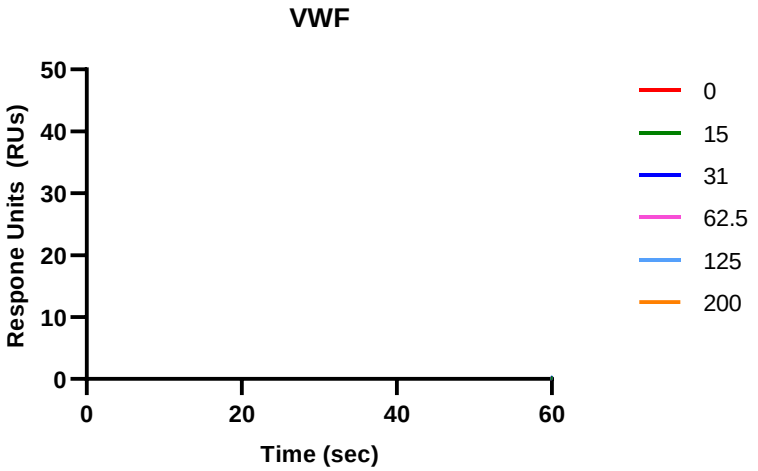
VWF
Respone Units (RUs)
50
40
30
20
10
0
0
20
40
60
Time (sec)
0
15
31
62.5
125
200

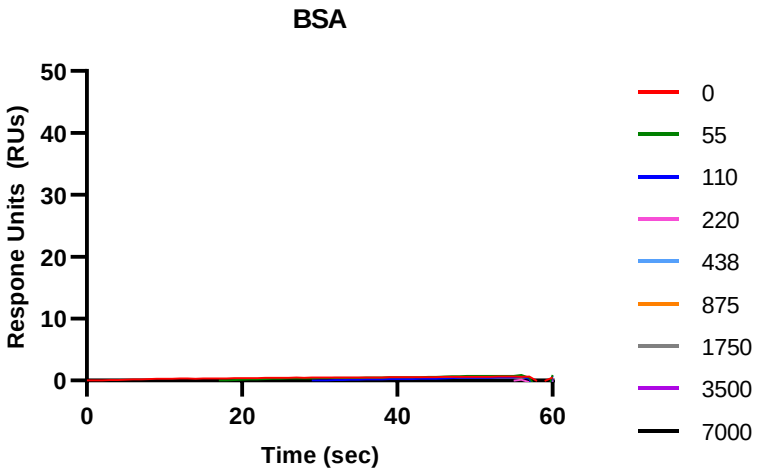
BSA
Respone Units (RUs)
50
40
30
20
10
0
0
20
40
60
Time (sec)
0
55
110
220
438
875
1750
3500
7000

Figure 30 - Binding Curves of Vn, VWF and BSA onto Immobilized MDTCS using SPR.

Vn, VWF, and BSA at varying concentrations 0-7 μM in HEPES-saline buffer at a flow rate of 20 μL/min were injected onto immobilized MDTCS for 60 seconds and the binding profiles were visualized by Biacore T200 evaluation software.

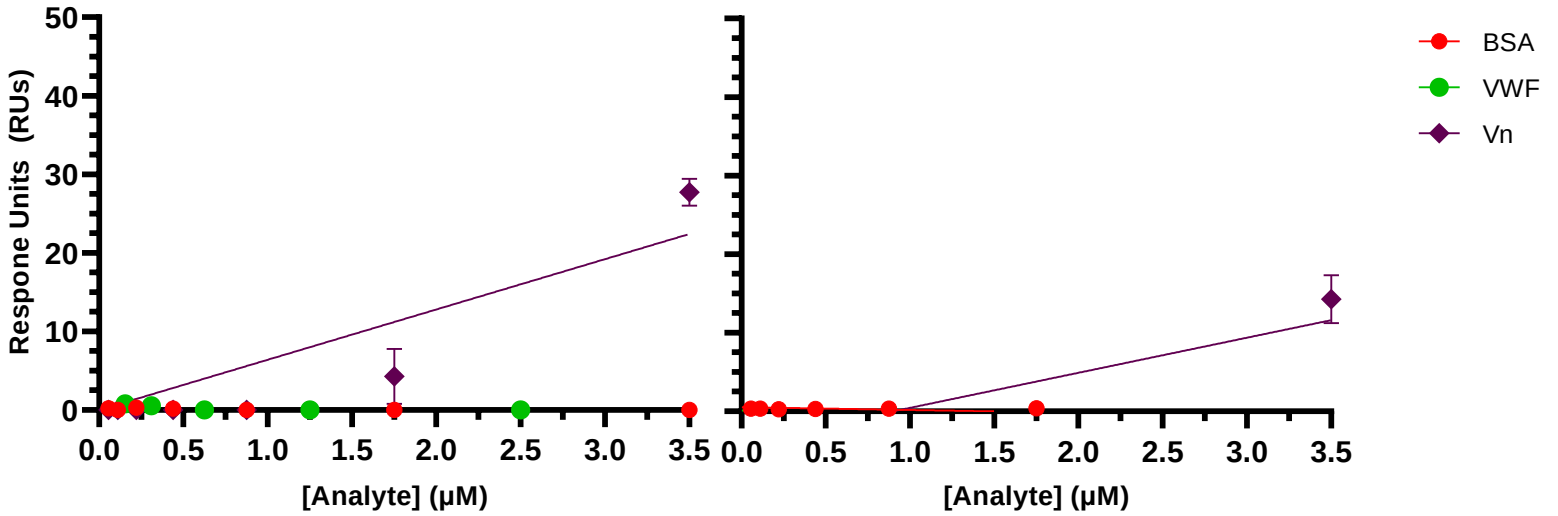

Figure 31 - Non-Linear Regression Models of Vn, VWF and BSA Binding to Immobilized ADAMTS13 and MDTCS.

Vn, VWF, and BSA at varying concentrations 0-7 µM in HEPES-saline buffer at a flow rate of 20 µL/min were injected onto immobilized ADAMTS13 (left) or MDTCS (right), and the binding profiles were visualized by GraphPad Prism using a one-site binding model.

After confirmation of ADAMTS13 binding to Glu-Pg, various forms of Pg were examined for binding to ADAMTS13 and MDTCS to map their binding interface. The binding profiles of the various forms of Pg increased in amplitude RUs as the concentration of the interacting analyte increased (Figures 32-34). With 7 μM of the analyte, Lys-Pg saturated near 240 RUs, Glu-Pg saturated near 120 RUs, and with 3.5 μM of analyte mini-Pg saturated near 70 RUs, and μ-Pg saturated near 30 RUs. In contrast, all of the various of Pg showed no dose-dependent binding to MDTCS (Figure 32). These binding profiles suggest that the TSP-CUB domains of ADAMTS13 bind to plasminogen. As the truncated form of Pg became smaller and the number of Kringle domains decreased (Glu-Pg > mini-Pg > micro-Pg) the binding affinity of Pg onto immobilized ADAMTS13 increased. This result was evident by the decrease in the dissociation constant, as the truncated form of Pg became smaller (Figures 33-34). The K_d values of the various forms of Pg binding onto immobilized ADAMTS13 were calculated to be Glu-Pg 2.78 ± 0.29 μM, Lys-Pg 0.98 ± 0.16 μM, Mini-Pg 1.48 ± 0.36 μM, and μ-Pg 11.36 ± 12.21 μM (Table 8).

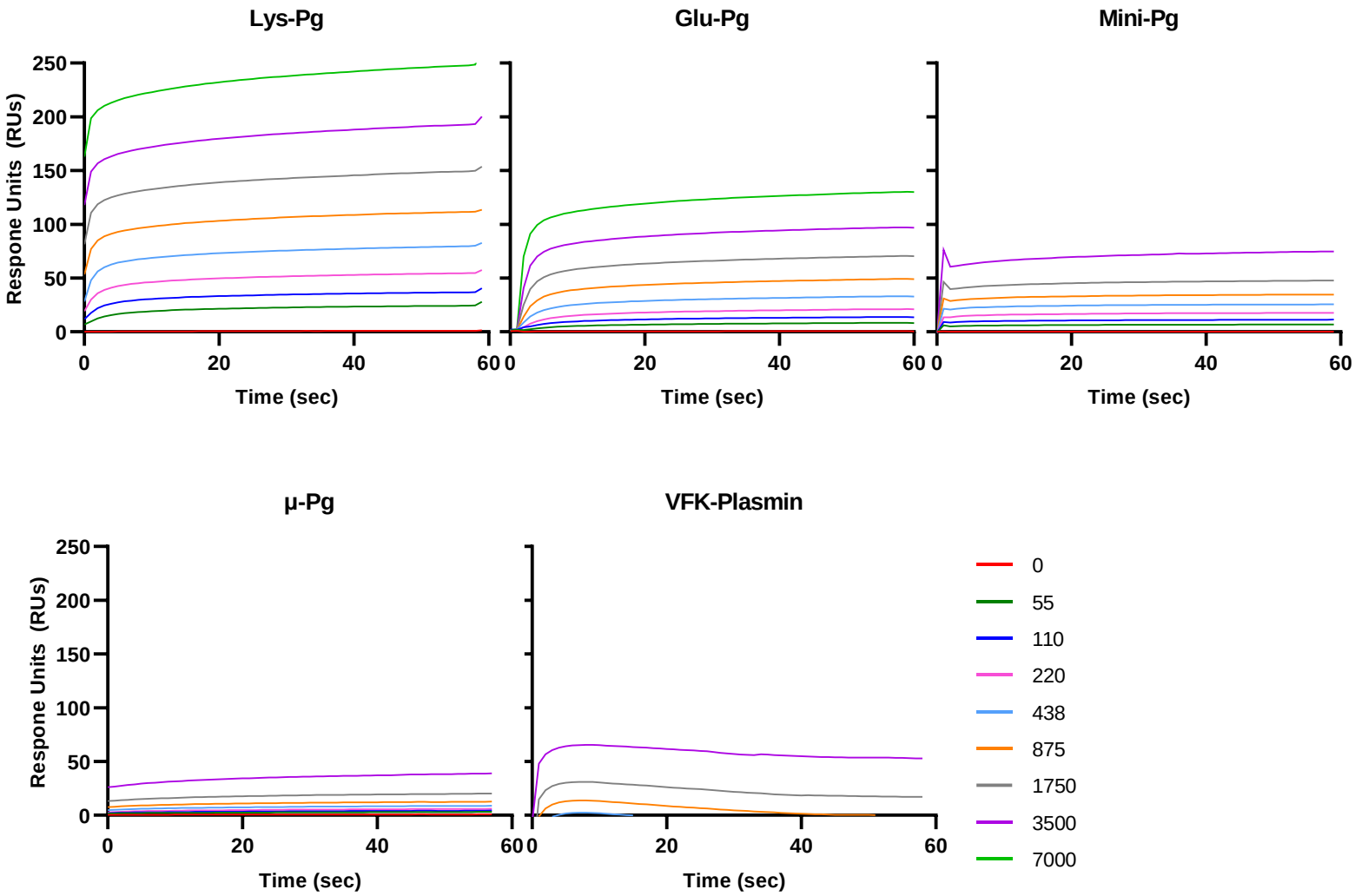
Lys-Pg
Glu-Pg
Mini-Pg
μ-Pg
VFK-Plasmin
Respone Units (RUs)
Time (sec)
0
20
40
60
50
100
150
200
250
0
55
110
220
438
875
1750
3500
7000

Figure 32 - Binding Curves of Various Forms of Plasminogen onto Immobilized ADAMTS13 using SPR.

Various forms of Plasminogen (Lys-Pg, Glu-Pg, mini-Pg, μ-Pg, VFK-plasmin) at varying concentrations 0-7 μM in HEPES-saline buffer at a flow rate of 20 μL/min were injected onto immobilized ADAMTS13 for 60 seconds and the binding profiles were visualized by Biacore T200 evaluation software.

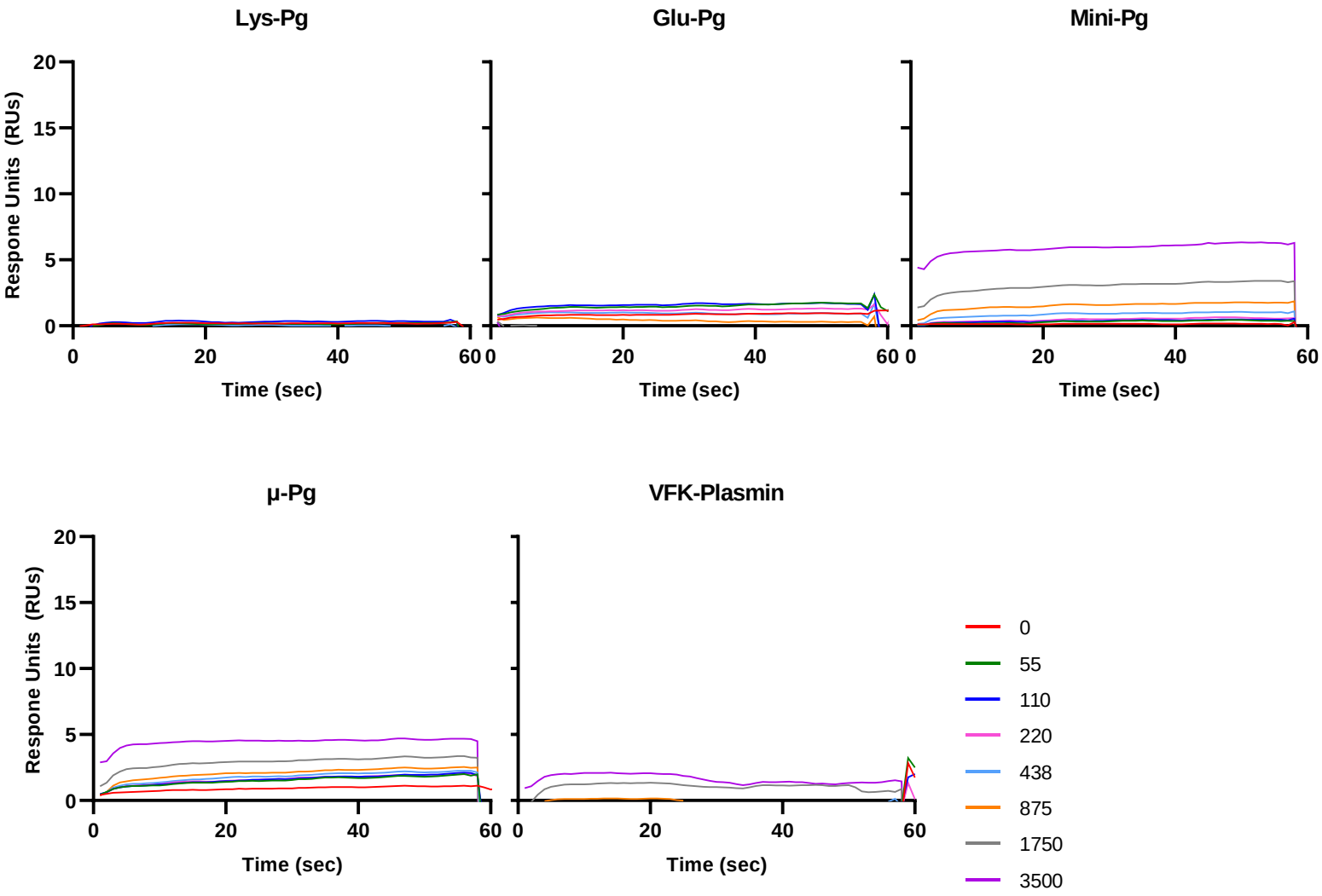
Lys-Pg
Glu-Pg
Mini-Pg
μ-Pg
VFK-Plasmin
Respone Units (RUs)
Time (sec)
0
20
40
60
5
10
15
0
55
110
220
438
875
1750
3500

Figure 33 - Binding Curves of Various Analytes onto Immobilized MDTCS using SPR.

Various forms of Plasminogen (Lys-Pg, Glu-Pg, mini-Pg, μ-Pg, VFK-plasmin) at varying concentrations 0-7 μM in HEPES-saline buffer at a flow rate of 20 μL/min were injected onto immobilized MDTCS for 60 seconds and the binding profiles were visualized by Biacore T200 evaluation software.

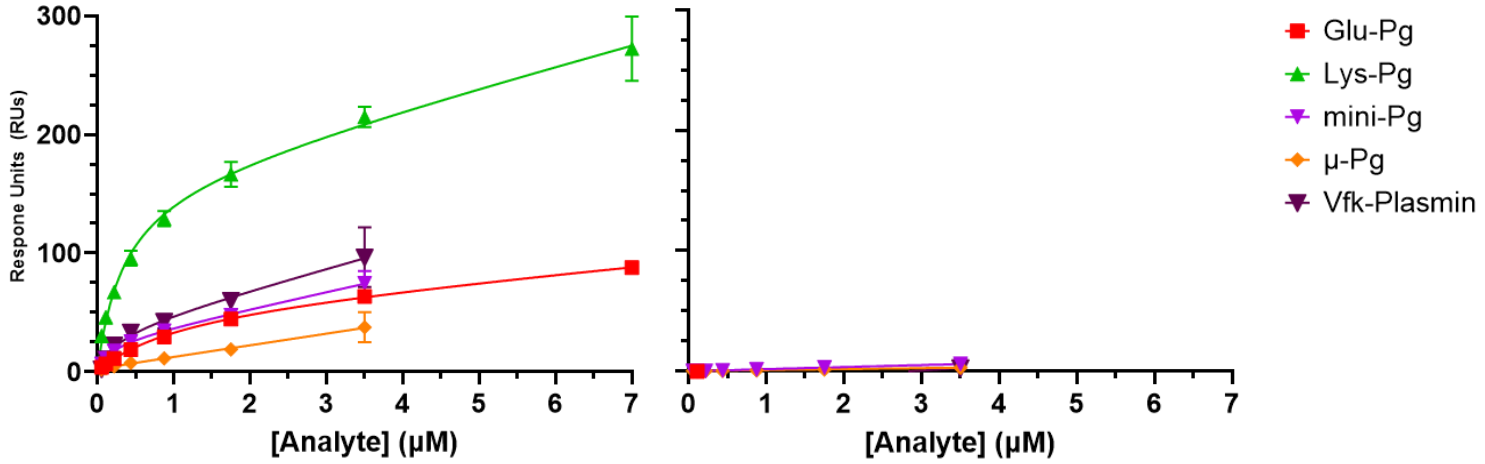

Figure 34 - Non-Linear Regression Models of Various Analytes' Affinity to Immobilized ADAMTS13 and MDTCS.

Various forms of Plasminogen (Lys-Pg, Glu-Pg, mini-Pg, and μ-Pg) at varying concentrations 0-7 μM in HEPES-saline buffer at a flow rate of 20 μL/min were injected onto immobilized ADAMTS13 (left) or MDTCS (right) and the binding profiles were visualized by GraphPad Prism using a one-site binding model.

Table 8 - Binding affinities of various forms of plasminogen's affinity onto immobilized ADAMTS13.

Analyte	**ADAMTS13**
	K_D (μM)
Lys-Pg	0.98 ± 0.16
Glu-Pg	2.78 ± 0.29
Mini-Pg	1.48 ± 0.36
μ-Pg	11.36 ± 12.21

These domain truncation experiments suggested that the C-terminus of ADAMTS13 was binding to the Kringle domains of plasminogen. Plasminogen contains 5 Kringle domains that play an important role in plasminogen activation and plasmin activity (325). For example, Kringle I and Kringle V bind to exposed lysine residues on fibrinogen and accelerate plasminogen activation by tPA and plasmin degradation (325). Therefore, we next performed competition with the anti-fibrinolytic agents tranexamic acid (TXA) or epsilon aminocaproic acid (EACA) to examine the importance of the lysine-binding Kringle domains to the interaction between plasminogen and ADAMTS13. The response in the binding affinity of Lys-Pg or Glu-Pg to immobilized ADAMTS13 decreased as the concentration of the lysine analogue, EACA or TXA, increased (Figure 35). Using 5 mM EACA, Glu-Pg and Lys-Pg decreased to 25 RUs and 15 RUs respectively. In contrast, using 5 mM EACA, Glu-Pg and Lys-Pg decreased to 16 RUs and 8 RUs respectively (Figure 33). The determined IC_{50} values of EACA and TXA were similar when almost doubled when comparing Glu-Pg to Lys-Pg (Table 9). The determined IC_{50} values of EACA to Glu-Pg and Lys-Pg were 409.6 ± 96.5 µM and 175.2 ± 69.0 µM respectively. In addition, the determined IC_{50} values of TXA to Glu-Pg and Lys-Pg were 98.1 ± 23.0 µM and 46.7 ± 12.2 µM respectively. This suggests that the closed-form of Pg (Glu-Pg) requires a higher concentration of the lysine analogue to be displaced from ADAMTS13. Furthermore, the IC_{50} values for TXA were lower, about one-fourth lower, than EACA, consistent with TXA's higher potency compared to EACA.

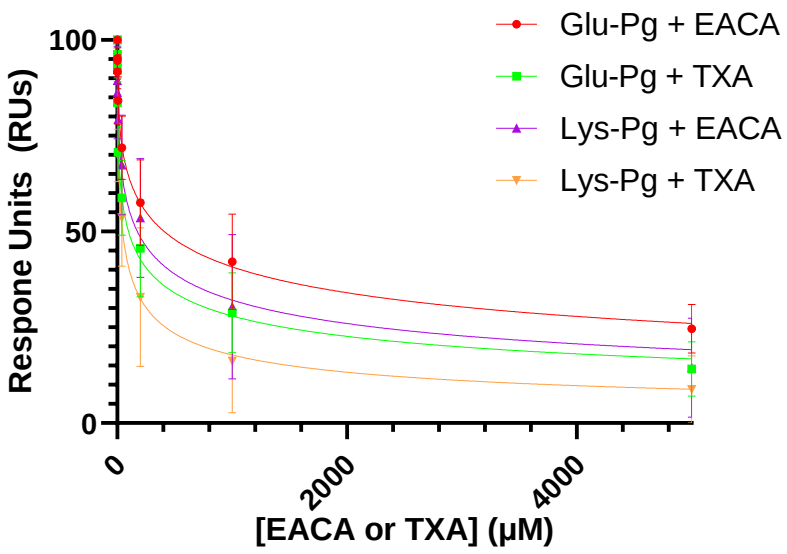

Figure 35 - Non-Linear Regression Models of Glu-Pg/Lys-Pg's Affinity to Immobilized ADAMTS13 in the Presence of the Lysine Analogues EACA/TXA.

Increasing concentration, 0-5 mM, of EACA or TXA was injected along with 2 µM Glu-Pg or Lys-Pg onto immobilized ADAMTS13, and the effect of the lysine analogues on the binding profiles was visualized by GraphPad Prism (V9) using a "[inhibitor] vs normalized response – variable slope" model.

Table 9 - IC_{50} of EACA/TXA Lysine Analogues on the Binding Interaction between Glu-Pg/Lys-Pg and Immobilized ADAMTS13.

	Glu-Pg		**Lys-Pg**	
	EACA	TXA	EACA	TXA
IC_{50} (µM)	409.6 ± 96.5	98.1 ± 23.0	175.2 ± 69.0	46.7 ± 12.2

These domain truncation experiments along with lysine-analogue experiments suggested that the C-terminus of ADAMTS13 was binding to the Kringle domains of plasminogen. Therefore, we next performed binding experiments with Kringle-domain proteins (FXII, prothrombin, Apo(a), LDL, Lp(a), modified Apo(a), and modified Glu-Pg) along with proteins identified in our BioID screen (vitronectin (Vn) and VWF) and a control (BSA) to examine the binding interactions between ADAMTS13 and other analytes.

Prothrombin did not display any binding interaction to ADAMTS13 nor MDTCS. Some binding was observed between FXII and ADAMTS13 with a saturation RUs of about 90 using 3.5 μM FXII, but not MDTCS (Figures 36-38). However, the calculated binding affinity was 56.0 ± 7245.5 μM, which is outside the range of concentrations tested and is not reliable. Therefore, we conclude that FXII is not a relevant ligand for ADAMTS13.

Other various Kringle-containing proteins (lipoprotein A (Lp(a)), apolipoprotein-A (Apo(a)), low-density lipoprotein (LDL), and the citrilated forms of Apo(a) and Glu-Pg) were examined for their binding interaction with ADAMTS13. The binding profiles of the various analytes demonstrated a lack of binding, except for modified Glu-Pg, to immobilized ADAMTS13 as evident by the 0 RUs with increasing concentration of analyte (Figure 39). Modified Glu-Pg demonstrated poor binding and a saturation RUs of 18 with 3.5 μM. Thus, due to the lack of binding of these analytes onto immobilized ADAMTS13, a binding affinity (K_d value) could not be determined.

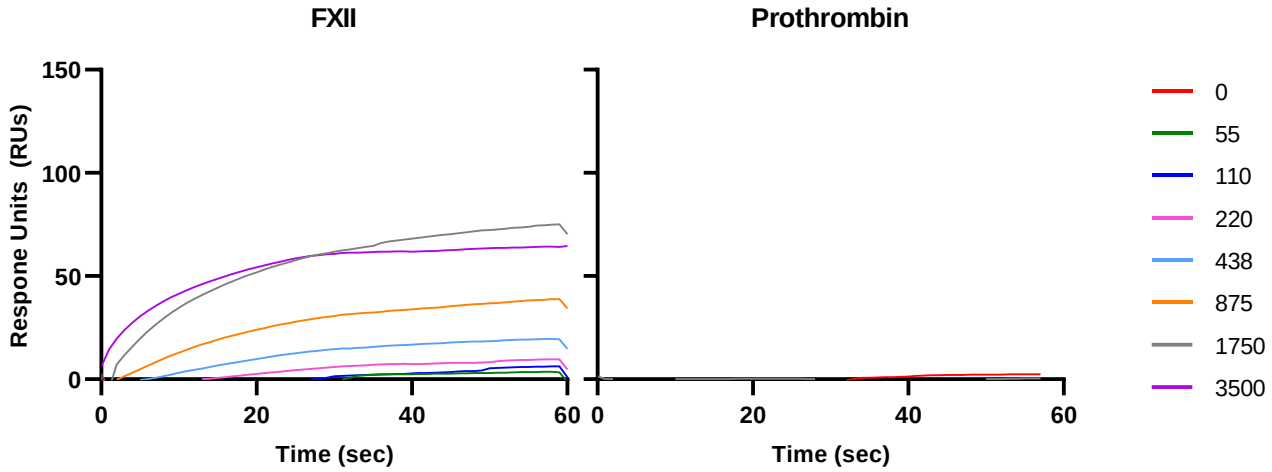

Figure 36 - Binding Curves of FXII and Prothrombin onto Immobilized ADAMTS13 using SPR.

FXII and prothrombin at varying concentrations 0-3.5 µM in HEPES-saline buffer at a flow rate of 20 µL/min were injected onto immobilized ADAMTS13 for 60 seconds and the binding profiles were visualized by Biacore T200 evaluation software.

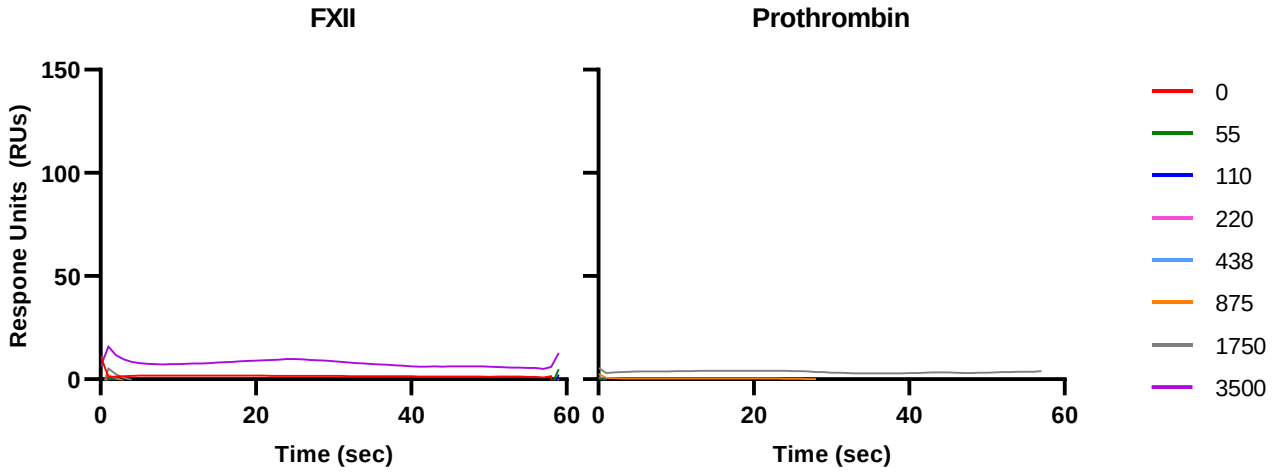

Figure 37 - Binding Curves of FXII and Prothrombin onto Immobilized MDTCS using SPR.

FXII and prothrombin at varying concentrations 0-3.5 μM in HEPES-saline buffer at a flow rate of 20 μL/min were injected onto immobilized MDTCS for 60 seconds and the binding profiles were visualized by Biacore T200 evaluation software.

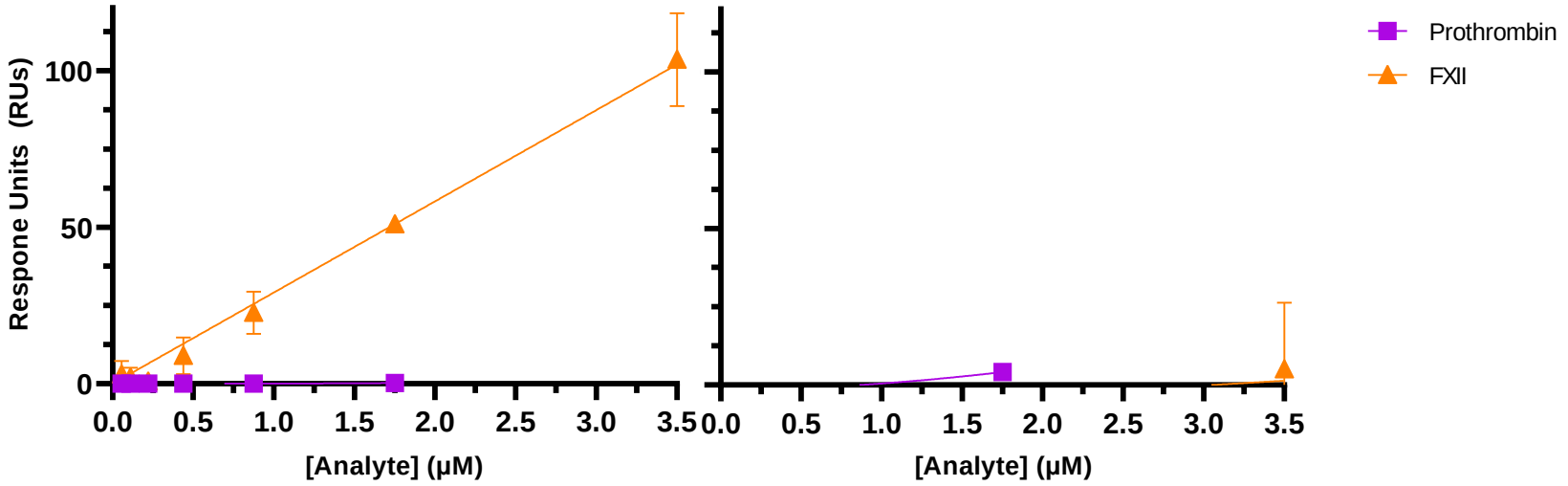

Figure 38 - Non-Linear Regression Models of FXII and prothrombin Affinity to Immobilized ADAMTS13 and MDTCS.

FXII and prothrombin at varying concentrations 0-7 µM in HEPES-saline buffer at a flow rate of 20 µL/min were injected onto immobilized ADAMTS13 (left) or MDTCS (right) and the binding profiles were visualized by GraphPad Prism using a one-site binding model.

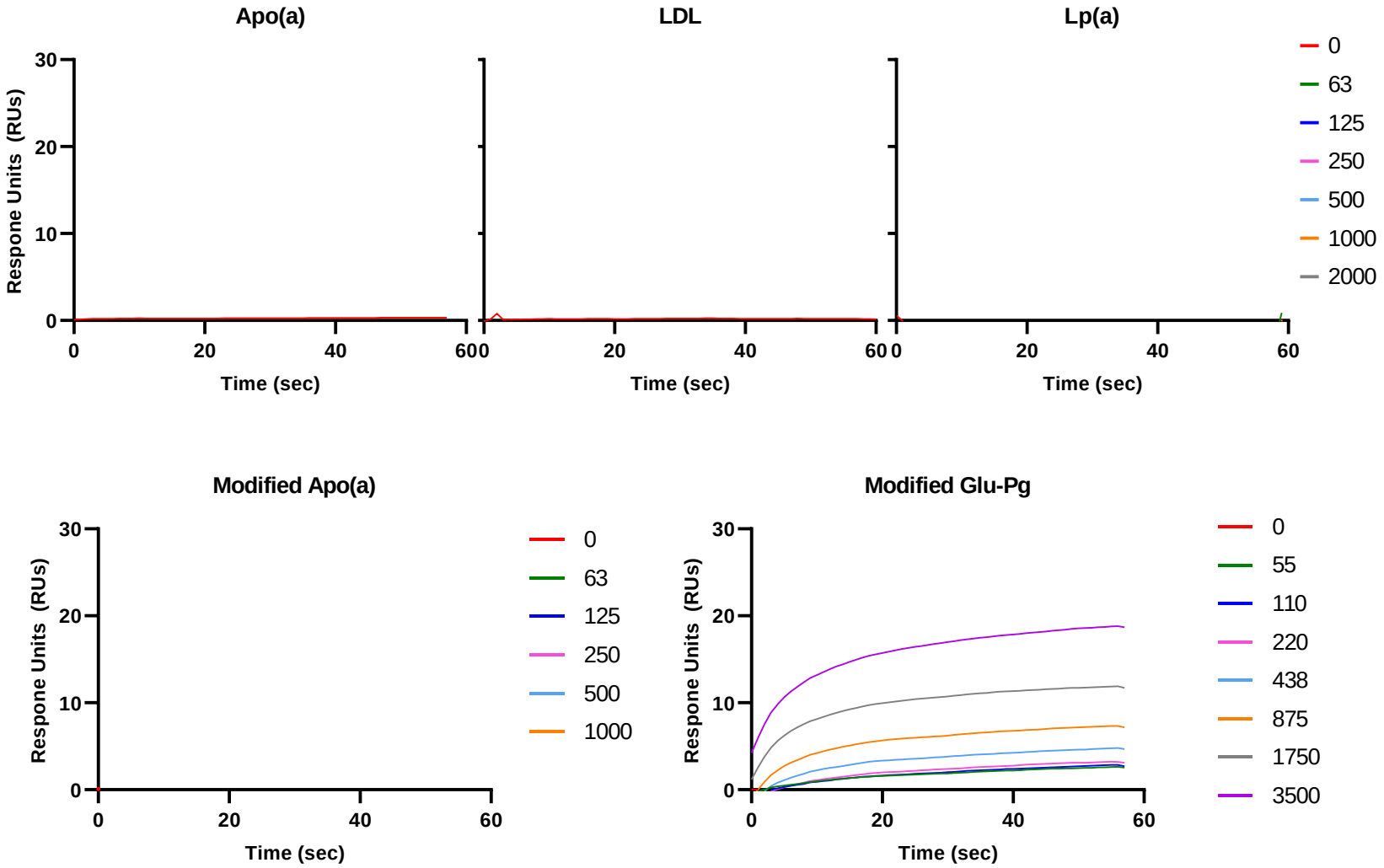
Apo(a)
LDL
Lp(a)
Respone Units (RUs)
Time (sec)
0
63
125
250
500
1000
2000
Modified Apo(a)
Modified Glu-Pg
55
110
220
438
875
1750
3500

Figure 39 - Binding Curves of Kringle Domain-Containing Analytes onto Immobilized ADAMTS13 using SPR.

Various analytes (Apo(a), LDL, Lp(a), modified Apo(a), and modified Glu-Pg) at varying concentrations 0-3.5 μM in HEPES-saline buffer at a flow rate of 20 μL/min were injected onto immobilized ADAMTS13 for 60 seconds and the binding profiles were visualized by Biacore T200 evaluation software. Association time was 60 sec, and dissociation time was 300 sec.

3.5. Proteolytic Degradation of ADAMTS13

3.5.1. *In-Silico* Analysis of Protease Sensitive Sites in ADAMTS13

The discovery of the interaction between plasminogen and ADAMTS13 prompted further investigation into the mechanism of ADAMTS13 regulation by proteolysis. Previous work has shown that plasmin, thrombin, and FXIa can cleave ADAMTS13, releasing the CUB domains (239). ADAMTS13 lacking CUB domains has been shown to exhibit a lower capacity to cleave VWF strings under flow (326).

The literature was searched for evidence on the proteolytic degradation of ADAMTS13 by various enzymes, while primarily focusing on serine proteases, and the findings were compiled into Figures 40-41. *In-silico* approaches, such as PROSPER (Protease specificity prediction server – Monash University), ExPASy Peptide Cutter (SIB Swiss Institute of Bioinformatics), and NEBcutter (v2.0, New England Biolabs) predicted various neutrophil-derived enzymes, such as cathepsin G, Cathepsin K, and elastase, and coagulation proteases, such as FXa, and thrombin, to cleave ADAMTS13 at various sites on ADAMTS13 (320–322). These techniques utilized the amino acid sequence of ADAMTS13 and compare it to known protease cleavage motifs. On the other hand, experimental findings in literature utilized N-terminal sequencing and gel electrophoresis and have identified the relative proteolytic sites of the neutrophil-derived enzyme, elastase, and human proteinase 3, coagulation enzymes, plasmin, thrombin, and FXIa onto ADAMTS13 (81, 239, 318, 319).

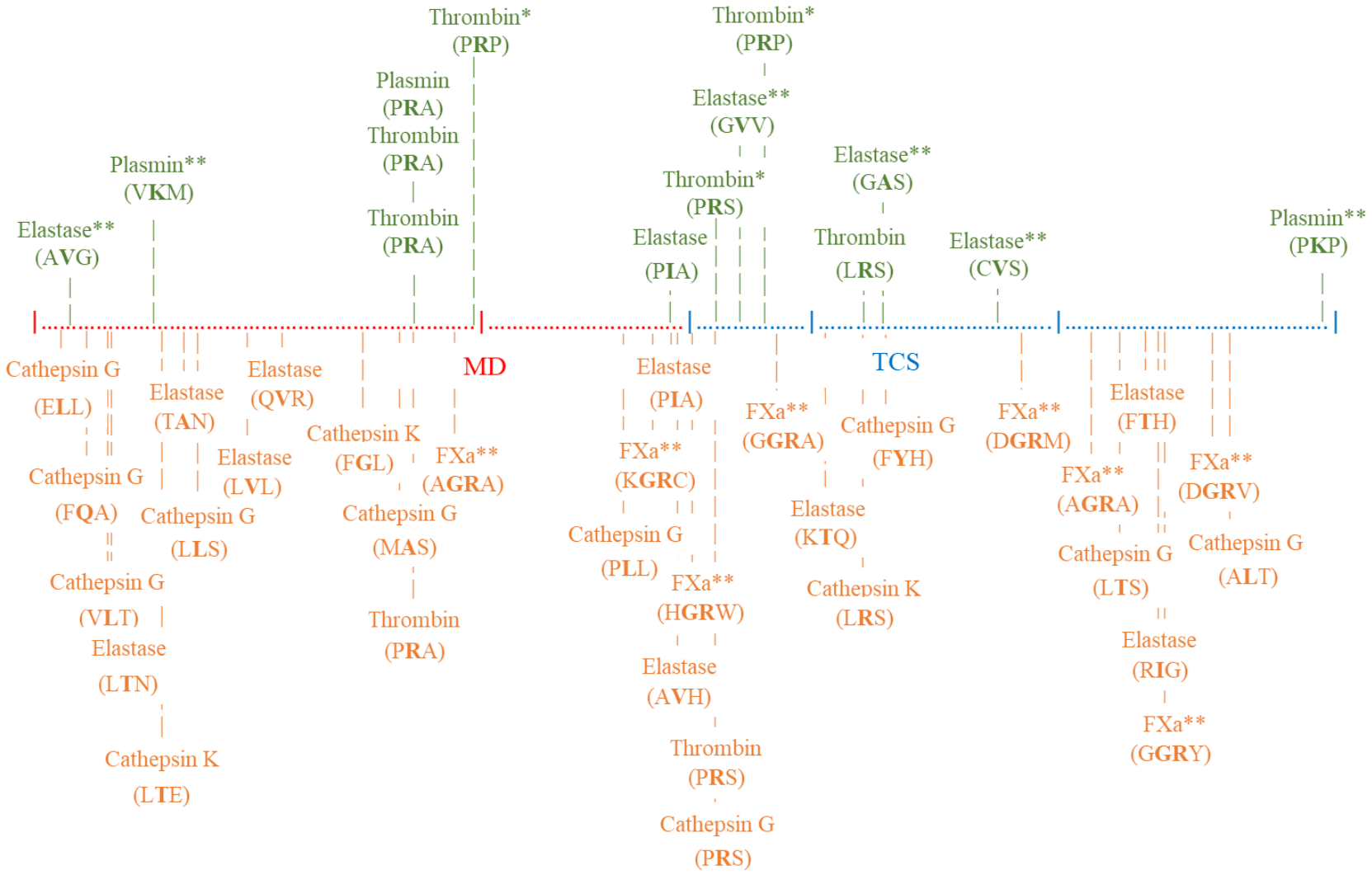
Thrombin*
(PRP)
Plasmin
(PRA)
Thrombin
(PRA)
Thrombin
(PRA)
Plasmin**
(VKM)
Elastase**
(AVG)
Cathepsin G
(ELL)
Cathepsin G
(FQA)
Cathepsin G
(VLT)
Elastase
(LTN)
Cathepsin K
(LTE)
Elastase
(TAN)
Cathepsin G
(LLS)
Elastase
(QVR)
Elastase
(LVL)
Cathepsin K
(FGL)
Cathepsin G
(MAS)
Thrombin
(PRA)
FXa**
(AGRA)
MD
Thrombin*
(PRP)
Elastase**
(GVV)
Thrombin*
(PRS)
Elastase
(PIA)
Elastase
(PIA)
FXa**
(KGRC)
Cathepsin G
(PLL)
FXa**
(HGRW)
Elastase
(AVH)
Thrombin
(PRS)
Cathepsin G
(PRS)
FXa**
(GGRA)
Elastase**
(GAS)
Thrombin
(LRS)
Cathepsin G
(FYH)
Elastase
(KTQ)
Cathepsin K
(LRS)
TCS
Elastase**
(CVS)
FXa**
(DGRM)
Plasmin**
(PKP)
Elastase
(FTH)
FXa**
(AGRA)
Cathepsin G
(LTS)
Elastase
(RIG)
FXa**
(GGRY)
FXa**
(DGRV)
Cathepsin G
(ALT)

Figure 40 - *In-Silico* Literature Survey of Proteases Capable of Cleaving ADAMTS13 (MDTCS Region)

*Potential and cleavage sites identified on the proteolytic degradation of ADAMTS13's proximal domains MDTCS by the various coagulation and neutrophil-derived proteases. The colour shade of each site represents the technique and source used to identify the potential cleavage site was identified (green - experimental and orange - computational). Each . represents 3 amino acids, * encodes for non-preferential cleavage sites, and ^ encodes for potential, yet non-confirmed cleavage sites.*

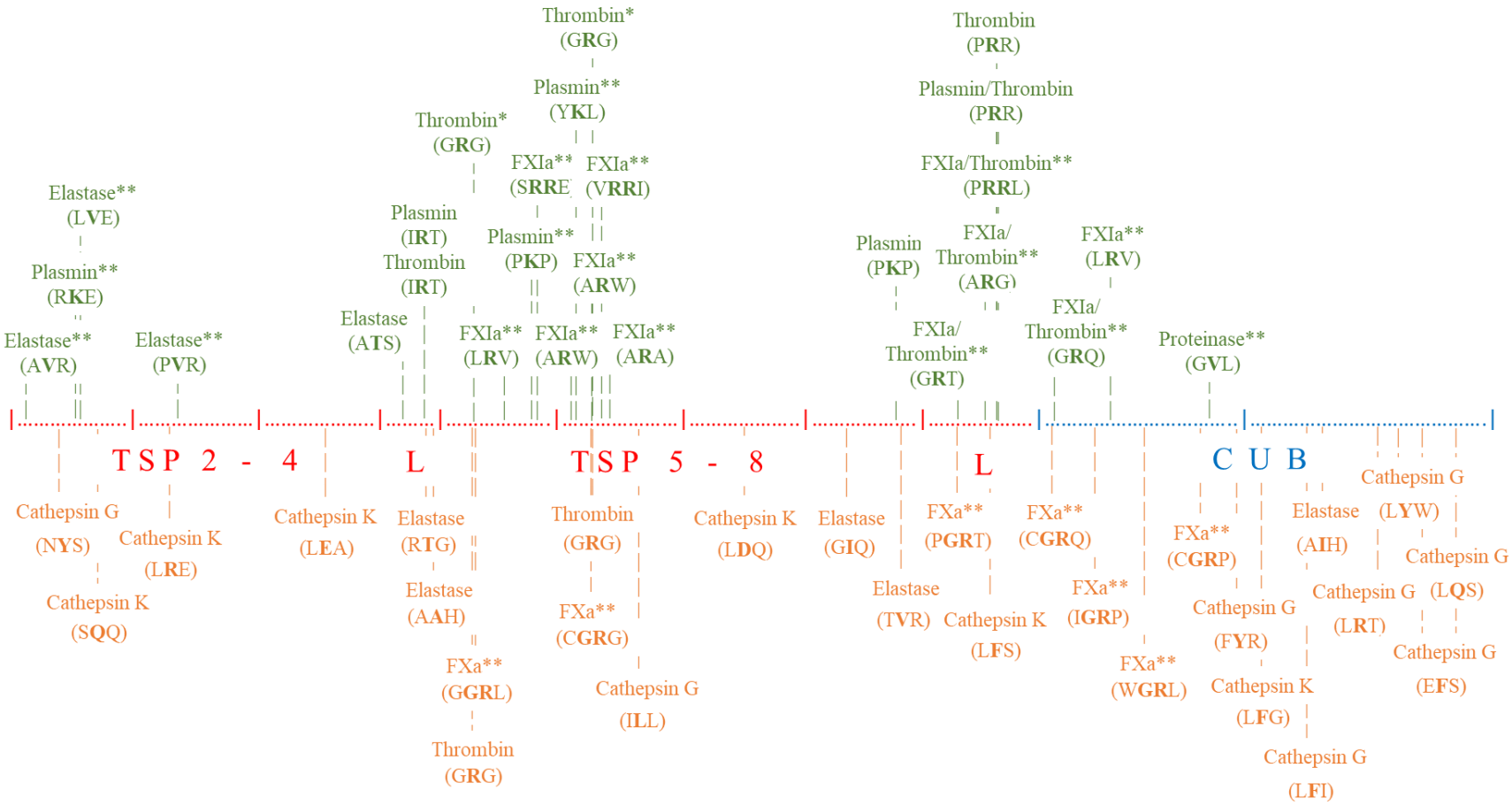
Thrombin*
(GRG)
Plasmin**
(YKL)
Thrombin*
(GRG)
FXIa**
(SRRE)
FXIa**
(VRRI)
Plasmin
(IRT)
Plasmin**
(PKP)
FXIa**
(ARW)
Thrombin
(IRT)
Elastase**
(LVE)
Plasmin**
(RKE)
Elastase**
(AVR)
Elastase**
(PVR)
Elastase
(ATS)
FXIa**
(LRV)
FXIa**
(ARW)
FXIa**
(ARA)
Thrombin
(PRR)
Plasmin/Thrombin
(PRR)
FXIa/Thrombin**
(PRRL)
Plasmin
(PKP)
FXIa/
Thrombin**
(ARG)
FXIa**
(LRV)
FXIa/
Thrombin**
(GRT)
FXIa/
Thrombin**
(GRQ)
Proteinase**
(GVL)
TSP 2 - 4
L
TSP 5 - 8
L
CUB
Cathepsin G
(NYS)
Cathepsin K
(LRE)
Cathepsin K
(SQQ)
Cathepsin K
(LEA)
Elastase
(RTG)
Elastase
(AAH)
FXa**
(GGRL)
Thrombin
(GRG)
Thrombin
(GRG)
FXa**
(CGRG)
Cathepsin G
(ILL)
Cathepsin K
(LDQ)
Elastase
(GIQ)
Elastase
(TVR)
FXa**
(PGRT)
Cathepsin K
(LFS)
FXa**
(CGRQ)
FXa**
(IGRP)
FXa**
(WGRL)
FXa**
(CGRP)
Cathepsin G
(FYR)
Cathepsin K
(LFG)
Cathepsin G
(LFI)
Elastase
(AIH)
Cathepsin G
(LRT)
Cathepsin G
(LYW)
Cathepsin G
(LQS)
Cathepsin G
(EFS)

Figure 41 - *In-Silico* Literature Survey of Proteases Capable of Cleaving ADAMTS13 (TSP-CUB Region).

*Potential and cleavage sites identified on the proteolytic degradation of ADAMTS13's distal domains TSP-CUB by the various coagulation and neutrophil-derived proteases. The colour shade of each site represents the technique and source used to identify the potential cleavage site was identified (green - experimental and orange - computational). Each . represents 3 amino acids, * encodes for non-preferential cleavage sites, and ^ encodes for potential, yet non-confirmed cleavage sites.*

3.5.2. Survey of Proteases Capable of Cleaving ADAMTS13

Following *in-silico* examination of protease-sensitive sites within ADAMTS13, we next performed a survey of select proteases to test their capacity to degrade ADAMTS13 *in-vitro*. Thus, 200 nM ADAMTS13 was incubated with 100 nM of various proteases (plasmin, thrombin, FVIIa, FIXa, FXa, FXIa, FXIIa, activated protein C (APC), tPa) or controls (thrombomodulin (TM) and fibrinogen). Preliminary data found that a 2-hour incubation of ADAMTS13 with plasmin, thrombin, FXIa, FXa, and tPa at 37°C cleaved ADAMTS13, resulting in a 150 kDa band along with one or more additional bands (Figure 42). On the other hand, activated protein C (APC), FVIIa, FIXa, and FXIIa did not cleave ADAMTS13 (Figure 42). The proteolysis of ADAMTS13 using plasmin, FXa, FXIa, and thrombin was repeated and analyzed using a total protein stain and western blot utilizing an anti-M domain ADAMTS13 antibody. Through analysis of the proteolytic fragment profiles of each enzyme, and their comparison to the initial *in-silico* findings, the various cut regions on ADAMTS13 were postulated (Figure 43).

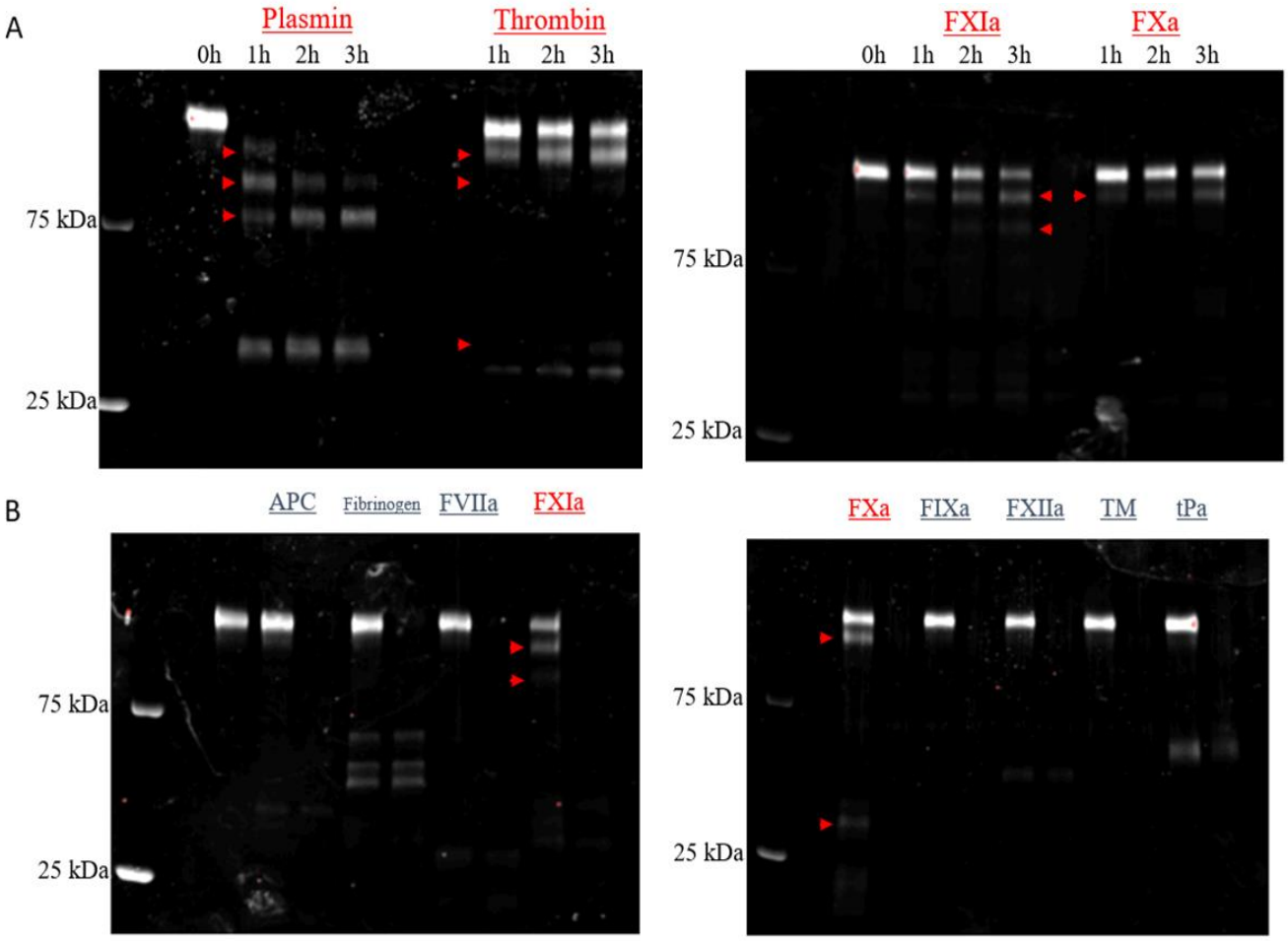
A
Plasmin
Thrombin
0h 1h 2h 3h 1h 2h 3h
75 kDa
25 kDa
FXIa
FXa
0h 1h 2h 3h 1h 2h 3h
75 kDa
25 kDa
B
APC
Fibrinogen
FVIIa
FXIa
75 kDa
25 kDa
FXa
FIXa
FXIIa
TM
tPa
75 kDa
25 kDa

Figure 42 - Survey of Proteases Capable of Cleaving ADAMTS13.

200 nM ADAMTS13 was incubated with various proteases (100 nM) for various time points (0 – 3 hours, A) or 2 hours (B) at 37°C then separated using SDS-PAGE under reducing conditions and analyzed through a total protein stain using SYPRO-RUBY. The red arrows represent the cleaved bands of ADAMTS13. Proteases in red were able to cleave ADAMTS13.

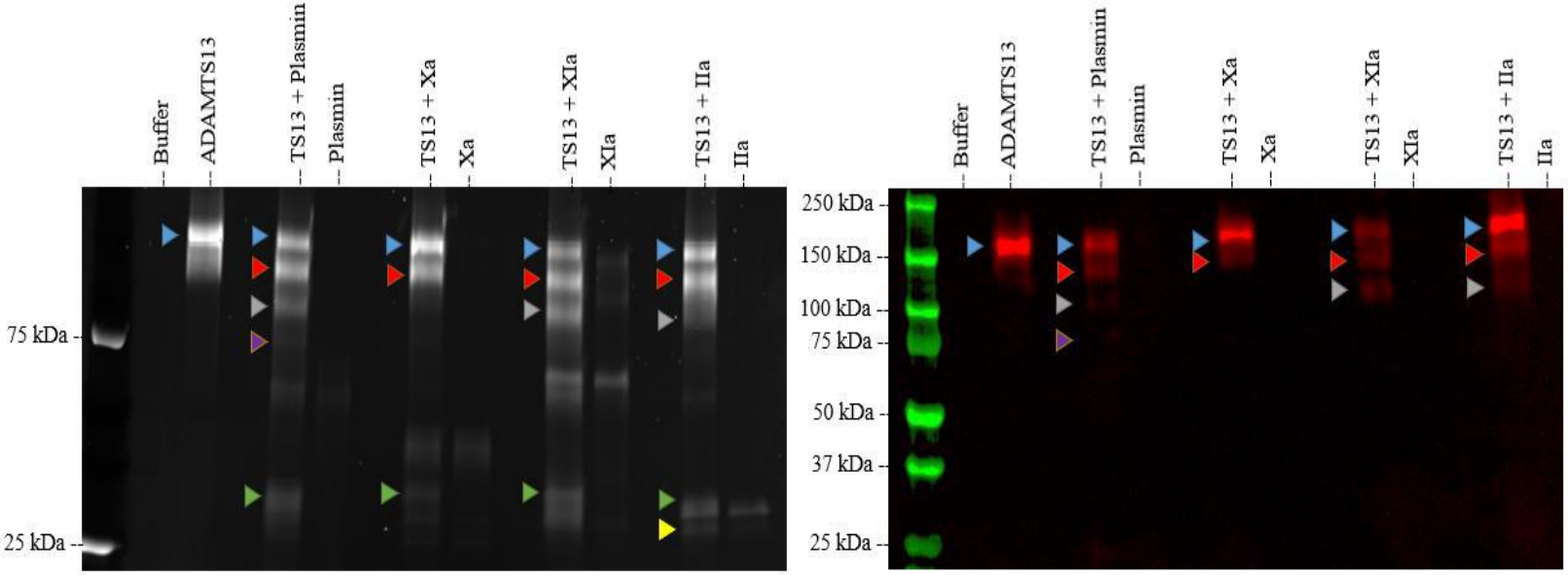

Band Color	Band Size (~kDa)	ADAMTS13 Domains	Enzymes	Cut Region
Blue	180	Full Length	-	-
Red	150	MDTCS-TSP2-8	Plasmin*, FIIa, FXIa, FXa	T8 Linker
Green	120	MDTCS-T2-T4	Plasmin, FXIa	T4 Linker
Purple	80	MDTCS	Plasmin	S/T2
Orange	40	T4L-T8L or CUB1-2	Plasmin*, FIIa, FXIa, FXa	T4/T8 Linkers
Yellow	30	CUB1-2	FIIa	T8 Linker

Figure 43 - Survey of Coagulation Proteases Capable of Cleaving ADAMTS13.

200 nM ADAMTS13 was incubated with 100 nM various coagulation proteases (plasmin, FXa, FXIa, and thrombin) for 2 hours at 37°C then separated using SDS-PAGE under reducing conditions and analyzed through a total protein stain using SYPRO-RUBY (top-left) and anti-M western blot (top-right). The blue arrows represent the uncleaved band of ADAMTS13, and all other colored arrows represent the cleaved bands of ADAMTS13. Cleaved fragments of ADAMTS13 were characterized based on their size, which postulated the cut region by each enzyme.

3.5.3. Proteolytic Degradation of ADAMTS13 by Activated Neutrophils

Neutrophil activation is known to occur at sites of vascular injury and inflammation where VWF dependent platelet recruitment is needed (70). Therefore, the capacity of neutrophil-derived proteases to degrade ADAMTS13 was tested. A 1/10 serial dilution of neutrophils were activated with PMA to stimulate degranulation and protease release and titrated into a cell count curve ranging from 0 – 500,000 cells. ADAMTS13 was added to the activated cells (refer to 2.7.2), and the proteolytic effect of the enzymes produced by activated neutrophils was examined by western blot. As the cell count increased, more proteolysis of ADAMTS13 was observed, as evident by the loss of the intact ADAMTS13 band on the western blot (Figure 44).

To better identify the family of enzymes produced by the activated neutrophils and responsible for the degradation of ADAMTS13, AEBSF or EDTA were added to the reaction to inhibit serine proteases or metalloproteases, respectively (Figure 45). The addition of 2mM AEBSF to the reaction attenuated degradation of ADAMTS13 up to 500,000 activated neutrophils (Figure 45). The addition of 5 mM EDTA to the reaction attenuated ADAMTS13 degradation up to 5000 activated neutrophils (Figure 45). ADAMTS13 was completely degraded in the absence of either inhibitor, except for 50 activated neutrophils or lower. This result indicated that serine proteases are primarily responsible for the degradation of ADAMTS13 by activated neutrophils.

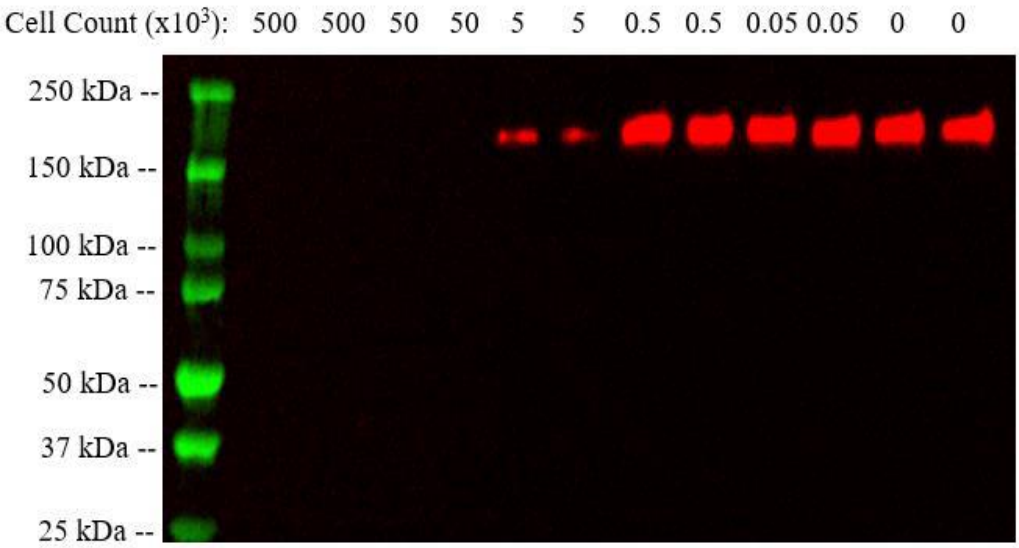

Figure 44 - Proteolytic Degradation of ADAMTS13 by Activated Neutrophils.

100 nM ADAMTS13 was incubated with an increasing count, 0 – 500,000, of PMA-simulated neutrophils for 2 hours at 37°C, then separated using SDS-PAGE under reducing conditions and analyzed through a western blot using the anti-ADAMTS13 antibody. Degradation of ADAMTS13 is represented by the decrease in the intensity of the ADAMTS13 band.

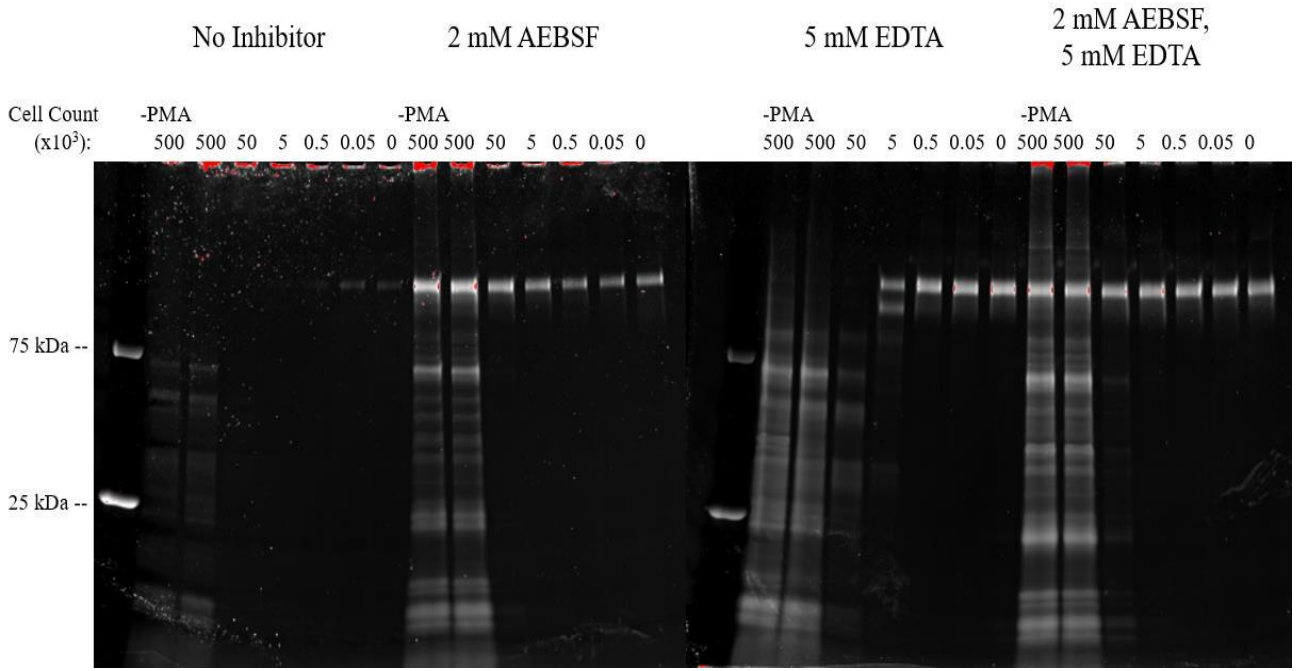

Figure 45 - Effect of Protease Inhibitors on the Proteolytic Degradation of ADAMTS13 by Activated Neutrophils.

100 nM ADAMTS13 was incubated with an increasing count, 0 – 500,000, of PMA-simulated neutrophils for 2 hours at 37°C, in the presence/absence of the protease inhibitors AEBSF (2 mM) or EDTA (5 mM) or both. The reactions were then separated using SDS-PAGE under reducing conditions and analyzed through a SYPRO-RUBY total protein stain. Degradation of ADAMTS13 is represented by the presence of the smaller bands, and the decrease in the intensity of the ADAMTS13 band (~180 kDa).

To identify the most important neutrophil-derived serine proteases for degrading ADAMTS13, we next tested neutrophil elastase, cathepsin G, and human proteinase 3 for their ability to cleave ADAMTS13 (Figures 46-47). ADAMTS13 was analyzed for cleavage using the anti-ADAMTS13 in the western blot and cleaved ADAMTS13 was represented by the absence of ~180 kDa ADAMTS13 band. 100 nM of neutrophil elastase degraded ADAMTS13 in a similar pattern as thrombin and FXIa (Figures 42-43, 46-47). Interestingly, 100 nM of cathepsin G was shown to completely degrade ADAMTS13 by the 1-hour time point. Therefore, the concentration of cathepsin G was decreased to 20 nM, which showed a comparable banding pattern as thrombin and neutrophil elastase (Figures 43, 46). The efficient capacity of cathepsin G to degrade ADAMTS13 may suggest that it is an efficient regulator of ADAMTS13 activity *in-vivo*. To better analyze the proteolytic profiles of each of the neutrophil-derived enzymes, while also examining the effect of hPR3, the experiment was repeated, and the findings were compared to the initial search to better postulate the cut regions on ADAMTS13 (Figure 47).

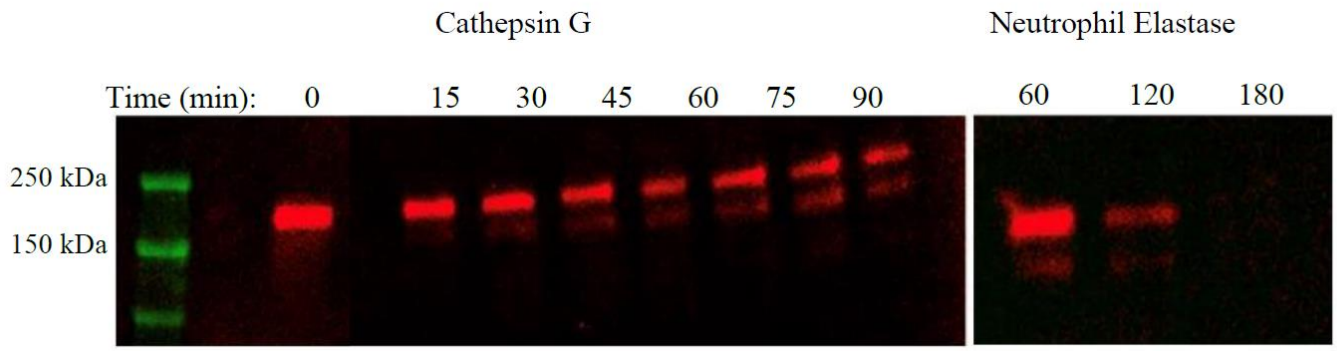

Figure 46 - Proteolysis of ADAMTS13 by Cathepsin G and Elastase.

200 nM ADAMTS13 was incubated with 20 nM cathepsin G or 100 nM neutrophil elastase for various time points (0 – 180 minutes) at 37°C, then separated using SDS-PAGE under reducing conditions and analyzed through a western blot using the anti-ADAMTS13 antibody. Degradation of ADAMTS13 is represented by the appearance of the smaller band and/or the decrease in the intensity of the ADAMTS13 band.

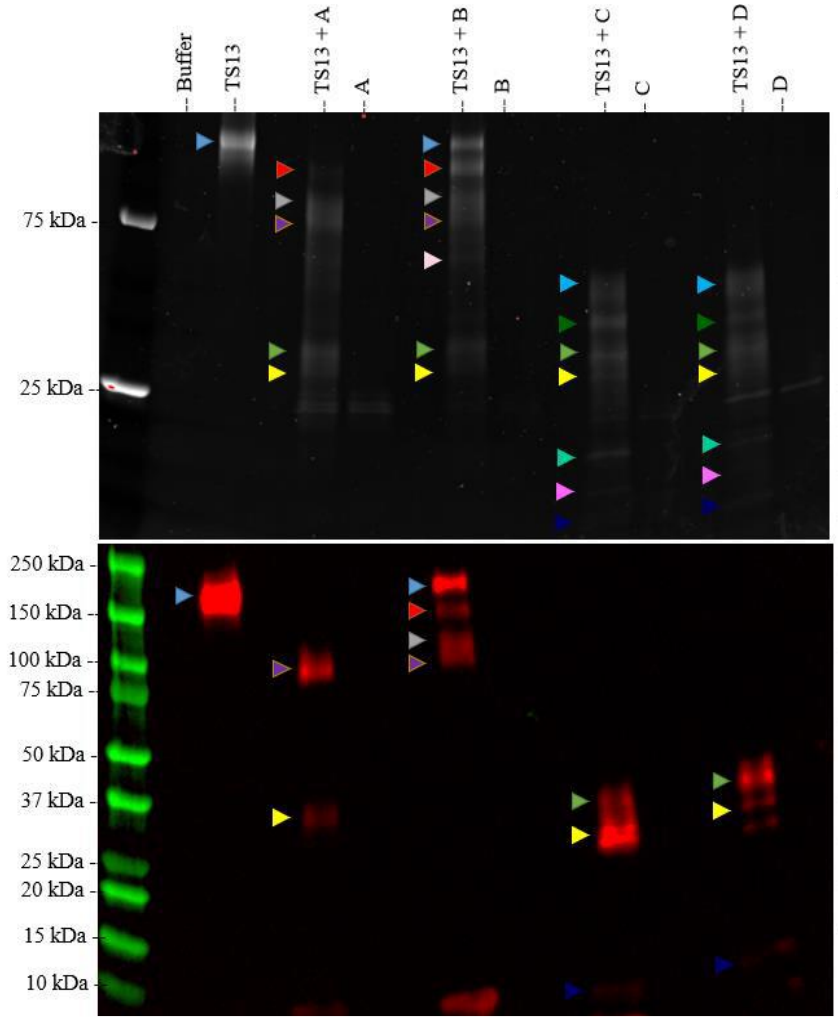

A) Cathepsin G (100 nM)
B) Cathepsin G (20 nM)
C) Elastase
D) hPR3

Band Color	Band Size (~kDa)	ADAMTS13 Domains	Enzymes	Cut Region
Blue	180	Full Length	-	-
Red	150	MDTCS-TSP2-8	Cathepsin G	T8 Linker
Green	120	MDTCS-T2-T4	Cathepsin G	T4 Linker
Purple	80	MDTCS	Cathepsin G	S/T2
White	70	?	Cathepsin G	?
Sky Blue	65	?	Elastase, hPR3	?
Dark Green	50	?	Elastase, hPR3	?
Orange	40	MDT	Cathepsin G, Elastase, hPR3	T
Yellow	30	MD	Cathepsin G, Elastase, hPR3	D
Teal	15	?	Elastase, hPR3	?
Pink	10	?	Elastase, hPR3	?
Navy Blue	5	M?	Elastase, hPR3	M

Figure 47 - Survey of Neutrophil-Derived Proteases Capable of Cleaving ADAMTS13.

200 nM ADAMTS13 was incubated with 20 or 100 nM various neutrophil-derived proteases (cathepsin G, elastase, and hPR3) for 2 hours at 37°C then separated using SDS-PAGE under reducing conditions and analyzed through a total protein stain using SYPRO-RUBY (top-left) and anti-M western blot (bottom-left). The blue arrows represent the uncleaved band of ADAMTS13, and all other colored arrows represent the cleaved bands of ADAMTS13. Cleaved fragments of ADAMTS13 were characterized based on their size, which postulated the cut region by each enzyme.

3.5.4. Protease Inhibitors

To identify the most important neutrophil-derived serine protease responsible for degrading ADAMTS13, we next tested activated neutrophils for their ability to cleave ADAMTS13 in the presence of specific protease inhibitors (Figure 48). The inhibitors used in this assay were against cathepsin G (Cathepsin G Inhibitor I), elastase (Sivelestat), or serine proteases (AEBSF). ADAMTS13 was analyzed for cleavage using the anti-ADAMTS13 in the western blot and cleaved ADAMTS13 was represented by the absence of ~180 kDa ADAMTS13 band. 5 mM of AEBSF was required to attenuate the proteolysis of ADAMTS13 by activated neutrophils, as evident by the intact full-length ADAMTS13 band (180 kDa) on the western blot (Figure 48). Interestingly, 50 mM Sivelestat was able to partially attenuate the proteolysis of ADAMTS13 by activated neutrophils (Figure 48). In contrast, 5 mM of Cathepsin G Inhibitor I was able to slightly attenuate proteolysis of ADAMTS13 by activated neutrophils, as evident by the very faint intact full-length ADAMTS13 band (180 kDa) on the western blot (Figure 48). The efficient capacity of Sivelestat to inhibit the proteolysis of ADAMTS13 by activated neutrophils may suggest that neutrophil elastase is the most potent regulator of ADAMTS13 released by activated neutrophils. To better analyze the proteolytic effect of each enzyme on ADAMTS13, the proteolysis experiments were repeated alongside a FRETS-VWF73 assay to better understand the effect proteolytic degradation has on ADAMTS13 activity.

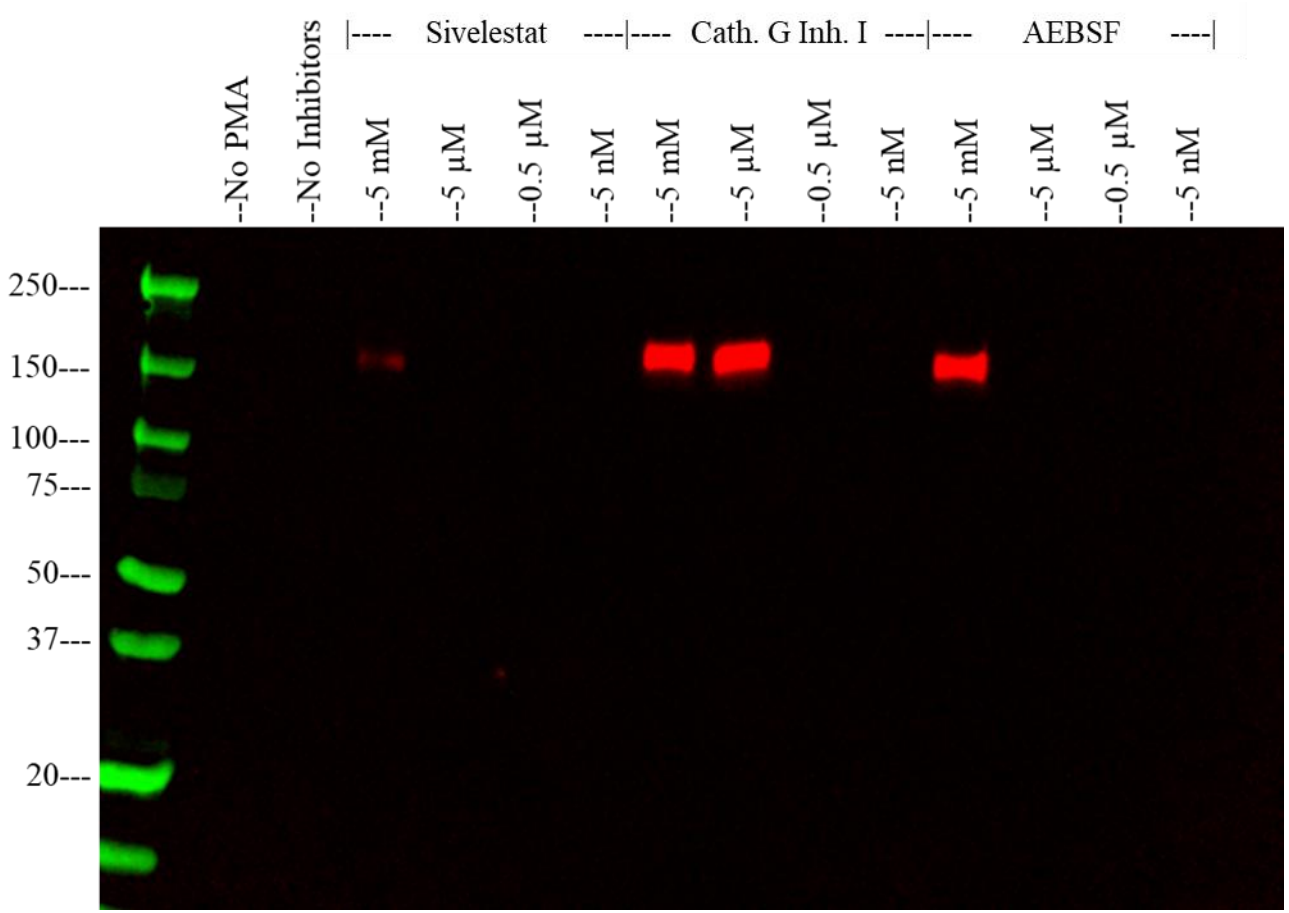
|---- Sivelestat ----|---- Cath. G Inh. I ----|---- AEBSF ----|
--No PMA
--No Inhibitors
--5 mM
--5 µM
--0.5 µM
--5 nM
--5 mM
--5 µM
--0.5 µM
--5 nM
--5 mM
--5 µM
--0.5 µM
--5 nM
250---
150---
100---
75---
50---
37---
20---

Figure 48 - Effect of Serine Protease Inhibitors on the Proteolytic Degradation of ADAMTS13 by Activated Neutrophils.

50 nM ADAMTS13 was incubated with 50,000 PMA-simulated neutrophils for 2 hours at 37°C, in the presence/absence of a varying concentration of 5 nM – 5 mM Sivelestat, Cathepsin G Inhibitor I or AEBSF. The reactions were separated using SDS-PAGE under reducing conditions and analyzed through an anti-M western blot. Degradation of ADAMTS13 is represented by the decrease in the intensity of the intact full-length ADAMTS13 band (~180 kDa).

3.5.5. Effect of Proteolytic Degradation on ADAMTS13 Activity

To evaluate the effect of proteolytic degradation on ADAMTS13, we repeated the proteolysis experiments using a lower concentration of protein (100 nM wt-ADAMTS13 and 50 nM protease) and examined the activity of proteolytically degraded ADAMTS13 using a FRETS-VWF73 assay. In contrast to previous experiments (Figures 42-43), FXIa and FXIIa did not cleave ADAMTS13 as evident by the absence of any bands other than the intact full-length ADAMTS13 band (180 kDa) as well as the lack of decrease in intensity of the intact full-length ADAMTS13 band (Figure 49A). This difference could be a result of a non-functional FXIIa. In comparison, thrombin, neutrophil elastase, and cathepsin G proteolytically degraded ADAMTS13 as evident by the similar banding pattern on the western blot (Figure 49A). In addition, thrombin demonstrated an additional band at ~30 kDa and cathepsin G had an additional band at ~50 kDa (Figure 49A).

The effect of proteolytic degradation has on ADAMTS13 activity was evaluated through the FRETS-VWF73 assay. Proteolytically degraded ADAMTS13 by FXIIa, FXIa, thrombin, elastase, or cathepsin G observed a rate in the range of ~3800 ΔRfu/s and ~5000 ΔRfu/s. In comparison, intact full-length ADAMTS13 observed a rate of ~3500 ΔRfu/s. Interestingly, in the absence of ADAMTS13, none of the proteases cleaved VWF73 except for neutrophil elastase which observed a rate of ~3100 ΔRfu/s, where literature has shown before (327). Although these data suggest that the cleaved form of ADAMTS13 may not lose activity towards VWF73 (consistent with cleavage sites outside the MDTCS region), these experiments are limited by the fact that ADAMTS13 in the reactions exist in both cleaved and uncleaved forms. Therefore, future studies will repeat this experiment with

ADAMTS13 that is more completely degraded by the tested proteases. In addition, future experiments will utilize AEBSF in the reactions to avoid the influence of the serine proteases in the reaction.

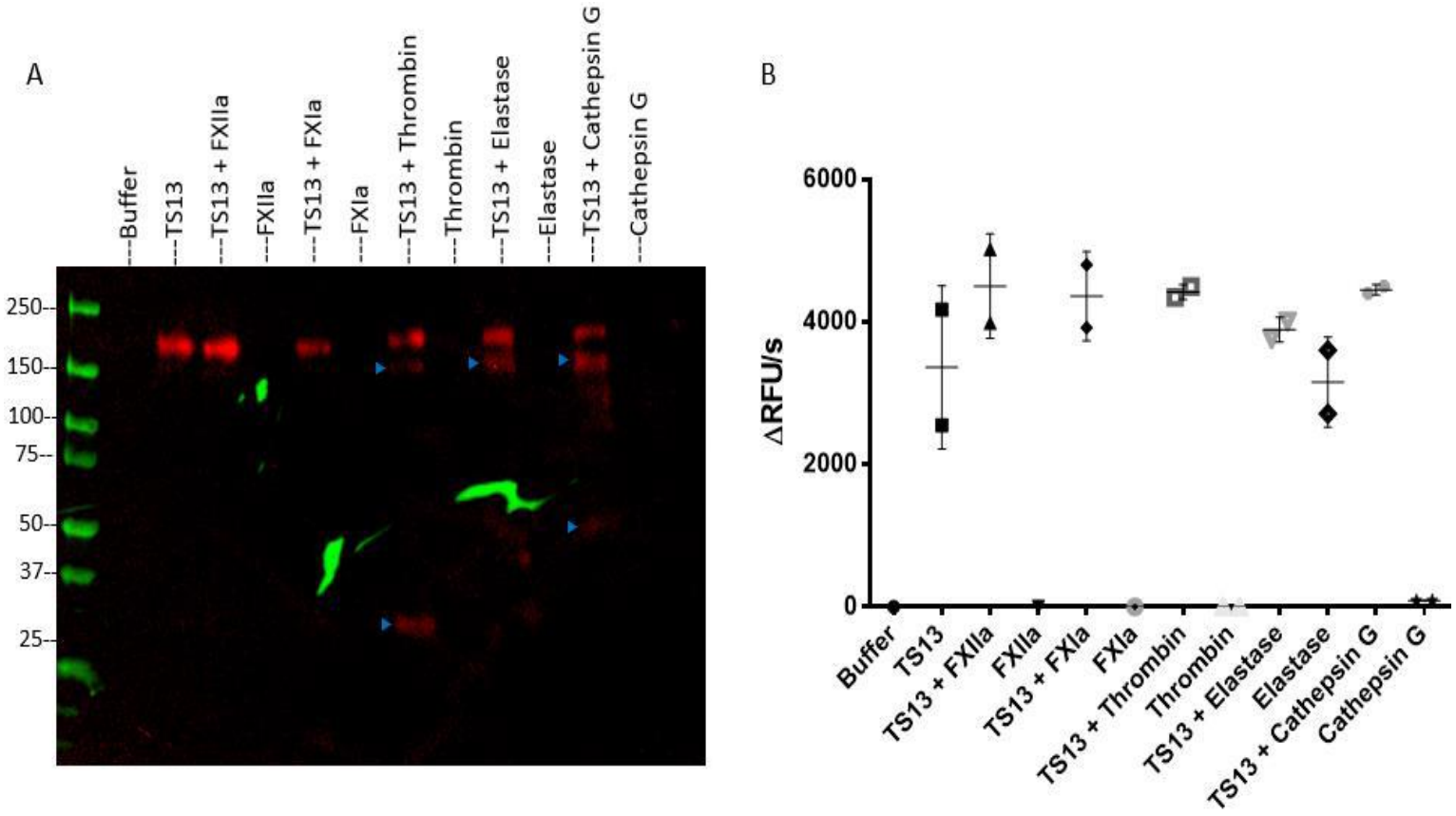
A
Buffer
TS13
TS13 + FXIIa
FXIIa
TS13 + FXIa
FXIa
TS13 + Thrombin
Thrombin
TS13 + Elastase
Elastase
TS13 + Cathepsin G
Cathepsin G
250
150
100
75
50
37
25
B
ΔRFU/s
6000
4000
2000
0
Buffer
TS13
TS13 + FXIIa
FXIIa
TS13 + FXIa
FXIa
TS13 + Thrombin
Thrombin
TS13 + Elastase
Elastase
TS13 + Cathepsin G
Cathepsin G

Figure 49 - Effect of Proteolytic Degradation on ADAMTS13 Activity.

100 nM ADAMTS13 was incubated with 50 nM of various proteases for 2 hours at 37°C. The reactions were then: (A) separated using SDS-PAGE under reducing conditions and analyzed through a western blot using the anti-M domain ADAMTS13 antibody; (B) measured the enzymes' rate of activity using FRETS-VWF73, using either 2 nM wt-ADAMTS13 or 1 nM protease (FXIIa, FXIa, thrombin, elastase, cathepsin G), or both, with 1 μM VWF73 substrate. Degradation of ADAMTS13 is represented by the appearance of the smaller band and is highlighted by the blue arrow (A).

3.5.6. The Influence of DNase I on the Proteolytic Degradation of ADAMTS13

Exogenous and microbial-derived DNase I is known to inhibit the function of NETs, which are produced by activated neutrophils (328). Thus, the influence of DNase I on the ability of activated neutrophils to degrade ADAMTS13 was examined. Increasing numbers of neutrophils were activated in the absence or presence of DNase I, before incubation with ADAMTS13 (refer to 2.7.3). Following a 1-hour incubation, ADAMTS13 was degraded by a 10x lower cell count in the presence of DNase I than in the absence of DNase I (Figure 50 A/B). These reactions were also analyzed for ADAMTS13 activity using the FRETS-VWF73 assay (Figure 50C). Interestingly, in the presence of DNase I, the rate of activity for ADAMTS13 increased ~3300 ΔRfu/s as the number of activated neutrophils increased to 5000 cells. On the other hand, in the absence of DNase I, the rate of activity for ADAMTS13 decreased ~800 ΔRfu/s as the number of activated neutrophils increased to 5000 cells. DNase I cleaves NETs which may influences the space availability of ADAMTS13 to be degraded by the neutrophil-derived proteases. Thus, future studies will examine longer DNase I incubation times to determine the influence the breakdown of NETS has on the capability of proteases to degrade ADAMTS13.

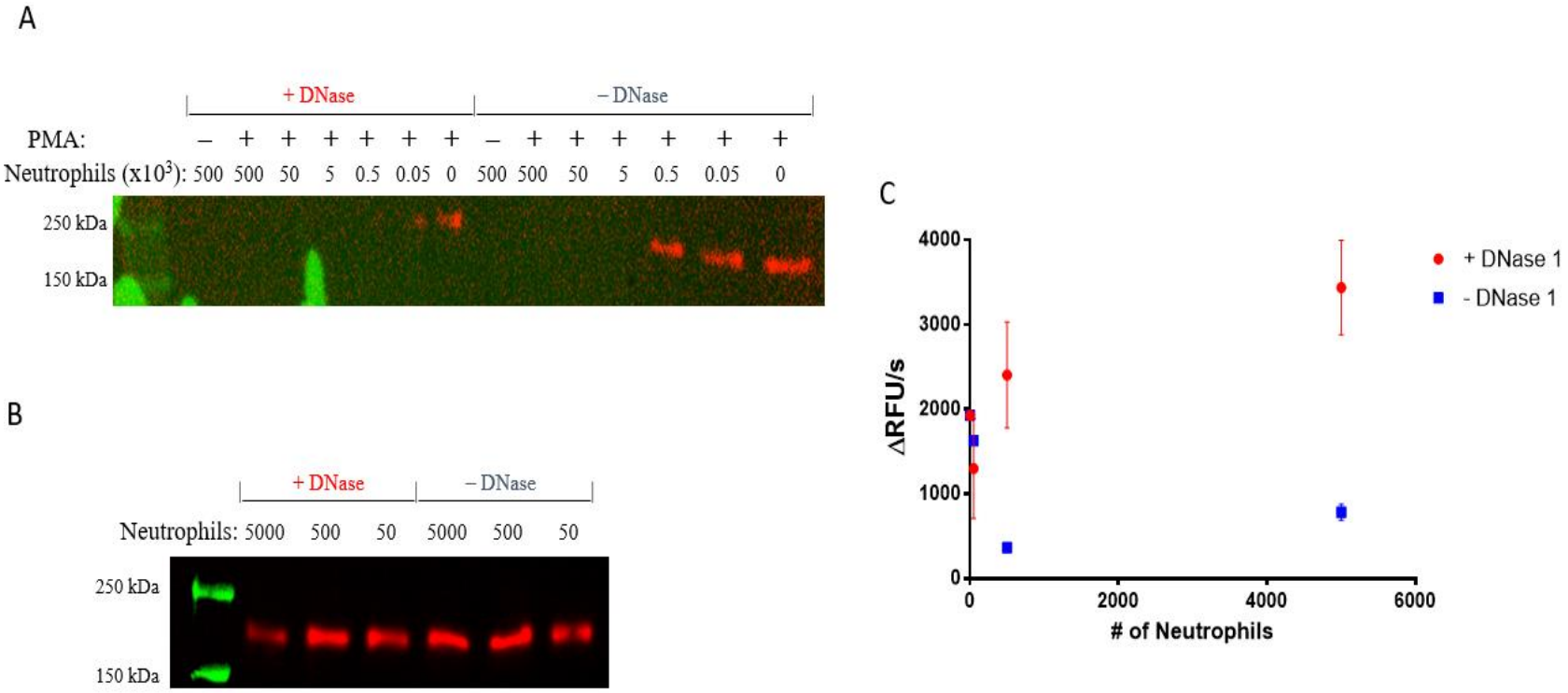

Figure 50 - Influence of DNase I on the Proteolytic Degradation of ADAMTS13 by Activated Neutrophils.

Isolated neutrophils were set up into reactions containing various cell counts (0 - 500,000 cells), diluted as needed using RPMI, in the presence or absence of DNase I at a final concentration of 20 µg/mL, and activated with 100 nM PMA for 4 hours at 37°C. 100 nM of wt-ADAMTS13 was added to the activated neutrophil reactions and incubated for 1 hour at 37°C. The reactions were then: (A/B) separated using SDS-PAGE under reducing conditions and analyzed through a western blot using the anti-

ADAMTS13 antibody; (C) measured wt-ADAMTS13's rate of activity using FRETS-VWF73, using 2 nM of the potentially degraded wt-ADAMTS13 with 1 µM VWF73 substrate. Degradation of ADAMTS13 is represented by the decrease in the intensity of the ADAMTS13 band.

3.5.7. Developing a Protease-Resistant Form of ADAMTS13

After surveying several coagulation and neutrophil-derived enzymes for their proteolytic degradation on ADAMTS13, possible cleavage sites were identified based on the banding patterns observed from the ADAMTS13 cleavage assays. All proteases capable of cleaving ADAMTS13 cleaved ADAMTS13 near the CUB domains, and around the TSP 2-8 region (Figure 51). Furthermore, neutrophil-derived enzymes also cleaved in additional areas, specifically in the M, D, T, and directly after the S domains. In comparison to the *in-silico* findings (Figures 40-41), the suspected areas of proteolysis are postulated to be the linker regions within the TSP 2-8 region, which are the T4 Linker region (T4L) and the T8 Linker region (T8L), which are devoid of secondary structure and may be ideally suited as a substrate for proteases (Figure 51).

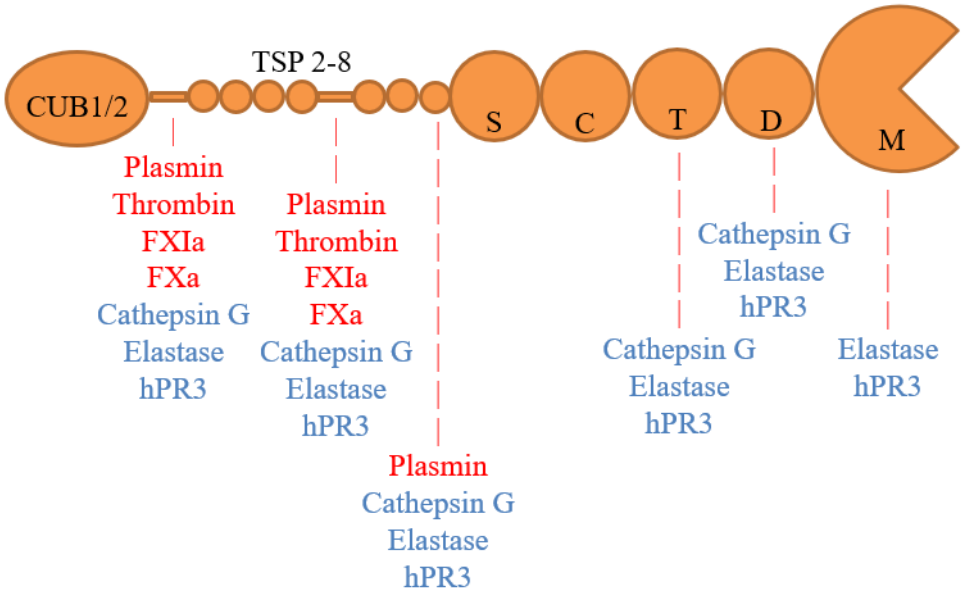

Figure 51 - Postulated Sites of Cleavage on ADAMTS13.

Protease-resistant ADAMTS13 mutants, whereby T4L, or T8L, or both linkers were mutated to a GSSS linker and expressed (refer to section 2.2). The ability of these mutants to resist proteolysis was evaluated using plasmin and PMA-stimulated neutrophils.

ADAMTS13 at a concentration of 100 nM and as wild-type, T4L mutant, T8L mutant, or T4L/T8L mutant was incubated with 100 nM of plasmin, in the presence or absence of plasmin inhibitor (VfKcK), for 2 hours and the ability to resist proteolysis was evaluated through a western blot (refer to section 2.7.3). The plasmin inhibitor, VfKcK, was added at the same time as the ADAMTS13; thus, VfKcK acted to slow down the proteolysis of ADAMTS13 by plasmin. Hence, the second band was observed in all reactions containing VfKcK (Figure 52). Proteolysis of ADAMTS13 was determined by the absence of the ADAMTS13 band on the western blot. Interestingly, plasmin successfully cleaved ADAMTS13 in all forms within 2 hours except for the double mutant, as evident by the prominent intact full-length ADAMTS13 band on the western blot (Figure 52). This is indicative of T4L/T8L mutant's resistance to proteolysis by plasmin.

Similar to the plasmin experiment, ADAMTS13 at a concentration of 100 nM and as wild-type, T4L mutant, T8L mutant, or T4L/T8L mutant was incubated with 50,000 activated neutrophils for 5, 30, and 60 minutes and the ability to resist proteolysis was evaluated through a western blot (refer to section 2.7.3). The activated neutrophils cleaved wild-type ADAMTS13 and T8L mutant within a 5-minute reaction, except for the 60-minute reaction for T8L (Figure 53). The unexpected result in the 60-minute reaction with T8L suggests an experimental repeat. In comparison, the T4L and T4L/T8L mutants resisted proteolysis by activated neutrophils within 60 minutes as evident by the prominent

intact full-length ADAMTS13 band on the western blot (Figure 53). This is indicative of T4L and T4L/T8L mutant's resistance to proteolysis by activated neutrophils.

In both cases, T4L/T8L demonstrated resistance to proteolysis by plasmin and activated neutrophils (Figures 52-53).

.

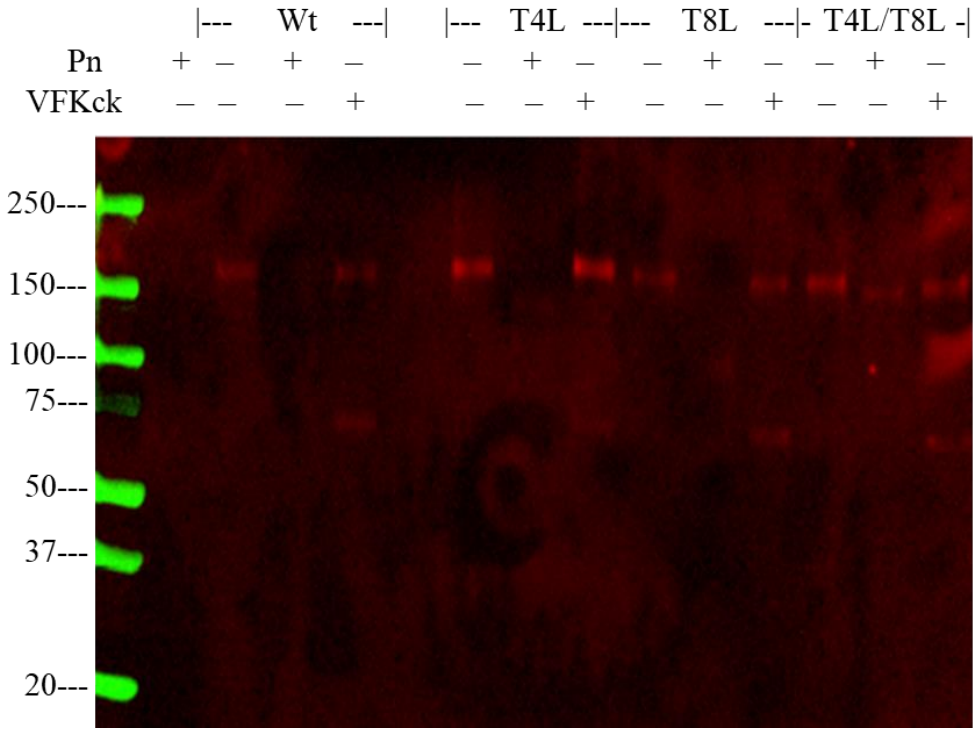

Figure 52 - Effect of Plasmin on ADAMTS13-Resistant Mutants.

100 nM ADAMTS13, as wild-type, T4L mutant, T8L mutant, or T4L/T8L mutant, was incubated with 100 nM of Plasmin for 2 hours at 37°C, then separated using SDS-PAGE under reducing conditions and analyzed through a western blot using the anti-ADAMTS13 antibody. Degradation of ADAMTS13 is represented by the decrease in the intensity of the ADAMTS13 band.

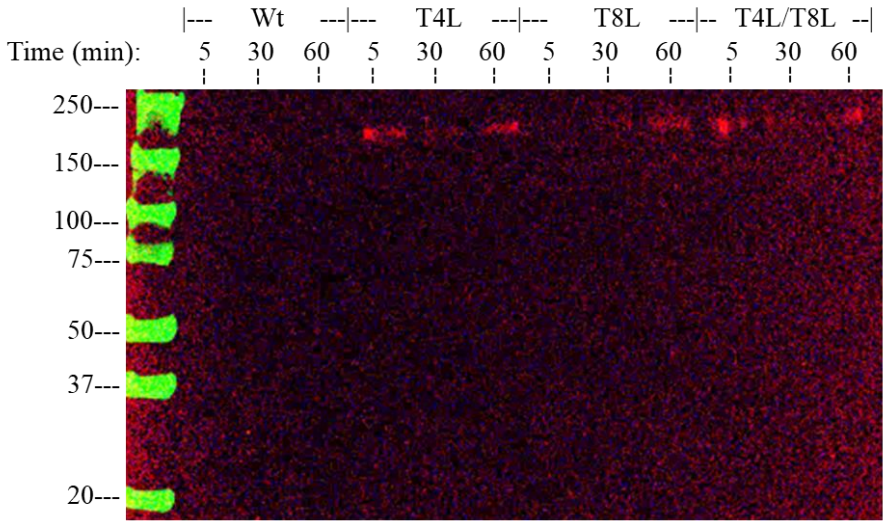

Figure 53 - Effect of Activated Neutrophils on ADAMTS13-Resistant Mutants.

100 nM ADAMTS13, as wild-type, T4L mutant, T8L mutant, or T4L/T8L mutant, was incubated with 50,000 PMA-simulated neutrophils for 5, 30, or 60 minutes at 37°C, then separated using SDS-PAGE under reducing conditions and analyzed through a western blot using the anti-ADAMTS13 antibody. Degradation of ADAMTS13 is represented by the decrease in the intensity of the ADAMTS13 band.

4. DISCUSSION

The studies described in this thesis were undertaken to examine the mechanisms that regulate ADAMTS13. Many investigators in the field postulate that the open/closed conformation serves to regulate ADAMTS13 activity *in vivo*. In circulation, ADAMTS13 exists in a closed conformation and upon binding to VWF, it adopts an open conformation and is poised for proteolysis (190, 201). Despite these conformational changes, ADAMTS13's activity is retained in both the open and closed conformation, suggesting that this is not a significant mechanism for regulating ADAMTS13 function in circulation (190, 201). The goals of the project were to (a) develop and optimize *in-vitro* plasma BioID to identify novel interactions to ADAMTS13, (b) validate novel interactions using BLI and SPR, (c) identify proteases capable of degrading ADAMTS13 and their proteolytic sites, and (d) develop a protease-resistant ADAMTS13, pr-ADAMTS13, as a potentially novel therapeutic to treat thrombosis.

Previous work by Guo *et al* confirmed that ADAMTS13 is not susceptible to inhibition by tissue inhibitors of metalloproteases (TIMPs), consistent with its long half-life in circulation (219). Therefore, ADAMTS13 is not regulated by canonical pathways of metalloprotease regulation in circulation. We hypothesized that other plasma proteins may contribute to the regulation of ADAMTS13. Therefore, we sought to perform an unbiased BioID screen to identify novel ligands of ADAMTS13 that may be important to its regulation.

Our BioID screen identified 5 plasma proteins significantly labelled by ADAMTS13-BirA*. Vitronectin was substantially labelled by unconjugated BirA* and was subsequently found not to bind ADAMTS13. Plasminogen was also substantially labelled by unconjugated BirA* and was found to bind ADAMTS13 with high affinity. The interaction between ADAMTS13 and plasminogen was mediated by the c-terminal domains of ADAMTS13 (TSP2-8-CUB1-2) and the Kringle domains of plasminogen in a lysine-dependent manner. ADAMTS13 is rapidly degraded by plasmin *in-vitro* and is protected from plasmin by TXA and EACA at therapeutic concentrations. These data demonstrate that *in-vitro* BioID is a useful technique to identify protein-protein interactions in plasma and identified proteolysis as a potential mechanism of ADAMTS13 regulation. Subsequent studies expanded the list of proteases capable of degrading ADAMTS13 to include FXIa and neutrophil-derived proteases such as Cathepsin G, elastase, and hPR3. These data suggest that activated neutrophils may play an important role in regulating the activity of ADAMTS13 *in-vivo*. Lastly, we identified the most common proteolytic sites on ADAMTS13 and engineered various protease-resistant forms of ADAMTS13. These variants of ADAMTS13 are resistant to degradation by plasmin and activated neutrophils, suggesting that they may serve as novel therapies to treat thrombosis. Overall, this project developed and deployed a novel screening tool to investigate protease biology, and identified and characterized a novel mechanism for the regulation of ADAMTS13.

4.1. BioID ADAMTS13

BioID is a unique technique for discovering protein-protein interactions and mapping protein interactomes. By covalently attaching biotin to interacting proteins, BioID identifies new substrates or protein-protein interactions. BioID might appear to be a "fishing expedition", that may result in no new discoveries. However, BioID is a proven concept that is both specific and sensitive in many biological systems (272, 273, 290, 304, 329). We aim to adapt the BioID technique to an *in-vitro* plasma system to further explore the interactome of ADAMTS13 and investigate its regulatory mechanism.

Our BioID studies aim to revisit the concept that the open/closed conformation is the primary mechanism for ADAMTS13 regulation. In addition, these studies are also positioned to identify potentially novel substrates of ADAMTS13, challenging the current understanding that its substrate is VWF (211). The goals of our BioID studies were to (a) identify novel ligands or substrates, and (b) validate potential novel interactions, to explore their role in the regulatory mechanism of ADAMTS13. This chapter contains a detailed discussion on the development and utilization of our BioID assay, emphasizing the optimization of the *in-vitro* plasma BioID technique and its use in advancing the understanding of the ADAMTS13 regulatory mechanism. In the next chapter, we demonstrate and characterize in more detail the additional proteases capable of degrading ADAMTS13 and their potential role in regulating ADAMTS13 activity. Further exploring the regulatory mechanism of ADAMTS13 may provide significant insight into ADAMTS13's role in the cardiovascular system, potentially leading to a better understanding and easier detection of blood clot diseases.

Roux *et al* termed BioID after the use of a promiscuous biotin ligase, fused with an intermediate filament protein Lamin A, in a eukaryotic cell system (272). Since then, many groups have adapted the BioID technique to other environments and advance forms of the BirA*, yet none have utilized a plasma system. Although no known study has reported on the use of BioID in plasma, we can postulate that *in-vitro* plasma BioID can be developed. This hypothesis is supported by the development of ivBioID whereby Remnant *et al* demonstrated *in-vitro* BirA* activity via the addition of exogenous ATP and biotin onto eukaryotic cells (308). As a result, the addition of exogenous ATP and biotin into plasma rendered BirA* active, which was demonstrated in our BioID studies.

The efficiency of BirA* to label in an environment that was not established before was crucial in the development of this project. Although the rate of biotinylation activity by BirA* was not directly quantified, it was qualitatively assessed in the presence versus the absence of BirA*. The SDS-PAGE and SYPRO-RUBY total protein stain of the BioID reactions provided evidence of non-specific protein labelling and therefore biotinylation activity. Increasing the concentration of BirA* in the reactions resulted in more protein detection on the gel, suggesting increased protein labeling. However, we avoided saturating the labelling reactions with BirA* activity to increase the specificity of the labelling to ligands of ADAMTS13 (305, 329). Thus, 100 nM of BirA* was chosen as the optimal concentration for our initial SDS-PAGE and LC/MS/MS studies.

For further confirmation on the use of the BioID technique in a plasma system, the first trial test of the BioID experiment's LC/MS/MS analysis was performed. As characterized by Roux *et al*, the labeling vicinity of BirA* is within a 10 nm radius, which

includes auto-labeling of BirA* and its attached protein (330). As demonstrated by Branon *et al*, the highest labeling signal represents auto-biotinylation (305). Based on the LC/MS/MS results, and literature, the highest number of hits for labeled ADAMTS13 was anticipated. However, the overall low labeling count indicated a need for optimization.

BirA* consumes ATP and biotin during the biotinylation reaction. We can postulate that the labeling count could improve through increased availability of the limiting reagents. As demonstrated by Gorman *et al*, the half-life of ATP in citrated plasma can be up to ~5 minutes (324). Gorman *et al* measured the half-life of ATP through a luciferase assay and identified that the stability of ATP in citrated plasma is greatly influenced by the presence of ATPases and phosphatases (324). These enzymes also consume ATP during their ATP hydrolysis and energy-producing reactions (324). Thus, we hypothesize that the use of ATPase and phosphatase inhibitors could improve ATP stability in citrated plasma and increase the labeling efficiency of the BirA*.

As demonstrated by Gorman *et al*, $NaVO_4$, IBMX, and NBTI increased the half-life of ATP in plasma and were among the inhibitors chosen for our assay (324). $NaVO_4$ is a competitive ATPase inhibitor that acts as a transition-state phosphate analogue, trapping ATPases during the transfer of the phosphate group (331). IBMX is a competitive non-specific phosphatase inhibitor that is derived from the purine xanthine and blocks the binding site of various phosphatases (332). NBTI is an adenosine analogue that inhibits ATP consumption competitively by competing with adenosine-containing molecules such as ATP (333). EDTA is a strong chelator of divalent cations and chelates Mg^{2+} and Ca^{2+}

which are often utilized by ATPases during ATP hydrolysis reactions and was thus used as a control (324).

The use of various ATPase inhibitors ($NaVO_4$, IBMX, and NBTI) in combination was able to slightly prolong the half-life of ATP in the citrated plasma. However, inhibition of phosphatase activity appeared to also affect the biotinylation activity of BirA*, resulting in lower labeling of plasma proteins. Further, as the strongest inhibitor, the use of EDTA increased the half-life of ATP in citrated plasma the most. However, EDTA also completely inhibited the labeling activity of BirA*. BirA*, along with many ATPases, hydrolyzes ATP in the form of MgATP whereby Mg^{2+} is needed (315). The Mg^{2+} ions create a complex with ATP molecules to allow the hydrolysis of ATP to take place, thus allowing ATP to be readily available in the form of MgATP (334). Thus, using a strong chelator such as EDTA inhibits the ATP hydrolysis reaction required for BirA* activity. In addition, the use of other inhibitors inhibited BirA* like that of ATPases or phosphatases, and as a result reduced the labelling efficiency of BirA*. These data suggest that improving ATP stability in plasma by inhibiting phosphatase and ATPase activity is not a viable approach to improving BioID labelling efficiency in citrated plasma. As a result, our BioID assay required serial supplementation of ATP into the reaction over the labelling period.

In another optimization strategy, the anticoagulant utilized was changed from citrate to hirudin. Citrate chelates free divalent cations including Mg^{2+}, $Ca^{2+,}$ and Zn^{2+}, but is not as strong as EDTA and will not easily chelate these divalent cations bound to protein (313). Mg^{2+} is utilized in the ATP hydrolysis reaction and the labeling reaction of BirA*, whereas Ca^{2+} and Zn^{2+} are required in the interaction between ADAMTS13 and VWF and

the proteolysis of VWF (315, 335). When both Ca^{2+} and Zn^{2+} are present, ADAMTS13 proteolysis of VWF multimer increases 6-fold (236). Changing the anticoagulant to Hirudin was used to restore the resemblance of a physiological state of the ions in plasma without the formation of blood clots. Our LC/MS/MS analysis of a Hirudin-based plasma system demonstrated an increase in labelled proteins from 14 to 32. However, a closer look revealed that the high count was caused by improper sample washes after immunoprecipitation. The LC/MS/MS data was statistically analyzed, and only four significant hits were identified. Thus, the strategy of changing the anticoagulant appeared to not improve labelling efficiency and was abolished.

After identifying the optimized conditions for the *in-vitro* BioID assay, a final BioID analysis run was performed. Through the LC/MS/MS analysis of the optimized BioID experiment, 199 proteins were uniquely identified by ADAMTS13, and 108 proteins were significant to ADAMTS13.

Unexpectedly, ADAMTS13-BirA* plasma BioID identified intracellular and cell-associated proteins like actin and tubulin. These proteins were consistently identified throughout all ADAMTS13-BirA* BioID experiments and not in unconjugated BirA* conditions. While plasma does not contain hematopoietic cells, it may contain microparticles derived from hematopoietic and non-hematopoietic cells such as endothelial cells. The identification of actin and tubulin may reflect the labeling of receptors on the surface of plasma microparticles such as CD36 (199). ADAMTS13 binds to the cell surface receptor CD36 via TSP-1 repeats contained at its C-terminus (199). CD36 binding to ADAMTS13 is consistent with CD36 involvement in localizing ADAMTS13 on the

endothelial cell surface and platelets, where ADAMTS13 can regulate the size of VWF multimers (199). However, since both actin and tubulin are intracellular proteins, they were disregarded from further analysis. Therefore, validation studies primarily focussed on known extracellular plasma proteins.

4.2. Validation of Novel Interactions

One of the unique properties of ADAMTS13 is its only known interaction is with VWF (336). However, that is unlikely as other metalloproteases, including other ADAMTS proteins, have multiple substrates (214). Our BioID studies identified potential interactions between ADAMTS13 and 5 other proteins including plasminogen. The goal of our validation studies is to confirm or refute the potential novel interactions with ADAMTS13. We have shown that ADAMTS13's CUB domains interact with the Kringle domains of plasminogen in a lysine-dependent manner. In addition, we have refuted the interaction between ADAMTS13 and vitronectin as well as any other Kringle domain-containing proteins. Plasminogen is activated into plasmin whereby their Kringle domains are conserved (38, 325). Previous work by Feys *et al* demonstrated that ADAMTS13 deficiency in TTP patients could be caused by plasmin proteolytically degrading ADAMTS13 (337). Thus, we hypothesize that locally high concentrations of proteases regulate the ADAMTS13 mechanism through proteolytic degradation.

Vitronectin, an anti-fibrinolytic molecule, was identified on the list of potential proteins interacting with ADAMTS13 (338). Through an ELISA plate binding assay, the

interaction between vitronectin and ADAMTS13 was refuted due to vitronectin binding to BirA*. In contrast, using BLI demonstrated a binding affinity average, K_d, of 91 nM between vitronectin and ADAMTS13 in a static environment. However, this test needed to be repeated in the presence of ADAMTS13-BirA* to see the binding effect that BirA* may have on vitronectin. In contrast, further analysis of the interaction between vitronectin and ADAMTS13 using SPR in a flow system could not accurately determine the binding affinity. Thus, the non-specific labelling of vitronectin might have been the consequence of interaction with BirA* suggesting that ADAMTS13 does not interact with vitronectin (339). However, these data do demonstrate that vitronectin is a potential false-positive in future plasma BioID studies of other target proteins due to its interaction with the BirA* enzyme.

VWF, the only known substrate for ADAMTS13, was also identified with a low number of spectral counts. The FRETS-VWF73 clinical assay revealed that BirA* did not affect the proteolytic activity of ADAMTS13. As a result, ADAMTS13-BirA* should be capable of labeling VWF. However, the low degree of VWF labeling by ADAMTS13-BirA* could be attributed to the reaction taking place in the absence of flow conditions, and that sufficient fluid shear stress was required to optimize their interaction (126, 323). In fact, only 3% of ADAMTS13 interacts with VWF in circulation under low shear conditions (323). ADAMTS13 has both shear-independent and shear-dependent interactions with VWF. The shear-dependent interactions are mediated between MDTCS and the unfolded A2 domain (210). The shear-independent interaction is mediated between the ADAMTS13-CUB domains and the D4-CK domains of VWF (190). The shear-

independent interaction may have been attenuated because of the BirA* fusion to the CUB domains, thereby resulting in lower spectra counts in the mass spec data of this experiment. Lastly, citrate chelates available Ca^{2+} ions which are required for the interaction between ADAMTS13 and VWF (315, 335). To label VWF specifically, the BioID assay needed further optimization which is discussed further in our future studies.

Under high shear stress, the binding affinity of VWF to ADAMTS13 is 79 nM (200). In contrast, using BLI demonstrated a binding affinity average, K_d, of <1 pM between multimeric VWF and ADAMTS13 in a non-flow environment. In contrast, further analysis of the interaction between multimeric VWF and ADAMTS13 using SPR in a flow system could not accurately determine the binding affinity. The difference in K_d values and/or the inability to determine an accurate binding affinity could be to the various sizes of VWF multimers inserted into the system. Thus, the validation studies of novel interactions were confirmed by comparison to negative controls, such as BSA, and not by comparison to VWF. Future studies could utilize a VWF monomer or the VWF73 substrate, without the FRETS system, to provide a more accurate binding affinity between VWF and ADAMTS13.

Plasminogen was also another protein identified with an average of 30 peptide counts as a novel interaction with ADAMTS13. Plasminogen is the inactive precursor of the fibrinolytic serine protease plasmin. Plasmin is activated by t-PA or u-PA and primarily targets and degrades fibrin but can also degrade other blood-circulating proteases such as ADAMTS13 (36, 239). Human plasminogen is a 92 kDa glycoprotein with five kringle domains (kI → kV) followed by a protease domain (P), and it can be found in closed (Glu-

Pg) or open form (Lys-Pg) (36, 340). Lower molecular weight forms of plasminogen also exist, such as mini-Pg (58 kDa, containing only Kringle 5 domain) and μ-Pg (30 kDa, containing no Kringle domains) (340). These lower molecular weight forms of plasminogen are generated by auto-digestion *in-vitro* or by proteolytic degradation by elastase, plasmin, and other proteolytic enzymes (340). However, both mini-Pg and μ-Pg have poor physiological relevance due to their poor fibrinolytic capacity once converted to mini-plasmin and μ-plasmin (340). Thus, mini-Pg and μ-Pg are generally generated and utilized to further study the roles of the plasminogen domains.

Our SPR studies demonstrated that various forms of Pg (Lys-Pg, Glu-Pg, and mini-Pg) interacted with immobilized ADAMTS13. All these forms share the common plasminogen structure (protease domain, disulfide bridge, and Kringle domains) except for mini-Pg having only one kringle domain KV. Kringle domains are protein domains that fold into large loops that are held together by three disulfide bridges (340, 341). However, the interactions of the various forms of Pg (Lys-Pg, Glu-Pg, and mini-Pg) were limited to full-length ADAMTS13 and not MDTCS, implying that the c-terminal TSP-2-8 or CUB domains play a role in the interaction. Furthermore, using the lysine analogues EACA and TXA, which block lysine binding sites on plasminogen's Kringle domains, mainly KV (342), reduced the binding interaction between ADAMTS13 and Pg. This finding points to the discovery of a novel interaction between the CUB domains of ADAMTS13 and the Pg Kringle domains. Since the interaction between ADAMTS13 and Pg may be related to the Kringle domains of Pg, it would be interesting to see what other proteins interact with

ADAMTS13 via a similar interaction. This discovery also raises the question of how many other Kringle domain-containing proteins in plasma can interact with ADAMTS13.

Other plasma proteins with Kringle domains such as FXII, prothrombin, and apolipoprotein A (343–346), were also tested for ADAMTS13 interaction. Our data indicate that neither FXII nor prothrombin bind to ADAMTS13, suggesting that ADAMTS13 does not possess general kringle binding properties. The FXII Kringle domain shares low sequence similarity with plasminogen Kringle 4 domain, and although FXII has fibrin-binding properties, it is unclear whether it is through lysine-mediated binding of the Kringle domain (347, 348). The 2 kringle domains in prothrombin share sequence similarity with plasminogen Kringle 1 domain but lack the ability to bind to lysine residues (349, 350). Therefore, the inability of ADAMTS13 to bind to FXII and prothrombin may reflect an inability of these kringle domains to bind lysine residues. While FXII and prothrombin were not identified to have a significant interaction with ADAMTS13 using the BioID screen, these analytes were still tested for a binding interaction using SPR as they contained a Kringle domain. Interestingly, prothrombin did not interact with ADAMTS13, but FXII may have done so. However, due to the binding profile of ADAMTS13 to FXII and the K_d value calculated, further tests are suggested to confirm the interaction between the two proteins.

The various forms of apolipoprotein A, as Apo(a), LDL, or Lp(a), were investigated for their interaction with ADAMTS13 and unfortunately, our data indicates that none of these analytes bound to the immobilized ADAMTS13. Lipoprotein A, Lp(a), another Kringle domains-containing protein is composed of a lipid core, low-density lipoprotein

(LDL), and is surrounded by apolipoprotein-B, Apo(b), which is linked via disulfide bond to apolipoprotein A, Apo(a). Apo(a) is made up of a protease-like domain and several Kringle domains with a shared resemblance to that of plasminogen's K-IV domain (346). Lp(a) is a protein that plays a contributing role in the process of atherogenesis, and its levels can predict the risk of myocardial infarctions (MIs) (346, 351). Low levels of ADAMTS13 were found to be associated with an increased risk of MIs through the influence of lipid levels (352). Particularly, ADAMTS13 levels were positively correlated with cholesterol and triglycerides, and negatively correlated with high-density lipoprotein-cholesterol levels (352). These clinical observations would be consistent with ADAMTS13 binding to Lp(a), which is also consistent with ADAMTS13 binding to plasminogen kringle domains, which share >80% sequence homology to Lp(a). We were therefore surprised to find that ADAMTS13 did not bind to Lp(a) in our studies. Future studies will revaluate the interaction between ADAMTS13 and Lp(a). The Apo(a) proteins' large size may be a limiting factor in this system. Alternatively, this finding indicated that the interaction between ADAMTS13 and Pg was not solely based on K-IV domains and may have also been the result of the involvement of another Kringle domain. Another possibility is that the glycosylation pattern on Apo(a) may have prevented it from interacting with ADAMTS13. Lastly, it may be possible that ADAMTS13 interacts with Lp(a), and further research into this interaction, if found to be positive, may lead to the discovery of new preventative measures for treating, combating, or lowering the risk of MIs.

Overall, BioID is a proven method that we have adapted and optimized for use in plasma. As technology advances, the BioID assay can be further optimized by employing

newer biotin ligases, such as MiniTurbo and TurboID, which were generated from yeast display-based direction evolution to the original promiscuous biotin ligase and have been shown to consume less ATP and label in 10 minutes what the original BirA* labelled in 18 hours (304, 305). The availability of ATP was the most important factor in the assay's optimization, and thus, by requiring less ATP, the newer biotin ligases will provide a higher resolution and labeling efficiency. Furthermore, this may enable us to identify protease substrates with rapid turnover as opposed to just ligands that exist in equilibrium between bound and unbound states. As the BioID technique is further developed, the BioID assay can be implemented in other environments, such as with purified platelets, red blood cells, or leukocytes. In addition, other plasma proteins such as coagulation factors could also be studied. BioID can also be applied to the rest of the ADAMTS family proteases and other proteases and substrates, such as VWF, in the coagulation system. This innovative strategy allowed us to identify the new interaction between the CUB domains of ADAMTS13 to the Kringle domains of plasminogen, possibly alluding to the discovery of new roles and a better understanding of ADAMTS13 in the cardiovascular system. As a result, this strategy provides an opportunity for ground-breaking research progress in the coagulation system, and the findings from this project may apply to a variety of blood disorders, including TTP, VWD, and others.

4.3. Proteolytic Degradation of ADAMTS13

ADAMTS13 is constitutively secreted as an active protease, yet VWF retains its capacity to recruit platelets despite normal ADAMTS13 levels during a hemostatic response. This ability makes ADAMTS13 an enigmatic protease with an unknown regulatory mechanism. Our data demonstrated that plasminogen bind to ADAMTS13, and that plasmin cleaves ADAMTS13 in a lysine-dependent mechanism. Plasmin activity has been detected in TTP patient samples, suggesting plasmin-mediated degradation may be a novel and important mechanism for the regulation of ADAMTS13 *in vivo* (337). We, therefore, sought to systematically examine other proteases in coagulation and inflammation for their capacity to cleave and regulate ADAMTS13 activity *in vivo*. In addition, we identified 2 linker regions within the tsp repeats as the most common proteolytically degraded sites on ADAMTS13 and produced proteolytic-resistant variants of ADAMTS13. Future studies will examine the therapeutic benefit of a protease-resistant form of ADAMTS13 to thrombotic disorders such as TTP, ischemic stroke, or VTE (166, 265, 353).

Our data provides a comprehensive and systematic examination of circulating proteases capable of degrading ADAMTS13 and identify the sites of cleavage. The ability of these enzymes to cleave ADAMTS13 likely contributes to the regulation of ADAMTS13 activity. Our survey of proteases revealed that plasmin, thrombin, FXa, FXIa, and tPa can cleave ADAMTS13 and that APC, FVIIa, FIXa, and FXIIa could not cleave ADAMTS13. This was consistent with previous studies that have shown that ADAMTS13 is cleaved by several proteases such as plasmin, thrombin, and FXIa (239). Our data further suggests that

there are more enzymes capable of proteolytically degrading ADAMTS13. Furthermore, because neutrophil activation can contribute to hemostasis and thrombosis under conditions of inflammation (53), neutrophil-derived proteases including neutrophil elastase, cathepsin G, and hPR3 were also tested. Both proteases cleaved ADAMTS13, with Cathepsin G completely degrading ADAMTS13 under the same conditions as the other tested proteases. Reducing Cathepsin G concentration produced a banding pattern similar to thrombin and neutrophil elastase. Cathepsin G's ability to degrade ADAMTS13 efficiently may imply that it is an effective regulator of ADAMTS13 activity *in-vivo*. Previous work by Ono *et al* demonstrated that ADAMTS13 deficiency, an increase in ultra-large VWF multimers, and lower molecular weight forms of ADAMTS13 were present in more than half of sepsis-induced disseminated intravascular coagulation patients (354). This observation is consistent with our hypothesis that ADAMTS13 can be proteolytically regulated at sites of vascular injury. Taken together with our data, ADAMTS13 is postulated to be proteolytically degraded by neutrophil-derived enzymes which further enhances the hypothesis that ADAMTS13 activity is regulated by proteolytic degradation. In addition, neutrophil-derived enzymes are more effective at regulating ADAMTS13 activity, and thus may play a greater role in regulating ADAMTS13 activity *in-vivo*.

Previous work by Garland *et al* demonstrated plasmin, thrombin and FXIa initially remove the CUB domains of ADAMTS13 (239). In addition, Garland *et al* demonstrated that the removal of the CUB domains, via proteolytic degradation or its inhibition via an antibody, drastically reduces the capacity of ADAMTS13 to bind and cleave VWF in a flow chamber assay (239). Thus, the removal of ADAMTS13 CUB domains is postulated

to remove the ability for ADAMTS13 to cleave VWF multimers. Our survey of proteases revealed the proteolysis of ADAMTS13 in a banding pattern similar to Garland *et al*, beginning with the truncation of the CUB domains at the T8-linker (239). In all our coagulation proteases capable of cleaving ADAMTS13, the first band to appear is ~150 kDa and is representative of ADAMTS13 without the CUB domains. In addition, when reducing the concentration of the neutrophil-derived enzymes, the ~150 kDa was also prominent which further emphasized that the removal of the CUB domains is the first step in the proteolytic degradation of ADAMTS13. These data, along with previous work by Garland *et al*, further emphasizes the importance of the CUB domains in the regulatory mechanism of ADAMTS13. Furthermore, Banno *et al*, demonstrated that C57BL/6 mice have an ADAMTS13 gene that lacks the CUB domains, and that plasma from these mice are less effective at cleaving VWF in a flow chamber than plasma from 129/Sv mice, which possess a full-length ADAMTS13 gene (326).

In contrast, previous studies showed that the removal of the CUB domains does not affect ADAMTS13's proteolytic activity towards small biochemical substrates like FRETS-VWF73 (190). Using the clinical FRETS-VWF73 assay, ADAMTS13 lacking CUB domains exhibits twice the activity rate in cleaving the VWF substrate (190). In comparison, our FRETS-VWF73 data also demonstrated an increase in enzymatic activity using proteolytically degraded ADAMTS13, which is consistent with previous work by South *et al* (190). The FRETS-VWF73 substrate is a 73 amino acid VWF peptide of the A2 domain which is utilized to test the activity of ADAMTS13 in the absence of shear stress (139). In addition, the VWF peptide lacks the D4-CK domains which interact with

ADAMTS13's CUB domains in promoting VWF proteolysis (139). After the initial interaction, the ADAMTS13 Spacer domain is exposed which initiates exosite binding to the VWF A2 domain (139). Thus, truncated ADAMTS13 is more effective at cleaving the VWF73 peptide because the exposed Spacer domain is more readily available to interact and initiate exosite binding with VWF73 (190). Hence, the proteolysis of ADAMTS13 is postulated to be a mechanism that partially controls ADAMTS13's ability to modulate VWF platelet binding activity *in vivo*. Therefore, proteolytically degraded ADAMTS13 may exhibit similar activity in biochemical and clinical assays that quantify ADAMTS13 by FRETS-VWF73 assay. However, because of the removal of the CUB domains, these degraded forms of ADAMTS13 possess drastically reduced anti-thrombotic activity *in vivo*. This may be relevant in sepsis where the correlation between ADAMTS13 activity and antigen levels have a poor correlation. Sepsis patients can experience DIC due to unregulated protease activity. This protease-rich state may degrade adamts13 and reduce its capacity to regulate massive quantities of VWF released by endothelial cell activation. Therefore, while ADAMTS13 activity levels may be normal in sepsis patients, its capacity to down-regulate the prothrombotic state caused by high VWF levels may be impaired. Protease-resistant variants of ADAMTS13 may therefore be useful in the treatment of sepsis-related thrombosis and DIC.

In contrast to the literature and our findings, proteolytically degraded ADAMTS13 by neutrophil elastase demonstrated a decrease in activity when considering the rate of ADAMTS13 alone. By subtracting the activity rate of neutrophil elastase, the activity rate of ADAMTS13 was decreased greatly, but not abolished, when compared to other cleaved

forms of ADAMTS13. This data suggests that neutrophil elastase (a) is a more potent regulator of ADAMTS13 activity, and (b) targets ADAMTS13 differently than other proteases. This observation caused us to further examine the role activated neutrophils may have in regulating ADAMTS13 activity.

Activated neutrophils secrete neutrophil extracellular traps (NETS) and numerous proteases as a defence mechanism against foreign microbes (355). These proteins can influence the activities of both ADAMTS13 and VWF. Reduced ADAMTS13 activity, along with increased VWF levels, has been associated with systemic inflammation in thrombotic microangiopathies (TMAs), such as sepsis, sepsis-induced disseminated intravascular coagulation (DIC), and autoimmune diseases (356, 357). Although the mechanism is not fully understood, activated neutrophils contribute to the decrease in ADAMTS13 levels through proteolytic degradation of ADAMTS13 by the secreted enzymes, and/or oxidation of ADAMTS13 by the release of hypochlorous acid that is produced by myeloperoxidase (357, 358). We demonstrated that PMA-stimulated neutrophils are capable of degrading ADAMTS13 as evident by the intensity of the ADAMTS13 band in our western blot which decreased as the number of activated neutrophils increased. This implies that the higher cell count secreted a greater number of neutrophil-derived proteases, thus, accelerating the degradation of ADAMTS13. Furthermore, by utilizing the serine protease inhibitor AEBSF and the metalloprotease inhibitor EDTA, we demonstrated that serine proteases have a greater impact on ADAMTS13 proteolytic degradation than the metalloprotease family of proteins. Additionally, by utilizing the specific serine protease inhibitors Sivelstat (elastase

inhibitor), Cathepsin-G Inhibitor I, and AEBSF, we demonstrated that neutrophil elastase has the greatest impact on ADAMTS13 proteolytic degradation. These findings reiterate the fact that neutrophil elastase (a) is a more potent regulator of ADAMTS13 activity, and (b) targets ADAMTS13 differently than other proteases. Therefore, targeting and inhibiting neutrophil elastase could be utilized as a therapeutic strategy to normalize the ADAMTS13 activity levels in thrombosis and sepsis.

Activated neutrophils are known to release neutrophil extracellular traps (NETs), a web-like structure of DNA containing many proteases as a mechanism for combating pathogens (328). In addition, VWF has been shown to bind to NETs and form a network capable of recruiting both platelets and leukocytes, inducing thrombosis (150). To examine the contribution of NETs to ADAMTS13 degradation by neutrophil-derived proteases, we performed activated neutrophil degradation studies in the presence of DNase I to digest the DNA of NETs (359, 360). We demonstrated that the presence of DNase I accelerated the degradation of ADAMTS13 by activated neutrophils. This is caused by an improvement in the solubility of the neutrophil-derived proteases mixing with ADAMTS13 allowing for greater accessibility and proteolysis to ADAMTS13. In vivo, the high viscosity of NETs may limit the mixing of neutrophil granular contents with the surrounding environment and prevent the widespread and disseminated proteolytic activity of neutrophil proteases. Interestingly, the activity rate on the proteolysis of VWF73 increased as the number of activated neutrophils increased in the presence of DNase I, and the activity rate drastically decreased in the absence of DNase I. This data suggests that activated neutrophils secreted enzymes capable of cleaving VWF73 or proteolytically degraded ADAMTS13 in a way

that increases its activity rate, such as in the case of Cathepsin G. In contrast, DNase I cleaved NETs which provided a free environment whereby the secreted enzymes, along with ADAMTS13, have an easier chance of finding and cleaving VWF73. To better understand the effect of activated neutrophils in the presence of DNase I has on the activity rate of ADAMTS13, AEBSF will be utilized in future replicates. Overall, our data along with literature suggest that activated neutrophils may regulate ADAMTS13 activity through proteolytic regulation by neutrophil-derived serine proteases.

While these studies demonstrated that ADAMTS13 can be degraded in purified systems, it remains unclear whether this is an important mechanism of its regulation *in vivo*. Our data identifies the first target by the proteases to be the T8-linker on ADAMTS13, followed by the T4-linker which is located between TSP4 and TSP5. Proteolysis of either linker facilitates the removal of ADAMTS13's CUB domains, limiting its capacity to regulate VWF platelet binding activity *in vivo*. Therefore, we sought to engineer a protease-resistant form of ADAMTS13, as T4L-, T8L-, or T4L/T8L- pr-ADAMTS13, that could be tested and compared to wt-ADAMTS13 for thrombolytic activity. If pr-ADAMTS13 is more effective *in vivo,* it would suggest that proteolytic degradation is an important regulator of ADAMTS13 activity. Pr-ADAMTS13 may also be a novel candidate thrombolytic agent or the treatment of microvascular thrombosis.

Initial characterization studies demonstrated that ADAMTS13 linker mutants are resistant to proteolysis by stimulated neutrophils and plasmin. Moreover, the double linker mutant demonstrated the highest resistance to proteolysis in comparison to the other mutants. However, these results are preliminary, and additional replicates are needed to

provide better conclusive evidence on the proteolytic resistance effect of the linker mutations. Our data also demonstrated that stimulated neutrophils and proteases such as plasmin cleave ADAMTS13 at multiple locations beginning with the T8-linker. Thus, we postulate that pr-ADAMTS13 mutants, specifically T4L/T8L-mutant, will be partially resistant to proteolysis and that the proteases will demonstrate delayed proteolysis of pr-ADAMTS13 mutants. This allows pr-ADAMTS13 mutants to have a longer half-life without hindering their clearance. Hence, pr-ADAMTS13 mutants could potentially be utilized as a novel therapeutic to thrombotic disorders whereby ADAMTS13 is acting as an anti-coagulant, such as in TTP, ischemic stroke, or VTE (166, 265, 353).

5. Future Directions

Understanding the role and regulatory mechanism of ADAMTS13 in biology will provide insight into the behavior of this enigmatic protease. ADAMTS13 having only one substrate, VWF, is unlikely as other metalloproteases including other members of the ADAMTS family have shown to have multiple substrates (214). ADAMTS13 appears to play important roles in many acute and chronic cardiovascular diseases. However, it remains unclear whether these roles are affected directly by ADAMTS13 or are a result of the multimeric distribution of VWF, or both. We have developed a BioID protocol for an *in-vitro* assay in plasma to identify novel interactions of proteins in plasma. This BioID assay is continuously being optimized and, as of right now, the assay was utilized to find novel substrates or protein-protein interactions to ADAMTS13. In the near future, we are updating our ADAMTS13-BirA* with the latest, higher resolution and faster labeling,

biotin ligases such as MiniTurbo and TurboID. The ability to label substrates and protein-protein interactions faster may resolve our low yield in labeling ADAMTS13's only known substrate, VWF.

After successful optimization of the *in-vitro* plasma BioID assay, the BioID assay can then be further enhanced for other environments and/or proteins, such as with purified platelets, red blood cells, leukocytes, or cultured endothelial cells. BioID can also be applied to the rest of the ADAMTS family proteases and other proteases and substrates, such as VWF, in the coagulation system. This innovative strategy is an opportunity for ground-breaking research progress in the coagulation system, and the findings from this project will be of relevance to many blood disorders such as TTP, VWD, and more.

The capability of ADAMTS13 to be degraded by active proteases is currently the only known mechanism of ADAMTS13 regulation. Previously, the regulation of ADAMTS13 was unclear because of its constitutive secretion as an active protease, and resistance to all known natural protease inhibitors. We have shown several proteases that are capable of degrading ADAMTS13. Even though the concentrations of coagulation proteases required to partially degrade ADAMTS13 are high and may not be of physiological relevance; the neutrophil-derived proteases showed that significantly a lower concentration of neutrophil proteases was required to partially degrade ADAMTS13; demonstrating that neutrophil proteases may be more significantly relevant in the regulation of ADAMTS13. Our next aim is to examine whether locally high protease concentrations at sites of vascular injury can degrade ADAMTS13 *in-vivo*. This objective will also overlap

in the understanding of how neutrophil-derived proteases, and the production of NETs, affect the activity of ADAMTS13.

Using FRETS-VWF73 to evaluate ADAMTS13 activity to VWF may not provide a full assessment of its activity since the truncated forms of ADAMTS13 can cleave VWF73 (209). To better evaluate the effect the proteolytic degradation has on the activity of ADAMTS13, there needs to be an additional step. Truncated forms of ADAMTS13, combined with inhibitors such as alpha-2-macroglobulin, will be evaluated for a decrease in ADAMTS13 activity using FRETS-VWF73. This project is currently being tested by my colleague Kanwal Singh. Another method to evaluate the effect the proteolytic degradation has on ADAMTS13 activity is to use VWF multimers and the presence of shear. Using a flow device, or a system that can induce shear force, the multimeric distribution of VWF will be evaluated for a change in multimeric distribution after ADAMTS13 is truncated by different proteases. The multimeric distribution will be observed on a VWF multimer gel or by a western through identification of the cleaved VWF by an anti-VWF antibody. The use of VWF multimers will help evaluate if the truncated CUB domain of ADAMTS13 can act as an inhibitor to ADAMTS13 proteolysis of VWF, as eluted by in literature (239). This line of investigation is currently being explored by my colleague Veronica DeYoung in the Kretz Lab.

Lastly, by identifying the proteases that can degrade ADAMTS13, we gained a closer step into a better understanding of how ADAMTS13 activity can be reduced at sites of vascular injury. After identifying the proteolytic sites on ADAMTS13 that are first cleaved by the various proteases, we aimed to and have generated potentially protease-

resistant ADAMTS13 mutants. Our preliminary results have shown these mutants to potentially have a protease-resistant ability; however, our findings remain preliminary and additional tests are needed to provide more conclusive evidence. Our next aim is to evaluate the proteolytic resistance of our developed protease-resistant ADAMTS13 mutants *in-vivo*. Potentially, our novel protease-resistant ADAMTS13 mutants may become of a therapeutic interest and be tested as a treatment possibility for the disorders affected by the low levels of ADAMTS13, such as TTP or sepsis.

In conclusion, the work of this thesis project developed plasma BioID, identified plasminogen and characterized its interaction with ADAMTS13, investigated other protease's capacity to regulate ADAMTS13, and developed a protease-resistant ADAMST13 that will be used to test the relevance of the ADAMTS13 mechanism of regulation *in vivo*.

REFERENCES

1. Versteeg, H. H., Heemskerk, J. W. M., Levi, M., and Reitsma, P. H. (2013) New Fundamentals in hemostasis. *Physiological Reviews*. 10.1152/physrev.00016.2011

2. Kretz, C. A., Weyand, A. C., and Shavit, J. A. (2015) Modeling Disorders of Blood Coagulation in the Zebrafish. *Current Pathobiology Reports*. 10.1007/s40139-015-0081-3

3. Mackman, N., Tilley, R. E., and Key, N. S. (2007) Role of the extrinsic pathway of blood coagulation in hemostasis and thrombosis. *Arteriosclerosis, Thrombosis, and Vascular Biology*. 10.1161/ATVBAHA.107.141911

4. Gailani, D., and Renné, T. (2007) The intrinsic pathway of coagulation: A target for treating thromboembolic disease? *Journal of Thrombosis and Haemostasis*. 10.1111/j.1538-7836.2007.02446.x

5. Levin, E. G., and Hanano, M. (1992) Endothelial cells and vascular hemostasis. *Nippon rinsho. Japanese journal of clinical medicine*

6. Stassen, J., Arnout, J., and Deckmyn, H. (2012) The Hemostatic System. *Current Medicinal Chemistry*. 10.2174/0929867043364603

7. Paulus, J. M. (1975) Platelet size in man. *Blood*. 10.1182/blood.v46.3.321.321

8. Stegner, D., and Nieswandt, B. (2011) Platelet receptor signaling in thrombus formation. *Journal of Molecular Medicine*. 10.1007/s00109-010-0691-5

9. Heemskerk, J. W. M., Kuijpers, M. J. E., Munnix, I. C. A., and Siljander, P. R. M. (2005) Platelet collagen receptors and coagulation. A characteristic platelet response as possible target for antithrombotic treatment. *Trends in Cardiovascular Medicine*. 10.1016/j.tcm.2005.03.003

10. Podoplelova, N. A., Sveshnikova, A. N., Kotova, Y. N., Eckly, A., Receveur, N., Nechipurenko, D. Y., Obydennyi, S. I., Kireev, I. I., Gachet, C., Ataullakhanov, F. I., Mangin, P. H., and Panteleev, M. A. (2016) Coagulation factors bound to procoagulant platelets concentrate in cap structures to promote clotting. *Blood*. 10.1182/blood-2016-02-696898

11. Blair, P., and Flaumenhaft, R. (2009) Platelet α-granules: Basic biology and clinical correlates. *Blood Reviews*. 10.1016/j.blre.2009.04.001

12. Yun, S. H., Sim, E. H., Goh, R. Y., Park, J. I., and Han, J. Y. (2016) Platelet activation: The mechanisms and potential biomarkers. *BioMed Research International*. 10.1155/2016/9060143

13. Shida, Y., Rydz, N., Stegner, D., Brown, C., Mewburn, J., Sponagle, K., Danisment, O., Crawford, B., Vidal, B., Hegadorn, C. A., Pruss, C. M., Nieswandt, B., and Lillicrap, D. (2014) Analysis of the role of von Willebrand factor, platelet glycoprotein VI-, and α2β1-mediated collagen binding in thrombus formation. *Blood*. 10.1182/blood-2013-09-521484

14. Dong, J. fei, Moake, J. L., Nolasco, L., Bernardo, A., Arceneaux, W., Shrimpton, C. N., Schade, A. J., McIntire, L. v., Fujikawa, K., and López, J. A. (2002) ADAMTS-13 rapidly cleaves newly secreted ultralarge von Willebrand factor multimers on the endothelial surface under flowing conditions. *Blood*. 10.1182/blood-2002-05-1401

15. Savage, B., Saldívar, E., and Ruggeri, Z. M. (1996) Initiation of platelet adhesion by arrest onto fibrinogen or translocation on von Willebrand factor. *Cell*. 10.1016/S0092-8674(00)80983-6

16. Tomokiyo, K., Kamikubo, Y., Hanada, T., Araki, T., Nakatomi, Y., Ogata, Y., Jung, S. M., Nakagaki, T., and Moroi, M. (2005) Von Willebrand factor accelerates platelet adhesion and thrombus formation on a collagen surface in platelet-reduced blood under flow conditions. *Blood*. 10.1182/blood-2004-05-1827

17. Gralnick, H. R., Williams, S. B., McKeown, L. P., Krizek, D. M., Shafer, B. C., and Rick, M. E. (1985) Platelet von Willebrand factor: Comparison with plasma von Willebrand factor. *Thrombosis Research*. 10.1016/0049-3848(85)90205-1

18. Varga-Szabo, D., Pleines, I., and Nieswandt, B. (2008) Cell adhesion mechanisms in platelets. *Arteriosclerosis, Thrombosis, and Vascular Biology*. 10.1161/ATVBAHA.107.150474

19. Pawlinski, R., Wang, J. G., Owens, A. P., Williams, J., Antoniak, S., Tencati, M., Luther, T., Rowley, J. W., Low, E. N., Weyrich, A. S., and Mackman, N. (2010) Hematopoietic and nonhematopoietic cell tissue factor activates the coagulation cascade in endotoxemic mice. *Blood*. 10.1182/blood-2009-12-259267

20. Tsai, H.-M. (2003) Platelet Activation and the Formation of the Platelet Plug. *Arteriosclerosis, Thrombosis, and Vascular Biology*. 10.1161/01.atv.0000058401.34021.d4

21. Crawley, J. T. B., de Groot, R., Xiang, Y., Luken, B. M., and Lane, D. A. (2011) Unraveling the scissile bond: How ADAMTS13 recognizes and cleaves von Willebrand factor. *Blood*. 10.1182/blood-2011-02-306597

22. Colman, R. W. (2006) Are hemostasis and thrombosis two sides of the same coin? *Journal of Experimental Medicine*. 10.1084/jem.20060217

23. Mackman, N. (2004) Role of tissue factor in hemostasis, thrombosis, and vascular development. *Arteriosclerosis, Thrombosis, and Vascular Biology*. 10.1161/01.ATV.0000130465.23430.74

24. Drake, T. A., Morissey, J. H., and Edgington, T. S. (1989) Selective cellular expression of tissue factor in human tissues. Implications for disorders of hemostasis and thrombosis. *American Journal of Pathology*

25. Petersen, L. C., Valentin, S., and Hedner, U. (1995) Regulation of the extrinsic pathway system in health and disease: The role of factor VIIa and tissue factor pathway inhibitor. *Thrombosis Research*. 10.1016/0049-3848(95)00069-4

26. Wu, Y. (2015) Contact pathway of coagulation and inflammation. *Thrombosis Journal*. 10.1186/s12959-015-0048-y

27. van Hinsbergh, V. W. M. (2001) The endothelium: vascular control of haemostasis. in *European Journal of Obstetrics and Gynecology and Reproductive Biology*, 10.1016/S0301-2115(00)00490-5

28. Riedel, T., Suttnar, J., Brynda, E., Houska, M., Medved, L., and Dyr, J. E. (2011) Fibrinopeptides A and B release in the process of surface fibrin formation. *Blood*. 10.1182/blood-2010-08-300301

29. Davie, E. W., Fujikawa, K., and Kisiel, W. (1991) The Coagulation Cascade: Initiation, Maintenance, and Regulation. *Biochemistry*. 10.1021/bi00107a001

30. Greenberg, C. S., Miraglia, C. C., Rickles, F. R., and Shuman, M. A. (1985) Cleavage of blood coagulation Factor XIII and fibrinogen by thrombin during in vitro clotting. *Journal of Clinical Investigation*. 10.1172/JCI111849

31. Roberts, H. R., Hoffman, M., and Monroe, D. M. (2006) A cell-based model of thrombin generation. *Seminars in Thrombosis and Hemostasis*. 10.1016/j.apnu.2005.08.008

32. Jesty, J., and Beltrami, E. (2005) Positive feedbacks of coagulation: Their role in threshold regulation. *Arteriosclerosis, Thrombosis, and Vascular Biology*. 10.1161/01.ATV.0000187463.91403.b2

33. Rezaie, A. R. (2010) Regulation of the Protein C Anticoagulant and Antiinflammatory Pathways. *Current Medicinal Chemistry*. 10.2174/092986710791233706

34. Li, W., Johnson, D. J. D., Esmon, C. T., and Huntington, J. A. (2004) Structure of the antithrombin-thrombin-heparin ternary complex reveals the antithrombotic mechanism of heparin. *Nature Structural and Molecular Biology*. 10.1038/nsmb811

35. Wiebe, E. M., Stafford, A. R., Fredenburgh, J. C., and Weitz, J. I. (2003) Mechanism of catalysis of inhibition of factor IXa by antithrombin in the presence of heparin or pentasaccharide. *Journal of Biological Chemistry*. 10.1074/jbc.M304803200

36. Henkin, J., Marcotte, P., and Yang, H. (1991) The plasminogen-plasmin system. *Progress in Cardiovascular Diseases*. 10.1016/0033-0620(91)90010-J

37. Chapin, J. C., and Hajjar, K. A. (2015) Fibrinolysis and the control of blood coagulation. *Blood Reviews*. 10.1016/j.blre.2014.09.003

38. Danø, K., Andreasen, P. A., Grøndahl-Hansen, J., Kristensen, P., Nielsen, L. S., and Skriver, L. (1985) Plasminogen Activators, Tissue Degradation, and Cancer. *Advances in Cancer Research*. 10.1016/S0065-230X(08)60028-7

39. Jung He Wu, and Diamond, S. L. (1995) Tissue plasminogen activator (tPA) inhibits plasmin degradation of fibrin: A mechanism that slows tPA-mediated fibrinolysis but does not require α2- antiplasmin or leakage of intrinsic plasminogen. *Journal of Clinical Investigation*. 10.1172/jci117949

40. Höfer, T., and Rodewald, H. R. (2018) Differentiation-based model of hematopoietic stem cell functions and lineage pathways. *Blood*. 10.1182/blood-2018-03-791517

41. Lee, M. S., and Kong, J. (2015) Heparin: Physiology, pharmacology, and clinical application. *Reviews in Cardiovascular Medicine*. 10.3909/ricm0778

42. Litvinov, R. I., and Weisel, J. W. (2017) Role of red blood cells in haemostasis and thrombosis. *ISBT Science Series*. 10.1111/voxs.12331

43. Duke, W. W. (1983) The relation of blood platelets to hemorrhagic disease. By W.W. Duke. *JAMA: The Journal of the American Medical Association*. 10.1001/jama.250.9.1201

44. Kroll, M. H., Michaelis, L. C., and Verstovsek, S. (2015) Mechanisms of thrombogenesis in polycythemia vera. *Blood Reviews*. 10.1016/j.blre.2014.12.002

45. Rother, R. P., Bell, L., Hillmen, P., and Gladwin, M. T. (2005) The clinical sequelae of intravascular hemolysis and extracellular plasma hemoglobin: A novel mechanism of human disease. *J Am Med Assoc*. 10.1001/jama.293.13.1653

46. Du, V. X., Huskens, D., Maas, C., al Dieri, R., de Groot, P. G., and de Laat, B. (2014) New insights into the role of erythrocytes in thrombus formation. *Seminars in Thrombosis and Hemostasis*. 10.1055/s-0033-1363470

47. Wautier, J. L., and Wautier, M. P. (2013) Molecular basis of erythrocyte adhesion to endothelial cells in diseases. *Clinical Hemorheology and Microcirculation*. 10.3233/CH-2012-1572

48. Flamm, M. H., and Diamond, S. L. (2012) Multiscale systems biology and physics of thrombosis under flow. *Annals of Biomedical Engineering*. 10.1007/s10439-012-0557-9

49. Abegaz, S. B. (2021) Human ABO Blood Groups and Their Associations with Different Diseases. *BioMed Research International*. 10.1155/2021/6629060

50. Anstee, D. J. (2010) The relationship between blood groups and disease. *Blood*. 10.1182/blood-2010-01-261859

51. Connor, J., Pak, C. C., and Schroit, A. J. (1994) Exposure of phosphatidylserine in the outer leaflet of human red blood cells. Relationship to cell density, cell age, and clearance by mononuclear cells. *Journal of Biological Chemistry*. 10.1016/s0021-9258(17)41959-4

52. Gregory, S. A., Morrissey, J. H., and Edgington, T. S. (1989) Regulation of tissue factor gene expression in the monocyte procoagulant response to endotoxin. *Molecular and Cellular Biology*. 10.1128/mcb.9.6.2752

53. Levi, M., van der Poll, T., and Büller, H. R. (2004) Bidirectional relation between inflammation and coagulation. *Circulation*. 10.1161/01.CIR.0000131660.51520.9A

54. Uderhardt, S., Ackermann, J. A., Fillep, T., Hammond, V. J., Willeit, J., Santer, P., Mayr, M., Biburger, M., Miller, M., Zellner, K. R., Stark, K., Zarbock, A., Rossaint, J., Schubert, I., Mielenz, D., Dietel, B., Raaz-Schrauder, D., Ay, C., Gremmel, T., Thaler, J., Heim, C., Herrmann, M., Collins, P. W., Schabbauer, G., Mackman, N., Voehringer, D., Nadler, J. L., Lee, J. J., Massberg, S., Rauh, M., Kiechl, S., Schett, G., O'Donnell, V. B., and Krönke, G. (2017) Enzymatic lipid oxidation by eosinophils propagates coagulation, hemostasis, and thrombotic disease. *Journal of Experimental Medicine*. 10.1084/jem.20161070

55. Caponegro, M., Thompson, K., Tayyab, M., and Tsirka, S. (2020) A Rigorous Quantitative Approach to Analyzing Phagocytosis Assays. *BIO-PROTOCOL*. 10.21769/bioprotoc.3698

56. Holstein, K., Matysiak, A., Witt, L., Sievers, B., Beckmann, L., Haddad, M., Renné, T., Voigtlaender, M., and Langer, F. (2020) LPS-induced expression and release of monocyte tissue factor in patients with haemophilia. *Annals of Hematology*. 10.1007/s00277-020-04075-6

57. Belaaouaj, A. A., Li, A., Wun, T. C., Welgus, H. G., and Shapiro, S. D. (2000) Matrix metalloproteinases cleave tissue factor pathway inhibitor: Effects on coagulation. *Journal of Biological Chemistry*. 10.1074/jbc.M004218200

58. Gragnano, F., Sperlongano, S., Golia, E., Natale, F., Bianchi, R., Crisci, M., Fimiani, F., Pariggiano, I., Diana, V., Carbone, A., Cesaro, A., Concilio, C., Limongelli, G., Russo, M., and Calabrò, P. (2017) The Role of von Willebrand Factor in Vascular Inflammation: From Pathogenesis to Targeted Therapy. *Mediators of Inflammation*. 10.1155/2017/5620314

59. Pendu, R., Terraube, V., Christophe, O. D., Gahmberg, C. G., de Groot, P. G., Lenting, P. J., and Denis, C. v. (2006) P-selectin glycoprotein ligand 1 and β2-integrins cooperate in the adhesion of leukocytes to von Willebrand factor. *Blood*. 10.1182/blood-2006-03-010322

60. Straat, M., van Hezel, M. E., Böing, A., Tuip-De Boer, A., Weber, N., Nieuwland, R., van Bruggen, R., and Juffermans, N. P. (2016) Monocyte-mediated activation of endothelial cells occurs only after binding to extracellular vesicles from red blood cell products, a process mediated by β-integrin. *Transfusion (Paris)*. 10.1111/trf.13851

61. Mukherjee, M., Lacy, P., and Ueki, S. (2018) Eosinophil extracellular traps and inflammatory pathologies-untangling the web! *Frontiers in Immunology*. 10.3389/fimmu.2018.02763

62. Marx, C., Novotny, J., Salbeck, D., Zellner, K. R., Nicolai, L., Pekayvaz, K., Kilani, B., Stockhausen, S., Bürgener, N., Kupka, D., Stocker, T. J., Weckbach, L. T., Pircher, J., Moser, M., Joner, M., Desmet, W., Adriaenssens, T., Neumann, F. J., Gerschlick, A. H., ten Berg, J. M., Lorenz, M., and Stark, K. (2019) Eosinophil-platelet interactions promote atherosclerosis and stabilize thrombosis with eosinophil extracellular traps. *Blood*. 10.1182/blood.2019000518

63. MacKman, N. (2019) Eosinophils, atherosclerosis, and thrombosis. *Blood*. 10.1182/blood.2019003027

64. Franco, C. B., Chen, C. C., Drukker, M., Weissman, I. L., and Galli, S. J. (2010) Distinguishing Mast Cell and Granulocyte Differentiation at the Single-Cell Level. *Cell Stem Cell*. 10.1016/j.stem.2010.02.013

65. Pizzolo, F., Castagna, A., Olivieri, O., Girelli, D., Friso, S., Stefanoni, F., Udali, S., Munerotto, V., Baroni, M., Cetera, V., Luciani, G. B., Faggian, G., Bernardi, F., and Martinelli, N. (2021) Basophil blood cell count is associated with enhanced factor ii plasma coagulant activity and increased risk of mortality in patients with

stable coronary artery disease: Not only neutrophils as prognostic marker in ischemic heart disease. *J Am Heart Assoc*. 10.1161/JAHA.120.018243

66. Borriello, F., Iannone, R., and Marone, G. (2017) Histamine release from mast cells and basophils. in *Handbook of Experimental Pharmacology*, 10.1007/164_2017_18

67. Chuang, Y. J., Swanson, R., Raja, S. M., and Olson, S. T. (2001) Heparin enhances the specificity of antithrombin for thrombin and factor Xa independent of the reactive center loop sequence. Evidence for an exosite determinant of factor Xa specificity in heparin-activated antithrombin. *Journal of Biological Chemistry*. 10.1074/jbc.M011550200

68. Guilarte, M., Sala-Cunill, A., Luengo, O., Labrador-Horrillo, M., and Cardona, V. (2017) The mast cell, contact, and coagulation system connection in anaphylaxis. *Frontiers in Immunology*. 10.3389/fimmu.2017.00846

69. Brunnée, T., Reddigari, S. R., Shibayama, Y., Kaplan, A. P., and Silverberg, M. (1997) Mast cell derived heparin activates the contact system: A link to kinin generation in allergic reactions. *Clinical and Experimental Allergy*. 10.1111/j.1365-2222.1997.tb01193.x

70. Ruf, W., and Ruggeri, Z. M. (2010) Neutrophils release brakes of coagulation. *Nature Medicine*. 10.1038/nm0810-851

71. Ferrer-Marín, F., Cuenca-Zamora, E. J., Guijarro-Carrillo, P. J., and Teruel-Montoya, R. (2021) Emerging role of neutrophils in the thrombosis of chronic myeloproliferative neoplasms. *International Journal of Molecular Sciences*. 10.3390/ijms22031143

72. Machovich, R., and Owen, W. G. (1990) The elastase-mediated pathway of fibrinolysis. *Blood Coagul Fibrinolysis*. 10.1097/00001721-199003000-00011

73. Scapini, P., Nesi, L., Morini, M., Tanghetti, E., Belleri, M., Noonan, D., Presta, M., Albini, A., and Cassatella, M. A. (2002) Generation of Biologically Active Angiostatin Kringle 1–3 by Activated Human Neutrophils. *The Journal of Immunology*. 10.4049/jimmunol.168.11.5798

74. Warejcka, D. J., and Twining, S. S. (2005) Specific conformational changes of plasminogen induced by chloride ions, 6-aminohexanoic acid and benzamidine, but not the overall openness of plasminogen regulate, production of biologically active angiostatins. *Biochemical Journal*. 10.1042/BJ20050907

75. Stief, T. (2005) Regulation of Hemostasis by Singlet-Oxygen (1ΔO2*). *Current Vascular Pharmacology*. 10.2174/1570161043385420

76. Kolaczkowska, E., and Kubes, P. (2013) Neutrophil recruitment and function in health and inflammation. *Nature Reviews Immunology*. 10.1038/nri3399

77. von Brühl, M. L., Stark, K., Steinhart, A., Chandraratne, S., Konrad, I., Lorenz, M., Khandoga, A., Tirniceriu, A., Coletti, R., Köllnberger, M., Byrne, R. A., Laitinen, I., Walch, A., Brill, A., Pfeiler, S., Manukyan, D., Braun, S., Lange, P., Riegger, J., Ware, J., Eckart, A., Haidari, S., Rudelius, M., Schulz, C., Echtler, K., Brinkmann, V., Schwaiger, M., Preissner, K. T., Wagner, D. D., Mackman, N., Engelmann, B., and Massberg, S. (2012) Monocytes, neutrophils, and platelets cooperate to initiate and propagate venous thrombosis in mice in vivo. *Journal of Experimental Medicine*. 10.1084/jem.20112322

78. Jochum, M., Lander, S., Heimburger, N., and Fritz, H. (1981) Effect of human granulocytic elastase on isolated human antithrombin iii. *Hoppe-Seyler's Zeitschrift fur Physiologische Chemie*. 10.1515/bchm2.1981.362.1.103

79. Borissoff, J. I., and ten Cate, H. (2011) From neutrophil extracellular traps release to thrombosis: An overshooting host-defense mechanism? *Journal of Thrombosis and Haemostasis*. 10.1111/j.1538-7836.2011.04425.x

80. Raife, T. J., Cao, W., Atkinson, B. S., Bedell, B., Montgomery, R. R., Lentz, S. R., Johnson, G. F., and Zheng, X. L. (2009) Leukocyte proteases cleave von Willebrand factor at or near the ADAMTS13 cleavage site. *Blood*. 10.1182/blood-2009-01-195461

81. Hiura, H., Matsui, T., Matsumoto, M., Hori, Y., Isonishi, A., Kato, S., Iwamoto, T., Mori, T., and Fujimura, Y. (2010) Proteolytic fragmentation and sugar chains of plasma ADAMTS13 purified by a conformation-dependent monoclonal antibody. *Journal of Biochemistry*. 10.1093/jb/mvq075

82. Kreuz, W. (2008) von Willebrand's disease: From discovery to therapy - Milestones in the last 25 years. *Haemophilia*. 10.1111/j.1365-2516.2008.01846.x

83. von Willebrand, E. A. (1926) Hereditär pseudohemofili. *Finska Läkarsällskapets Handlingar*. **67**, 7–12

84. Lenting, P. J., Casari, C., Christophe, O. D., and Denis, C. v. (2012) von Willebrand factor: The old, the new and the unknown. *Journal of Thrombosis and Haemostasis*. 10.1111/jth.12008

85. Favaloro, E. J. (2014) Diagnosing von Willebrand disease: A short history of laboratory milestones and innovations, plus current status, challenges, and solutions. *Seminars in Thrombosis and Hemostasis*. 10.1055/s-0034-1383546

86. Trachtman, H. (2013) Hus and Ttp. *Pediatr Clin North Am*

87. Chion, C. K. N. K., Doggen, C. J. M., Crawley, J. T. B., Lane, D. A., and Rosendaal, F. R. (2007) ADAMTS13 and von Willebrand factor and the risk of myocardial infarction in men. *Blood*. 10.1182/blood-2006-07-038166

88. Borchgrevink, Chr. F. (2009) Platelet Adhesion in Vivo in Patients with Bleeding Disorders. *Acta Medica Scandinavica*. 10.1111/j.0954-6820.1961.tb00234.x

89. Salzman, E. W. (1963) Measurement of platelet adhesiveness: a simple in vitro technique demonstrating an abnormality in von Willebrand's disease. *J Lab Clin Med*. **62**, 724–735

90. Alexander, B., and Goldstein, R. (1953) Dual hemostatic defect in pseudohemophilia. *Journal of Clinical Investigation*. **32**, 551–551

91. Larrieu, M. J., and Soulier, J. P. (1953) Deficiency of antihemophilic factor A in a girl associated with bleeding disorder. *Rev Hematol*. **8**, 361–370

92. Jenkins, C. S. P., Meyer, D., Dreyfus, M. D., and Larreu, M. -J (1974) Willebrand Factor and Ristocetin I. MECHANISM OF RISTOCETIN-INDUCED PLATELET AGGREGATION. *British Journal of Haematology*. 10.1111/j.1365-2141.1974.tb06675.x

93. Weiss, H. J., Hoyer, L. W., Rickles, F. R., Varma, A., and Rogers, J. (1973) Quantitative assay of a plasma factor deficient in von Willebrand's disease that is necessary for platelet aggregation. Relationship to factor VIII procoagulant activity and antigen content. *Journal of Clinical Investigation*. 10.1172/JCI107465

94. Sadler, J. E., Shelton-Inloes, B. B., Sorace, J. M., Harlan, J. M., Titani, K., and Davie, E. W. (1985) Cloning and characterization of two cDNAs coding for human von Willebrand factor. *Proc Natl Acad Sci U S A*. 10.1073/pnas.82.19.6394

95. Ginsburg, D., Handin, R. I., Bonthron, D. T., Donlon, T. A., Bruns, G. A. P., Latt, S. A., and Orkin, S. H. (1985) Human von Willebrand Factor (vWF): Isolation of complementary DNA (cDNA) clones and chromosomal localization. *Science (1979)*. 10.1126/science.3874428

96. Verweij, C. L., Diergaarde, P. J., Hart, M., and Pannekoek, H. (1986) Full-length von Willebrand factor (vWF) cDNA encodes a highly repetitive protein considerably larger than the mature vWF subunit. *EMBO J*. 10.1002/j.1460-2075.1986.tb04435.x

97. Ruggeri, Z. M., and Ware, J. (1992) The structure and function of von Willebrand factor. *Thromb Haemost*. **67**, 594–599

98. Peyvandi, F., Garagiola, I., and Baronciani, L. (2011) Role of von Willebrand factor in the haemostasis. *Blood Transfusion*. 10.2450/2011.002S

99. Lippok, S., Kolšek, K., Löf, A., Eggert, D., Vanderlinden, W., Müller, J. P., König, G., Obser, T., Röhrs, K., Schneppenheim, S., Budde, U., Baldauf, C., Aponte-Santamaría, C., Gräter, F., Schneppenheim, R., Rädler, J. O., and Brehm, M. A. (2016) Von Willebrand factor is dimerized by protein disulfide isomerase. *Blood*. 10.1182/blood-2015-04-641902

100. Denis, C. v. (2002) Molecular and cellular biology of von willebrand factor. *International Journal of Hematology*. 10.1007/BF02981972

101. Dang, L. T., Purvis, A. R., Huang, R. H., Westfield, L. A., and Sadler, J. E. (2011) Phylogenetic and functional analysis of histidine residues essential for pH-dependent multimerization of von willebrand factor. *Journal of Biological Chemistry*. 10.1074/jbc.M111.249151

102. de Meyer, S. F., Deckmyn, H., and Vanhoorelbeke, K. (2009) Von Willebrand factor to the rescue. *Blood*. 10.1182/blood-2008-10-165621

103. Leebeek, F. W. G., and Eikenboom, J. C. J. (2016) Von Willebrand's Disease. *New England Journal of Medicine*. 10.1056/NEJMra1601561

104. Ohmori, K., Fretto, L. J., Harrison, R. L., Switzer, M. E. P., Erickson, H. P., and McKee, P. A. (1982) Electron microscopy of human factor VIII/von willebrand glycoprotein: Effect of reducing reagents on structure and function. *Journal of Cell Biology*. 10.1083/jcb.95.2.632

105. Zheng, Y., Chen, J., and López, J. A. (2015) Flow-driven assembly of VWF fibres and webs in in vitro microvessels. *Nature Communications*. 10.1038/ncomms8858

106. Springer, T. A. (2014) Von Willebrand factor, Jedi knight of the bloodstream. *Blood*. 10.1182/blood-2014-05-378638

107. Bridges, A. B., McLaren, M., Scott, N. A., Pringle, T. H., McNeill, G. P., and Belch, J. J. F. (1993) Circadian variation of tissue plasminogen activator and its inhibitor, von Willebrand factor antigen, and prostacyclin stimulating factor in men with ischaemic heart disease. *British Heart Journal*. 10.1136/hrt.69.2.121

108. Haberichter, S. L. (2015) Von Willebrand factor propeptide: Biology and clinical utility. *Blood*. 10.1182/blood-2015-04-512731

109. Yee, A., and Kretz, C. A. (2014) Von Willebrand factor: Form for function. *Seminars in Thrombosis and Hemostasis*. 10.1055/s-0033-1363155

110. Huang, R. H., Wang, Y., Roth, R., Yu, X., Purvis, A. R., Heuser, J. E., Egelman, E. H., and Sadler, J. E. (2008) Assembly of Weibel-Palade body-like tubules from N-terminal domains of von Willebrand factor. *Proc Natl Acad Sci U S A*. 10.1073/pnas.0710079105

111. Wise, R. J., Pittman, D. D., Handin, R. I., Kaufman, R. J., and Orkin, S. H. (1988) The propeptide of von Willebrand Factor independently mediates the assembly of von Willebrand multimers. *Cell*. 10.1016/0092-8674(88)90511-9

112. Voorberg, J., Fontijn, R., van Mourik, J. A., and Pannekoek, H. (1990) Domains involved in multimer assembly of von Willebrand factor (vWF): Multimerization is independent of dimerization. *EMBO Journal*. 10.1002/j.1460-2075.1990.tb08176.x

113. Valentijn, K. M., Sadler, J. E., Valentijn, J. A., Voorberg, J., and Eikenboom, J. (2011) Functional architecture of Weibel-Palade bodies. *Blood*. 10.1182/blood-2010-09-267492

114. Paroutis, P., Touret, N., and Grinstein, S. (2004) The pH of the secretory pathway: Measurement, determinants, and regulation. *Physiology*. 10.1152/physiol.00005.2004

115. Purvis, A. R., and Sadler, J. E. (2004) A covalent oxidoreductase intermediate in propeptide-dependent von Willebrand factor multimerization. *Journal of Biological Chemistry*. 10.1074/jbc.M408727200

116. Wagner, D. D., Saffaripour, S., Bonfanti, R., Sadler, J. E., Cramer, E. M., Chapman, B., and Mayadas, T. N. (1991) Induction of specific storage organelles by von Willebrand factor propolypeptide. *Cell*. 10.1016/0092-8674(91)90648-I

117. Haberichter, S. L., Fahs, S. A., and Montgomery, R. R. (2000) Von Willebrand factor storage and multimerization: 2 independent intracellular processes. *Blood*. 10.1182/blood.v96.5.1808.h8001808_1808_1815

118. Voorberg, J., Fontijn, R., Calafat, J., Janssen, H., van Mourik, J. A., and Pannekoek, H. (1993) Biogenesis of von Willebrand factor-containing organelles in heterologous transfected CV-1 cells. *EMBO Journal*. 10.1002/j.1460-2075.1993.tb05709.x

119. Przeradzka, M. A., Meems, H., van der Zwaan, C., Ebberink, E. H. T. M., van den Biggelaar, M., Mertens, K., and Meijer, A. B. (2018) The D 0 domain of von Willebrand factor requires the presence of the D3 domain for optimal factor VIII binding. *Biochemical Journal*. 10.1042/BCJ20180431

120. Chauhan, A. K., Kisucka, J., Lamb, C. B., Bergmeier, W., and Wagner, D. D. (2007) Von Willebrand factor and factor VIII are independently required to form stable occlusive thrombi in injured veins. *Blood*. 10.1182/blood-2006-06-028241

121. Sadler, J. E., Budde, U., Eikenboom, J. C. J., Favaloro, E. J., Hill, F. G. H., Holmberg, L., Ingerslev, J., Lee, C. A., Lillicrap, D., Mannucci, P. M., Mazurier, C., Meyer, D., Nichols, W. L., Nishino, M., Peake, I. R., Rodeghiero, F.,

Schneppenheim, R., Ruggeri, Z. M., Srivastava, A., Montgomery, R. R., and Federici, A. B. (2006) Update on the pathophysiology and classification of von Willebrand disease: A report of the Subcommittee on von Willebrand factor. *Journal of Thrombosis and Haemostasis*. 10.1111/j.1538-7836.2006.02146.x

122. Hilbert, L., Nurden, P., Caron, C., Nurden, A. T., Goudemand, J., Meyer, D., Fressinaud, E., and Mazurier, C. (2006) Type 2N von Willebrand disease due to compound heterozygosity for R854Q and a novel R763G mutation at the cleavage site of von Willebrand factor propeptide. *Thrombosis and Haemostasis*. 10.1160/TH06-03-0157

123. Wise, R. J., Dorner, A. J., Krane, M., Pittman, D. D., and Kaufman, R. J. (1991) The role of von Willebrand factor multimers and propeptide cleavage in binding and stabilization of factor VIII. *Journal of Biological Chemistry*. 10.1016/s0021-9258(18)54729-3

124. Casonato, A., Sartorello, F., Cattini, M. G., Pontara, E., Soldera, C., Bertomoro, A., and Girolami, A. (2003) An Arg760Cys mutation in the consensus sequence of the von Willebrand factor propeptide cleavage site is responsible for a new von Willebrand disease variant. *Blood*. 10.1182/blood-2002-04-1046

125. Springer, T. A. (2011) Biology and physics of von Willebrand factor concatamers. *Journal of Thrombosis and Haemostasis*. 10.1111/j.1538-7836.2011.04320.x

126. Gogia, S., and Neelamegham, S. (2015) Role of fluid shear stress in regulating VWF structure, function and related blood disorders. *Biorheology*. 10.3233/BIR-15061

127. Titani, K., Kumar, S., Takio, K., Ericsson, L. H., Wade, R. D., Ashida, K., Walsh, K. A., Chopek, M. W., Sadler, J. E., and Fujikawa, K. (1986) Amino Acid Sequence of Human von Willebrand Factor. *Biochemistry*. 10.1021/bi00359a015

128. Blenner, M. A., Dong, X., and Springer, T. A. (2014) Structural basis of regulation of von Willebrand factor binding to glycoprotein Ib. *Journal of Biological Chemistry*. 10.1074/jbc.M113.511220

129. Cruz, M. A., Handin, R. I., and Wise, R. J. (1993) The interaction of the von Willebrand factor-A1 domain with platelet glycoprotein Ib/IX. The role of glycosylation and disulfide bonding in a monomeric recombinant A1 domain protein. *Journal of Biological Chemistry*. 10.1016/s0021-9258(19)36916-9

130. Ishihara, J., Ishihara, A., Starke, R. D., Peghaire, C. R., Smith, K. E., McKinnon, T. A. J., Tabata, Y., Sasaki, K., White, M. J. V., Fukunaga, K., Laffan, M. A., Lutolf, M. P., Randi, A. M., and Hubbell, J. A. (2019) The heparin binding domain

of von Willebrand factor binds to growth factors and promotes angiogenesis in wound healing. *Blood*. 10.1182/blood.2019000510

131. Borthakur, G., Cruz, M. A., Dong, J. F., Mcintire, L., Li, F., López, J. A., and Thiagarajan, P. (2003) Sulfatides inhibit platelet adhesion to von Willebrand factor in flowing blood. *Journal of Thrombosis and Haemostasis*. 10.1046/j.1538-7836.2003.00156.x

132. Hoylaerts, M. F., Yamamoto, H., Nuyts, K., Vreys, I., Deckmyn, H., and Vermylen, J. (1997) Von Willebrand factor binds to native collagen VI primarily via its A1 domain. *Biochemical Journal*. 10.1042/bj3240185

133. Okhota, S., Melnikov, I., Avtaeva, Y., Kozlov, S., and Gabbasov, Z. (2020) Shear stress-induced activation of vonwillebrand factor and cardiovascular pathology. *International Journal of Molecular Sciences*. 10.3390/ijms21207804

134. Aponte-Santamaría, C., Lippok, S., Mittag, J. J., Obser, T., Schneppenheim, R., Baldauf, C., Gräter, F., Budde, U., and Rädler, J. O. (2017) Mutation G1629E Increases von Willebrand Factor Cleavage via a Cooperative Destabilization Mechanism. *Biophysical Journal*. 10.1016/j.bpj.2016.11.3202

135. Sadler, J. E. (2005) Von Willebrand factor: Two sides of a coin. in *Journal of Thrombosis and Haemostasis*, 10.1111/j.1538-7836.2005.01369.x

136. Zhang, Q., Zhou, Y. F., Zhang, C. Z., Zhang, X., Lu, C., and Springer, T. A. (2009) Structural specializations of A2, a force-sensing domain in the ultralarge vascular protein von Willebrand factor. *Proc Natl Acad Sci U S A*. 10.1073/pnas.0903679106

137. Xu, A. J., and Springer, T. A. (2012) Calcium stabilizes the von Willebrand factor A2 domain by promoting refolding. *Proc Natl Acad Sci U S A*. 10.1073/pnas.1121261109

138. Shim, K., Anderson, P. J., Tuley, E. A., Wiswall, E., and Sadler, J. E. (2008) Platelet-VWF complexes are preferred substrates of ADAMTS13 under fluid shear stress. *Blood*. 10.1182/blood-2007-05-093021

139. Kokame, K., Nobe, Y., Kokubo, Y., Okayama, A., and Miyata, T. (2005) FRETS-VWF73, a first fluorogenic substrate for ADAMTS13 assay. *British Journal of Haematology*. 10.1111/j.1365-2141.2005.05420.x

140. Lynch, C. J., Lane, D. A., and Luken, B. M. (2014) Control of VWF A2 domain stability and ADAMTS13 access to the scissile bond of full-length VWF. *Blood*. 10.1182/blood-2013-11-538173

141. Huizinga, E. G., van der Plas, R. M., Kroon, J., Sixma, J. J., and Gros, P. (1997) Crystal structure of the A3 domain of human von Willebrand factor: Implications for collagen binding. *Structure*. 10.1016/s0969-2126(97)00266-9

142. Flood, V. H., Lederman, C. A., Wren, J. S., Christopherson, P. A., Friedman, K. D., Hoffmann, R. G., and Montgomery, R. R. (2010) Absent collagen binding in a VWF A3 domain mutant: Utility of the VWF:CB in diagnosis of VWD. *Journal of Thrombosis and Haemostasis*. 10.1111/j.1538-7836.2010.03869.x

143. Legendre, P., Navarrete, A. M., Rayes, J., Casari, C., Boisseau, P., Ternisien, C., Caron, C., Fressinaud, E., Goudemand, J., Veyradier, A., Denis, C. v., Lenting, P. J., and Christophe, O. D. (2013) Mutations in the A3 domain of Von Willebrand factor inducing combined qualitative and quantitative defects in the protein. *Blood*. 10.1182/blood-2012-09-456038

144. Zhou, Y. F., Eng, E. T., Nishida, N., Lu, C., Walz, T., and Springer, T. A. (2011) A pH-regulated dimeric bouquet in the structure of von Willebrand factor. *EMBO Journal*. 10.1038/emboj.2011.297

145. Xu, E. R., von Bülow, S., Chen, P. C., Lenting, P. J., Kolšek, K., Aponte-Santamaría, C., Simon, B., Foot, J., Obser, T., Schneppenheim, R., Gräter, F., Denis, C. v., Wilmanns, M., and Hennig, J. (2019) Structure and dynamics of the platelet integrin-binding C4 domain of von Willebrand factor. *Blood*. 10.1182/blood-2018-04-843615

146. Shapiro, S. E., Nowak, A. A., Wooding, C., Birdsey, G., Laffan, M. A., and McKinnon, T. A. J. (2014) The von Willebrand factor predicted unpaired cysteines are essential for secretion. *Journal of Thrombosis and Haemostasis*. 10.1111/jth.12466

147. Sadler, J. E. (1998) Biochemistry and genetics of von Willebrand factor. *Annual Review of Biochemistry*. 10.1146/annurev.biochem.67.1.395

148. Brinkmann, V., Reichard, U., Goosmann, C., Fauler, B., Uhlemann, Y., Weiss, D. S., Weinrauch, Y., and Zychlinsky, A. (2004) Neutrophil Extracellular Traps Kill Bacteria. *Science (1979)*. 10.1126/science.1092385

149. Steinert, M., Ramming, I., and Bergmann, S. (2020) Impact of Von Willebrand Factor on Bacterial Pathogenesis. *Frontiers in Medicine*. 10.3389/fmed.2020.00543

150. Fuchs, T. A., Brill, A., Duerschmied, D., Schatzberg, D., Monestier, M., Myers, D. D., Wrobleski, S. K., Wakefield, T. W., Hartwig, J. H., and Wagner, D. D. (2010) Extracellular DNA traps promote thrombosis. *Proc Natl Acad Sci U S A*. 10.1073/pnas.1005743107

151. Ward, C. M., Tetaz, T. J., Andrews, R. K., and Berndt, M. C. (1997) Binding of the von Willebrand factor A1 domain to histone. *Thrombosis Research*. 10.1016/S0049-3848(97)00096-0

152. Badimon, L., and Vilahur, G. (2014) Thrombosis formation on atherosclerotic lesions and plaque rupture. *Journal of Internal Medicine*. 10.1111/joim.12296

153. Ed Rainger, G., Chimen, M., Harrison, M. J., Yates, C. M., Harrison, P., Watson, S. P., Lordkipanidzé, M., and Nash, G. B. (2015) The role of platelets in the recruitment of leukocytes during vascular disease. *Platelets*. 10.3109/09537104.2015.1064881

154. Burger, P. C., and Wagner, D. D. (2003) Platelet P-selectin facilitates atherosclerotic lesion development. *Blood*. 10.1182/blood-2002-07-2209

155. Kong, D. H., Kim, Y. K., Kim, M. R., Jang, J. H., and Lee, S. (2018) Emerging roles of vascular cell adhesion molecule-1 (VCAM-1) in immunological disorders and cancer. *International Journal of Molecular Sciences*. 10.3390/ijms19041057

156. Doddapattar, P., Dhanesha, N., Chorawala, M. R., Tinsman, C., Jain, M., Nayak, M. K., Staber, J. M., and Chauhan, A. K. (2018) Endothelial cell–derived von willebrand factor, but not platelet-derived, promotes atherosclerosis in apolipoprotein e–deficient mice. *Arteriosclerosis, Thrombosis, and Vascular Biology*. 10.1161/ATVBAHA.117.309918

157. van Galen, K. P. M., Tuinenburg, A., Smeets, E. M., and Schutgens, R. E. G. (2012) Von Willebrand factor deficiency and atherosclerosis. *Blood Reviews*. 10.1016/j.blre.2012.05.002

158. Gandhi, C., Khan, M. M., Lentz, S. R., and Chauhan, A. K. (2012) ADAMTS13 reduces vascular inflammation and the development of early atherosclerosis in mice. *Blood*. 10.1182/blood-2011-09-376202

159. Davis, G. E., and Senger, D. R. (2005) Endothelial extracellular matrix: Biosynthesis, remodeling, and functions during vascular morphogenesis and neovessel stabilization. *Circulation Research*. 10.1161/01.RES.0000191547.64391.e3

160. Carmeliet, P. (2003) Angiogenesis in health and disease. *Nature Medicine*. 10.1038/nm0603-653

161. Starke, R. D., Paschalaki, K. E., Ferraro, F., Dryden, N. H., McKinnon, T. A. J., Sutton, R. E., Payne, E. M., Haskard, D. O., Hughes, A. D., Cutler, D. F., Laffan, M. A., and Randi, A. M. (2012) Endothelial Von Willebrand factor regulates angiogenesis. *Vascular Pharmacology*. 10.1016/j.vph.2011.08.038

162. Olsson, A. K., Dimberg, A., Kreuger, J., and Claesson-Welsh, L. (2006) VEGF receptor signalling - In control of vascular function. *Nature Reviews Molecular Cell Biology*. 10.1038/nrm1911

163. Gerhardt, H. (2008) VEGF and endothelial guidance in angiogenic sprouting. *Organogenesis*. 10.4161/org.4.4.7414

164. Majerus, E. M., Zheng, X., Tuley, E. A., and Sadler, J. E. (2003) Cleavage of the ADAMTS13 Propeptide Is Not Required for Protease Activity. *Journal of Biological Chemistry*. 10.1074/jbc.M309872200

165. Zheng, X. L. (2015) ADAMTS13 and von willebrand factor in thrombotic thrombocytopenic purpura. *Annual Review of Medicine*. 10.1146/annurev-med-061813-013241

166. Levy, G. G., Nichols, W. C., Lian, E. C., Foroud, T., McClintick, J. N., McGee, B. M., Yang, A. Y., Siemieniak, D. R., Stark, K. R., Gruppo, R., Sarode, R., Shurin, S. B., Chandrasekaran, V., Stabler, S. P., Sabio, H., Bouhassira, E. E., Upshaw, J. D., Ginsburg, D., and Tsai, H. M. (2001) Mutations in a member of the ADAMTS gene family cause thrombotic thrombocytopenic purpura. *Nature*. 10.1038/35097008

167. Zhou, W., Inada, M., Lee, T. P., Benten, D., Lyubsky, S., Bouhassira, E. E., Gupta, S., and Tsai, H. M. (2005) ADAMTS13 is expressed in hepatic stellate cells. *Laboratory Investigation*. 10.1038/labinvest.3700275

168. Tati, R., Kristoffersson, A. C., Ståhl, A. lie, Mörgelin, M., Motto, D., Satchell, S., Mathieson, P., Manea-Hedström, M., and Karpman, D. (2011) Phenotypic expression of ADAMTS13 in glomerular endothelial cells. *PLoS ONE*. 10.1371/journal.pone.0021587

169. Moschcowitz, E. L. I. (1924) Hyaline thrombosis of the terminal arterioles and capillaries: a hitherto undescribed disease. *Proc NY Pathol Soc*. **24**, 21–24

170. JY, W., Horstman, L. L., Arce, M., and Ahn, Y. S. (1992) Clinical significance of platelet microparticles in autoimmune thrombocytopenias. *The Journal of Laboratory and Clinical Medicine*. 10.5555/uri:pii:0022214392902005

171. SCHULMAN, I., PIERCE, M., LUKENS, A., and CURRIMBHOY, Z. (1960) Studies on thrombopoiesis. I. A factor in normal human plasma required for platelet production; chronic thrombocytopenia due to its deficiency. *Blood*. 10.1182/blood.v16.1.943.943

172. Upshaw, J. D. (1978) Congenital Deficiency of a Factor in Normal Plasma That Reverses Microangiopathic Hemolysis and Thrombocytopenia. *New England Journal of Medicine*. 10.1056/nejm197806152982407

173. Kinoshita, S., Yoshioka, A., Park, Y. D., Ishizashi, H., Konno, M., Funato, M., Matsui, T., Titani, K., Yagi, H., Matsumoto, M., and Fujimura, Y. (2001) Upshaw-schulman syndrome revisited: A concept of congenital thrombotic thrombocytopenic purpura. *International Journal of Hematology*. 10.1007/BF02982558

174. Moake, J. L., Rudy, C. K., Troll, J. H., Weisntein, M. J., Colannino, N. M., Azocar, J., Seder, R. H., and Hong, S. L. (1982) Moake JL, Rudy CK, Troll JH, Weinstein MJ, Colannino NM, Azocar J, Seder RH, Hong SL, Deykin D. Unusually large plasma factor VIII: von Willebrand factor multimers in chronic relapsing thrombotic thrombocytopenic purpura. *New England Journal of Medicine*. **307**, 1432–1435

175. Furlan, M., Robles, R., and Lämmle, B. (1996) Partial purification and characterization of a protease from human plasma cleaving von Willebrand factor to fragments produced by in vivo proteolysis. *Blood*. 10.1182/blood.v87.10.4223.bloodjournal87104223

176. Tsai, H. M. (1996) Physiologic cleavage of von Willebrand factor by a plasma protease is dependent on its conformation and requires calcium ion. *Blood*. 10.1182/blood.v87.10.4235.bloodjournal87104235

177. Fujikawa, K., Suzuki, H., McMullen, B., and Chung, D. (2001) Purification of human von Willebrand factor-cleaving protease and its identification as a new member of the metalloproteinase family. *Blood*. 10.1182/blood.V98.6.1662

178. Gerritsen, H. E., Robles, R., Lämmle, B., and Furlan, M. (2001) Partial amino acid sequence of purified von Willebrand factor-cleaving protease. *Blood*. 10.1182/blood.V98.6.1654

179. Zheng, X., Chung, D., Takayama, T. K., Majerus, E. M., Sadler, J. E., and Fujikawa, K. (2001) Structure of von Willebrand Factor-cleaving Protease (ADAMTS13), a Metalloprotease Involved in Thrombotic Thrombocytopenic Purpura. *Journal of Biological Chemistry*. 10.1074/jbc.C100515200

180. Gao, W., Zhu, J., Westfield, L. A., Tuley, E. A., Anderson, P. J., and Sadler, J. E. (2012) Rearranging exosites in noncatalytic domains can redirect the substrate specificity of ADAMTS proteases. *Journal of Biological Chemistry*. 10.1074/jbc.M112.380535

181. Santamaria, S., and de Groot, R. (2020) ADAMTS proteases in cardiovascular physiology and disease. *Open Biology*. 10.1098/rsob.200333

182. Mead, T. J., and Apte, S. S. (2018) ADAMTS proteins in human disorders. *Matrix Biology*. 10.1016/j.matbio.2018.06.002

183. Bekhouche, M., and Colige, A. (2015) The procollagen N-proteinases ADAMTS2, 3 and 14 in pathophysiology. *Matrix Biology*. 10.1016/j.matbio.2015.04.001

184. Gomis-Rüth, F. X., Botelho, T. O., and Bode, W. (2012) A standard orientation for metallopeptidases. *Biochimica et Biophysica Acta - Proteins and Proteomics*. 10.1016/j.bbapap.2011.04.014

185. Bode, W., Gomis-Rüth, F. X., and Stöckler, W. (1993) Astacins, serralysins, snake venom and matrix metalloproteinases exhibit identical zinc-binding environments (HEXXHXXGXXH and Met-turn) and topologies and should be grouped into a common family, the "metzincins." *FEBS Letters*. 10.1016/0014-5793(93)80312-I

186. Apte, S. S. (2020) ADAMTS Proteins: Concepts, Challenges, and Prospects. in *Methods in Molecular Biology*, 10.1007/978-1-4939-9698-8_1

187. Yamamoto, K., Murphy, G., and Troeberg, L. (2015) Extracellular regulation of metalloproteinases. *Matrix Biology*. 10.1016/j.matbio.2015.02.007

188. Colige, A., Sieron, A. L., Li, S. W., Schwarze, U., Petty, E., Wertelecki, W., Wilcox, W., Krakow, D., Cohn, D. H., Reardon, W., Byers, P. H., Lapière, C. M., Prockop, D. J., and Nusgens, B. v. (1999) Human ehlers-danlos syndrome type VII C and bovine dermatosparaxis are caused by mutations in the procollagen I N-proteinase gene. *American Journal of Human Genetics*. 10.1086/302504

189. Muia, J., Zhu, J., Gupta, G., Haberichter, S. L., Friedman, K. D., Feys, H. B., Deforche, L., Vanhoorelbeke, K., Westfield, L. A., Roth, R., Tolia, N. H., Heuser, J. E., and Sadler, J. E. (2014) Allosteric activation of ADAMTS13 by von Willebrand factor. *Proc Natl Acad Sci U S A*. 10.1073/pnas.1413282112

190. South, K., Luken, B. M., Crawley, J. T. B., Phillips, R., Thomas, M., Collins, R. F., Deforche, L., Vanhoorelbeke, K., and Lane, D. A. (2014) Conformational activation of ADAMTS13. *Proc Natl Acad Sci U S A*. 10.1073/pnas.1411979112

191. Loechel, F., Overgaard, M. T., Oxvig, C., Albrechtsen, R., and Wewer, U. M. (1999) Regulation of human ADAM 12 protease by the prodomain. Evidence for a functional cysteine switch. *Journal of Biological Chemistry*. 10.1074/jbc.274.19.13427

192. Cao, J., Hymowitz, M., Conner, C., Bahou, W. F., and Zucker, S. (2000) The propeptide domain of membrane type 1-matrix metalloproteinase acts as an

intramolecular chaperone when expressed in trans with the mature sequence in COS-1 cells. *Journal of Biological Chemistry*. 10.1074/jbc.M001920200

193. de Groot, R., Bardhan, A., Ramroop, N., Lane, D. A., and Crawley, J. T. B. (2009) Essential role of the disintegrin-like domain in ADAMTS13 function. *Blood*. 10.1182/blood-2008-11-187914

194. Gardner, M. D., Chion, C. K. N. K., Groot, R. de, Shah, A., Crawley, J. T. B., and Lane, D. A. (2009) Afunctional calcium-binding site in the metalloprotease domain ofADAMTS13. *Blood*. 10.1182/blood-2008-03-144683

195. Petri, A., Kim, H. J., Xu, Y., de Groot, R., Li, C., Vandenbulcke, A., Vanhoorelbeke, K., Emsley, J., and Crawley, J. T. B. (2019) Crystal structure and substrate-induced activation of ADAMTS13. *Nature Communications*. 10.1038/s41467-019-11474-5

196. Zheng, X. L. (2013) Structure-function and regulation of ADAMTS-13 protease. *Journal of Thrombosis and Haemostasis*. 10.1111/jth.12221

197. Lu, D., Chung, K. F., Xia, M., Lu, X., Scully, M., and Kakkar, V. (2006) Integrin binding characteristics of the disintegrin-like domain of ADAM-15. *Thrombosis and Haemostasis*. 10.1160/TH06-07-0395

198. Xiang, Y., de Groot, R., Crawley, J. T. B., and Lane, D. A. (2011) Mechanism of von Willebrand factor scissile bond cleavage by a disintegrin and metalloproteinase with a thrombospondin type 1 motif, member 13 (ADAMTS13). *Proc Natl Acad Sci U S A*. 10.1073/pnas.1018559108

199. Davis, A. K., Makar, R. S., Stowell, C. P., Kuter, D. J., and Dzik, W. H. (2009) ADAMTS13 binds to CD36: A potential mechanism for platelet and endothelial localization of ADAMTS13. *Transfusion (Paris)*. 10.1111/j.1537-2995.2008.01978.x

200. Feys, H. B., Anderson, P. J., Vanhoorelbeke, K., Majerus, E. M., and Sadler, J. E. (2009) Multi-step binding of ADAMTS-13 to von Willebrand factor. *Journal of Thrombosis and Haemostasis*. 10.1111/j.1538-7836.2009.03620.x

201. South, K., Freitas, M. O., and Lane, D. A. (2016) Conformational quiescence of ADAMTS-13 prevents proteolytic promiscuity. *Journal of Thrombosis and Haemostasis*. 10.1111/jth.13445

202. de Groot, R., Lane, D. A., and Crawley, J. T. B. (2015) The role of the ADAMTS13 cysteine-rich domain in VWF binding and proteolysis. *Blood*. 10.1182/blood-2014-08-594556

203. Fang, X., Lin, J., Fang, Y., and Wu, J. (2018) Prediction of spacer-α6 complex: A novel insight into binding of ADAMTS13 with A2 domain of von Willebrand factor under forces. *Scientific Reports*. 10.1038/s41598-018-24212-6

204. South, K., Freitas, M. O., and Lane, D. A. (2017) A model for the conformational activation of the structurally quiescent metalloprotease ADAMTS13 by von willebrand factor. *Journal of Biological Chemistry*. 10.1074/jbc.M117.776732

205. Pos, W., Crawley, J. T. B., Fijnheer, R., Voorberg, J., Lane, D. A., and Luken, B. M. (2010) An autoantibody epitope comprising residues R660, Y661, and Y665 in the ADAMTS13 spacer domain identifies a binding site for the A2 domain of VWF. *Blood*. 10.1182/blood-2009-06-229203

206. Pos, W., Sorvillo, N., Fijnheer, R., Feys, H. B., Kaijen, P. H. P., Vidarsson, G., and Voorberg, J. (2011) Residues arg568 and phe592 contribute to an antigenic surface for anti-adamts13 antibodies in the spacer domain. *Haematologica*. 10.3324/haematol.2010.036327

207. Deforche, L., Roose, E., Vandenbulcke, A., Vandeputte, N., Feys, H. B., Springer, T. A., Mi, L. Z., Muia, J., Sadler, J. E., Soejima, K., Rottensteiner, H., Deckmyn, H., de Meyer, S. F., and Vanhoorelbeke, K. (2015) Linker regions and flexibility around the metalloprotease domain account for conformational activation of ADAMTS-13. *Journal of Thrombosis and Haemostasis*. 10.1111/jth.13149

208. Jian, C., Xiao, J., Gong, L., Skipwith, C. G., Jin, S. Y., Kwaan, H. C., and Zheng, X. L. (2012) Gain-of-function ADAMTS13 variants that are resistant to autoantibodies against ADAMTS13 in patients with acquired thrombotic thrombocytopenic purpura. *Blood*. 10.1182/blood-2011-12-399501

209. Gao, W., Anderson, P. J., Majerus, E. M., Tuley, E. A., and Sadler, J. E. (2006) Exosite interactions contribute to tension-induced cleavage of von Willebrand factor by the antithrombotic ADAMTS13 metalloprotease. *Proc Natl Acad Sci U S A*. 10.1073/pnas.0607264104

210. de Groot, R., Lane, D. A., and Crawley, J. T. B. (2010) The ADAMTS13 metalloprotease domain: Roles of subsites in enzyme activity and specificity. *Blood*. 10.1182/blood-2009-12-258780

211. Schneppenheim, R., and Budde, U. (2011) Von Willebrand factor and ADAMTS13 balancing primary hemostasis. *Hämostaseologie*. 10.5482/ha-1167

212. Furlan, M., and Lammle, B. (1998) Deficiency of von Willebrand factor-cleaving protease in familial and acquired thrombotic thrombocytopenic purpura. *Bailliere's Clinical Haematology*. 10.1016/S0950-3536(98)80064-4

213. Kretz, C. A., Tomberg, K., van Esbroeck, A., Yee, A., and Ginsburg, D. (2018) High throughput protease profiling comprehensively defines active site specificity for thrombin and ADAMTS13. *Scientific Reports*. 10.1038/s41598-018-21021-9

214. Kelwick, R., Desanlis, I., Wheeler, G. N., and Edwards, D. R. (2015) The ADAMTS (A Disintegrin and Metalloproteinase with Thrombospondin motifs) family. *Genome Biology*. 10.1186/s13059-015-0676-3

215. Tortorella, M. D., Liu, R. Q., Burn, T., Newton, R. C., and Arner, E. (2002) Characterization of human aggrecanase 2 (ADAM-TS5): Substrate specificity studies and comparison with aggrecanase 1 (ADAM-TS4). *Matrix Biology*. 10.1016/S0945-053X(02)00069-0

216. Glasson, S. S., Askew, R., Sheppard, B., Carito, B., Blanchet, T., Ma, H. L., Flannery, C. R., Peluso, D., Kanki, K., Yang, Z., Majumdar, M. K., and Morris, E. A. (2005) Deletion of active ADAMTS5 prevents cartilage degradation in a murine model of osteoarthritis. *Nature*. 10.1038/nature03369

217. Kumar, S., Sharghi-Namini, S., Rao, N., and Ge, R. (2012) ADAMTS5 functions as an anti-angiogenic and anti-tumorigenic protein independent of its proteoglycanase activity. *American Journal of Pathology*. 10.1016/j.ajpath.2012.05.022

218. Heuberger, D. M., Franchini, A. G., Madon, J., and Schuepbach, R. A. (2019) Thrombin cleaves and activates the protease-activated receptor 2 dependent on thrombomodulin co-receptor availability. *Thrombosis Research*. 10.1016/j.thromres.2019.02.032

219. Guo, C., Tsigkou, A., and Lee, M. H. (2016) ADAMTS13 and 15 are not regulated by the full length and N-terminal domain forms of TIMP-1, -2, -3 and -4. *Biomedical Reports*. 10.3892/br.2015.535

220. Shelat, S. G., Ai, J., and Zheng, X. L. (2005) Molecular biology of ADAMTS13 and diagnostic utility of ADAMTS13 proteolytic activity and inhibitor assays. *Seminars in Thrombosis and Hemostasis*. 10.1055/s-2005-925472

221. Fujimura, Y., Matsumoto, M., Isonishi, A., Yagi, H., Kokame, K., Soejima, K., Murata, M., and Miyata, T. (2011) Natural history of Upshaw-Schulman syndrome based on ADAMTS13 gene analysis in Japan. *Journal of Thrombosis and Haemostasis*. 10.1111/j.1538-7836.2011.04341.x

222. Thompson, E. A., and Howard, M. A. (1986) Proteolytic cleavage of human von Willebrand factor induced by enzyme(s) released from polymorphonuclear cells. *Blood*. 10.1182/blood.v67.5.1281.1281

223. Jeleńska, M., Bykowska, W., Kopeć, M., Vigh, Z., Scharrer, I., and Breddin, K. (1990) Effects of human elastase on von willebrand factor in highly purified factor VIII concentrate and in cryoprecipitate. *Thrombosis Research*. 10.1016/0049-3848(90)90132-V

224. Xu, H., Cao, Y., Yang, X., Cai, P., Kang, L., Zhu, X., Luo, H., Lu, L., Wei, L., Bai, X., Zhu, Y., Zhao, B. Q., and Fan, W. (2017) ADAMTS13 controls vascular remodeling by modifying VWF reactivity during stroke recovery. *Blood*. 10.1182/blood-2016-10-747089

225. Saint-Lu, N., Oortwijn, B. D., Pegon, J. N., Odouard, S., Christophe, O. D., de Groot, P. G., Denis, C. v., and Lenting, P. J. (2012) Identification of galectin-1 and galectin-3 as novel partners for von willebrand factor. *Arteriosclerosis, Thrombosis, and Vascular Biology*. 10.1161/ATVBAHA.111.240309

226. Markowska, A. I., Jefferies, K. C., and Panjwani, N. (2011) Galectin-3 protein modulates cell surface expression and activation of vascular endothelial Growth factor receptor 2 in human endothelial cells. *Journal of Biological Chemistry*. 10.1074/jbc.M111.226423

227. Flori, H. R., Ware, L. B., Milet, M., and Matthay, M. A. (2007) Early elevation of plasma von Willebrand factor antigen in pediatric acute lung injury is associated with an increased risk of death and prolonged mechanical ventilation. *Pediatric Critical Care Medicine*. 10.1097/01.PCC.0000257097.42640.6F

228. Ware, L. B., Eisner, M. D., Thompson, B. T., Parsons, P. E., and Matthay, M. A. (2004) Significance of Von Willebrand factor in septic and nonseptic patients with acute lung injury. *American Journal of Respiratory and Critical Care Medicine*. 10.1164/rccm.200310-1434OC

229. Rubin, D. B., Wiener-Kronish, J. P., Murray, J. F., Green, D. R., Turner, J., Luce, J. M., Montgomery, A. B., Marks, J. D., and Matthay, M. A. (1990) Elevated von Willebrand factor antigen is an early plasma predictor of acute lung injury in nonpulmonary sepsis syndrome. *Journal of Clinical Investigation*. 10.1172/JCI114733

230. Lee, M., Rodansky, E. S., Smith, J. K., and Rodgers, G. M. (2012) ADAMTS13 promotes angiogenesis and modulates VEGF-induced angiogenesis. *Microvascular Research*. 10.1016/j.mvr.2012.05.004

231. Nemerson, Y., Furie, B., and Jackson, C. M. (1980) Zymogens and cofactors of blood coagulatio. *Critical Reviews in Biochemistry and Molecular Biology*. 10.3109/10409238009105472

232. Krishnaswamy, S. (2013) The transition of prothrombin to thrombin. *Journal of Thrombosis and Haemostasis*. 10.1111/jth.12217

233. Turner-Gomes, S. O., Mitchell, L., Williams, W. G., and Andrew, M. (1994) Thrombin regulation in congenital heart disease after cardiopulmonary bypass operations. *Journal of Thoracic and Cardiovascular Surgery*. 10.1016/S0022-5223(12)70103-4

234. Wang, W. M., Gaoxiang, G. E., Lim, N. H., Nagase, H., and Greenspan, D. S. (2006) TIMP-3 inhibits the procollagen N-proteinase ADAMTS-2. *Biochemical Journal*. 10.1042/BJ20060630

235. Tortorella, M. D., Arner, E. C., Hills, R., Easton, A., Korte-Sarfaty, J., Fok, K., Wittwer, A. J., Liu, R. Q., and Malfait, A. M. (2004) α2-Macroglobulin Is a Novel Substrate for ADAMTS-4 and ADAMTS-5 and Represents an Endogenous Inhibitor of These Enzymes. *Journal of Biological Chemistry*. 10.1074/jbc.M313041200

236. Anderson, P. J., Kokame, K., and Sadler, J. E. (2006) Zinc and calcium ions cooperatively modulate ADAMTS13 activity. *Journal of Biological Chemistry*. 10.1074/jbc.M504540200

237. Han, Y., Xiao, J., Falls, E., and Zheng, X. L. (2011) A shear-based assay for assessing plasma ADAMTS13 activity and inhibitors in patients with thrombotic thrombocytopenic purpura. *Transfusion (Paris)*. 10.1111/j.1537-2995.2010.03020.x

238. Crawley, J. T. B., Lam, J. K., Rance, J. B., Mollica, L. R., O'Donnell, J. S., and Lane, D. A. (2005) Proteolytic inactivation of ADAMTS13 by thrombin and plasmin. *Blood*. 10.1182/blood-2004-03-1101

239. Garland, K. S., Reitsma, S. E., Shirai, T., Zilberman-Rudenko, J., Tucker, E. I., Gailani, D., Gruber, A., McCarty, O. J. T., and Puy, C. (2017) Removal of the C-terminal domains of ADAMTS13 by activated coagulation factor XI induces platelet adhesion on endothelial cells under flow conditions. *Frontiers in Medicine*. 10.3389/fmed.2017.00232

240. Wagenman, B. L., Townsend, K. T., Mathew, P., and Crookston, K. P. (2009) The Laboratory Approach to Inherited and Acquired Coagulation Factor Deficiencies. *Clinics in Laboratory Medicine*. 10.1016/j.cll.2009.04.002

241. Rodeghiero, F., Castaman, G., and Dini, E. (1987) Epidemiological investigations of the prevalence of von Willebrand's disease. *Blood*. 10.1182/blood.v69.2.454.454

242. Eikenboom, J. C. J., Matsushita, T., Reitsma, P. H., Tuley, E. A., Castaman, G., Briët, E., and Sadler, J. E. (1996) Dominant type 1 von Willebrand disease caused by mutated cysteine residues in the D3 domain of von Willebrand factor. *Blood*. 10.1182/blood.v88.7.2433.bloodjournal8872433

243. Sadler, J. E. (1994) A revised classification of von Willebrand disease. For the Subcommittee on von Willebrand Factor of the Scientific and Standardization Committee of the International Society on Thrombosis and Haemostasis. *Thrombosis and Haemostasis*. 10.1055/s-0038-1642471

244. Eikenboom, J. C. J., van Marion, V., Putter, H., Goodeve, A., Rodeghiero, F., Castaman, G., Federici, A. B., Batlle, J., Meyer, D., Mazurier, C., Goudemand, J., Schneppenheim, R., Bubbe, U., Ingerslev, J., Vorlova, Z., Habart, D., Holmberg, L., Lethagen, S., Pasi, J., Hill, F., and Peak, I. (2006) Linkage analysis in families diagnosed with type 1 von Willebrand disease in the European study, molecular and clinical markers for the diagnosis and management of type 1 VWD. *Journal of Thrombosis and Haemostasis*. 10.1111/j.1538-7836.2006.01823.x

245. Goodeve, A. (2007) Genetics of type 1 von Willebrand disease. *Current Opinion in Hematology*. 10.1097/MOH.0b013e32826f4b41

246. James, P. D., Notley, C., Hegadorn, C., Leggo, J., Tuttle, A., Tinlin, S., Brown, C., Andrews, C., Labelle, A., Chirinian, Y., O'Brien, L., Othman, M., Rivard, G., Rapson, D., Hough, C., and Lillicrap, D. (2007) The mutational spectrum of type 1 von Willebrand disease: Results from a Canadian cohort study. *Blood*. 10.1182/blood-2006-05-021105.

247. Connell, N. T., Flood, V. H., Brignardello-Petersen, R., Abdul-Kadir, R., Arapshian, A., Couper, S., Grow, J. M., Kouides, P., Laffan, M., Lavin, M., Leebeek, F. W. G., O'Brien, S. H., Ozelo, M. C., Tosetto, A., Weyand, A. C., James, P. D., Kalot, M. A., Husainat, N., and Mustafa, R. A. (2021) Ash isth nhf wfh 2021 guidelines on the management of von willebrand disease. *Blood Advances*. 10.1182/BLOODADVANCES.2020003264

248. Lillicrap, D. (2007) Von Willebrand disease-Phenotype versus genotype: Deficiency versus disease. *Thrombosis Research*. 10.1016/j.thromres.2007.03.014

249. O'Brien, L. A., Sutherland, J. J., Weaver, D. F., and Lillicrap, D. (2005) Theoretical structural explanation for Group I and Group II, type 2A von Willebrand disease mutations [2]. *Journal of Thrombosis and Haemostasis*. 10.1111/j.1538-7836.2005.01219.x

250. Federici, A. B., Mannucci, P. M., Castaman, G., Baronciani, L., Bucciarelli, P., Canciani, M. T., Pecci, A., Lenting, P. J., and Groot, P. G. D. (2009) Clinical and

molecular predictors of thrombocytopenia and risk of bleeding in patients with von Willebrand disease type 2B: A cohort study of 67 patients. *Blood*. 10.1182/blood-2008-04-152280

251. Goodeve, A. C. (2010) The genetic basis of von Willebrand disease. *Blood Reviews*. 10.1016/j.blre.2010.03.003

252. Lynch, C. J., Cawte, A. D., Millar, C. M., Rueda, D., and Lane, D. A. (2017) A common mechanism by which type 2A von Willebrand disease mutations enhance ADAMTS13 proteolysis revealed with a von Willebrand factor A2 domain FRET construct. *PLoS ONE*. 10.1371/journal.pone.0188405

253. Zheng, X., Majerus, E. M., and Sadler, J. E. (2002) ADAMTS13 and TTP. *Current Opinion in Hematology*. 10.1097/00062752-200209000-00001

254. Chiasakul, T., and Cuker, A. (2018) Clinical and laboratory diagnosis of TTP: An integrated approach. *Hematology (United States)*. 10.1182/asheducation-2018.1.530

255. Bukowski, R. M. (1982) Thrombotic thrombocytopenic purpura: a review. *Prog Hemost Thromb*

256. Rock, G. A., Shumak, K. H., and Buskard, N. A. (1991) Comparison of plasma exchange with plasma infusion in the treatment of thrombotic thrombocytopenic purpura. *Annals of Internal Medicine*. 10.1056/nejm199108083250604

257. Sadler, J. E. (2017) Pathophysiology of thrombotic thrombocytopenic purpura. *Blood*. 10.1182/blood-2017-04-636431

258. Cataland, S. R., and Wu, H. M. (2015) Acquired thrombotic thrombocytopenic purpura: New therapeutic options and their optimal use. *Journal of Thrombosis and Haemostasis*. 10.1111/jth.12934

259. Velásquez Pereira, L. C., Roose, E., Graça, N. A. G., Sinkovits, G., Kangro, K., Joly, B. S., Tellier, E., Kaplanski, G., Falter, T., von Auer, C., Rossmann, H., Feys, H. B., Reti, M., Prohászka, Z., Lämmle, B., Voorberg, J., Coppo, P., Veyradier, A., de Meyer, S. F., Männik, A., and Vanhoorelbeke, K. (2021) Immunogenic hotspots in the spacer domain of ADAMTS13 in immune-mediated thrombotic thrombocytopenic purpura. *Journal of Thrombosis and Haemostasis*. 10.1111/jth.15170

260. Lancellotti, S., Peyvandi, F., Pagliari, M. T., Cairo, A., Abdel-Azeim, S., Chermak, E., Lazzareschi, I., Mastrangelo, S., Cavallo, L., Oliva, R., and de Cristofaro, R. (2016) The D173G mutation in ADAMTS-13 causes a severe form of congenital

thrombotic thrombocytopenic purpura: A clinical, biochemical and in silico study. *Thrombosis and Haemostasis*. 10.1160/TH15-02-0119

261. Korkmaz, S., Keklik, M., Sivgin, S., Yildirim, R., Tombak, A., Kaya, M. E., Acik, D. Y., Esen, R., Hacioglu, S. K., Sencan, M., Kiki, I., Tiftik, E. N., Kuku, I., Okan, V., Yilmaz, M., Demir, C., Sari, I., Altuntas, F., Unal, A., and Ilhan, O. (2013) Therapeutic plasma exchange in patients with thrombotic thrombocytopenic purpura: A retrospective multicenter study. *Transfusion and Apheresis Science*. 10.1016/j.transci.2013.04.016

262. Sadler, J. E. (2015) What's new in the diagnosis and pathophysiology of thrombotic thrombocytopenic purpura. *Hematology (United States)*. 10.1182/asheducation-2015.1.631

263. Motto, D. G., Chauhan, A. K., Zhu, G., Homeister, J., Lamb, C. B., Desch, K. C., Zhang, W., Tsai, H. M., Wagner, D. D., and Ginsburg, D. (2005) Shigatoxin triggers thrombic thrombocytopenic purpura in genetically susceptible ADAMTS13-deficient mice. *Journal of Clinical Investigation*. 10.1172/JCI26007

264. Yamashita, E., Okada, H., Yorioka, H., Fujita, S., Nishi, K., Komiyama, Y., and Kanzaki, H. (2012) Successful management of pregnancy-associated thrombotic thrombocytopenic purpura by monitoring ADAMTS13 activity. *Journal of Obstetrics and Gynaecology Research*. 10.1111/j.1447-0756.2011.01742.x

265. Sonneveld, M. A. H., de Maat, M. P. M., Portegies, M. L. P., Kavousi, M., Hofman, A., Turecek, P. L., Rottensteiner, H., Scheiflinger, F., Koudstaal, P. J., Ikram, M. A., and Leebeek, F. W. G. (2015) Low ADAMTS13 activity is associated with an increased risk of ischemic stroke. *Blood*. 10.1182/blood-2015-05-643338

266. Newnham, M., South, K., Bleda, M., Auger, W. R., Barberà, J. A., Bogaard, H., Bunclark, K., Cannon, J. E., Delcroix, M., Hadinnapola, C., Howard, L. S., Jenkins, D., Mayer, E., Ng, C., Rhodes, C. J., Screaton, N., Sheares, K., Simpson, M. A., Southwood, M., Su, L., Taboada, D., Traylor, M., Trembath, R. C., Villar, S. S., Wilkins, M. R., Wharton, J., Gräf, S., Pepke-Zaba, J., Laffan, M., Lane, D. A., Morrell, N. W., and Toshner, M. (2019) The ADAMTS13–VWF axis is dysregulated in chronic thromboembolic pulmonary hypertension. *European Respiratory Journal*. 10.1183/13993003.01805-2018

267. Singh, K., Kwong, A. C., Madarati, H., Kunasekaran, S., Sparring, T., Fox-Robichaud, A. E., Liaw, P. C., and Kretz, C. A. (2021) Characterization of ADAMTS13 and von Willebrand factor levels in septic and non-septic ICU patients. *PLoS ONE*. 10.1371/journal.pone.0247017

268. Chen, X., Cheng, X., Zhang, S., and Wu, D. (2019) ADAMTS13: An emerging target in stroke therapy. *Frontiers in Neurology*. 10.3389/fneur.2019.00772

269. Eerenberg, E. S., Teunissen, P. F. A., van den Born, B. J., Meijers, J. C. M., Hollander, M. R., Jansen, M., Tijssen, R., Beliën, J. A. M., van de Ven, P. M., Aly, M. F., Kamp, O., Niessen, H. W., Kamphuisen, P. W., Levi, M., and van Royen, N. (2016) The role of ADAMTS13 in acute myocardial infarction: Cause or consequence? *Cardiovascular Research*. 10.1093/cvr/cvw097

270. de Meyer, S. F., Savchenko, A. S., Haas, M. S., Schatzberg, D., Carroll, M. C., Schiviz, A., Dietrich, B., Rottensteiner, H., Scheiflinger, F., and Wagner, D. D. (2012) Protective anti-inflammatory effect of ADAMTS13 on myocardial ischemia/reperfusion injury in mice. *Blood*. 10.1182/blood-2012-06-439935

271. Tinnefeld, V., Sickmann, A., and Ahrends, R. (2014) Catch me if you can: Challenges and applications of cross-linking approaches. *European Journal of Mass Spectrometry*. 10.1255/ejms.1259

272. Roux, K. J., Kim, D. I., and Burke, B. (2013) BioID: A screen for protein-protein interactions. *Current Protocols in Protein Science*. 10.1002/0471140864.ps1923s74

273. Varnaitė, R., and MacNeill, S. A. (2016) Meet the neighbors: Mapping local protein interactomes by proximity-dependent labeling with BioID. *Proteomics*. 10.1002/pmic.201600123

274. Leitner, Z. A. (1947) Vitamin H. *BMJ*. 10.1136/bmj.1.4497.354

275. Pacheco-Alvarez, D., Solórzano-Vargas, R. S., and del Río, A. L. (2002) Biotin in metabolism and its relationship to human disease. *Archives of Medical Research*. 10.1016/S0188-4409(02)00399-5

276. Pendini, N. R., Bailey, L. M., Booker, G. W., Wilce, M. C., Wallace, J. C., and Polyak, S. W. (2008) Microbial biotin protein ligases aid in understanding holocarboxylase synthetase deficiency. *Biochimica et Biophysica Acta - Proteins and Proteomics*. 10.1016/j.bbapap.2008.03.011

277. He, L., Hamm, J. A., Reddy, A., Sams, D., Peliciari-Garcia, R. A., McGinnis, G. R., Bailey, S. M., Chow, C. W., Rowe, G. C., Chatham, J. C., and Young, M. E. (2016) Biotinylation: A novel posttranslational modification linking cell autonomous circadian clocks with metabolism. *American Journal of Physiology - Heart and Circulatory Physiology*. 10.1152/ajpheart.00959.2015

278. Altin, J. G., and Pagler, E. B. (1995) A one-step procedure for biotinylation and chemical cross-linking of lymphocyte surface and intracellular membrane-associated molecules. *Analytical Biochemistry*. 10.1006/abio.1995.1054

279. Shinya, T., Osada, T., Desaki, Y., Hatamoto, M., Yamanaka, Y., Hirano, H., Takai, R., Che, F. S., Kaku, H., and Shibuya, N. (2010) Characterization of receptor proteins using affinity cross-linking with biotinylated ligands. *Plant and Cell Physiology*. 10.1093/pcp/pcp185

280. Chapman-Smith, A., and Cronan, J. E. (1999) The enzymatic biotinylation of proteins: A post-translational modification of exceptional specificity. *Trends in Biochemical Sciences*. 10.1016/S0968-0004(99)01438-3

281. LANE, M. D., ROMINGER, K. L., YOUNG, D. L., and LYNEN, F. (1964) THE ENZYMATIC SYNTHESIS OF HOLOTRANSCARBOXYLASE FROM APOTRANSCARBOXYLASE AND (+)-BIOTIN. II. INVESTIGATION OF THE REACTION MECHANISM. *J Biol Chem*

282. Fairhead, M., and Howarth, M. (2015) Site-specific biotinylation of purified proteins using BirA. *Methods in Molecular Biology*. 10.1007/978-1-4939-2272-7_12

283. Rhee, E. C., and Schulman, H. (2004) Promiscuous protein biotinylation by Escherichia coli biotin protein ligase - Choi-Rhee - 2008 - Protein Science - Wiley Online Library. *Protein Science*

284. Kim, D. I., Birendra, K. C., Zhu, W., Motamedchaboki, K., Doye, V., and Roux, K. J. (2014) Probing nuclear pore complex architecture with proximity-dependent biotinylation. *Proc Natl Acad Sci U S A*. 10.1073/pnas.1406459111

285. Elzi, D. J., Song, M., Hakala, K., Weintraub, S. T., and Shiio, Y. (2014) Proteomic analysis of the EWS-Fli-1 interactome reveals the role of the lysosome in EWS-Fli-1 turnover. *Journal of Proteome Research*. 10.1021/pr500387m

286. Ritchie, C., Cylinder, I., Platt, E. J., and Barklis, E. (2015) Analysis of HIV-1 Gag Protein Interactions via Biotin Ligase Tagging. *Journal of Virology*. 10.1128/jvi.03584-14

287. le Sage, V., Cinti, A., Valiente-Echeverría, F., and Mouland, A. J. (2015) Proteomic analysis of HIV-1 Gag interacting partners using proximity-dependent biotinylation. *Virology Journal*. 10.1186/s12985-015-0365-6

288. Fields, S., and Song, O. K. (1989) A novel genetic system to detect protein-protein interactions. *Nature*. 10.1038/340245a0

289. Brückner, A., Polge, C., Lentze, N., Auerbach, D., and Schlattner, U. (2009) Yeast two-hybrid, a powerful tool for systems biology. *International Journal of Molecular Sciences*. 10.3390/ijms10062763

290. Adile, A. A., and Vujovic, A. (2018) Use of BioID to detect protein-protein interactions. *Canadian Journal of Undergraduate Research*

291. Liu, X., Salokas, K., Weldatsadik, R. G., Gawriyski, L., and Varjosalo, M. (2020) Combined proximity labeling and affinity purification−mass spectrometry workflow for mapping and visualizing protein interaction networks. *Nature Protocols*. 10.1038/s41596-020-0365-x

292. Yadav, L., Tamene, F., Göös, H., van Drogen, A., Katainen, R., Aebersold, R., Gstaiger, M., and Varjosalo, M. (2017) Systematic Analysis of Human Protein Phosphatase Interactions and Dynamics. *Cell Systems*. 10.1016/j.cels.2017.02.011

293. Liu, X., Salokas, K., Tamene, F., Jiu, Y., Weldatsadik, R. G., Öhman, T., and Varjosalo, M. (2018) An AP-MS- and BioID-compatible MAC-tag enables comprehensive mapping of protein interactions and subcellular localizations. *Nature Communications*. 10.1038/s41467-018-03523-2

294. Free, R. B., Hazelwood, L. A., and Sibley, D. R. (2009) Identifying novel protein-protein interactions using co-immunoprecipitation and mass spectroscopy. *Current Protocols in Neuroscience*. 10.1002/0471142301.ns0528s46

295. Lee, C. (2007) Coimmunoprecipitation assay. *Methods in Molecular Biology*. 10.1385/1-59745-257-2:401

296. Rhee, H. W., Zou, P., Udeshi, N. D., Martell, J. D., Mootha, V. K., Carr, S. A., and Ting, A. Y. (2013) Proteomic mapping of mitochondria in living cells via spatially restricted enzymatic tagging. *Science (1979)*. 10.1126/science.1230593

297. Mortensen, A., and Skibsted, L. H. (1997) Importance of Carotenoid Structure in Radical-Scavenging Reactions. *Journal of Agricultural and Food Chemistry*. 10.1021/jf970010s

298. Hung, V., Zou, P., Rhee, H. W., Udeshi, N. D., Cracan, V., Svinkina, T., Carr, S. A., Mootha, V. K., and Ting, A. Y. (2014) Proteomic Mapping of the Human Mitochondrial Intermembrane Space in Live Cells via Ratiometric APEX Tagging. *Molecular Cell*. 10.1016/j.molcel.2014.06.003

299. DeMoss, J. A., Genuth, S. M., and Novelli, G. D. (1956) THE ENZYMATIC ACTIVATION OF AMINO ACIDS VIA THEIR ACYL-ADENYLATE DERIVATIVES. *Proceedings of the National Academy of Sciences*. 10.1073/pnas.42.6.325

300. Chen, C. L., and Perrimon, N. (2017) Proximity-dependent labeling methods for proteomic profiling in living cells. *Wiley Interdisciplinary Reviews: Developmental Biology*. 10.1002/wdev.272

301. Echols, N., Harrison, P., Balasubramanian, S., Luscombe, N. M., Bertone, P., Zhang, Z., and Gerstein, M. (2002) Comprehensive analysis of amino acid and nucleotide composition in eukaryotic genomes, comparing genes and pseudogenes. *Nucleic Acids Research*. 10.1093/nar/30.11.2515

302. Tourasse, N. J., and Li, W. H. (2000) Selective constraints, amino acid composition, and the rate of protein evolution. *Molecular Biology and Evolution*. 10.1093/oxfordjournals.molbev.a026344

303. Lam, S. S., Martell, J. D., Kamer, K. J., Deerinck, T. J., Ellisman, M. H., Mootha, V. K., and Ting, A. Y. (2014) Directed evolution of APEX2 for electron microscopy and proximity labeling. *Nature Methods*. 10.1038/nmeth.3179

304. Kim, D. I., Jensen, S. C., Noble, K. A., Kc, B., Roux, K. H., Motamedchaboki, K., and Roux, K. J. (2016) An improved smaller biotin ligase for BioID proximity labeling. *Molecular Biology of the Cell*. 10.1091/mbc.E15-12-0844

305. Branon, T. C., Bosch, J. A., Sanchez, A. D., Udeshi, N. D., Svinkina, T., Carr, S. A., Feldman, J. L., Perrimon, N., and Ting, A. Y. (2018) Efficient proximity labeling in living cells and organisms with TurboID. *Nature Biotechnology*. 10.1038/nbt.4201

306. Khan, M., Youn, J. Y., Gingras, A. C., Subramaniam, R., and Desveaux, D. (2018) In planta proximity dependent biotin identification (BioID). *Scientific Reports*. 10.1038/s41598-018-27500-3

307. Uezu, A., Kanak, D. J., Bradshaw, T. W. A., Soderblom, E. J., Catavero, C. M., Burette, A. C., Weinberg, R. J., and Soderling, S. H. (2016) Identification of an elaborate complex mediating postsynaptic inhibition. *Science (1979)*. 10.1126/science.aag0821

308. Remnant, L., Booth, D. G., Vargiu, G., Spanos, C., Kerr, A. R. W., and Earnshaw, W. C. (2019) In vitro BioID: Mapping the CENP-A microenvironment with high temporal and spatial resolution. *Molecular Biology of the Cell*. 10.1091/mbc.E18-12-0799

309. Chojnowski, A., Sobota, R. M., Ong, P. F., Xie, W., Wong, X., Dreesen, O., Burke, B., and Stewart, C. L. (2018) 2C-BioID: An Advanced Two Component BioID System for Precision Mapping of Protein Interactomes. *iScience*. 10.1016/j.isci.2018.11.023

310. Schopp, I. M., Amaya Ramirez, C. C., Debeljak, J., Kreibich, E., Skribbe, M., Wild, K., and Béthune, J. (2017) Split-BioID a conditional proteomics approach to monitor the composition of spatiotemporally defined protein complexes. *Nature Communications*. 10.1038/ncomms15690

311. Mathew, J., and Bhimji, S. S. (2018) *Physiology, Blood Plasma*

312. C Costello, L. (2016) Plasma Citrate Homeostasis: How It Is Regulated; And Its Physiological and Clinical Implications. An Important, But Neglected, Relationship in Medicine. *Human Endocrinology*. 10.24966/HE-9640/100005

313. Mann, K. G., Whelihan, M. F., Butenas, S., and Orfeo, T. (2007) Citrate anticoagulation and the dynamics of thrombin generation. *Journal of Thrombosis and Haemostasis*. 10.1111/j.1538-7836.2007.02710.x

314. Chen, Z., Chen, B., Yao, X. Q., Gui, B. S., Ou, Y., and Ouyang, J. M. (2012) Anticoagulation of diethyl citrate and its comparison with sodium citrate in an animal model. *Blood Purification*. 10.1159/000330891

315. Sloane, V., Blanchard, C. Z., Guillot, F., and Waldrop, G. L. (2001) Site-directed mutagenesis of ATP binding residues of biotin carboxylase: Insight into the mechanism of catalysis. *Journal of Biological Chemistry*. 10.1074/jbc.M101472200

316. Gorman, M. W., Marble, D. R., Ogimoto, K., and Feigl, E. O. (2003) Measurement of adenine nucleotides in plasma. *Luminescence*. 10.1002/bio.721

317. Gibson, D. G., Young, L., Chuang, R. Y., Venter, J. C., Hutchison, C. A., and Smith, H. O. (2009) Enzymatic assembly of DNA molecules up to several hundred kilobases. *Nature Methods*. 10.1038/nmeth.1318

318. Lam, J. K., Chion, C. K. N. K., Zanardelli, S., Lane, D. A., and Crawley, J. T. B. (2007) Further characterization of ADAMTS-13 inactivation by thrombin. *Journal of Thrombosis and Haemostasis*. 10.1111/j.1538-7836.2007.02514.x

319. Fu, Z., Thorpe, M., Akula, S., Chahal, G., and Hellman, L. T. (2018) Extended cleavage specificity of human neutrophil elastase, human proteinase 3, and their distant ortholog clawed frog PR3-three elastases with similar primary but different extended specificities and stability. *Frontiers in Immunology*. 10.3389/fimmu.2018.02387

320. Song, J., Tan, H., Perry, A. J., Akutsu, T., Webb, G. I., Whisstock, J. C., and Pike, R. N. (2012) PROSPER: An Integrated Feature-Based Tool for Predicting Protease Substrate Cleavage Sites. *PLoS ONE*. 10.1371/journal.pone.0050300

321. Gasteiger, E., Hoogland, C., Gattiker, A., Duvaud, S., Wilkins, M. R., Appel, R. D., and Bairoch, A. (2005) Protein Identification and Analysis Tools on the ExPASy Server. in *The Proteomics Protocols Handbook*, 10.1385/1-59259-890-0:571

322. Vincze, T., Posfai, J., and Roberts, R. J. (2003) NEBcutter: A program to cleave DNA with restriction enzymes. *Nucleic Acids Research*. 10.1093/nar/gkg526

323. Crawley, J. T. B., de Groot, R., and Luken, B. M. (2009) Circulating ADAMTS-13-von Willebrand factor complexes: An enzyme on demand. *Journal of Thrombosis and Haemostasis*. 10.1111/j.1538-7836.2009.03621.x

324. Gorman, M. W., Marble, D. R., Ogimoto, K., and Feigl, E. O. (2003) Measurement of adenine nucleotides in plasma. *Luminescence*. 10.1002/bio.721

325. Castellino, F. J., and McCance, S. G. (1997) The kringle domains of human plasminogen. *CIBA Foundation Symposia*. 10.1002/9780470515457.ch4

326. Banno, F., Chauhan, A. K., Kokame, K., Yang, J., Miyata, S., Wagner, D. D., and Miyata, T. (2009) The distal carboxyl-terminal domains of ADAMTS13 are required for regulation of in vivo thrombus formation. *Blood*. 10.1182/blood-2008-07-169359

327. Wohner, N., Kovács, A., MacHovich, R., and Kolev, K. (2012) Modulation of the von Willebrand factor-dependent platelet adhesion through alternative proteolytic pathways. *Thrombosis Research*. 10.1016/j.thromres.2011.11.021

328. Fuchs, T. a, Brill, A., and Wagner, D. D. (2012) NET impact on deep vein thrombosis. *Arterioscler Thromb Vasc Biol*. 10.1161/ATVBAHA.111.242859.NET

329. May, D. G., Scott, K. L., Campos, A. R., and Roux, K. J. (2020) Comparative Application of BioID and TurboID for Protein-Proximity Biotinylation. *Cells*. 10.3390/cells9051070

330. Roux, K. J., Kim, D. I., Raida, M., and Burke, B. (2012) A promiscuous biotin ligase fusion protein identifies proximal and interacting proteins in mammalian cells. *Journal of Cell Biology*. 10.1083/jcb.201112098

331. Davies, D. R., and Hol, W. G. J. (2004) The power of vanadate in crystallographic investigations of phosphoryl transfer enzymes. *FEBS Letters*. 10.1016/j.febslet.2004.10.022

332. Essayan, D. M. (2001) Cyclic nucleotide phosphodiesterases. *Journal of Allergy and Clinical Immunology*. 10.1067/mai.2001.119555

333. Yu, F. X., Goh, S. R., Dai, R. P., and Luo, Y. (2009) Adenosine-containing molecules amplify glucose signaling and enhance Txnip expression. *Molecular Endocrinology*. 10.1210/me.2008-0383

334. Gout, E., Rébeillé, F., Douce, R., and Bligny, R. (2014) Interplay of Mg2+, ADP, and ATP in the cytosol and mitochondria: Unravelling the role of Mg2+ in cell respiration. *Proc Natl Acad Sci U S A*. 10.1073/pnas.1406251111

335. di Stasio, E., Lancellotti, S., Peyvandi, F., Palla, R., Mannucci, P. M., and de Cristofaro, R. (2008) Mechanistic studies on ADAMTS13 catalysis. *Biophysical Journal*. 10.1529/biophysj.108.131532

336. Sadler, J. E. (2008) Von Willebrand factor, ADAMTS13, and thrombotic thrombocytopenic purpura. *Blood*. 10.1182/blood-2008-02-078170

337. Feys, H. B., Vandeputte, N., Palla, R., Peyvandi, F., Peerlinck, K., Deckmyn, H., Lijnen, H. R., and Vanhoorelbeke, K. (2010) Inactivation of ADAMTS13 by plasmin as a potential cause of thrombotic thrombocytopenic purpura. *Journal of Thrombosis and Haemostasis*. 10.1111/j.1538-7836.2010.03942.x

338. Zhou, A., Huntington, J. A., Pannu, N. S., Carrell, R. W., and Read, R. J. (2003) How vitronectin binds PAI-1 to modulate fibrinolysis and cell migration. *Nature Structural Biology*. 10.1038/nsb943

339. Crescente, M., Thomas, G. M., Demers, M., Voorhees, J. R., Wong, S. L., Ho-Tin-Noe, B., and Wagner, D. D. (2012) ADAMTS13 exerts a thrombolytic effect in microcirculation. *Thrombosis and Haemostasis*. 10.1160/TH12-01-0046

340. Shi, G. Y., and Wu, H. L. (1988) Isolation and characterization of microplasminogen. A low molecular weight form of plasminogen. *Journal of Biological Chemistry*. 10.1016/s0021-9258(18)37499-4

341. Patthy, L. (1985) Evolution of the proteases of blood coagulation and fibrinolysis by assembly from modules. *Cell*. 10.1016/S0092-8674(85)80046-5

342. Nielsen, V. G., and Ford, P. M. (2018) The ratio of concentrations of aminocaproic acid and tranexamic acid that prevent plasmin activation of platelets does not provide equivalent inhibition of plasmatic fibrinolysis. *Journal of Thrombosis and Thrombolysis*. 10.1007/s11239-018-1705-3

343. Shi, G. Y., Wu, D. H., and Wu, H. L. (1991) Kringle domains and plasmin denaturation. *Biochemical and Biophysical Research Communications*. 10.1016/0006-291X(91)91822-T

344. Jones, D. W., Nicholls, P. J., Donohoe, S., Gallimore, M. J., and Winter, M. (2002) Antibodies to factor XII are distinct from antibodies to prothrombin in patients

with the anti-phospholipid syndrome. *Thrombosis and Haemostasis*. 10.1055/s-0037-1613021

345. Hughes, A. L. (2000) Modes of evolution in the protease and kringle domains of the plasminogen-prothrombin family. *Molecular Phylogenetics and Evolution*. 10.1006/mpev.1999.0685

346. Ikeo, K., Takahashi, K., and Gojobori, T. (1991) Evolutionary origin of numerous kringles in human and simian apolipoprotein(a). *FEBS Letters*. 10.1016/0014-5793(91)80036-3

347. McMullen, B. A., and Fujikawa, K. (1985) Amino acid sequence of the heavy chain of human α-factor XIIa (activated Hageman factor). *Journal of Biological Chemistry*. 10.1016/s0021-9258(18)89026-3

348. Hofman, Z. L. M., Clark, C. C., Sanrattana, W., Nosairi, A., Parr, N. M. J., Živkovic, M., Krause, K., Mahnke, N. A., Scheffel, J., Erik Hack, C., Maurer, M., de Maat, S., and Coen Maas, X. (2020) A mutation in the kringle domain of human factor XII that causes autoinflammation, disturbs zymogen quiescence, and accelerates activation. *Journal of Biological Chemistry*. 10.1074/jbc.RA119.009788

349. Castellino, F. J., and Beals, J. M. (1987) The genetic relationships between the kringle domains of human plasminogen, prothrombin, tissue plasminogen activator, urokinase, and coagulation factor XII. *Journal of Molecular Evolution*. 10.1007/BF02101155

350. Arni, R. K., Padmanabhan, K., Padmanabhan, K. P., Wu, T. P., and Tulinsky, A. (1994) Structure of the non-covalent complex of prothrombin kringle 2 with PPACK-thrombin. *Chemistry and Physics of Lipids*. 10.1016/0009-3084(94)90124-4

351. Paré, G., Çaku, A., McQueen, M., Anand, S. S., Enas, E., Clarke, R., Boffa, M. B., Koschinsky, M., Wang, X., and Yusuf, S. (2019) Lipoprotein(a) levels and the risk of myocardial infarction among 7 ethnic groups. *Circulation*. 10.1161/CIRCULATIONAHA.118.034311

352. Crawley, J. T. B., Lane, D. A., Woodward, M., Rumley, A., and Lowe, G. D. O. (2008) Evidence that high von Willebrand factor and low ADAMTS-13 levels independently increase the risk of a non-fatal heart attack. *Journal of Thrombosis and Haemostasis*. 10.1111/j.1538-7836.2008.02902.x

353. Karakaya, B., Tombak, A., Serin, M. S., and Tiftik, N. (2016) Change in plasma a disintegrin and metalloprotease with thrombospondin type-1 repeats-13 and von

Willebrand factor levels in venous thromboembolic patients. *Hematology*. 10.1080/10245332.2015.1125079

354. Ono, T., Mimuro, J., Madoiwa, S., Soejima, K., Kashiwakura, Y., Ishiwata, A., Takano, K., Ohmori, T., and Sakata, Y. (2006) Severe secondary deficiency of von Willebrand factor-cleaving protease (ADAMTS13) in patients with sepsis-induced disseminated intravascular coagulation: Its correlation with development of renal failure. *Blood*. 10.1182/blood-2005-03-1087

355. Majewski, P., Majchrzak-Gorecka, M., Grygier, B., Skrzeczynska-Moncznik, J., Osiecka, O., and Cichy, J. (2016) Inhibitors of serine proteases in regulating the production and function of neutrophil extracellular traps. *Frontiers in Immunology*. 10.3389/fimmu.2016.00261

356. Farkas, P., Csuka, D., Mikes, B., Sinkovits, G., Réti, M., Németh, E., Rácz, K., Madách, K., Gergely, M., Demeter, J., and Prohászka, Z. (2017) Complement activation, inflammation and relative ADAMTS13 deficiency in secondary thrombotic microangiopathies. *Immunobiology*. 10.1016/j.imbio.2016.10.014

357. Yang, J., Wu, Z., Long, Q., Huang, J., Hong, T., Liu, W., and Lin, J. (2020) Insights Into Immunothrombosis: The Interplay Among Neutrophil Extracellular Trap, von Willebrand Factor, and ADAMTS13. *Frontiers in Immunology*. 10.3389/fimmu.2020.610696

358. Wang, Y., Chen, J., Ling, M., López, J. A., Chung, D. W., and Fu, X. (2015) Hypochlorous acid generated by neutrophils inactivates ADAMTS13: An oxidative mechanism for regulating ADAMTS13 proteolytic activity during inflammation. *Journal of Biological Chemistry*. 10.1074/jbc.M114.599084

359. Lancellotti, S., Basso, M., and de Cristofaro, R. (2013) Proteolytic processing of Von Willebrand Factor by Adamts13 and Leukocyte Proteases. *Mediterranean Journal of Hematology and Infectious Diseases*. 10.4084/mjhid.2013.058

360. Weber, C., Jenke, A., Chobanova, V., Yazdanyar, M., Chekhoeva, A., Eghbalzadeh, K., Lichtenberg, A., Wahlers, T., Akhyari, P., and Paunel-Görgülü, A. (2019) Targeting of cell-free DNA by DNase I diminishes endothelial dysfunction and inflammation in a rat model of cardiopulmonary bypass. *Scientific Reports*. 10.1038/s41598-019-55863-8